
Electronic Thesis and Dissertation Repository

February 2015

Chromite Crystal Structure and Chemistry applied as an Exploration Tool

Patrick H.M. Shepherd
The University of Western Ontario

Supervisor
Dr. Roberta L. Flemming
The University of Western Ontario

Graduate Program in Geology

A thesis submitted in partial fulfillment of the requirements for the degree in Master of Science
© Patrick H.M. Shepherd 2015

Follow this and additional works at: <https://ir.lib.uwo.ca/etd>

 Part of the [Geology Commons](#)

Recommended Citation

Shepherd, Patrick H.M., "Chromite Crystal Structure and Chemistry applied as an Exploration Tool" (2015).
Electronic Thesis and Dissertation Repository. 2685.
<https://ir.lib.uwo.ca/etd/2685>

This Dissertation/Thesis is brought to you for free and open access by Scholarship@Western. It has been accepted for inclusion in Electronic Thesis and Dissertation Repository by an authorized administrator of Scholarship@Western. For more information, please contact wlsadmin@uwo.ca.

Chromite Crystal Structure and Chemistry Applied as an Exploration Tool

Patrick H.M. Shepherd

Supervisor

Roberta Flemming

The University of Western Ontario

Follow this and additional works at: <http://ir.lib.uwo.ca/etd>

 Part of the [Geology Commons](#)

Chromite Crystal Structure and Chemistry Applied as an Exploration Tool

(Thesis format: Integrated Article)

by

Patrick H.M. Shepherd

Graduate Program in Earth Science

A thesis submitted in partial fulfillment
of the requirements for the degree of
Master of Science

The School of Graduate and Postdoctoral Studies
The University of Western Ontario
London, Ontario, Canada

© Shepherd 2014

Abstract

Spinel group minerals have long been of interest in mineral exploration due to their use as indicator minerals. The unit cell parameter is a structural measurement primarily controlled by composition and this study has attempted to look at the applications of the unit cell parameter as a proxy for composition in exploration, with a focus on diamond exploration. The implementation of μ XRD for this purpose required the creation the Slice Integration Technique to improve the signal to noise ratio from 2D data. The compositions of spinels can be approximated through their correlation with unit cell with some ambiguity. Possible applications include the discrimination of diamond inclusion-related compositions for diamond exploration, or in gemology and curatorial studies, where the nondestructive nature of μ XRD is advantageous. Additional analysis of chromite indicator minerals was conducted using a field portable XRD which has demonstrated that unit cell data could be used in the field, in conjunction with other new field-portable technologies, such as XRF.

Keywords

Chromite, Unit Cell Parameter, Spinel, Mineral Exploration

Acknowledgments

No research undertaking is the result of a lone investigator's efforts, and as such, there are a great many individuals who have contributed to this project and who have made its completion possible.

I would first like to thank my supervisor Dr. Roberta Flemming, for her guidance and her willingness to always be available to help. I would also like to thank her for the opportunity to work in her X-ray lab as an RA, which has been a great experience and allowed me the ability to finish my thesis. I have benefited from her guidance during this project and her support.

Matthew Izawa deserves special thanks for having been extremely helpful during the final months of the project. His emotional and academic support was indispensable in the process of solving a number of standard difficulties that were encountered during the research process, and his many discussions were of the utmost help.

I am very grateful to Dr. Tom Nowicki for guidance and for graciously providing samples, and for much useful advice in understanding the industry. I would also like to thank Mineral Services Canada Inc for supplying samples.

Many thanks also to Dave Edey, Mike Craig, Alysha McNeil, Annemarie Pickersgill, Bethany Dean, Trevor Weiss, Sarah CoDyre, Diego Uribe, Mike Bramble, Dr. Phil McCausland,

Also deserving of recognition are Eleni and Sotiros Petrou, Ashley Piskor-Potter, Corey De Vlugt John Jardine, Catherine Jardine, Megan Simpson, Eva McGuire, Adam Helmers, Aaron Drahushchak, Steve Eckert, Ben Lamb, Cameron Beare, Charles Nolan, Justin Peter, Dan Freeman, Fr. Raymond DeSouza, Josh Vanleeuwen, Peter Ketelaars, Sean Wilson, David Johnson and the many other people who have been there to support me along my journey.

Many thanks to Michael McTaggart-Cook for graciously giving his time in reading and editing the final draft of this thesis the evening before submission.

Finally, my family has been an amazing source of support, especially my mother, who throughout my undergraduate degree and my masters degree has been there when I needed a quick edit, an ear to vent to or to ask for advice. Moreover, my sister Sarah has been a constant source of support. There is nothing like having a sister show up the night before thesis is due with a full dinner.

Table of Contents

Abstract.....	ii
Acknowledgments.....	iii
Table of Contents.....	iii
List of Tables	ix
List of Figures.....	x
List of Appendices	xiii
Chapter 1	1
1 Introduction.....	1
1.1 Overview.....	1
1.2 Spinel Structure and Unit Cell	2
1.3 Spinel Indicator Minerals.....	4
1.4 Spinel petrogenetic indicators.....	6
1.5 Kimberlites: History and Overview	6
1.6 Exploration Target and Strategy	9
1.7 Indicator Mineral Overview.....	10
1.8 Diamond Indicator Mineral Discrimination.....	13
1.9 Kimberlite Chemical Trends.....	14
1.10 Rationale for the Unit Cell Parameter as a Compositional Proxy.....	16
1.11 References	17
Chapter 2.....	24
2 Methods.....	24
2.1 Samples.....	24
2.2 General Methods.....	25
2.2.1 Micro X-ray Diffraction.....	25

2.2.2	Slice Integration Technique Overview	28
2.2.3	Error Determination	28
2.2.4	Terra X-Ray Diffraction /X-Ray Fluorescence Methods.....	29
2.2.5	The Unit Cell Parameter Refinement.....	29
2.2.6	Electron Probe Micro-Analysis (EPMA).....	29
2.3	References	33
	Co-Authorship Statement.....	34
	Chapter 3	35
3	Signal enhancement through a maximum intensity projection using Slice Integration of 2D-XRD data: Applications to unstrained crystallites (>100 micron grain size)....	35
3.1	Executive Summary	35
3.2	Introduction.....	36
3.3	Methods.....	37
3.3.1	In situ micro X-ray Diffraction	37
3.3.2	Pick Peak Method and 2D Slicing	38
3.3.3	Slice Integration Technique using the Additive Method	40
3.3.4	Slice Integration Technique using a Max Intensity Plot (MIP)	41
3.4	Results.....	42
3.4.1	Demonstrating Signal to Noise Improvement.....	42
3.4.2	Demonstrating the Max Plot	46
3.5	Discussion	49
3.5.1	Demonstrating Signal to Noise	49
3.5.2	Overslicing.....	50
3.5.3	Max Intensity Plot.....	52
3.6	Conclusions.....	53
3.7	References.....	54

Co-Authorship Statement.....	56
Chapter 4.....	57
4 The unit cell parameter a proxy for composition within defined terrains as applied to kimberlitic vs non-kimberlitic chromite	57
4.1 Executive Summary	57
4.2 Introduction.....	57
4.3 Methods.....	59
4.3.1 Samples	59
4.3.2 Major Elements	60
4.3.3 MicroXRD	61
4.4 Results.....	63
4.4.1 Overview.....	67
4.4.2 Micro X-ray Diffraction as applied to unit cell parameter and textural information.....	67
4.4.3 Unit Cell and Composition Correlations.....	70
4.4.4 Unit Cell Parameter in Reference to End-member Spinel	75
4.4.5 Unit Cell Applied to KIM vs Non-KIM discrimination	79
4.5 Conclusions.....	85
4.6 References.....	85
Co-Authorship Statement.....	89
Chapter 5.....	90
5 Portable Structural Refinement and Compositional proxy using a Terra XRD/XRF ..	90
5.1 Abstract.....	90
5.2 Introduction.....	90
5.3 Methods.....	91
5.3.1 Electron probe microanalysis (EPMA).....	91
5.3.2 Terra XRD/XRF Methods.....	92

5.3.3 Unit Cell.....	92
5.4 Results.....	93
5.4.1 Power XRD.....	93
5.4.2 Exposure Times	94
5.4.3 Powder XRF.....	95
5.5 Discussion.....	95
5.5.1 Estimating Al content from unit cell parameter.....	95
5.5.2 Field Proxy.....	98
5.6 Conclusions and Future work	99
5.7 References.....	100
Chapter 6.....	102
6 Conclusions and Future Directions	102
6.1 Slicing.....	102
6.2 Unit Cell Parameters.....	103
6.3 Field Proxy.....	104
Appendices.....	107
Resume.....	220

List of Tables

Table 1-1: Ionic Radii (O'Neill and Navrotsky 1983)	3
Table 1-2: Spinel group formula and unit cells (Deer et al. 1992)	4
Table 1-3: Indicator Minerals Relevant Attributes (adapted from Muggeridge 1995).....	11
Table 3-1: Slice Percentage	42
Table 3-2: Peak Locations for addition method.....	53
Table 4-1: Grains and Sample Locations.....	60

List of Figures

Figure 1-1: General spinel structure (Atoms Software, Dowty 1993).....	2
Figure 1-2: a) Trivalent spinel prism; b) divalent Spinel prism.....	5
Figure 1-3: Schematic diagram of descending geotherm under a craton into the diamond stability field. (Modified from Stachel and Harris 2008)	6
Figure 1-4: Kimberlite morphologies. Modified from (Scott Smith et al. 2013)	9
Figure 1-5: Polished probe chromite	13
Figure 1-6: The three kimberlite trends. a) the AMC trend b) first magmatic trend c) The second magmatic trend.	16
Figure 2-1: Bruker D8 Discover in situ μ XRD configuration.	25
Figure 2-2: Effect of detector distance.....	27
Figure 3-1: Skematic Diagram for Slice Method.....	38
Figure 3-2: Peak Position.....	39
Figure 3-3: Context Image and GADDS	40
Figure 3-4: Intensity vs Frame Percentage and the STD vs Frame Percentage.....	43/44
Figure 3-5: Figure Signal/Noise (normalized to 3 STD) vs frame percentage	45
Figure 3-6: Results additive pattern method	46
Figure 3-7: MIP method single phase results	47
Figure 3-8: MIP method Multi phase results	48
Figure 3-9: Oversliced intense peak..	49
Figure 3-10: Over sliced weak peak..	50

Figure 3-11: 400 Slices on a Weak Peak	51
Figure 3-12: Schulze Sample Sliced - 70 Slices.	52
Figure 4-1: Bruker D8 Discover configuration.....	61
Figure 4-2: Conventional vs Slice Integration.....	62
Figure 4-3: 1D *.dif pattern	63
Figure 4-4. The spinel prism. a) Trivalent prism; b) Divalent prism.....	64
Figure 4-5: Prism Face projections. a) Cr vs Fe^{3+} vs Al b) Cr vs Ti vs Al	65
Figure 4-6: Prism Projection: Side a) $\text{Fe}/(\text{Fe}+\text{Mg})$ versus $\text{Fe}^{3+}/(\text{Fe}^{3+}+\text{Al}+\text{Cr})$; b) Base $\text{Fe}^{2+}/(\text{Mg}+\text{Fe}^{2+})$ versus $\text{Cr}/(\text{Cr}+\text{Al})$	66
Figure 4-7 : Common discrimination plots used for diamond exploration. a) MgO vs Cr_2O_3 B) TiO_2 vs Cr_2O_3 C) Cr_2O_3 vs Al_2O_3	68/69
Figure 4-8. Unit cell vs. B cation. a) Cr plot, b) Al plot.	71
Figure 4-9: Unit cell vs. Fe^{3+}	72
Figure 4-10. Unit cell vs A cation a) Fe_{tot} plot b) Fe^{2+}	73
Figure 4-11: Unit cell vs A cation - Mg.....	74
Figure 4-12. Ternary projections with Unit Cell. a) Cr, Al, Fe^{3+} b) Cr, Al, Ti.....	76
Figure 4-13: Side view of spinel prism.....	77
Figure 4-14: Spinel prism base.	78
Figure 4-15: Cr_2O_3 vs Al_2O_3 discrimination diagram.....	80
Figure 4-16: TiO_2 vs Cr_2O_3 discrimination diagram.....	81
Figure 4-17: Cr_2O_3 vs MgO discrimination diagram.	83

Figure 4-18: Cr_2O_3 vs TiO_2 vs MgO : a 3D discrimination diagram.....	84
Figure 5-1: Terra powder XRD pattern of halite and chromite mixture.....	93
Figure 5-2: Terra XRD exposures plot.	94
Figure 5-3: Terra XRF pattern.	95
Figure 5-4: Aluminum content approximated through visual interpolation.	97
Figure 5-5: Aluminum content approximated through a best fit regression line.....	97
Figure 5-6: Terra XRD compositional proxy results	99

List of Appendices

Appendix A: Slice SLMS	109
Appendix B: Max Intesity Plot Macro.....	111
Appendix C: Autohot Key Files	127
Appendix D: Gadds Raw Images.....	128
Appendix E: Unit Cells	166
Appendix F: Chemistry Data	208
Appendix G: MatLab Code.....	210

Chapter 1

1 Introduction

1.1 Overview

Spinel is a group of minerals of great interest to petrogenetic studies, as indicator minerals in diamond exploration, and are frequently mined in chromite deposits (e.g. Bushveld complex). Spinel has the general formula $(A)[B]_2O_4$ and consists of a cubic closest-packed oxygen array, it can accommodate many ions as major constituents, including Zn^{2+} , Mn^{2+} , Mg^{2+} , Fe^{2+} , Fe^{3+} , Ni^{2+} , Al^{3+} , Cr^{3+} , and Ti^{4+} into both octahedral and tetrahedral sites in their structure. The chemical variability of spinel minerals results in a correspondingly wide range of geologic occurrences. Spinel is often used as petrogenetic indicators, because they are important carriers of certain elements (e.g., Cr in chromite, Fe^{3+} and Ti in titanomagnetite) and indicators of the pressure, temperature and chemical state of their formation environments.

One of the most common applications of spinel group minerals is as an exploration tool. Chromian spinels (predominantly chromite and magnesiochromite) have been used in diamond exploration around the world as an indicator of both kimberlites and the diamonds hosted within the deposits. Cr-spinels are important for petrogenetic studies because spinel grains are primary phases of kimberlites and, as such, are reflective of kimberlite host rocks (Roeder 1994). It is worth noting that there are both phenocryst and xenocryst spinels found during diamond exploration, which are a product of the formation of kimberlites entrapping spinels on route to the surface. Early evaluation of an area for kimberlites and for the existence of economic pipes is one of the primary uses of indicator minerals. Less than one percent of kimberlite pipes are economic; this means that the rapid elimination of these targets before undertaking more expensive bulk sampling is critical (Kjarsgaard and Levinson 2002). Traditionally, the crystal chemistry of Cr-spinels measured by electron beam methods (e.g., electron probe microanalysis) has been used in exploration through the analysis of glacial or stream sediment samples. Crystal chemical methods for Cr-spinel analysis in diamond exploration are well-

developed, but they require sample preparation and shipping, along with expensive analytical facilities and personnel. This study attempts to demonstrate the effectiveness of a new technique of *in-situ* X-ray diffraction performed with minimal sample preparation, and explores the potential for the unit cell parameter (a_0) to be an effective proxy for chemical composition, for exploration purposes.

1.2 Spinel Structure and Unit Cell

Spinel group minerals have the general formula AB_2O_4 and can be found in Figure 1-1, as created in the Atoms software package (Dowty 1993). In all (oxide) spinels there are 24 cations (8 cations in the tetrahedral site and 16 cations in the octahedral site) and 32 oxygen atoms, with the oxygen atoms alternating with cations in a cubic closest packed arrangement (Deer et al. 1992; Hill et al. 1979). Spinel can be structurally normal (A cations in tetrahedral sites, B cations in octahedral sites), inverse (B cations are evenly divided among the tetrahedral and octahedral sites), or partially inverse (B cations are unevenly divided among the tetrahedral and octahedral sites). Spinel is cubic, with the space group $Fd\bar{3}m$.

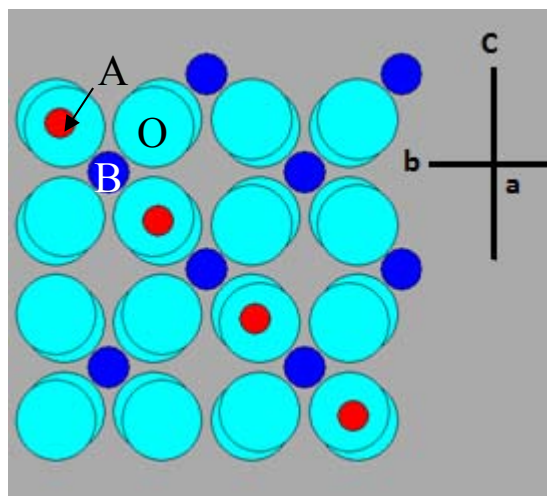


Figure 1-1: General spinel structure, where light blue symbols are oxygen, red symbols are A-cations and dark blue are B cations. (Atoms Software, Dowty 1993)

The unit cell is the smallest repeating unit of a crystal structure that has the properties and symmetry of the bulk mineral (Klein et al. 2008). The cubic structure, where $a=b=c$ and $\alpha=\beta=\gamma=90^\circ$ has only one variable parameter (a_0) would allow unit cell to be a simple, straightforward and easily-reportable proxy for chemical composition. This use as a potential proxy will be examined for its potential applications spinel minerals in general and to the kimberlite indicator mineral (KIM) Cr-spinel specifically.

The chemical composition of Cr-spinel $(\text{Fe,Mg})[\text{Cr, Al}]_2\text{O}_4$, is variable and our study demonstrates the correlated effect of chemical substitution on both the tetrahedral and octahedral sites with unit cell parameter.

The unit cell parameter of spinel group minerals ranges from 8.080 Å to 8.536 Å, and our relevant end-members range from 8.103 Å (spinel) and 8.536 Å (ulvospinel) (Deer et al. 1992). In spinel group minerals, the unit cell parameter is driven primarily by composition and not by temperature and pressure of crystallization, which makes it an ideal proxy for composition (Uchida et al. 2005). Unit cell variation occurs as cations with larger or smaller ionic radii are substituted for each other

(for radii see Table 1.1), there is an expansion or contraction of the unit cell parameter (values are from O'Neill and Navrotsky 1983), Table 1-2.

Atom	Ionic Radii Tetrahedral Site	Ionic Radii Octahedral Site
Al^{3+}	0.39	0.53
Cr	----	0.615
Fe^{3+}	0.485	0.645
Fe^{2+}	0.615	0.74
Mg^{2+}	0.585	0.715
Ti^{4+}	----	0.6

Table 1-1: Ionic Radii (O'Neill and Navrotsky 1983)

The use of the unit cell parameter as a proxy is effected by the order-disorder of cations between the octahedral and tetrahedral sites because of the variation in ionic radii in each site (O'Neill and Navrotsky 1983; Hamecher et al. 2013). This means partial inversion can lead to many potential combinations that cause increased ambiguity for the use of the unit cell parameter as a compositional proxy, since the same atom will have a different size in each site (See Table 1.1). This causes X-ray diffraction-based unit cell parameter compositional proxy method to be less complex and more applicable to normal spinel group minerals.

Previous work by Lenaz and co-workers (2010) shows the ability to discriminate terrains on the basis of single crystal XRD, but is limited to a small data set of 14 samples. Lenaz

et al. (2010) in addition to the unit cell parameter uses the oxygen positional parameter (u) parameter of spinel to discriminate between ultramafic and mafic rocks. Single crystal methods have the advantage of being able to measure more detailed structural properties including oxygen-metal distance parameters. Combining unit cell parameter with oxygen positional parameter has been shown to effectively discriminate between different Cr-spinel parageneses (Uchida et al. 2005; Lenaz et al. 2010; Lenaz et al. 2009). Our study focused on unit cell, due to the potential use of the unit cell parameter in the field, through the employment of field-portable instrumentation or due to the potential to scale up the measurement process using rapid, *in situ* micro XRD methods, which require minimal sample preparation. These X-ray methods, while incapable of measuring crystal structure with the same detail and precision as single-crystal methods (e.g., metal oxygen distance parameters cannot be extracted from these data), do demonstrate promise for rapid sample screening and analysis at field sites.

1.3 Spinel Indicator Minerals

The indicator minerals of interest for this study are Cr-spinels, due to their widespread occurrence and resistance to erosion and chemical re-equilibration, a typical epoxy mount of our samples can be seen in Figure 1-4.

Oxide spinels can broadly be broken into three series: the spinel series (Al), hercynite ($\text{Fe}^{2+}\text{Al}_2\text{O}_4$), spinel (*sensu stricto*) (MgAl_2O_4), gahnite (ZnAl_2O_4) and galaxite (MnAl_2O_4); the magnetite series (Fe^{3+}): magnesioferrite ($\text{MgFe}^{3+}_2\text{O}_4$), franklinite ($\text{ZnFe}^{3+}_2\text{O}_4$), jacobsite ($\text{MnFe}^{3+}_2\text{O}_4$), trevorite ($\text{NiFe}^{3+}_2\text{O}_4$) and magnetite ($\text{Fe}^{2+}\text{Fe}^{3+}_2\text{O}_4$); and the chromite series (Cr): magnesiochromite (MgCr_2O_4) and chromite ($\text{Fe}^{2+}\text{Cr}_2\text{O}_4$) (Deer et al. 1992). This study focuses on the seven relevant end-members spinel, hercynite, chromite, magnesiochromite, magnetite, magnesioferrite and

Table 1-2: Spinel group formula and unit cells (Deer et al. 1992)

Mineral	Formula	a(Å)
Spinel	MgAl_2O_4	8.103
Hercynite	$\text{Fe}^{2+}\text{Al}_2\text{O}_4$	8.135
Magnesioferrite	$\text{MgFe}^{3+}_2\text{O}_4$	8.383
Ulvospinel	$\text{Fe}^{2+}_2\text{TiO}_4$	8.536
Magnesiochromite	MgCr_2O_4	8.334
Chromite	$\text{Fe}^{2+}\text{Cr}_2\text{O}_4$	8.378
Magnetite	$\text{Fe}^{2+}\text{Fe}^{3+}_2\text{O}_4$	8.396

ulvöspinel. Table 1-2 lists the relevant unit cell parameters. The composition of spinel can be visualized using the projections of the spinel prism that were first developed by Stevens (1944) and later used by Mitchell for kimberlites (Haggerty 1986). In order to display all relevant end-members, two spinel prisms are required: a reduced or trivalent prism and an oxidized or divalent prism (Figure 1-2a/b).

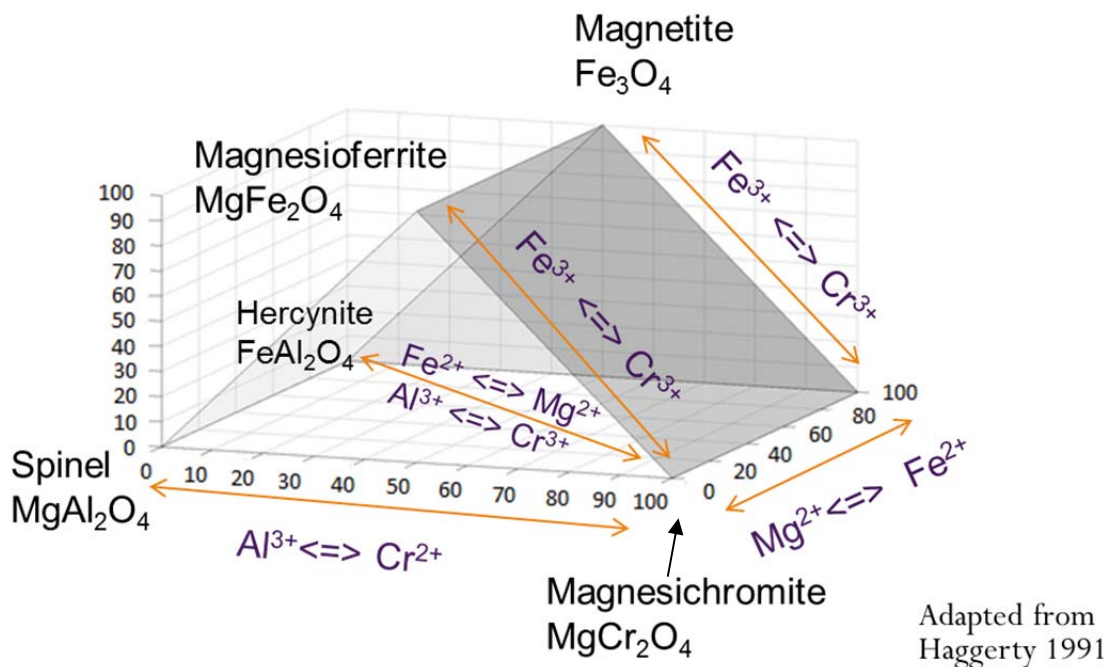
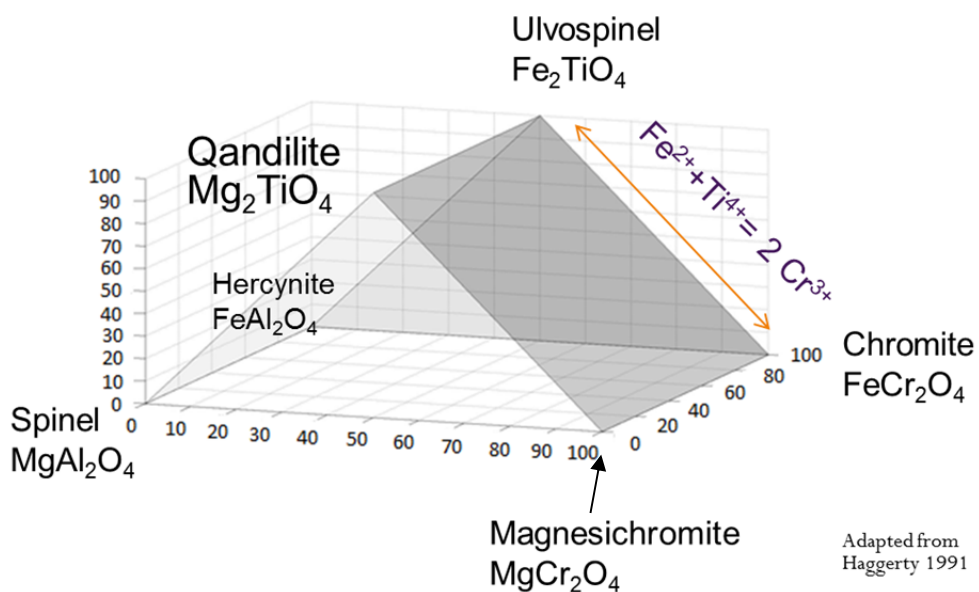


Figure 1-2: a) Trivalent spinel prism and b) divalent spinel prism showing substitution relationship



1.4 Spinel petrogenetic indicators

Extensive work has been done with spinel as a petrologic indicator since it was first shown to be useful in 1965 (Irvine 1965). Cr-spinel makes an excellent petrologic indicator due to its extensive solid solution, spanning over a broad range conditions and because Cr-spinel is typically one of the first phases to crystallize (Barnes 2001). Additionally, spinel are resistant to alteration and relatively refractory compared to other high temperature minerals like olivine (Barnes 2001).

Cr-Spinel compositions are directly related to the melt composition, and as different minerals crystallize, the composition of spinel will adjust accordingly (Roeder 1994). Compositions of Cr-spinel between chromite and magnetite are uncommon due to the crystallization of clinopyroxene (Roeder 1994). This does not mean that spinels in the “gap” will be unstable, but they are less common and the “gap” will vary depending on composition of a melt, the temperature, and pressure (Roeder 1994; Hill and Roeder 1974).

1.5 Kimberlites: History and Overview

Kimberlites are mafic magmatic rocks rich in H_2O and CO_2 that originate from greater than 150 km depth based on high pressure experiments, diamond xenocryst and mantle nodule examination, but some have estimated depths of greater than 450-650 km based on majorite inclusions (Kavanagh and Sparks 2009; McClenaghan and Kjarsgaard 2007). Diamonds form at

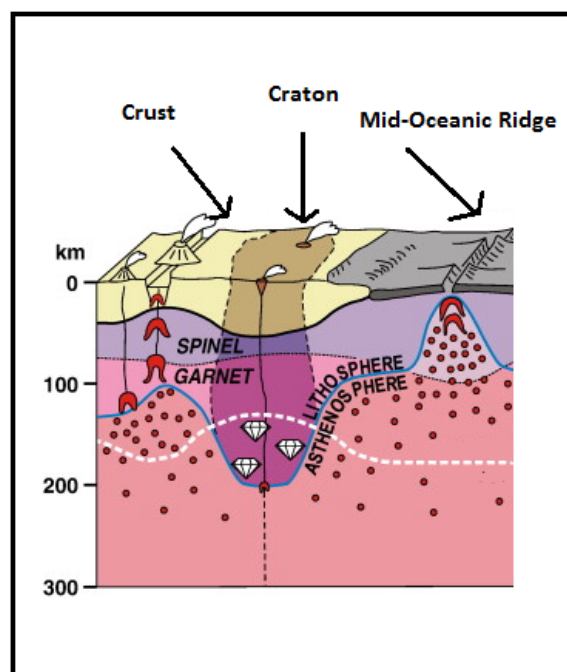


Figure 1-3: Schematic diagram of descending geotherm under a craton into the diamond stability field. (Modified from Stachel and Harris 2008)

the base of thick stable cratons at great depth and have been brought to surface in order to be mined (Gurney et al. 2010). They can come to the surface through both igneous and tectonic processes, but only the former has produced diamond deposits of economic grade (Gurney et al. 2010). Kimberlites are a common route by which diamonds are brought to the surface allowing for diamond mining. Prior to the discovery of the first kimberlite, secondary deposits were the primary economic source for diamonds, which included alluvial deposits, wind-borne, marine and paleoplacer deposits (Gurney et al. 2010). Kimberlites are thought to be formed by partial melting of the mantle, and are relatively explosive when they erupt (Clement 1975; McClenaghan and Kjarsgaard 2001; Moore and Gurney 1989). Diamonds can be found from Archean cratons and the surrounding Proterozoic belts, as seen in Figure 1-2 (Stachel and Harris 2008) coming from depths of at least 150 to 200 km. Without exceeding temperatures of 1200 °C, they are thought to have formed in relatively cool lithospheric roots (Stachel and Harris 2008; Boyd et al. 1985). These thick cratonic roots lead to an increased diamond stability field as they create downward deflected isotherms (Haggerty 1986).

Kimberlites derive their name from the original discovery location in Kimberly, South Africa (Mitchell, 1986). The first mines were found in October of 1869 on two farms, Bultfontein and Dorstfontein, and subsequently in Koffiefontein and Jagersfontein (Mitchell 1986). The term initially was adopted in 1887 at the British Association for the Advancement of Science in Manchester when presented by Henry Carvill Lewis. The first published reference to kimberlites was found in 1888 by Lewis and stressed the mafic nature of the rocks and their distinctive structure (Lewis 1888). The term initially was used to describe any igneous rock that had diamonds in it, regardless of the characteristics of the rock (Mitchell 1995). This confusion led to issues in creating an accurate rock description and eventually the term was divided into kimberlites and orangites (Mitchell 1995).

Smith (1983) divided kimberlites into two groups; group 1 (monticellite serpentine calcite) kimberlites derived from the asthenosphere, and group 2 (phlogopite) kimberlites from the lithosphere, on the basis of isotopes (Smith 1983). This would start further work differentiating the two types on the basis of age, petrography, megacrysts, xenocrysts,

isotopes, whole-rock geochemistry and xenoliths (Mitchell 1986). Furthermore, many authors added to the understanding of the division between these groups through mineralogy and geochemistry (Mitchell 1986; Mitchell 1995). Mitchell suggested that kimberlite groups 1 and 2 came from genetically distinct origins and had separate parent magmas (Mitchell 1986; Mitchell 1995). The second group of “kimberlites” were thus suggested to be renamed “orangites” in light of their discovery in the Orange Free State of South Africa (Mitchell 1995). This study focuses on the exploration of kimberlites, also known as group 1 kimberlites or monticellite serpentine calcite kimberlites in older literature.

Terminology for kimberlites has evolved significantly through the work of Dawson (Dawson 1971), Hawthorne (Hawthorne 1975), Clement and Skinner (Clement and Skinner 1985), Mitchell (Mitchell 1986; Mitchell 1991), Field and Scott Smith (Field and Scott Smith 1998) and Cas (Cas et al. 2008; Cas et al. 2009) and has led to confusion at times between kimberlite petrologists and traditional volcanologists (Smith et al. 2013). The work of Scott Smith et al. has attempted to reconcile the two disciplines in their 2013 work and, when possible, their terminology will be referenced (Smith et al. 2013). As these rocks erupt from depth they pick up mantle xenoliths, mantle xenocrysts and crustal xenoliths, resulting in a hybrid nature to these rocks, which are set in the groundmass matrix of the kimberlite melt with subhedral to euhedral xenocrysts (McClenaghan and Kjarsgaard 2001). The magma is composed of micro-phenocrysts of spinel, carbonate, phlogopite-kinoshitlite mica, ilmenite, monticellite, apatite, and has larger olivine and phlogopite xenocrysts (McClenaghan and Kjarsgaard 2007; Dawson 1971). Mantle xenoliths and megacrysts are composed of Mg-ilmenite, Cr-poor Ti-pyrope garnet, Cr-diopside, zircon, olivine and enstatite (Mineeva et al. 2007). The distinctive mineral assemblages that compose kimberlites allow for their exploration through the use of resistant and abundant minerals known as kimberlite indicator minerals, e.g. pyrope garnet, pyrope amandine garnet, Mg-ilmenite, Cr-diopside, Cr-spinel, forsteritic olivine and diamond (Muggeridge 1995), as described in section 1.7 (or using generic volcanology terms suggested by Smith et al. 2013, mantle derived xenocrysts minerals).

1.6 Exploration Target and Strategy

As an exploration target, kimberlites are relatively small, typically less than 2 km across, and can be as small as 50 m in diameter

(McClenaghan and Kjarsgaard 2007). They can be found either in a pipe of variable shape and size or as thin sills or dykes and small blows.

(McClenaghan and Kjarsgaard 2001). They have three characteristic morphologies, the crater, diatreme and root zone

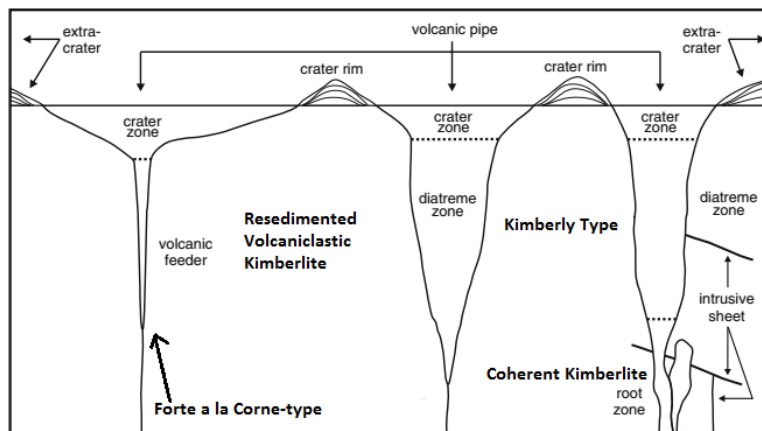


Figure 1-4: Three types of kimberlite morphologies diatreme, feeder and root zones. Overlain on Kimberly and Forte a la Corne type kimberlites. Modified from Scott Smith et al. (2013)

within these carrot-shaped pipes, Figure 1-3, which are akin to the older volcaniclastic, diatreme and hypabyssal facies, the differences being discussed extensively by Scott-Smith et al (Smith et al. 2013; Clement 1975). The smallest diamond exploration targets, known as hypabyssal facies dykes, are small, typically 1 to 10 m in width, but they are laterally extensive (McClenaghan and Kjarsgaard 2001). Kimberlites are often found in groups of clustered pipes known as kimberlite fields. The rocks are commonly eroded by glaciation or streams because they are softer and chemically less resistant than the country rock that hosts them (McClenaghan and Kjarsgaard 2007). This eroded material results in a larger footprint than the deposits themselves that can be explored using kimberlite indicator minerals. Less than one percent of kimberlites are economic worldwide. This, combined with the small target size, means that exploring for kimberlites is challenging. This necessitates strategy to be employed to find these indicator minerals.

When exploring for kimberlites, four basic questions need to be answered (Muggeridge 1995):

- 1) Is there a tectonic correlation to diamondiferous kimberlites?
- 2) Are primary diamond-type or related intrusive deposits in the area?
- 3) Are detrital diamonds found in the area?
- 4) Are kimberlite indicator minerals present?

At the regional scale, it is important to first look for tectonic features that may be relevant to kimberlites, and the exploration can be done through aerial photos or satellite radar/imaging (Muggeridge 1995). This is especially important when using stream prospecting, where topographic variations can affect drainage and, as such, how many lithologies are sampled (Muggeridge 1995). Next, understanding the country rock is critical, especially when using preconcentration techniques in the field, as background mineralogy can mask the kimberlite signature and younger rock units can obscure older kimberlites (Muggeridge 1995). The type of overburden in the area has a clear ability to mask indicator signatures and should be kept in consideration for later geophysical surveys and drilling (Muggeridge 1995). Logistical constraints like accessibility and rugged terrain can have a significant effect in an area as to whether the development of a site may be possible (Muggeridge 1995). Finally, the climate of an area can have a major influence on field seasons, methods of exploration and erosion rates (Muggeridge 1995).

1.7 Indicator Mineral Overview

Common indicator minerals can be found in Table 1-2 below, adapted from Muggeridge. Many of these indicators can be found very distal to the deposits and are very resistant to weathering like Cr-spinel; but, others like olivine are more commonly found only in glaciated terrains or proximal to the source (McClenaghan and Kjarsgaard 2007). Exploration for indicator minerals uses eight typical methods, but the most common methods are stream, loam, and glacial till sampling. Sometimes burrow mound sampling, vegetation sampling, ground water sampling, rock sampling and geochemical soil sampling are employed (Muggeridge 1995). The relative abundance of different minerals

Table 1-3: Indicator Minerals Relevant Attributes (adapted from (Muggeridge 1995))						
Mineral	Composition	Crystal system	Colour	Typical grain Size (mm)	Visible diagnostic features	Main Source Rocks
Pyrope garnet	Mg Fe Ca Al silicate <i>Cr,Ti</i>	Isometric	Purple, crimson, red, mauve	1-5 mm Rarely up to 100	Kelphite rim, colour, anhedral, orange peel surface	Kimberlite, lamprophyre, peridotite
Pyrope amandine garnet	Mg Fe Ca Al silicate <i>Na,Ti</i>	Isometric	Orange	1-5 mm Rarely up to 25	Kelphite rim, colour, anhedral, orange peel surface	Eclogite
Mg-ilmenite	Mg Fe Ca Al oxide <i>Cr,Mn, Al</i>	Trigonal	Black	1-20 mm Rarely up to 100	White porcellaneous leucocene coating, perovskite overgrowth anhedral, rounded or blocky, conchoidal fracture	Kimberlite (some mafic volcanic rocks)
Cr-diopside	Ca Mg silicate, <i>Fe,Cr,Al,Na</i>	Monoclinic	Emerald green	1-5 mm Rarely up to 50	Colour, blocky, anhedral, 2 cleavage directions	Kimberlites, peridotite, (some ultramafic rocks)
Cr-spinel	Mg, Cr, Al, Fe oxide, <i>Mn, Ti</i>	Isometric	Black, reddish brown	0.5-1 mm Rarely up to 2	Reddish brown on broken edges, glassy surface on grains octahedral and irregular shapes	Kimberlites, lamproite, carbonatite, various ultramafic plutonic and volcanic rocks
Forsteritic olivine	Mg silicate, <i>Fe,N, Mn</i>	Orthorhombic	Pale yellow to green	2-10 mm Rarely up to 50	Colour, irregular crystal shape, vermiform etching	Kimberlites, lamproite, carbonatite, various ultramafic plutonic and volcanic rocks
Diamond	C native <i>N,B</i>	Isometric	Colourless, pale colours (brown and yellow)	0.5-10 mm Rarely up to 30	Crystal form, reabsorption features adamantine lustre	Kimberlite, lamproite (and rarely in certain ultrahigh pressure metamorphic rocks and lamphyres)

in non-glaciated terrains will vary with the proximity to the source. The mineralogy of the kimberlites is variable, which leads to different mixes of indicator minerals (Mitchell 1986). Indicator minerals like Cr-pyrope are typically 0.1 to 1.0 mm in size and experiences fracturing during decompression. In glacial or stream sediment, the relative amounts of minerals decrease downstream, primarily due to dilution (Kong et al. 1999). The main types of sediments used for mineral indicator work are stream sediments, kimberlite fragments, glaciofluvial sediments, beach sediments and till (McClenaghan and Kjarsgaard 2001). Kimberlite fragments are the most obvious indicator of a deposit and can be found in three deposits: within till (Carlson et al. 1999), within the pebble-cobble facies of eskers (McClenaghan and Kjarsgaard 2007) or modern stream sediments (Kong et al. 1999).

Stream sediments are best used for reconnaissance to recover kimberlites because they collect material from a greater area. They do not however have the clear directional transport history of glacial tills (McClenaghan and Kjarsgaard 2007). Sampling strategies vary depending on location, but in general, esker, fluvial, or beach sediments are sampled before till because they have deposited material from a larger area and from more rock types making them more useful for large scale reconnaissance. Indicator mineral surveys should match their collected sample volumes to historic sample volumes in the area to make a direct comparison. Follow up work to this will include systematic till sampling once the area is established following geophysical surveys (Carlson et al. 1999; Fipke et al. 1995; Jennings 1995). Sampling of till is done perpendicular to glacial ice direction when possible (McClenaghan and Kjarsgaard 2001; Kong et al. 1999).

After sampling, the next phase is concentration of indicator minerals, which involves removing quartz, carbonates, most ferro-magnesian minerals, and rock fragments. This reduces the samples to the kimberlite indicator minerals (McClenaghan and Kjarsgaard 2007) and is typically done in the lab setting, but can be done in a field setting. The first step is to remove the larger size fraction (>2 mm) through sieving and have lithological analysis conducted on the <2 mm material that is preconcentrated by density, grain size, or magnetic susceptibility before final density separation (McClenaghan and Kjarsgaard 2007). Density preconcentration can be done either in the field or in the lab setting using

methods such as jigging, and panning (Muggeridge 1995). In the lab, for methods such as dense media separator, a spiral shaking table can be used in conjunction with heavy liquid separation (McClenaghan and Kjarsgaard 2007). The most efficient separation procedures are dense media separator and heavy liquid separation, but these are not as inexpensive as tabling (McClenaghan and Kjarsgaard 2007). The final step of separation is done using either a magseparator for Cr-diopside or through heavy liquid separation using a liquid like methylene iodide.

1.8 Diamond Indicator Mineral Discrimination

Diamond indicator minerals are vectors to direct a search toward the diamond source and have been successfully used starting in the 1870s, when the association of garnets and diamonds was noticed (Kjarsgaard and Levinson 2002). The first systematic stream survey was done in the 1950s in Russia for primarily garnets (see Kjarsgaard and Levinson 2002). Kimberlite indicator minerals came to the forefront with the work of Gurney on garnets and were later made more accurate by Moore by adding the diamond / graphite division (for detailed discussion see Fipke et al. 1995; Gurney 1984). Cr-spinels are used as a vector to find diamond deposits due to their relative stability and resistance to erosion that provide a larger footprint for exploration (Fipke et al. 1995; Gurney 1989). Cr-spinels were first analyzed by electron probe microanalysis in 1968 by Boyd and Meyer in diamond inclusions (Meyer and Boyd 1968; Meyer and Boyd 1968; Meyer and Boyd 1969). Cr-rich spinels are predicted by experimental work to acquire Cr-numbers ($\text{Cr} \times 100 / \text{Cr} + \text{Al}$) of at least 80 to come from cratonic harzburgites and lherzolites, their predicted host rocks. Less than 2% of Cr-spinels, related to diamonds, have Cr-numbers lower than this predicted value (Stachel and Harris 2008). Spinel inclusions that do not have a Cr-number greater than 80



Figure 1-5: Selected polished probe chromite mount approximately 2.5 cm across

are thought to coexist with orthopyroxene and garnet in dunites (Stachel and Harris 2008).

Diamond inclusion spinels are thought to have a higher trapping temperature (the temperature at which the diamond crystallized around the inclusion) than ambient temperature or that the Cr-spinel inclusions in diamonds come from deeper levels than Cr-spinel found in general within kimberlite concentrates. The former hypothesis is typically preferred (Griffin et al. 1994).

Work on diamond inclusions was, for exploration purposes, followed by work with kimberlite concentrates instead of inclusions, which lead to the discrimination diagrams that this study uses. Cr-spinel has been carefully studied with well-defined regions for diamond-associated compositions clearly defined for the diamond-inclusion field for Cr-Spinel of >61% wt% Cr₂O₃, 10 to 16% wt% MgO, <8% Al₂O₃, <6 wt% Fe₂O₃ and <0.6% wt% TiO₂ (Fipke et al. 1995; Gurney 1984; Gurney 1989; Griffin et al. 1994; Sobolev 1977; Fipke et al. 1989; Fipke 1991; Grütter and Apter 1998; Kjarsgaard 1998; Griffin et al. 1997). The Cr₂O₃ vs MgO discrimination diagram is widely used in diamond exploration, along with Al₂O₃ vs Cr₂O₃ and TiO₂ vs Cr₂O₃ (e.g. Gurney 1984, Sobolev 1977, Grütter and Apter 1998). These distinctive grains are well associated with diamonds but are sometimes overlapped in composition by rocks that are not diamond-associated such as boninites and minnettes (Kjarsgaard 1998; Barnes 2001). Some grains might be also of this composition, but are in fact phenocryst grains, as discussed by Grütter and Apter (1998). This study builds on the work of these compositional diagrams, and has the same compositional limitations as these diagrams.

1.9 Kimberlite Chemical Trends

Three distinctive trends exist within Cr-spinel found in kimberlites, as seen on Figure 1-6 (Roeder 1994; Mitchell 1986; Barnes 2001). The macrocrystal (AMC) trend is found on the base of the spinel prisms between hercynite, chromite, magnetite and magnesiochromite. These Cr-spinels with typically less than 1 wt. % TiO₂ are known as

magnesian aluminous chromites or aluminous magnesian chromites (Mitchell 1986). These Cr-spinels evolve toward Cr and Fe at the expense of Al and Mg making a trend on the base of the spinel prism.

The first magmatic trend (Trend 1 in Figure 1-6), also known as the magnesian ulvöspinel trend or the kimberlite trend, is found almost exclusively in kimberlites and involves a decrease in $\text{Cr}/(\text{Cr}+\text{Al})$ simultaneous to an increase in $\text{Fe}^{3+}/(\text{Fe}^{3+}+\text{Al}+\text{Cr})$ with a constant value of $\text{Fe}^{2+}/(\text{Fe}^{2+}+\text{Mg})$ (Roeder 1994; Roeder 1994; Mitchell 1986; Barnes 2001; Roeder and Schulze 2008). This trend is likely caused by a major oxidation event in the late stages of kimberlite crystallization (Roeder 1994). The oxidizing event maintains a high Mg content, while converting ferrous to ferric iron; this likely results from evolution of gas near the surface (Mitchell 1986). Many Cr-spinels in the late stages of ascent are converted to magnesioferrite (Roeder 1994). Additional spinel populations falling within this trend may have a gap in crystallization between high temperature Cr-spinels and Ti-rich spinels (Mitchell 1986). This is due to the resorption of high temperature spinels at a reaction point, followed by a period of no crystallization and then crystallization of a stable Ti-rich spinel (Mitchell 1986). This magmatic trend can be contrasted to the typical igneous melts where $\text{Cr}/(\text{Cr}+\text{Al})$, $\text{Fe}^{3+}/(\text{Fe}^{3+}+\text{Al}+\text{Cr})$ and $\text{Fe}^{2+}/(\text{Fe}^{2+}+\text{Mg})$ all increase simultaneously (Roeder 1994; Roeder 1994; Mitchell 1986; Barnes 2001; Roeder and Schulze 2008). Similar to the magmatic trend 1 in kimberlites it is possible to have similar gaps in crystallization. These have been attributed to a reaction between spinel and pyroxene, or due to oxygen fugacity (Haggerty 1975).

The second magmatic trend in kimberlites (Trend 2 in Figure 1-6) is not as common as trend 1 and moves from aluminous magnesian chromites to titanian magnesian chromites to titanian chromites to ulvöspinel-magnetite. The trend starts with increasing $\text{Fe}/(\text{Fe}+\text{Mg})$ ratios along the base of the prism having high $\text{Cr}/\text{Cr}+\text{Al}$ with low Ti, then begins a rapid increase in Ti at high $\text{Fe}/(\text{Fe}+\text{Mg})$ ratios toward the apex (Mitchell 1986). Manganese enrichment can occur in the most evolved spinels with enrichment upwards of one percent Mn (Mitchell 1986). Trend 2 is thought to occur due to extensive phlogopite crystallization, resulting in depletion of Mg and Al in the magma (Mitchell 1986). Both trends have been found in the same kimberlite, but trend 2 is linked with the

micaceous facies (Mitchell 1986). These spinel trends are relevant to the study since composition trends are a common use for spinels and the compositional trends will have an effect on unit cell.

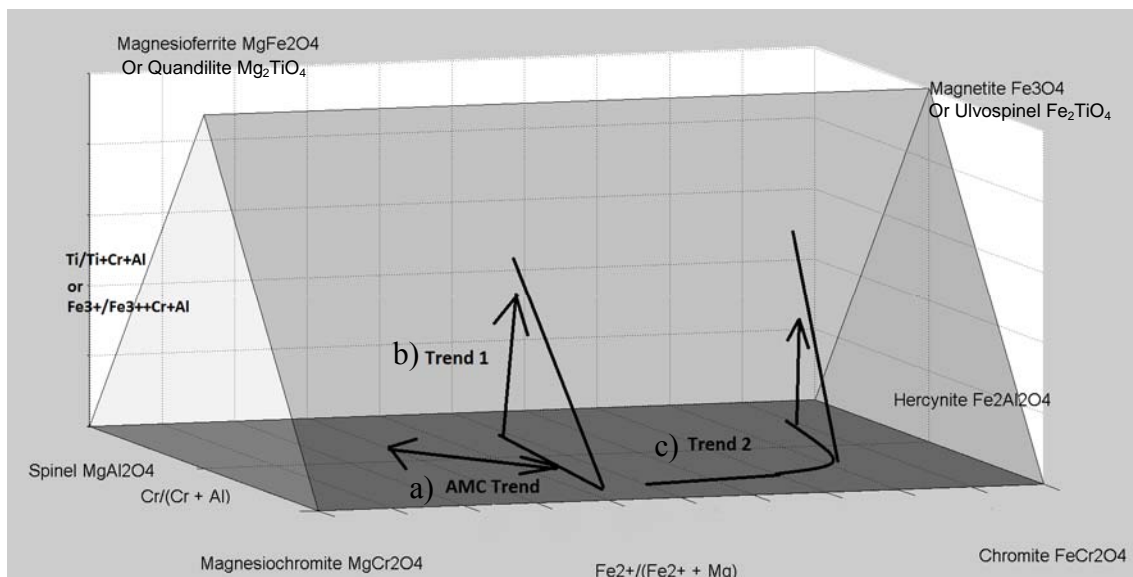


Figure 1-6: The three kimberlite trends. a) the AMC trend trends along the base of the prism evolving toward Cr and Fe at the expense of Al and Mg. b) The first magmatic trend involves a decrease in $\text{Cr}/(\text{Cr}+\text{Al})$ simultaneous to an increase in $\text{Fe}^{3+}/(\text{Fe}^{3+}+\text{Al}+\text{Cr})$ with a constant value of $\text{Fe}^{2+}/(\text{Fe}^{2+}+\text{Mg})$. c) The second magmatic trend in kimberlites is not as common as trend 1, increasing $\text{Fe}/(\text{Fe}+\text{Mg})$ ratios along the base of the prism with high $\text{Cr}/\text{Cr}+\text{Al}$ with low Ti, this phase is then followed by a rapid increase in Ti at high $\text{Fe}+(\text{Fe}+\text{Mg})$ ratios toward the apex.

1.10 Rationale for Unit Cell Parameter as a Compositional Proxy

Unit cell parameter in spinel provides the potential to be an easily reportable bulk proxy for composition. The advantage it ultimately has is due to the relative ease to collect unit

cell information with little or no mounting. This provides the potential for rapid discrimination but is limited by the inherent ambiguity of the measurement. This means that it is most useful in well-constrained systems. Unit cell parameter also is not limited to a laboratory setting as this can be collected in a field setting. This provides the possibility of using it as an exploration tool in the field.

This study expands and improves upon the study of Freckleton and Flemming (2009), which compared unit cell parameter in chromite spinels against chemical composition. Interpretation of the μ XRD data of Freckleton and Flemming (2009) was complicated by X-ray beam overlap, where multiple grains diffracted under the X-ray beam simultaneously, due to the 500 micron beam diameter. This study removed the overlap issue by switching to a 100 micron beam diameter and used five localities with three kimberlitic and two non-kimberlitic sources instead of the 4 sources used by the original study. The data analysis will also be expanded from bi-variant plots to multi-variant plots for ready comparison with conventional chemical plots used in exploration.

1.11 References

- Barnes, S.J. & Roeder P.L. (2001) The Range of Spinel Compositions in Terrestrial Mafic and Ultramafic Rocks. *Journal of Petrology*, 12, 2279-2302
- Boyd, F.R., Gurney, J.J. and Richardson, S.H. (1985) Evidence for a 150-200-km thick Archaean lithosphere from diamond inclusion thermobarometry. *Nature*, 387-389
- Carlson, S., Hillier, W., Hood, C., Pryde, R. and Skelton, D. (1999) The Buffalo Hills kimberlites: a newly-discovered diamondiferous kimberlite province in north-central Alberta, Canada. In *Proceedings of the 7th International Kimberlite Conference*, Cape Town, South Africa. Edited by JJ Gurney, JL Gurney, MD Pascoe and SH Richardson. Red Roof Design, Cape Town, South Africa, p. 109-116

- Cas, R., Porritt, L., Pittari, A. and Hayman, P. (2009) A practical guide to terminology for kimberlite facies: A systematic progression from descriptive to genetic, including a pocket guide. *Lithos*, 183-190
- Cas, R., Porritt, L., Pittari, A. and Hayman, P. (2008) A new approach to kimberlite facies terminology using a revised general approach to the nomenclature of all volcanic rocks and deposits: Descriptive to genetic. *Journal of Volcanology and Geothermal Research*, 1, 226-240
- Clement, C. and Skinner, E. (1985) A textural-genetic classification of kimberlites. *South African Journal of Geology*, 2, 403-409
- Clement, C.R. (1975) The emplacement of some diatreme-facies kimberlites. *Physics and Chemistry of the Earth*, 0, 51-59
- Dawson, J. (1971) Advances in kimberlite geology. *Earth-Science Reviews*, 4, 187-214
- Deer, W.A., Howie, R.A. and Zussman, J. (1992) An introduction to the rock-forming minerals Longman Scientific & Technical, Harlow, Essex, England
- Dowty, E. (1993) ATOMS: A computer program for displaying atomic structures. Shape Software
- Field, M. and Scott Smith, B. (1998) Textural and genetic classification schemes for kimberlites: a new perspective. In *Extended abstracts of the seventh international kimberlite conference*, Cape Town, South Africa, p. 214-216
- Fipke, C., Gurney, J. and Moore, R. (1995) Diamond exploration techniques emphasising indicator mineral geochemistry and Canadian examples

Fipke, C., Gurney, J., Moore, R. and Nassichuk, W. (1989) The development of advanced technology to distinguish between diamondiferous and barren diatremes. Geological Survey of Canada, Open File, 559

Fipke, C.E. (1991) Significance of chromite, ilmenite, G5 Mg-almandine garnet, zircon and tourmaline in heavy mineral detection of diamond bearing lamproite. Kimberlites, Related Rocks and Mantle Xenoliths, SPRM Spec.Publ.A, 1

Griffin, W., Fisher, N., Friedman, J. and Ryan, C. (1997) Statistical techniques for the classification of chromites in diamond exploration samples. Journal of Geochemical Exploration, 3, 233-249

Griffin, W., Ryan, C., Gurney, J., Sobolev, N. and Win, T. (1994) Chromite macrocrysts in kimberlites and lamproites: geochemistry and origin. Kimberlites, related rocks and mantle xenoliths.CPRM Spec Publ, 366-377

Grütter, H. and Apter, D. (1998) Kimberlite-and lamproite-borne chromite phenocrysts with “diamond-inclusion”-type chemistries. In Extended abstract 7th International Kimberlite Conference, Cape Town, p. 280-282

Gurney, J.J. (1989) Diamonds. In Kimberlites and Related Rocks: 2. Their Mantle/ Crust Setting, Diamonds and Diamond Exploration, p. 935-965. Geological Society of Australia Special Publication

Gurney, J. (1984) A correlation between garnets and diamonds in kimberlites. Kimberlite occurrence and origin, 143-166

Gurney, J.J., Helmstaedt, H.H., Richardson, S.H. and Shirey, S.B. (2010) Diamonds through time. Economic Geology, 3, 689-712

Haggerty, S.E. (1986) Diamond genesis in a multiply-constrained model

Haggerty, S.E. (1975) The chemistry and genesis of opaque minerals in kimberlites. *Physics and Chemistry of the Earth*, 0, 295-307

Hamecher, E.A., Antoshechkina, P.M., Ghiorso, M.S. and Asimow, P.D. (2013) The molar volume of FeO–MgO–Fe₂O₃–Cr₂O₃–Al₂O₃–TiO₂ spinels. *Contributions to Mineralogy and Petrology*, 1, 25-43

Hawthorne, J. (1975) Model of a kimberlite pipe. *Physics and Chemistry of the Earth*, 1-15

Hill, R. and Roeder, P. (1974) The crystallization of spinel from basaltic liquid as a function of oxygen fugacity. *The Journal of geology*, 709-729

Hill, R.J., Craig, J.R. and Gibbs, G.V. (1979) Systematics of the spinel structure type. *Physics and Chemistry of Minerals*, 4, 317-339

Irvine, T.N. (1965) Chromian Spinel as a Petrogenic Indicator: Part 1. Theory. *Canadian Journal of Earth Sciences*, 6, 648-672

Jennings, C. (1995) The exploration context for diamonds. *Journal of Geochemical Exploration*, 1, 113-124

Kavanagh, J.L. and Sparks, R.S.J. (2009) Temperature changes in ascending kimberlite magma. *Earth and Planetary Science Letters*, 3–4, 404-413

Kjarsgaard, B. (1998) Compositional trends of spinel and mica in alkali minettes, southern Alberta, Canada. In *Extended Abstracts, 7th International Kimberlite Conference, Cape Town, South Africa*, p. 435-437

Kjarsgaard, B. and Levinson, A. (2002) Diamonds in Canada. *Gems and Gemology*, 3, 208-238

Klein, C., Dutrow, B. and Dana, J.D. (2008) The 23rd edition of the manual of mineral science: after James D. Dana J. Wiley, Hoboken, N.J

Kong, J., Boucher, D. and Scott Smith, B. (1999) Exploration and geology of the Attawapiskat kimberlites, James Bay lowland, northern Ontario, Canada. In Proceedings of the VIIth International Kimberlite Conference, p. 452-467

Lenaz, D., Logvinova, A.M., Princivalle, F. and Sobolev, N.V. (2009) Structural parameters of chromite included in diamond and kimberlites from Siberia: A new tool for discriminating ultramafic source. *American Mineralogist*, 7, 1067-1070

Lenaz, D., De Min, A., Garuti, G., Zaccarini, F. and Princivalle, F. (2010) Crystal chemistry of Cr-spinels from the lherzolite mantle peridotite of Ronda. *American Mineralogist*, 8-9, 1323-1328

Lewis, H.C. (1888) The Matrix of the Diamond . *Geological Magazine*, New Series, 5, 129-131

McClenaghan, M. and Kjarsgaard, B. (2007) Indicator mineral and surficial geochemical exploration methods for kimberlite in glaciated terrain; examples from Canada. In W.D. Goodfellow, Ed., *Mineral deposits of Canada: a synthesis of major deposit-types, district metallogeny, the evolution of geological provinces, and exploration methods*, ed. Special Publication no. 5, p. 983-1009. Geological Association of Canada, Mineral Deposits Division

McClenaghan, M. and Kjarsgaard, B. (2001) Indicator mineral and geochemical methods for diamond exploration in glaciated terrain in Canada. Geological Society, London, *Special Publications*, 1, 83-123

Meyer, H.O.A. and Boyd, F.R. (1969) Mineral inclusions in diamonds. *Carnegie Inst. Wash., Year Book*, 67, 315-324

Meyer, H.O.A. and Boyd, F.R. (1968) Mineral inclusions in diamond. Carnegie Inst. Wash. Year Book, 67, 130-135

Mineeva, R., Speransky, A., Titkov, S. and Zudin, N. (2007) The ordered creation of paramagnetic defects at plastic deformation of natural diamonds. *Physics and Chemistry of Minerals*, 2, 53-58

Mitchell, R. (1991) Kimberlites and lamproites: Primary sources of diamond. *Geoscience Canada*, 1, 1-16

Mitchell, R.H. (1986) Mineralogy of kimberlites. In *Kimberlites*, p. 137-274. Springer

Mitchell, R.H. (1995) Kimberlites, orangeites, and related rocks Plenum Press, New York

Moore, R. and Gurney, J. (1989) Mineral inclusions in diamond from the Monastery kimberlite, South Africa. *Kimberlites and related rocks*, 1029-1041

Muggeridge, M.T. (1995) Pathfinder sampling techniques for locating primary sources of diamond: Recovery of indicator minerals, diamonds and geochemical signatures. *Journal of Geochemical Exploration*, 1, 183-204

O'Neill, H.S.C. and Navrotsky, A. (1983) Simple spinels; crystallographic parameters, cation radii, lattice energies, and cation distribution. *American Mineralogist*, 1-2, 181-194

Roeder, P.L. and Schulze, D.J. (2008) Crystallization of Groundmass Spinel in Kimberlite. *Journal of Petrology*, 8, 1473-1495

Roeder, P.L. (1994) Chromite; from the fiery rain of chondrules to the Kilauea Iki lava lake. *The Canadian Mineralogist*, 4, 729-746

- Smith, B.S., Nowicki, T., Russell, J., Webb, K., Mitchell, R., Hetman, C., Harder, M., Skinner, E. and Robey, J.A. (2013) Kimberlite terminology and classification. In Proceedings of 10th International Kimberlite Conference, p. 1-17. Springer
- Smith, C.B. (1983) Pb, Sr and Nd isotopic evidence for sources of southern African Cretaceous kimberlites. *Nature*, 5921, 51-54
- Sobolev, N.V. (1977) Deep-Seated Inclusions in Kimberlites and the Problem of the Composition of the Upper Mantle American Geophysical Union
- Stachel, T. and Harris, J. (2008) The origin of cratonic diamonds—constraints from mineral inclusions. *Ore Geology Reviews*, 1, 5-32
- Stevens, R.E. (1944) Composition of some chromites of the western hemisphere. *American Mineralogist*, 1-2, 1-64
- Uchida, H., Lavina, B., Downs, R.T. and Chesley, J. (2005) Single-crystal X-ray diffraction of spinels from the San Carlos Volcanic Field, Arizona: Spinel as a geothermometer. *American Mineralogist*, 11-12, 1900-1908

Chapter 2

2 Methods

2.1 Samples

Samples came from five localities, with three kimberlitic and two non-kimberlitic sources. The kimberlitic samples were collected from the Koala, Sheiba, and Misery pipes at Ekati Diamond mine (Northwest Territories, Canada) (Nowicki et al. 2004). The kimberlite samples are derived from crushed samples (~5 kg) of drill core intersecting each of the bodies (Nowicki pers. comm. 2014). The Koala and Misery pipes were deemed economic and were part of the Ekati mine site; meanwhile Sheiba was deemed to be sub-economic. The Lac de Gras area was, in the early stages, explored by chemical analysis of kimberlite indicator minerals including chromite. The original discovery region of indicator minerals was followed by discoveries of grains to the north of the region. East of the discovery region was found to be barren, indicating the eventual target area. The oxides, including spinels, in the kimberlites were typically small, ranging between 1 and 10 μm in their longest dimension (Nowicki et al. 2004).

The Koala kimberlite pipe is hosted in biotite granodiorite of the koala batholith. It is an economic deposit and is a part of the mine plan for Ekati, starting with open pit mining followed by underground mining. The deposit is a sub horizontal layered sequence composed of 7 geological domains and, unlike other Ekati pipes, has distinct margins between domains (Nowicki et al. 2004).

Misery is on the Southeastern portion of the claim and is composed of six kimberlite bodies. They are hosted between the Archæan metasedimentary rocks and the mica granite. Misery main, the largest pipe, is relatively small, approximately 15000 m^2 . It is steep-sided, elongated, is infilled with crater sediments, and has magmatic kimberlite at depth with minor xenolithic content (Nowicki et al. 2004).

The non-kimberlitic samples came from a stream sampling program from Gabon and are likely from dunites (Nowicki pers. comm. 2014). The actual host rock is, at this time,

unknown but is assumed to be non-kimberlitic on the basis of the lack of definitive kimberlitic chromite compositions. The second non-kimberlite was from soil sediments from eastern Botswana known as Matsitami/Tatumi (Nowicki pers. comm. 2014).

2.2 General Methods

2.2.1 Micro X-ray Diffraction

2.2.1.1 Overview

A Bruker D8 Discover Micro X-ray Diffractometer (μ XRD) in Earth Sciences at Western University, London, Ontario, was used to collect crystal unit cell parameter. It is configured with a $\text{CoK}\alpha$ source ($\lambda = 1.78897 \text{ \AA}$) and was run at 35 kV and 45 mA and has an angular resolution of 0.04-0.05°. The goal of this research was to compare unit cell parameter to composition,

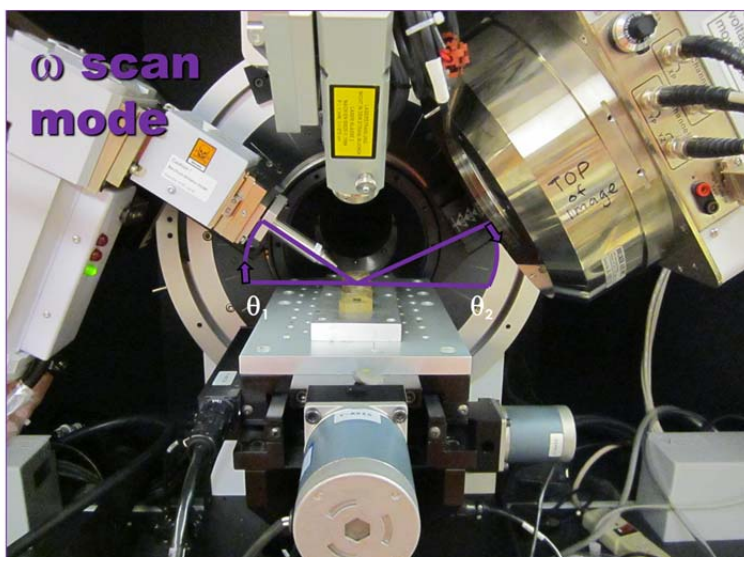


Figure 2-1: Bruker D8 Discover in situ μ XRD configuration.

in order to look for potential applications, particularly in exploration. The 2D detector enabled the measurement of diffracted X-ray intensity along the arc of the Debye rings (denoted χ) and the Bragg angle (2θ). The μ XRD has theta-theta geometry and is typically run at 35 kV and 40 mA configuration; the μ XRD can be seen in Figure 2-1. The sampling of individual grains required the use of a 60 mm Gobel mirror with a 100 micron pinhole snout and the use of omega scan mode. An omega scan is a scan where 2θ is kept constant while the detector and source are moved in a clock-wise manner by an angle omega (ω) around a stationary sample. This type of scan allows more lattice planes to satisfy Bragg's law. For more information on this technique refer to Flemming (2007).

2.2.1.2 Parameters

The μ XRD was upgraded from a Cu K α source as used by Freckleton and Flemming (2009) to a CoK α source in the current study (Freckleton and Flemming 2009). This caused a lowering of the intensity, which required the optimization of the operating parameters. This was resolved through iterative optimization of the operating parameters until the best parameters were established. This was done by starting with parameters that maximized the amount of 2θ coverage to increase the number of detectable peaks. This was generally very unsuccessful at satisfying Bragg's law, and as such the parameters were modified to cover less 2θ space and instead maximize the number of degrees the detector and source move clockwise during an omega scan. The parameters that were found to work best for *in situ* μ XRD of chromite using an omega scan were for frame one: Theta 1=15.5°, Theta 2= 40°, Width = 37.5° and 60 minutes, and the second frame: Theta 1=45.5°, Theta 2= 40°, Width = 7.5°, Time = 60 minutes.

2.2.1.3 Detector Distance Optimization

X-rays were detected with a 2-dimensional Hi-Star detector using General Area Detector Diffraction System (GADDS) software. The detector was moved from 15 to 12 cm in order to increase the amount of 2θ space collected during a single frame, Figure 2-2. The detector distance is inversely proportional to the range of data collected in degrees 2θ . This is because the diffracted rays that leave the sample will diverge apart, and a closer detector with less spread will pick up a greater angular proportion of the diffracted X-rays. However, the peak resolution will decrease with a closer detector. The detector resolution was originally 0.035-0.05 degrees of 2θ at 15 cm, as determined by Bruker. The detector resolution is estimated at 0.04-0.05 degrees per data point based on 1024 wires resolving 41° 2θ for the 12 cm detector configuration. This detector system and the μ XRD have the distinct advantage of being able to X-ray single crystals and powders. In two dimensions, the textural information is also available, where single crystal data appear as single spots whereas powders appear as homogenous Debye rings. Non-

uniformly strained (deformed) materials appear as streaking along the Debye rings (χ).

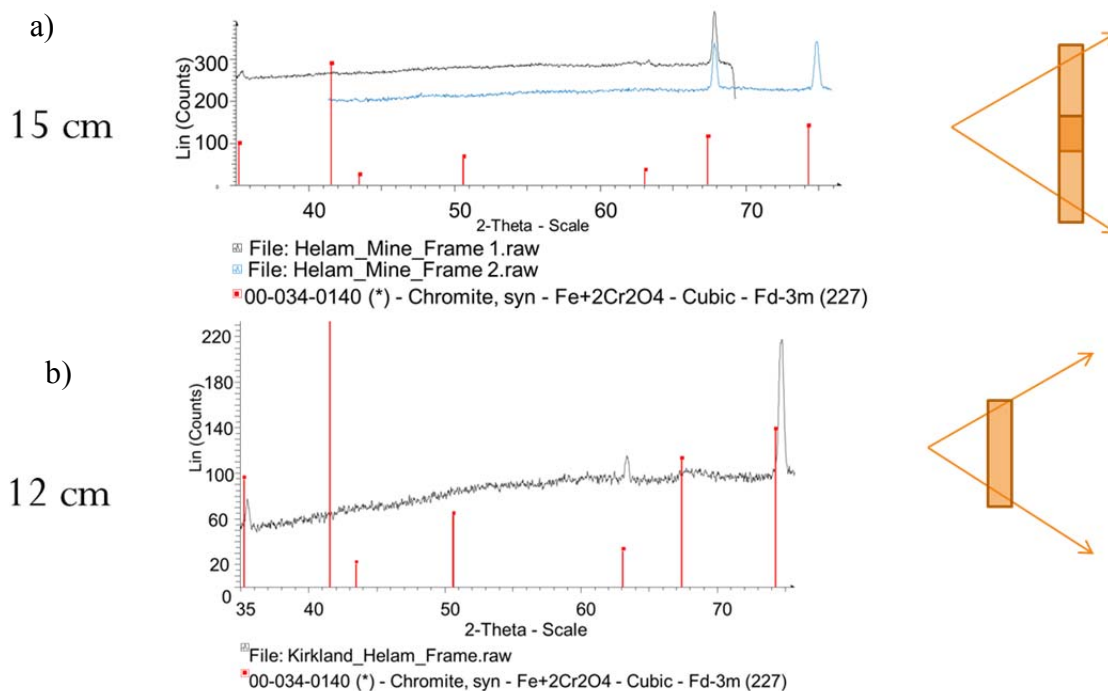


Figure 2-2: Effect of detector distance. a) Peaks were in two separate frames before detector move; b) After detector moved closer, all peaks were captured in a single frame.

2.2.1.4 Operation

The grains were first positioned using an optical microscope monitor, which allowed for the placement of the grain in X-Y space. This was followed by placement in the Z-axis using a vertical targeting laser. All samples were run using Bruker's omega scan geometry. After the positions were targeted, the locations were primarily X-rayed using the "Omega Scan" user interface program, but some were done using the manual input method. The "Omega Scan" user interface program was created for the purposes of this project and allows the user to automate scans overnight from many different samples with different sample names and numbers. The user interface program was designed to

“write” the scripting files required for the Bruker GADDS scripting language based on the user’s inputs into a C++ command line interface.

2.2.2 Slice Integration Technique Overview

The raw 2-dimensional (2D) X-ray data were subsequently processed using the simple Slice Integration Technique, by which the data were integrated in ten slices and then viewed together. This integration process converted the 2D diffraction pattern to a one-dimensional plot of intensity vs 2-theta, regardless of textural information. This slicing makes each peak more distinct in the selection process, and once the peaks are selected they are exported together as a *.dif file which is later used for unit cell parameter refinement. Using the omega scan technique, randomly-oriented single grains will not produce all of the diffraction peaks associated with the mineral (unlike powder diffraction). The lower number of peaks due to this preferred orientation resulted in each peak being of greater importance, and with many low-intensity peaks in the pattern, the use of the ‘Slice Integration Technique’ was required to maximize the number of usable peaks.

2.2.3 Error Determination

The unit cell parameter is accurate only when the d-spacing is input accurately. Otherwise, inaccuracies can occur due to misalignment, poor user peak selection, and/or poor calibration. Calibration is the most common issue when performing unit cell parameter refinement, since a poor calibration can change peak locations and shape. Calibration was achieved by analyzing a polycrystalline corundum standard (NIST #1976) over three frames. The parameters used were $\theta_1=20.5^\circ$, $\theta_2=7.0^\circ$, Width= 33.0° while using coupled scan mode. Each of the frames have an overlap region with neighboring frames and the overlapping peaks in these areas are used for calibration. The calibration corrected X, Y and detector distance, by minimizing the offset between peaks and from the corundum patterns (#43-1484 and #10-0173) from the International Centre for Diffraction Data (ICDD). The calibration was done until the difference between overlapping peaks in Frame one and Frame two were below 0.002 and for Frame two and Frame three below 0.0005. Previous work by Harwood (2009) showed that the standard

deviation caused by instrument error varied as a result of 2θ so the maximum deviation was assumed for all, which was determined to be 0.0006 Å. Errors of the peaks caused by user selection can be easily mitigated with an experienced user who ensures that peaks in the *.dif are placed at the centre of mass of the peak throughout the experiments. Beam alignment is another easily mitigated issue that rarely affects the unit cell parameter, as a poor beam alignment predominately results in a low intensity that is poor for refinements. A description of the beam alignment procedures is beyond the scope of this thesis.

2.2.4 Terra X-Ray Diffraction /X-Ray Fluorescence Methods

The kimberlitic indicator spinels used as a vector for exploration are very small and a Terra XRD/ XRF was used for analysis. The sealed Cu source (Cu K α radiation, $\lambda=1.5418$ Å) operating at 30 kV accelerating voltage and 10 W power was used to collect both XRD and XRF data. Terra instrument provides XRD data 5° to 55° 2θ (d-spacing: 1.668 to 17.660 Å) with 0.05° angular resolution using a 1024 x 256 pixel 2-dimensional Peltier-cooled charge-coupled device detector. Samples were run for 10.5 hours each to improve signal to noise, which is equivalent to 2800 individual frames.

The innovative sample holder vibrates a powder sample allowing for collection in the field and was based on the same design as used in the CheMin device on the Curiosity Rover on Mars, as designed by Sarrazin (Sarrazin et al. 2005). To fill the sample chamber, halite was used to supplement the sample volume for the spinel analysis. This supplement acts a dispersant that places more of the spinel sample within the X-ray beam for diffraction. This was done because the halite has only one overlapping peak with spinel. Additionally, halite is also easily dissolved and can be easily removed after use.

2.2.5 The Unit Cell Parameter Refinement

2.2.5.1 Software Selection

Two software programs were tested for the purpose of micro-XRD diffraction the unit cell parameter refinement. The software tested was Unit Cell (Holland and Redfern 1997) and Celref (Altermatt and Brown 1987). Both forms of software had been tested previously by Harwood (2009), and both data were in agreement.

Unit Cell and Celref both use a non-linear least squares refinement of observed d-spacings to output a refined unit cell dimension and standard deviation. Unlike Celref, Unit Cell does not need starting unit cell parameters because it requires user-indexed d-spacings as input, whereas Celref automatically indexed the observed d-spacings based on user-defined initial unit cell parameters. The initial unit cell parameters were selected from the best matching card from the International Centre for Diffraction Database.

Unit Cell requires a creation of an input file manually, and this was done by taking the d-spacings of each peak and manually assigning the corresponding Miller index. Although Harwood (2009) had previously partially automated this process, the process can be time consuming. In contrast, Celref provides a simpler alternative in which a graphical user interface is implemented while using Bruker dif output files. The ease of Celref, combined with the demonstrated small deviation between the two programs as seen by Harwood (2009) between programs resulted in the selection of Celref for the purposes of this study. The average refined values were 0.0084 and 0.0073 Å less for the Celref software than Unit Cell software for the two data sets. The ability to visually monitor the refinement, with the calculated peaks compared to observed data, also led to the conclusion that Celref was preferable.

2.2.5.2 Least Squares unit cell refinement

Non-Linear least squares refinement is done according to Altermatt and Brown (1987) using the observed data, crystal structure and the starting unit cell parameter. In the observed data, Bragg's law relates theta (θ) to the interplanar distance of d_{hkl} , the wavelength (λ) and the zero angular shift ($\Delta\theta$), equation 1.

$$\theta = \Delta\theta + \sin^{-1} \frac{\lambda}{2d} \quad (1)$$

The zero angular shift is variable with θ . If there is a sample displacement error with a goniometer displacement, then the shift will be constant according to equation 2. The radius of the goniometer in the equation is defined as R.

$$\Delta\theta = \frac{e}{R} \cos \theta \quad (2)$$

The relationship between a^* , b^* , c^* , α^* , β^* and γ^* , which are reciprocal cell parameters, and d is given by equation 3.

$$\frac{1}{d_{hkl}^2} = (ha^*)^2 + (kb^*)^2 + (lc^*)^2 + 2hka^*b^* \cos \gamma^* + 2klb^*c^* \cos \alpha^* + 2lhc^*a^* \cos \beta^* \quad (3)$$

This is simplified to the relevant terms for a cubic system and converted to direct space in equation 4.

$$d_{hkl}^2 = a^2/(h^2+k^2+l^2) \quad (4)$$

Equation 4 is finally rearranged to equation 5, in order to determine a , upon which a non-linear least squares refinement is completed.

$$a = \sqrt{d_{hkl}^2 * (h^2+k^2+l^2)} \quad (5)$$

2.2.5.3 Error Determination

For all samples, Celref calculated a standard deviation, which is included in appendix E with the refined unit cell parameters. Standard deviation (STD) can be misleading due to local minima when picking a starting value for refinement. The chance of a local minimum for STD instead of the true minimum could be reduced by comparing the calculated peaks visually to a known unit cell parameter (sometimes adjusted using the ‘Tune Cell’ function in the EVA Diffracplus software package (EVA)). The unit cell parameter could not be refined for patterns with fewer than three peaks, as the refinement then becomes underconstrained; therefore refinements were only completed for patterns with three or more peaks.

2.2.6 Electron Probe Micro-Analysis (EPMA)

Electron probe micro analysis (EPMA) data were collected through Mineral Services Canada Inc. (North Vancouver, BC, Canada) and Renaud Geological consulting (London, ON, Canada). The technique was used as a calibration set for the unit cell parameter data to compare composition to the structural data (unit cell parameter). Electron Beam techniques use a beam of electrons to generate characteristic X-rays in the sample, and

the X-rays from each element in the sample go through a curved crystal spectrometer and are counted using sealed proportional or gas-flow detectors.

The data for the creation of a baseline for the structural data was provided by Mineral Services Canada Inc. (North Vancouver, BC) and was performed using a LEO 1450 Scanning Electron Microscope (SEM) using combined energy dispersive X-ray spectrometry (EDX) and wave-length dispersive spectrometry (WDS) (Oxford Instruments spectrometers). Relevant major and minor elements were detected at an operating voltage of 20 kV and a beam current of 30 nA on the EDX detector. The detection limits are approximately 0.01% with 60 second counts. The standards for quantitative work were other kimberlite indicator minerals of known composition.

The field portable grains were analyzed at Renauld Geological Consulting on a JEOL JXA-733 electron microprobe equipped with an energy-dispersive X-ray spectrometer (EDX) and 5-wavelength-dispersive spectrometers (WDS). The operating accelerating voltage was 15 kV and 11 nA probe current. The 5 micron beam was targeted on a peak for 10 seconds for Fe, Mg, Si and for 50 seconds for trace elements, Ti, Ni, Ca, Mn, Co, and Na. The background signal was counted for 20 seconds for major elements and 50 seconds for minor elements. The detection limits (DL) for trace elements were better than 60 ppm and 0.01 wt% for major elements.

Acknowledgements:

Alysha McNeil is thanked for help crystal bond mounting samples. Natalie Pietrzak-Renaud is thanked for electron probe microanalysis. Paul Mann (U of Winnipeg) and Matt Izawa are thanked for collecting the Terra data. Matt Izawa is thanked for reviewing this chapter and for discussions.

2.3 References

- Altermatt, U. and Brown, I. (1987) A real-space computer-based symmetry algebra. *Acta Crystallographica Section A: Foundations of Crystallography*, 1, 125-130
- Flemming, R.L. (2007) Micro X-ray diffraction (μ XRD): a versatile technique for characterization of Earth and planetary materials. *Canadian Journal of Earth Sciences*, 44, 1333-1346
- Freckelton, C.N. and Flemming, R.L. (2009) Crystal-Chemical Correlations in Chromites from Kimberlitic and Non-Kimberlitic Sources. *EOS Trans. AGU*, 22, Abstract MA71C-05
- Harwood, B. (2009) Crystal chemical relationships in kimberlitic and non-kimberlitic garnets and ilmenites. M.Sc. Thesis, University of Western Ontario.
- Holland, T. and Redfern, S. (1997) UNITCELL: a nonlinear least-squares program for cell-parameter refinement and implementing regression and deletion diagnostics. *Journal of Applied Crystallography*, 1, 84-84
- Nowicki, T. (2014) Chomite and Kimberlite vs Non-Kimberlite Discrimination
- Nowicki, T., Crawford, B., Dyck, D., Carlson, J., McElroy, R., Oshust, P. and Helmstaedt, H. (2004) The geology of kimberlite pipes of the Ekati property, Northwest Territories, Canada. *Lithos*, 1–4, 1-27
- Sarrazin, P., Blake, D., Feldman, S., Chipera, S., Vaniman, D. and Bish, D. (2005) Field deployment of a portable X-ray diffraction/X-ray fluorescence instrument on Mars analog terrain. *Powder diffraction*, 02, 128-133

Co-Authorship Statement

The μ XRD and refinements were collected by myself at Western University. I also developed the ideas, and wrote the paper. Dr. Flemming provided guidance and instrument training and Matt Izawa for guidance in the writing of the paper.

Chapter 3

3 Signal enhancement through a maximum intensity projection using Slice Integration of 2D-XRD data: Applications to unstrained crystallites (>100 micron grain size)

3.1 Executive Summary

A common problem in the application of micro X-ray diffraction (μ XRD) with two-dimensional (2D) detection is that ‘large’ (greater than ~ 100 micron) crystallites produce only a ‘few spots’ within the area of the 2D detector corresponding to diffracted rays from only a subset of lattice planes diffracting. The ‘omega scan’ rotating optics method, designed to maximize the number of lattice planes that satisfy Bragg’s Law under the beam, minimizes the amount of time each lattice plane spends in diffraction condition. This can lead to the intensity of a peak “disappearing” relative to the noise when the area of the peak is integrated as part of the entire detector area to produce an integrated diffraction pattern. This chapter describes a new data processing technique, the ‘Slice Integration Technique’, which improves sensitivity and signal-to-noise ratios in μ XRD data. Chi (χ) is the spread of the data on a 2D detector parallel to the Debye rings and perpendicular to the 2θ axis. The standard method of processing 2D XRD data for phase identification is to integrate the entire detected area of a 2D XRD image at once, to produce a conventional intensity vs 2θ pattern. The technique demonstrated herein, the “Slice Integration Technique”, integrates a series of areas smaller than the full frame at various chi angles. This results in the background noise being more uniform in each slice, and allows originally faint peaks to be detected. The pattern slices can be used as separate patterns, though the process may be labour intensive. A single pattern can be created from the slices by stitching them together using a maximum intensity plot. It has been demonstrated that there is a threshold to ensure one has not taken too many slices, termed “overslicing”. We propose a potential method to determine the optimal number of slices and to avoid the overslicing threshold. The technique is best used for unstrained

crystallites, and does have some application to grains demonstrating asterism. This technique has been applied to μ XRD data from two examples: a diamond inclusion to show signal to noise improvement and a multiphase thin-section to demonstrate the enhancement of phase recognition using the technique. This technique can be used for phase identification of minor phases that are difficult to identify due to poor signal, or for samples which diffract poorly (e.g., low atomic number materials).

3.2 Introduction

Typically, 2D XRD data is converted into a conventional 1D-diffraction pattern by integration of detected X-ray counts along the Debye rings (here referred to as the χ -direction) to produce a plot of intensity vs. 2θ (or integrated diffraction pattern) which is then interpreted using databases of reference powder XRD patterns (Flemming 2007). A common observation is that many weak peaks discernible by visual inspection in the 2D image are often not visible in the integrated intensity vs. 2θ plot (Flemming 2007; Bramble et al. 2015; Izawa et al. 2011; Izawa et al. 2010). Due to non-uniformity of detector noise, or simply due to averaging of a weak peak over large areas of noisy data, weak peaks tend to disappear, that is, to be undetectable above the background after integration. The Slice Integration Technique developed in this work enables improvement of both the intensity of peaks and their signal-to-noise ratio.

For the purposes of this study, the technique has been applied to data from an *in situ* micro X-ray diffraction (μ XRD) study of a polished diamond inclusion, and a polished thin-section, using the omega scan method. The omega scan method is used for non-polycrystalline samples, such as single crystals or large crystals in thin section, to increase the number of lattice planes that satisfy Bragg's Law. This is done by rotating both the detector and the source clockwise by an omega angle (ω) with fixed 2θ . During the scan, from the frame of reference of the detector, it appears that the sample has rotated by $-\omega$, which increases the number of lattice planes passing through the diffraction condition. A general disadvantage of μ XRD as compared to powder XRD is that for crystallites that are a significant fraction of the beam footprint, only a few lattice planes will be in diffraction condition, in a situation analogous to extreme preferred

orientation or very coarse particle size in conventional powder XRD (Jenkins and Snyder 1996; Azároff and Buerger 1958).

Operating the μ XRD in ‘omega scan’ mode (Flemming 2007) reduces but does not eliminate these problems. An additional problem presented by the omega scan method is that most lattice planes will only be in diffraction condition for a short duration, resulting in peaks that are very weak. A possible solution is to extend the counting time; however, because signal-to-noise ratio will generally scale as the square root of elapsed time, the times required becomes impractically long (days or more) for many samples of interest. The slice technique enables the merging of intensity-2 θ data produced by integration over selected sub-regions of a 2D diffraction image, resulting in substantial improvement in signal-to-noise ratios without increased counting times. This technique has broad applicability to μ XRD analysis, including for strongly absorbing samples, very small sample volumes, poorly diffracting materials, and large crystals that cannot be prepared as powders (e.g., objects of value, thin sections required for other analyses, and others). The Slice Integration Technique is most applicable to unstrained crystallites, but can be applied with caution to some grains that show asterism. Asterism is produced by a series of orientationally-related crystallites (such as subgrains formed in non-uniformly strained minerals), resulting in a series of smaller spotty peaks. This technique can potentially resolve those peaks better. The technique was performed using three methods that varied according to how the data was processed: the Peak Pick method, the Additive method, and the Max Intensity Plot method.

3.3 Methods

3.3.1 In situ micro X-ray Diffraction

In order to demonstrate the effectiveness of the Slice Integration Technique, we performed two *in situ* micro X-ray diffraction studies using a Bruker D8 Discover Micro X-ray diffractometer at Western University in London, Ontario, Canada. This instrument has the advantage of theta-theta geometry which enables the sample to remain stationary and horizontal. The XRD used Cobalt radiation (Co K α , λ = 1.78897 Å), generated in a sealed-tube source operated at 35 kV and 45 mA with Göbel mirror parallel-beam optics

system to reduce the effects of non-flat sample surfaces, and used a pinhole collimator snout giving a nominal beam diameter of 100 microns. Two-dimensional XRD data were collected using a Hi Star detector with General Area Detector Diffraction System (GADDS), at 12 cm detector distance. This configuration enables the targeting of specific points with the X-ray diffractometer and gives the great advantages of being entirely non-destructive and the ability to analyze small volumes of material *in situ*, unlike conventional powder XRD (Flemming 2007). Analysis of unstrained crystallites using this technique requires the use of the omega scan method.

3.3.2 Pick Peak Method and 2D Slicing

The Slice Integration Technique uses the programming capability available in GADDS (Slm file) and a user-programmed macro that automatically subdivides the 2D XRD data into adjustable increments of χ . This is clearly illustrated in Figure 3-1 for 10 slices, where the areas enclosed by the light blue lines show the slice areas for 10 slices and the dark blue lines show the entire area of a traditional integration. The Peak Pick manual method of data processing started with the raw 2D GADDS images that had been integrated along a

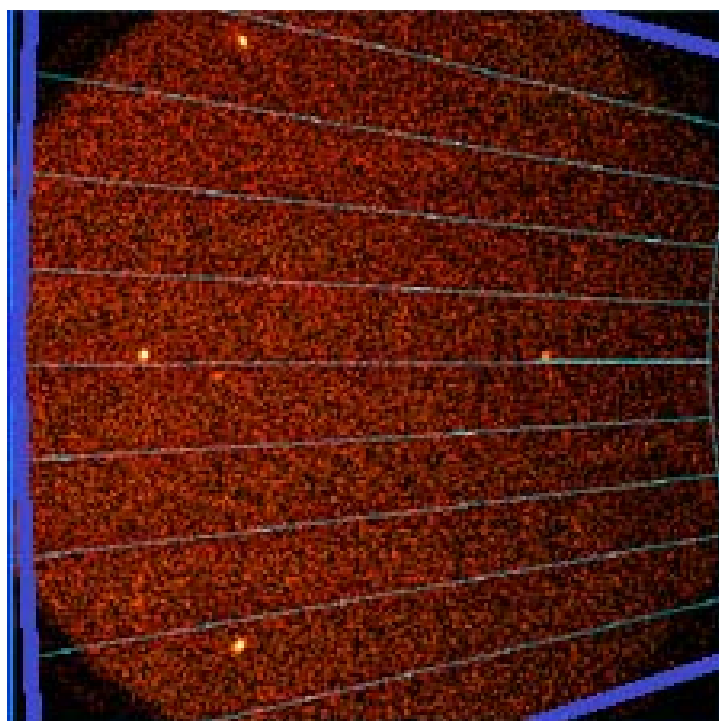


Figure 3-1: The slice method subdivides the integrated area of the X-ray detector (the area is integrated is seen between the thin blue lines) instead of the traditional integration method which integrates the area over the entire frame (thick blue lines). This GADDS image is from a chromite grain from Gabon, Southern Africa (courtesy of Dr. Nowicki, Mineral Services Canada, Vancouver, BC.)

selected number of χ° slices to produce a series of one-dimensional diffraction patterns of intensity versus 2θ . Each of the series were searched for peaks, and for any

increments that contained peaks, those peaks were picked and all peaks were combined to create a *.dif pattern. Figure 3-2 shows a peak from one slice (conventional full frame integration) as compared to the same peak from one slice from the 50 slice pattern, for demonstration purposes.

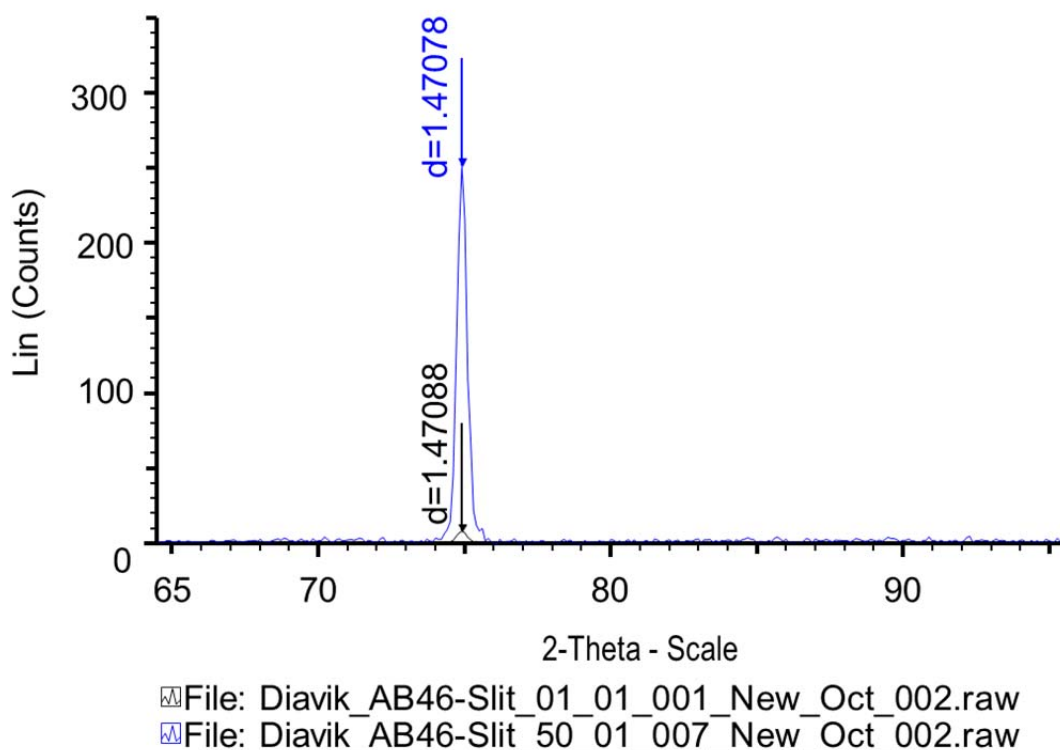


Figure 3-2: The Peak Position for 1 Slice as compared with 50 Slices and is 0.0001 d, which is within the 0.0005 Å acceptable range of machine error for Peak 1. (The sample is a chromite inclusion in a diamond (AB-46) from Diavik Kimberlite A154 South pipe, courtesy of Dr. Van Rythoven and Dr. Schulze, U of Toronto. (from the sample set in Van Rythoven 2013)

In cases where peaks showed up in multiple frames of the series of slices, the slices containing the most intense peaks were used for the final pattern. This qualitatively improved the signals, but required manual selection of peaks and the addition of these peaks into a single *.dif file. After processing, it was possible to get sufficient peaks to enable refinement of the unit cell parameters to within acceptable uncertainties (~ 0.005 Å). Slicing was limited to ten slices for this method in order to minimize any possibility of hitting the overslicing threshold. As will be discussed further in the paper, peak position was not found to vary with the number of slices unless overslicing had occurred.

Once the overslicing threshold was reached, peak shapes became distorted or in extreme cases, peak position would move. This was observed well over 10 slices, which was used for the basic peak pick pattern method. When searching in a stack plot of patterns, one must select all of the peaks in all patterns independently, and then save them together as a *.dif, which can then be searched.

3.3.3 Slice Integration Technique using the Additive Method

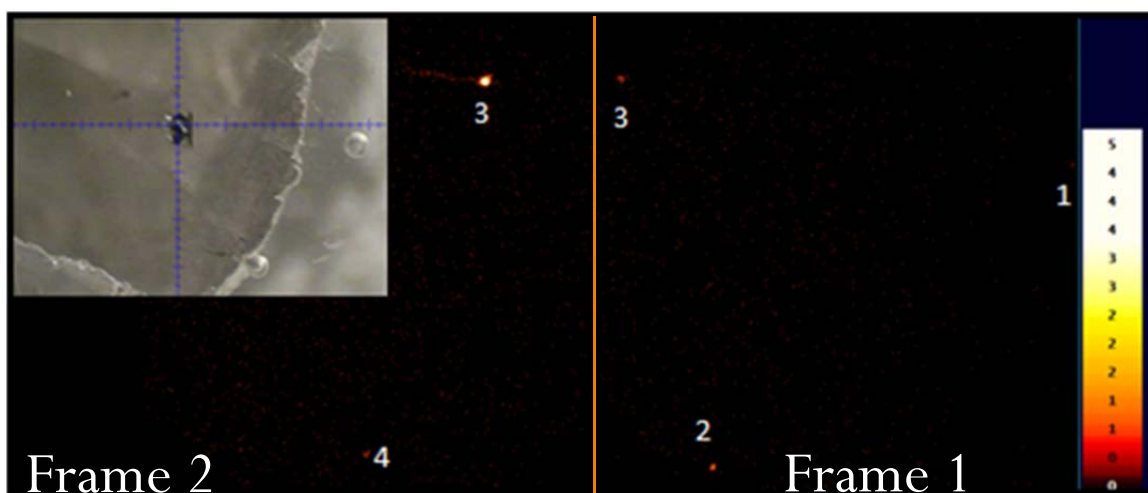


Figure 3-3: Context Image and GADDS clearly shows three very weak peaks but only one peak is visible when integrated over the entire frame using the traditional approach (Peak 3). The sample is a chromite inclusion in a diamond (AB-46) from Diavik Kimberlite A154 South diatreme, courtesy of Dr. Van Rythoven and Dr. Schulze, U of Toronto, Toronto, ON

The simplest way to process the 2D data into a 1D diffraction pattern was using EVA DiffracPlus Evaluation (EVA) software to add all of the first frames and then all second frames, followed by a manual merging of the frames. Three types of merges were attempted; the first was a traditional merge where first frame is scaled to match the second frame using EVA. The second type of merge used does not scale the second frame, it only adds the frames together. The third way attempted was to merge first frames together and second frames together instead of adding all Frames before merging Frames 1 and 2. The second and third methods of merging were done using the non-multiplying Bruker Merge standalone program.

The second method of merging resulted in lower frame 1 peak intensities than the traditional multiplying merge function used in the EVA program, but this kept the signal to noise ratio more consistent between frames after merging. Peaks were shown to remain within the instrument error with an increased number of slices (See Discussion). To analyse the signal- to-noise ratio, the background must be isolated. The peaks are identified from the data set by visual inspection, then removed once imported into Microsoft ExcelTM to separate the noise where the mean is calculated, and compared to maximum signal or average peak intensity as explained below. Patterns that did not cover the entire 2 θ range, i.e. those at the edges of the GADDS frame, could not be added together as it resulted in an elevated range over the subsection being added. As a result, only peaks contained in slices covering the entire 2 θ range were included in the data analysis. This can be used as an approximation of the signal to noise relationship that occurs with all the sets. The GADDS image was integrated over the entire area and then was subdivided into 2 and then into 10-slice increments from 20 to 90. It is anticipated that similar materials, run under the same settings, should require the same number of slices, and so a calibration slice test will only be necessary for the first sample in a set and subsequent runs will employ the optimal number of slices as determined by the calibration test. The creation of an automatic determination for the ideal number of slices is beyond the scope of this current paper. The advantage of the Max Intensity Plot method (discussed next) instead of the additive slice method described here is that it allows the user access to the entire range of 2D data, not only the areas which contain a complete 2 θ range in 1D. This becomes relevant when peaks are either high or low in χ , that is, near the edges of the 2D detector.

3.3.4 Slice Integration Technique using a Max Intensity Plot (MIP)

The use of a Max Intensity Plot (MIP) allows for the rapid creation of a single pattern to combine slices and has the potential to be automated. In order to automate or quantify, one must decide on the appropriate number of slices – for which a calibration needs to be done. This is required due to the variability of data depending on the detector distance, and the sample characteristics. This could be done by automatically generating an increasing number of slices, and then by background subtracting the *.raw files and converting them to *.plv files using PowDLL (Kourkouvelis 2013), after which the data can be read by external data processing programs.

Two frames were sliced, as can be seen in Table 3-1. Then, with a user created macro in Excel, the data was stitched back together by performing a Max Intensity Plot of the slices. This was done by inputting all of the scans from the 2θ vs intensity data sets for each of the slices, matching all the slice data together (i.e. taking all data sets which contained an intensity value for each 2θ value and linking these), and finally selecting most intense value for each 2θ . Afterwards, an output file was created with the complete pattern of 2θ vs intensity. This was followed by a conversion of the data back into *.raw files for merging the frames. The frames were then converted to *.raw files and imported into the EVA application, and the two frames were merged together. Crossing the overslicing threshold can occur within plots, which will distort peak shape and locations, and the user will be required to decide if a pattern has become over sliced and if peak shapes have been distorted or moved. This will be discussed further below.

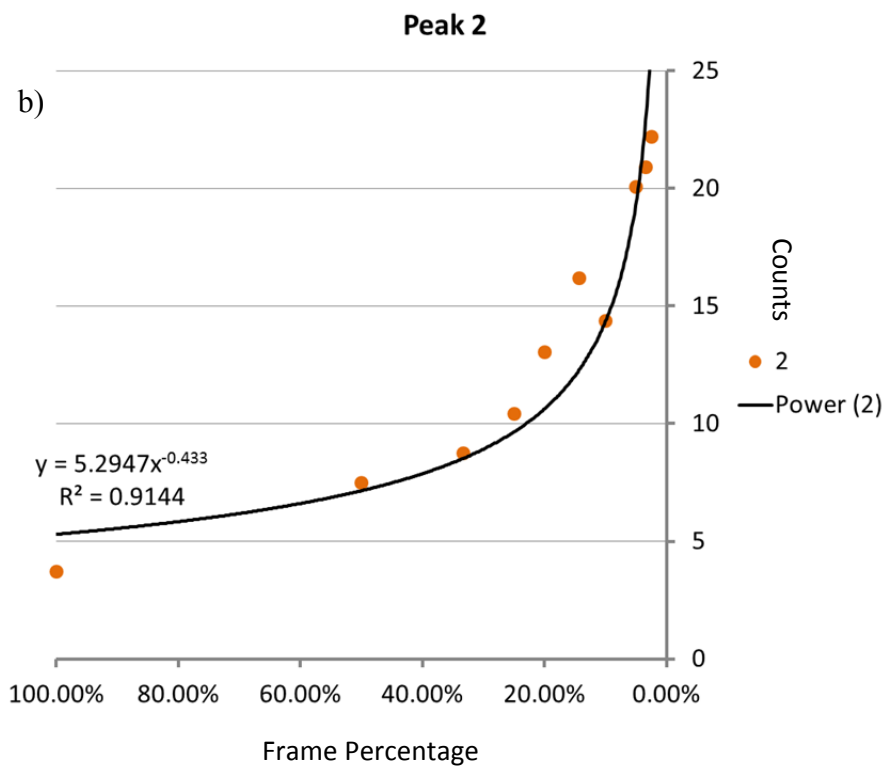
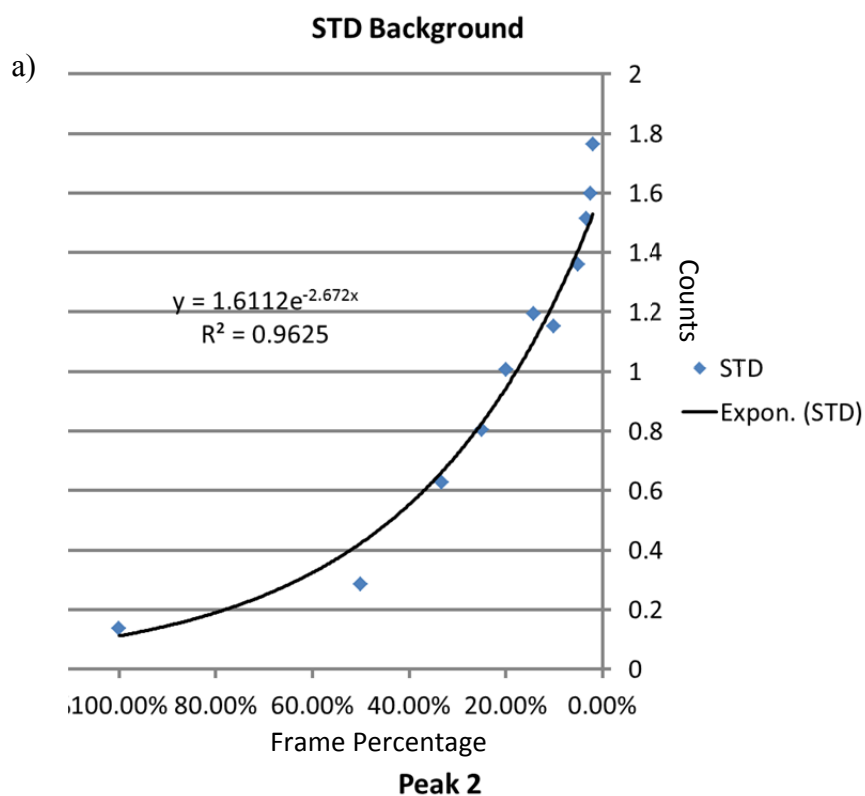
Table 3-1: Slice Percentage			
Slice #	% of Full Frame	Frame 1 Slice (χ°)	Frame 2 Slice (χ°)
1	100	60	42
2	50	30	21
3	33.3	19.98	13.986
4	25	15	10.5
5	20	12	8.4
7	14.28	8.568	5.9976
10	10	6	4.2
20	5	3	2.1
30	3.33	1.998	1.3986
40	2.5	1.5	1.05
50	2	1.2	0.84
60	1.67	1.002	0.7014
70	1.42	0.852	0.5964
80	1.25	0.75	0.525
90	1.11	0.666	0.4662

3.4 Results

3.4.1 Demonstrating Signal to Noise Improvement

The Slice Integration Technique – additive method has been performed on a chromite diamond inclusion. This single phase example was done to demonstrate the increase in intensity and simultaneous decrease in signal to noise ratio achieved for weak diffraction peaks by the Slice Integration Technique. See Figure 3-3 for context image of the diamond inclusion and 2D GADDS image containing the raw data. This sample was selected to show the ability to produce a pattern from a sample that does not produce many strong peaks. This is a common scenario with the small sample sizes often used in *in situ* micro X-ray diffraction studies (Flemming 2007). The intensity of the three peaks being tracked increases as a power function with the number of slices, as can be seen in Figure 3-4: Intensity vs Frame Percentage and the STD vs Frame Percentage. The first peak in the pattern was on the edge of the 2D detector, which behaved erratically, so it

was discounted from calculations and plots. The noise can be best described by the standard deviation of the mean; the mean of the noise is arbitrary and can be based on the processing of the data.



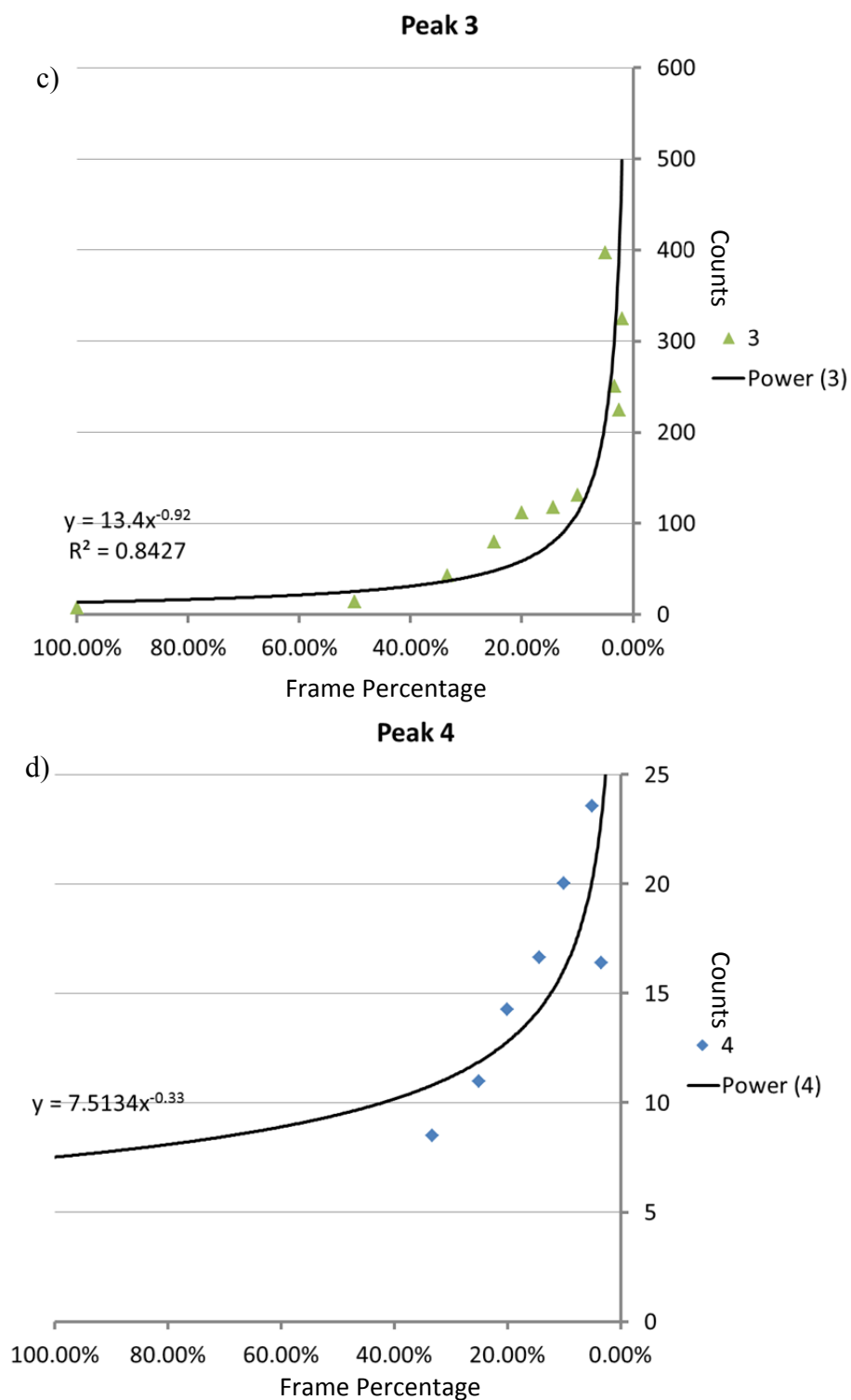
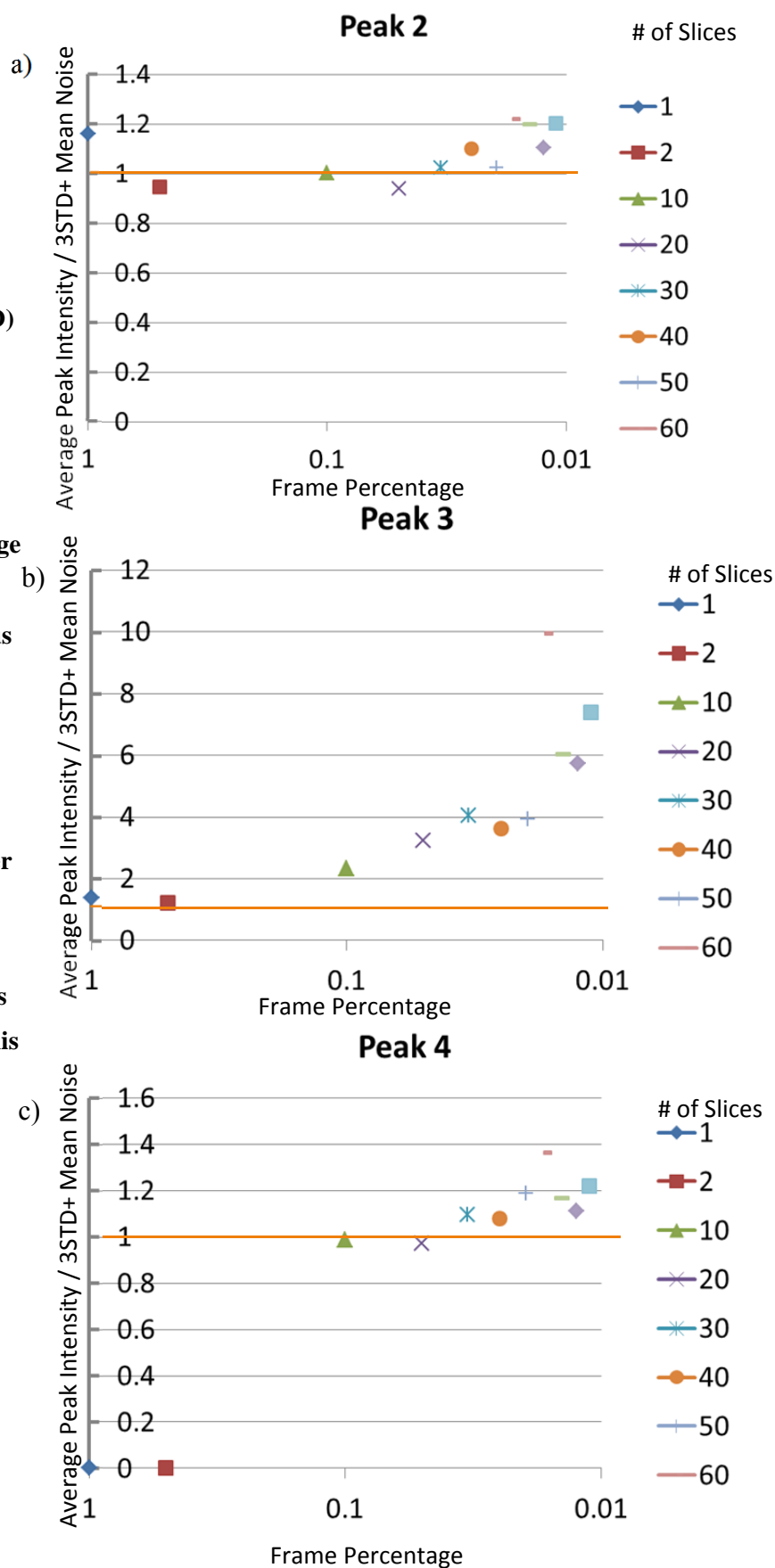


Figure 3-4: Intensity vs Frame Percentage and the STD vs Frame Percentage. a) The standard deviation (STD) can be used to approximate noise and increases with frame percentage. The intensity of the three peaks visible in Figure 3-3 (b) Peak 2, c) Peak 3, d) Peak 4) compared to peak intensity can be clearly seen to increase with an increasing

Figure 3-5: Figure Signal/Noise (normalized to 3 STD) vs frame percentage. The three peaks (a) Peak 2, b) Peak 3, c) Peak 4) were plotted comparing the average peak divided by the mean of the noise plus 3STD to the frame percentage. Once all peaks are over the 3STD level it is suggested that further slicing only risks overslicing and the ideal number of slices has been found. In this case 30 slices was found to be optimal.



The standard deviation, however, shows the spread in the noise, and as such is a better descriptive statistic in this context. It can be seen that the noise also increases with increasing number of slices, but at a slower rate than the intensity in Figure 3-4. The signal to noise ratio also can be seen to improve with more slices, as seen numerically in Figure 3-5: signal of the average peak (normalized to 3 STD) vs frame percentage. For this study, it is suggested that the correct number of slices occurs once all peaks are above the 3 STD thresholds. A 3 STD limit minimum was used because this limit represents 95% of noise and so it was assumed that peaks above this threshold were actually peaks and not noise. Average peak intensity was used for this metric since it is more sensitive to the creation of subdomains by slicing as subdomains will create local intensity minimas. The additive method can be seen stack plotted in Figure 3-6.

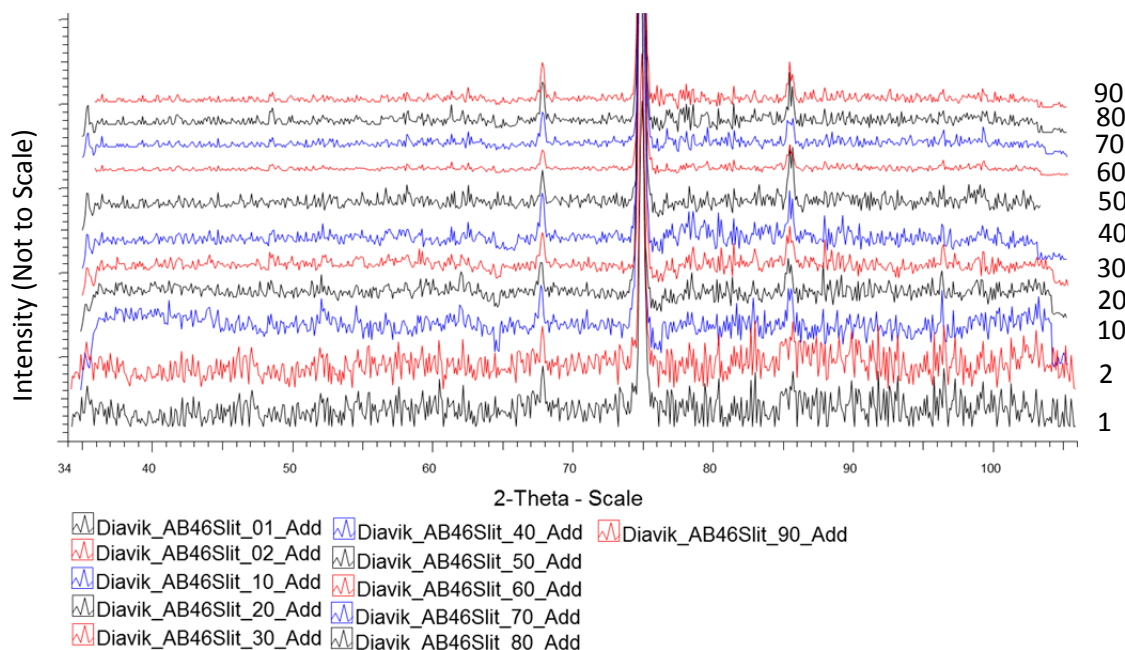


Figure 3-6: The results of additive pattern method of slicing shows only two peaks in the pattern but three peaks after the slicing has been employed. The effects of overslicing become evident in slice 40 and 80 when the peaks are subdivided extra times. (The sample is the same chromite inclusion as shown in the GADDS image in Fig. 3-3) (Note that the intensity of the patterns is not to scale.)

3.4.2 Demonstrating the Max Plot

3.4.2.1 Single phase example

The same sample that was analyzed manually was also run using the Max Intensity Plot (MIP) i.e. chromite inclusion in the diamond, which allows for automation of the process. The Max

Intensity Plot program cannot be used for fewer than 20 subdivisions because of edge effects that occur at the intersection of the 2D mask and the pattern. Once there are more than 20 slices, the size of this margin is small enough that removing 1.2° from the top and bottom of the pattern negates the issue. The MIP method was applied from 20 – 90 slices in increments of 10 slices. The initial pattern only showed two distinct peaks, but once sliced at least 20 times, three peaks become visible. The changes in the patterns are illustrated in Figure 3-7. The intensity of a peak was considered less important than the ratio of signal to noise, which can be understood as the amount a peak “stands” out relative to noise. This prominence is critical for phase identification.

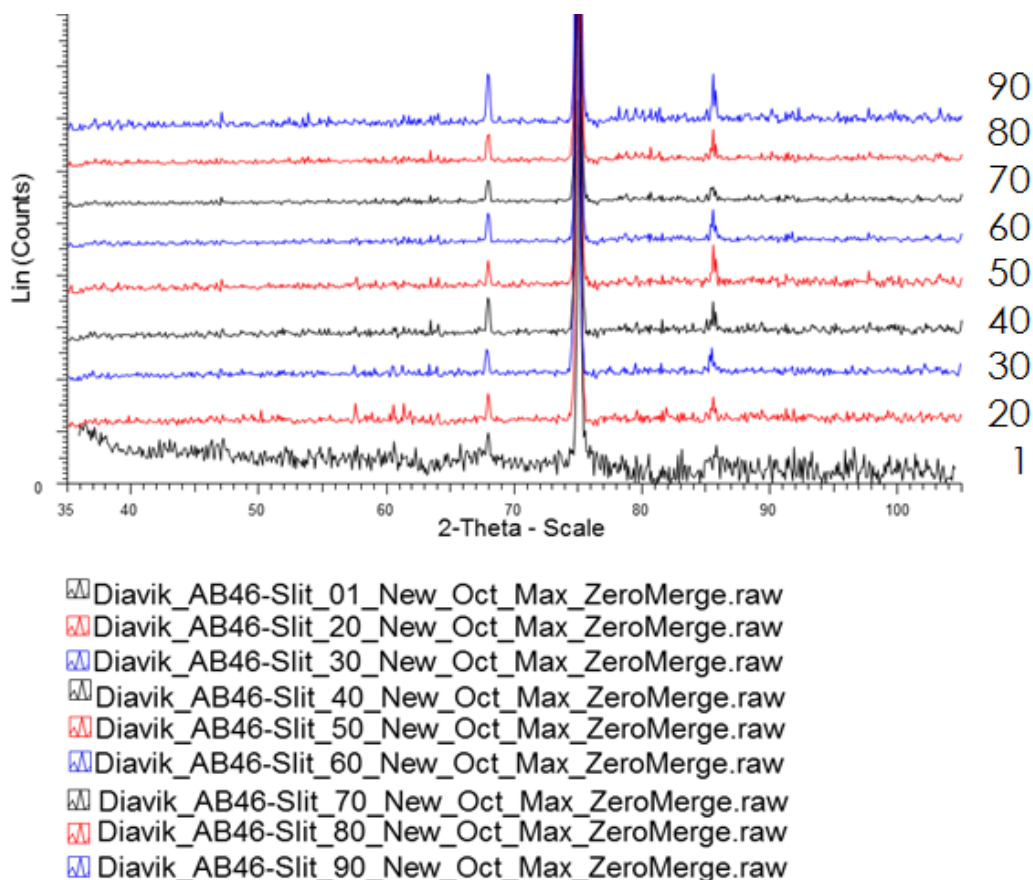


Figure 3-7: The comparison of the 20, 30, 40, 50, 60, 70, 80, 90 slice plots to 1D single slice plot. The implementation of the MIP method on a single phase shows the clear improvement of Peak 4 allowing for a more accurate identification. Thirty slices is suggested as the optimal number of slices in this instance because overslicing, as explained below, becomes visible with the subdivision of Peak 4 with 40 slices.

3.4.2.2 Multiple phase example

The MIP method was also applied to a multiphase example, which only showed one peak in the original integrated diffraction pattern but showed six visible peaks after slicing and combination (Figure 3-8). When the 1D 70 slice plot is compared to 1D single slice plot, it is clear that 5 new peaks are visible, enabling a phase identification that was not possible before the application of the slicing technique, as seen in Figure 3-12 below.

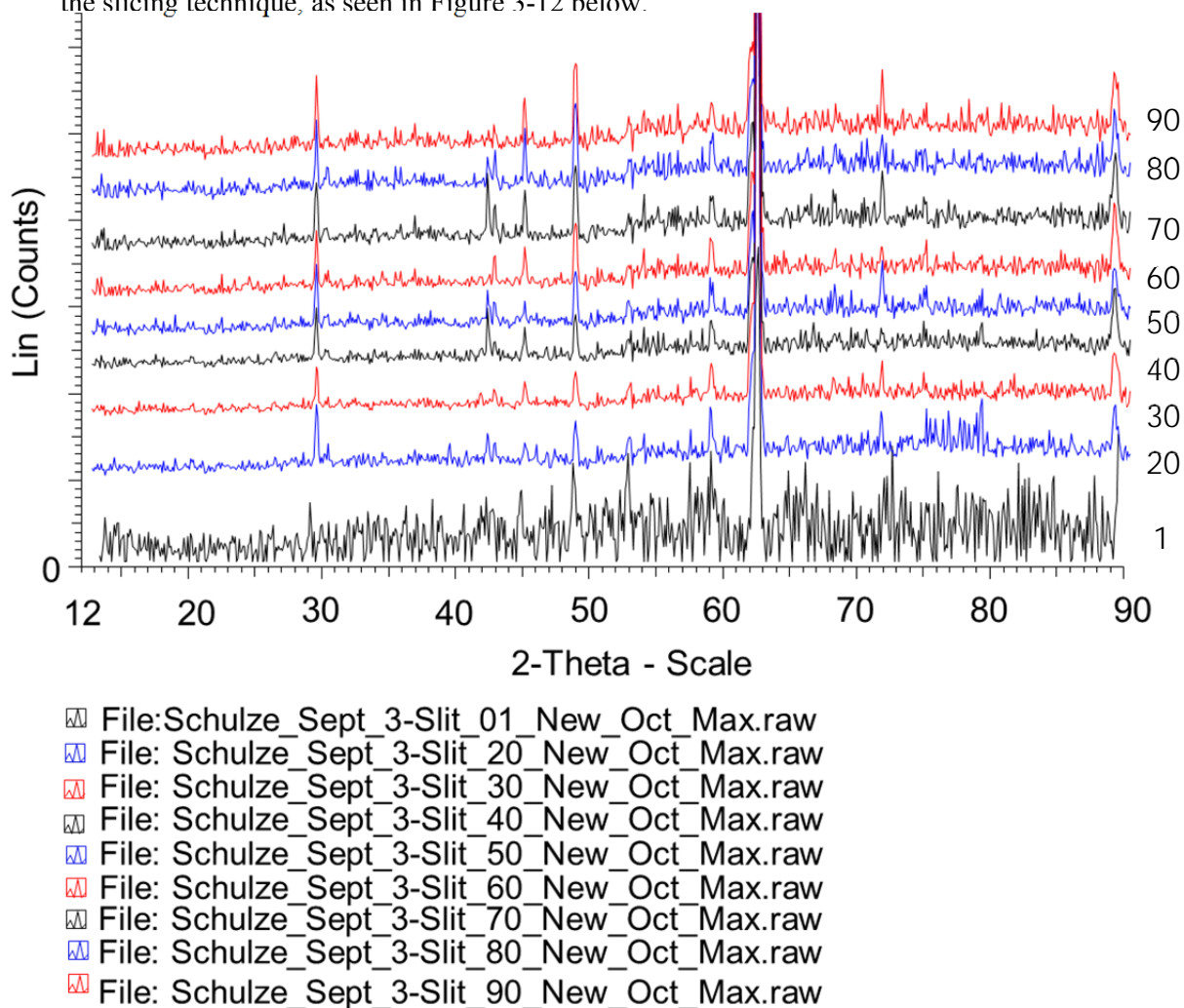


Figure 3-8: The comparison of the 20, 30, 40, 50, 60, 70, 80, 90 slice plots to 1D single slice plot. The implementation of the MIP method on a multiphase sample from Schulze (similar to that reported in Schulze et al. 2014). In the one slice there is only one resolved peak as compared up to seven peaks resolved in the other patterns. The 70 slice pattern is further processed for phase ID in Figure 3-11.

3.5 Discussion

3.5.1 Demonstrating Signal to Noise

The Slice Integration Technique significantly improved both the signal to noise ratio, and the intensity of all peaks. In this example a traditional integration technique would have been unable to identify the magnesiochromite because only two peaks would have been insufficient for identification but the third makes a more convincing match to the standard magnesiochromite pattern. Additionally, when choosing a calibration frame, one with fewer slices is preferable, because one needs to be careful to prevent peak splitting. In the single phase example using the thirty slice data, the three peaks show up clearly in the Additive pattern, with all peaks exhibiting greater than three standard deviations of single to noise ratio. The least-improved peak in the thirty slice

data (Peak 3) showed an almost 250% improvement of maximum intensity from the single slice (full image integration)

and the most-improved peak showed close to 1530% improvement in intensity (Peak 2). The signal to noise ratio

improved 28.94 % for the least-improved peak, with the most- improved peak showing a 670.1% improvement from the single slice data using the average for the peak. The average was considered more sensitive to overslicing since the subdivision of a peak with the creation of minimas would be detectable since it would reduce the average unlike the maximum. The advantages of the stitched-together pattern (Additive or MIP Methods) over simply taking the peak positions and creating a *.dif are that it is easier to search directly for patterns and it is more intuitive for users. Both methods are much more labour intensive than the MIP technique.

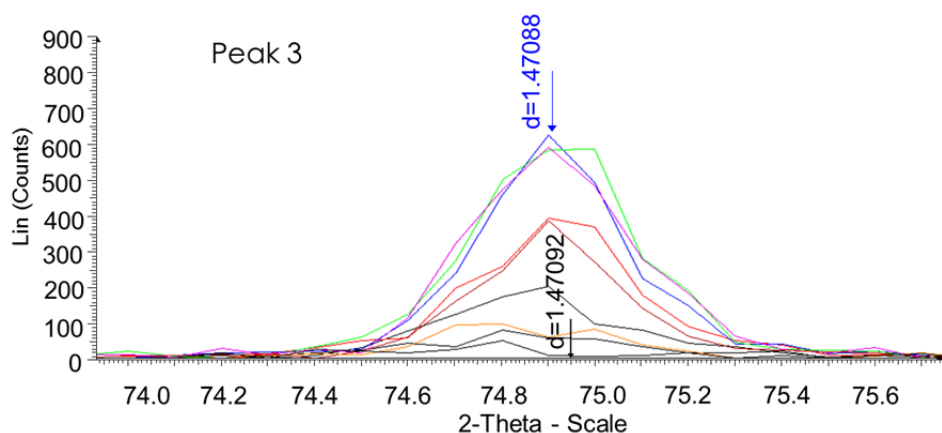


Figure 3-9: Oversliced intense peak. An intense peak is sliced 400 times and the peak centre of the intense peak is still within error of the original one-slice peak. The patterns displayed are the patterns which show Peak 4 within the 400 slices.

3.5.2 Overslicing

Overslicing should be considered a threshold that slicing should be kept below. When overslicing occurs, a peak distorts its shape, creates subdomains and local minima, or reduces intensity. The easiest method for identifying overslicing was through visual identification. As the number of slices increases, the peaks should keep a consistent shape, especially once a standard peak shape has been observed. The only aspect of the peak that should change before the overslicing threshold is peak intensity, which should improve with increased number of slices. This likely occurs due to a lack of symmetry within the 2D data, which when sliced will shift the peak toward a local maxima or show local minima within the peak in the 2D data.

When peaks are left intact or minimally subdivided by the area of the slice relative to the peak on the 2D image, the peak position remains consistent as can be seen in Figure 3-2 (peak position in 1 Slice vs 50 Slices), the peak position in a single frame, intermediate number of frames, and the final peak position stay within the 0.0005 degree error of the technique. Strong peaks with good peak shape can often be subdivided with the Slice integration method without significant issue, as long as the user uses the highest intensity peak, as can be seen in Figure 3-9.

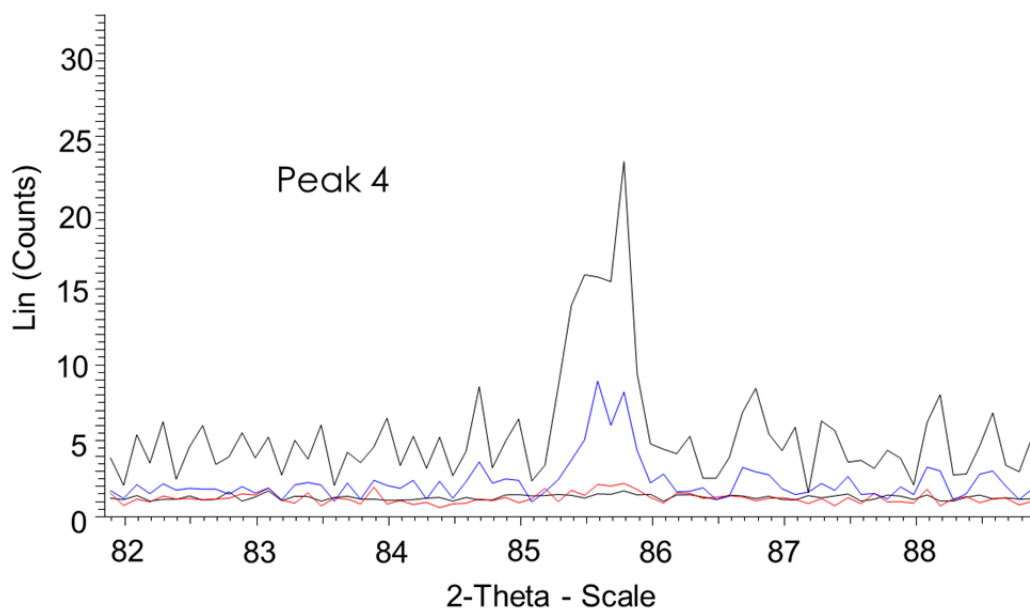


Figure 3-10: Over sliced weak peak. A weak peak when overslice will rapidly distort. Although an improvement occurs in the 10 and 60 slice pattern, a clear distortion of peak shape occurs at 100 slices, as a byproduct of overslicing (Sample as in Fig 3-3). Black base pattern 1 slice Red pattern 10 Slices, Blue pattern 60 slices, Black top pattern 100 slices.

The intense peak sliced 400 times shows approximately the same peak centre and shape as the 1 slice centre, within the error of the instrument, even though the other slices vary. However, a weak peak is more subject to localized change; as a weak peak is sliced through, it can eventually lead to an array of local maxima that are not representative of the peak as a whole. A weak peak can be subdivided too many times, as can be seen in Figure 3-9, where this oversliced weak peak clearly deforms at 100 slices. The peak shown in Figure 3-10 is not detected by traditional full frame integration (= 1 slice); examples at 10 slices and 60 slices both show a clearly formed peak, but the 100 slice example shows a localized effect of the centre of peak and is not reflective of the peak as a whole.

The 400 slice version of a weak peak is used to demonstrate what can occur when a weak peak is sliced into many separate peaks. In this case, it cleaves the peak into three peaks, meaning it virtually disappears into the background noise, as seen in Figure 3-11. The advantage of this method is that it retains intensity lost after merging. For peaks close to the edges of the detector, we are, at this time, unable to merge them into the pattern unless the lack of overlap is very small, and this merge method does risk reducing intensity.

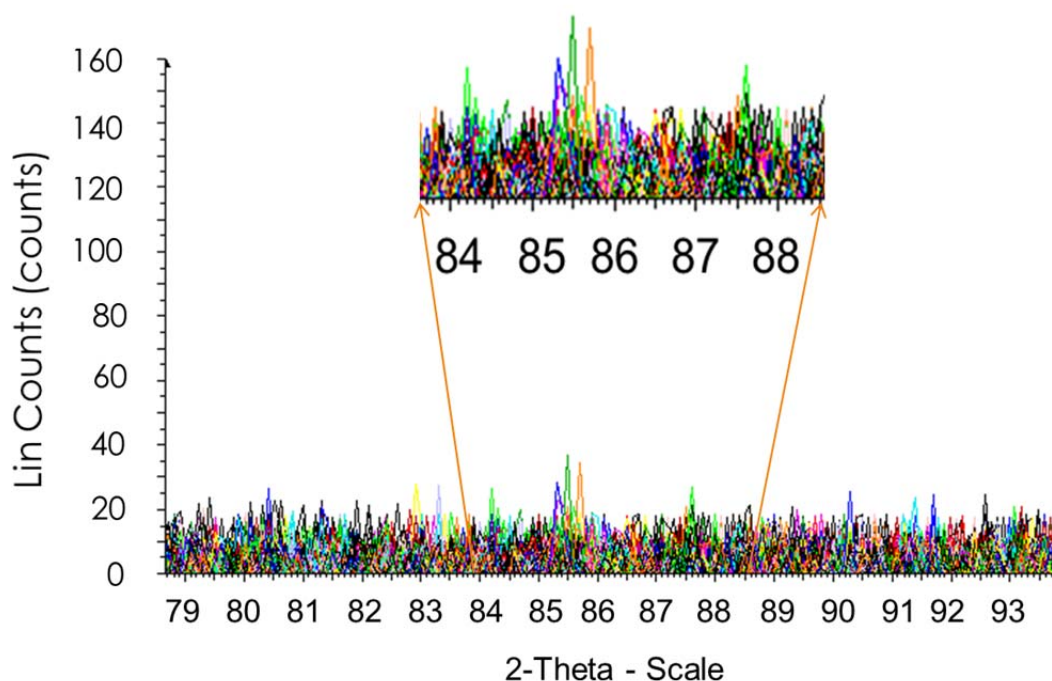


Figure 3-11: 400 Slices were applied to a weak peak in order to demonstrate the splicing of a peak into tiny sub domains that are barely visible over the background. Peak 4 Sample as in Figure 3-3.

3.5.3 Max Intensity Plot

The Max Intensity Plot Slice Integration Technique is a means to implement the Slice Integration Technique in an automated form. The automation of this process is the next step for this project as both semi-automated examples from a single phase and a multiphase have been shown to be effective.

All sliced patterns produced all peaks seen through visual inspection and, in this case, the pattern having the least number of slices that showed no visual distortion should be selected. The 70 slice pattern was chosen to be the preferred pattern for the multiphase example. Three phases were identified that would not have been identifiable without the MIP technique, Figure 3-12.

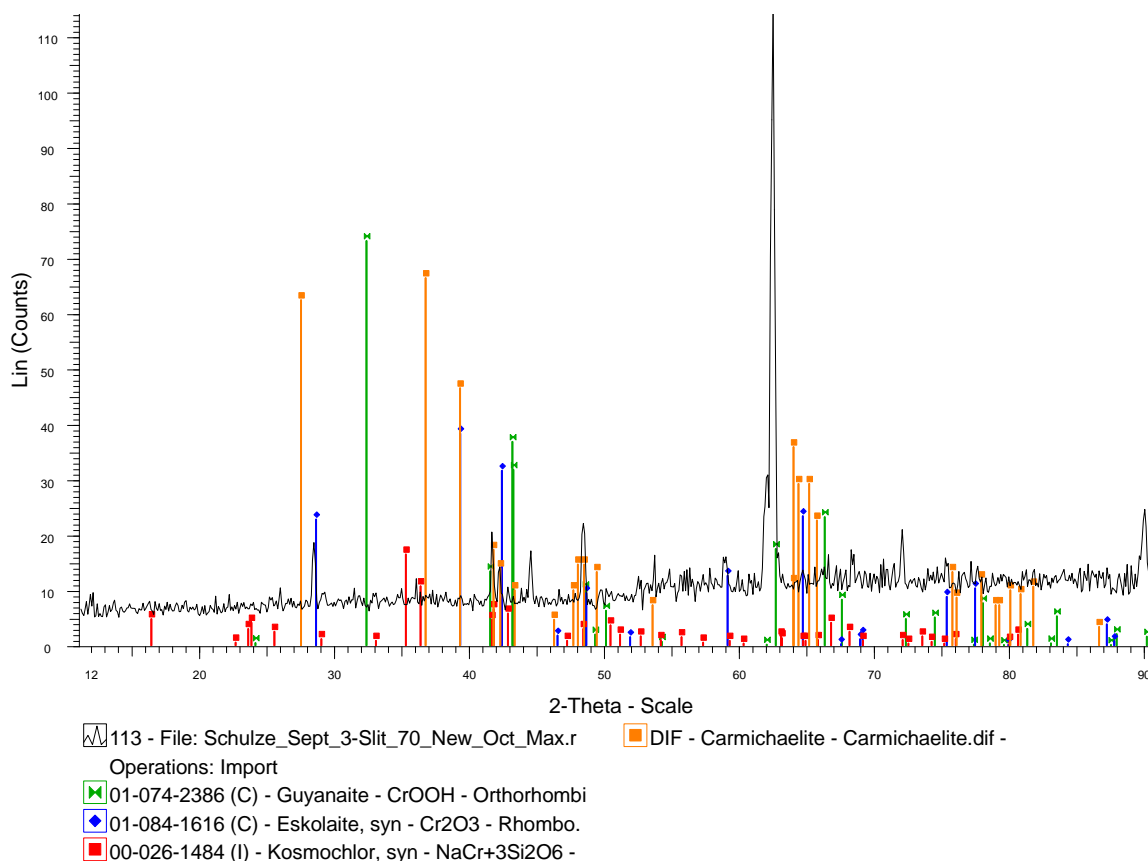


Figure 3-12: Schulze sample sliced 70 times showing three phases that were previously undetectable with only the single slice. Eskolaite, guyanaite and carmichaelite are all detectable phases.

3.6 Conclusions

The Slice Integration Technique is a simple and effective way to improve the signal-to-noise ratio in 2D XRD. This technique has improved peak intensity on the thirty slice data above background by 6.47% for the least

improved and 189% for the most improved compared to the single slice option (conventional full frame integration) using the addition method. (See Figure 3-6) Additionally, we have observed an improvement from a single visible peak in the 1D pattern to upwards of six peaks, making it now possible using the Max Intensity Plot method to identify samples that were previously unidentifiable.

Crossing the overslicing threshold of peaks can cause a problem that must be avoided, and can be easily identified through visual inspection by looking

for obvious distortions of the peak shape. Future work using the MIP technique may enable a rapid and automated method to determine the calibration of slices for XRD identification. The dramatic improvements in signal-to-noise ratio using the slicing technique developed here can enable the enhancement of existing data and recognition of new data on GADDS images, leading to additional phase-identification and crystal structural (i.e. unit cell) information from μ XRD data for a wide range of target materials.

Table 3-2: Peak Locations for addition method

Max Intensity Peak	Intensity			
Zero Merge 1			Zero Merge 50	
67.8	3.721921		Peak	
74.9	6.873275		67.8	14.38336
			74.9	131.0947
			85.5	20.02876
Zero Merge 2			Zero Merge 60	
Peak			Peak	
67.8	7.491467		67.8	20.05411
74.9	13.9424		74.9	396.6188
			85.5	23.5446
Zero Merge 10			Zero Merge 70	
Peak			Peak	
67.8	8.730936		67.8	20.88618
74.9	42.70143		74.9	250.8833
85.5	8.503182		85.3	17.31067
85.7	8.471775		85.5	16.38765
Zero Merge 20			Zero Merge 80	
Peak			Peak	
67.8	10.43472		67.8	22.19564
74.9	79.26569		74.9	224.2009
85.5	10.97974		85.5	25.71748
85.7	10.13855			
Zero Merge 30			Zero Merge 90	
Peak			Peak	
67.8	13.03245		67.8	27.59929
74.9	111.9708		74.9	324.2057
85.5	14.25529		85.5	27.97485
Zero Merge 40				
Peak				
67.8	16.18101			
74.9	117.4966			
85.5	16.65316			

Acknowledgements:

Dan Schulze for providing the guyanaite-containing mantle xenolith sample and Adrian Van Rythoven and Dan Schulze for providing the Diavik Diamond with its enclosed chromite inclusion. Dr. Rapheal Bahatti and Matt Izawa are thanked for their help with mathematical concepts Phil McCausland and Matt Izawa are thanked for reviewing versions of this paper.

3.7 References

Azároff, L.V. and Buerger, M.J. (1958) The powder method in X-ray crystallography McGraw-Hill, New York

Bramble, M.S., Flemming, R.L. and McCausland, P.J.A. (2014) Grain size measurement from two-dimensional micro-X-ray diffraction: Laboratory application of a radial integration technique. Submitted to American Mineralogist in Sept 2014.

Flemming, R.L. (2007) Micro X-ray diffraction (uXRD): a versatile technique for characterization of Earth and planetary materials. Canadian Journal of Earth Sciences, 9, 1333-1346

Izawa, M.R., Flemming, R.L., Banerjee, N.R. and McCausland, P.J. (2011) Micro-X-ray diffraction assessment of shock stage in enstatite chondrites. Meteoritics & Planetary Science, 5, 638-651

Izawa, M., Flemming, R., McCausland, P., Southam, G., Moser, D. and Barker, I. (2010) Multi-technique investigation reveals new mineral, chemical, and textural heterogeneity in the Tagish Lake C2 chondrite. Planetary and Space Science, 10, 1347-1364

Izawa M.R.M., Flemming, R.L., Banerjee, N.R. and Mateev, S. (2011) QUE 94204: A primitive enstatite achondrite produced by the partial melting of an E chondrite-like protolith. Meteoritics & Planetary Science, 11, 1742-1753

Jenkins, R. and Snyder, R.L. (1996) Introduction to X-ray powder diffractometry
Wiley, New York

Kourkouvelis, N. (2013) PowDLL, a reusable .NET component for interconverting
powder diffraction data: Recent developments. In L. O'Neil, Ed., ICDD Annual Spring
Meetings, p. 137

Co-Authorship Statement

I conducted the microXRD and refinements at Western University. The calibration data's chemistry was provided by Mineral Services Canada Inc. Dr. Flemming provided guidance and instrument training. This paper I wrote and I further developed the idea originally from Dr.Flemming. Editing and guidance on the writing of this paper was given by Matt Izawa and Dr.Flemming.

Chapter 4

4 The unit cell parameter a proxy for composition within defined terrains as applied to kimberlitic vs non-kimberlitic chromite

4.1 Executive Summary

Exploration for mineral deposits has long relied on indicator minerals to act as vectors to point the way to the next deposit. Spinel is one of the best known and most widely studying minerals due to its use in mineral exploration, as a resource and as a petrogenetic indicator. The unit cell parameter is a structural measure controlled by the sum of chemical substitutions within the crystal lattice. Therefore, under restricted conditions (e.g. binaries, low Fe^{3+} , low Ti^{4+}) it is possible to use the unit cell parameter as a proxy for composition. The conditions of formation will affect the order-disorder relationship meaning that understanding natural samples is required to understand the sorts of compositional restrictions mentioned above. Additionally, micro-XRD provides the potential for rapid discrimination with the correct configuration (2-8 min of XRD time). This study was undertaken to do an examination of the unit cells of natural kimberlitic and non-kimberlitic samples to look at the potential for its use within exploration.

4.2 Introduction

Spinel group minerals have the general formula AB_2O_4 , and display considerable chemical variability. Typical A cations include Mg^{2+} , Fe^{2+} , Zn^{2+} , Mn^{2+} , and typical B cations include Al^{3+} , Fe^{3+} , and Cr^{3+} . Cation ordering phenomena are important in spinels and lead to two general types of structure, termed normal and inverse. In normal spinel, the A cations are all located in tetrahedral sites and the B cations are all located in octahedral sites. In an inverse spinel, the B cations are evenly divided among the tetrahedral and octahedral sites (Hill et al. 1979) and the A and B cations share the octahedral site. Many spinel-group minerals occur in a range of intermediate ordering

states between fully normal and fully inverse (O'Neill and Navrotsky 1983). Chromite ($\text{Fe}^{2+}\text{Cr}_2\text{O}_4$) is a member of the spinel group, and is an important mineral in the petrogenesis of mafic and ultramafic rocks. Chromite is also economically important, both as an important carrier of chromium and platinum-group elements and as an important indicator mineral in diamond exploration. The chemical composition of chromite spinel is variable, with multiple possible substitutions among both A and B cations. Chromites from kimberlites have distinctive chemical signatures which have long been used in diamond exploration to search for diamondiferous kimberlites. Because the size of the chromite unit cell parameter (a_0) is determined in a large part by the identities of the A and B cations, the parameter a_0 may be a useful proxy for the chemical composition. In this study, we have explored variations in the chromite unit cell parameter within the compositional subspace $(\text{Fe}^{2+}, \text{Mg})[\text{Cr}, \text{Al}, \text{Fe}^{3+}, \text{Ti}]_2\text{O}_4$. Under some conditions (e.g. low Fe^{3+} , low Ti^{4+}), the relationship between unit cell dimension and crystal chemistry may enable crystal-structural measurements to be used as a proxy for the measurement of chemical composition.

The unit cell is the smallest defined repeating unit of a mineral that has the properties and symmetry of the mineral (Klein and Dutrow 2008). In general, as cations with larger or smaller ionic radii are substituted for each other, there is a concomitant expansion or shrinking the unit cell, as discussed by several researchers (Hill et al. 1979; O'Neill and Navrotsky 1983; O'Neill and Navrotsky 1983; O'Neill and Navrotsky 1983; Hamecher et al. 2013; Hamecher et al. 2013). Because structure determination by X-ray diffraction averages over many thousands of unit cells, order-disorder effects cause XRD-derived unit cell parameters to vary as a function of cation ordering (Hill et al. 1979; O'Neill and Navrotsky 1983). The unit cell parameter for spinel group minerals ranges from 8.080 Å to 8.536 Å and those of end-members relevant to this study range from 8.103 Å to 8.536 Å (Deer et al. 1992).

Kimberlite indicator minerals (KIMs) are used as a vector to find diamond deposits due to their relative stability and resistance to erosion that provides a larger footprint for exploration (McClenaghan and Kjarsgaard 2001). Chromite composition has been used for this purpose and through careful study, the chemical composition space for diamond-

associated chromites has been clearly defined (McClenaghan and Kjarsgaard 2001). This study builds on the work of (Freckelton and Flemming 2009), which found, on the basis of a unit cell parameter (a_0) of a chromite, that kimberlitic and non-kimberlitic chromite could be discriminated using bi-variant plots of chromite crystal-chemical and structural data from four sample locations. The XRD data of (Freckelton and Flemming 2009) were difficult to unambiguously interpret due to a beam overlap issue that resulted in multiple adjacent grains being sampled during each experiment.

This study has removed the overlap issue and used chromites from five localities with three kimberlitic and two non-kimberlitic sources. The data analysis was expanded from bi-variant to multi-variant plots, enabling direct comparison with well-established chemical plots used in exploration. This study is unable to discern a constant Cr trend with variable Mg (the non-KIM trend) from the KIM trends with varying Cr, which is an important discriminator for diamond exploration (Nowicki pers.comm. 2014). This limits the use of μ XRD to reconnaissance in known kimberlitic terrains; this method alone cannot perform KIM vs non-KIM discrimination.

4.3 Methods

4.3.1 Samples

Samples were collected from three kimberlites and two non-kimberlite localities. The kimberlites were from Misery, Koala and Sheiba (Ekati, Slave Province, NWT) (Nowicki et al. 2004; Gurney et al. 2004). Grains were already mounted in epoxy and were supplied together with the compositional data. The non-kimberlites were from stream sediments (Gabon, Africa) and soil sediments (Matsitami/Tutume, Botswana) (Nowicki pers.comm. 2014). Table 1: Sample Summary, summarizes localities and the number of grains sampled. The average grain size was ~ 300 microns with an average spacing of 200-300 microns between grains on the probe mount. There was a random sampling of euhedral and sub-euhedral grains with textures varying from pitted to smooth.

Table 4-1: Grains and Sample Locations				
Sample	Disc	Locality	No. of Grains Successfully Refined	No. of Grains attempted.
MSL04/0095PM	1	Gabon	19	27
WO02/048PM	3	Koala	18	28
WO02/084PM	3	Sheiba	10	12
WO03/058PM	8	Misery	19	27
WO00/062PU	3	Matsitami/ Tutume	12	21

4.3.2 Major Elements

Major element chemistry was provided by Mineral Services Canada Inc. (North Vancouver, BC) for Koala, Sheiba, Gabon, and Misery samples. They were performed using a LEO 1450 Scanning Electron Microscope (SEM) using combined energy dispersive (EDS) and wave-length dispersive (WDS) spectrometry (Oxford Instruments spectrometers). ED spectrometry was used for the determination of the relevant major and minor elements and were performed at an operating voltage of 20 kV and a beam current of 30 nA. Live counting times for standard quality EDS analyses are 60 seconds and detection limits are approximately 0.01 wt%. Kimberlite indicator minerals with compositions similar to the unknowns are used as standards in most cases and concentrations used in-house natural silicate and oxide mineral standards.

4.3.3 MicroXRD

A Bruker D8 Discover Micro X-ray Diffractometer (μ XRD) at the University of Western Ontario was used to obtain structural information *in-situ* for the purposes of this study (Figure 4-1). It is configured with a $\text{CoK}\alpha$ source ($\lambda = 1.79026 \text{ \AA}$) and was run at 35 kV and 45 mA. The X-ray beam was collimated to a nominal 100 μm diameter to interrogate individual grains mounted close together in an epoxy puck.

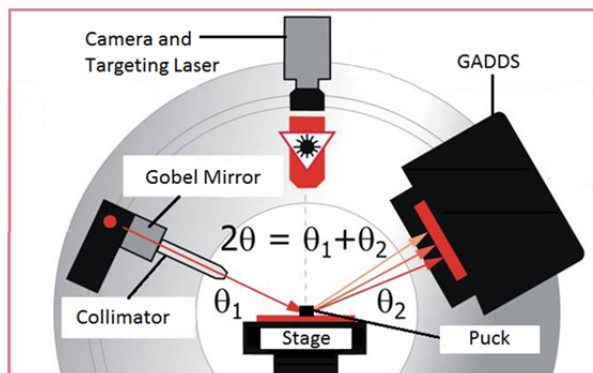


Figure 4-1: Bruker D8 Discover configuration. AXS modified Shepherd 2014 (Modified from Bruker AXS)

Detection was performed using a 2-dimensional Hi-Star detector with General Area Detector Diffraction

System (GADDS) software placed at a detection distance of 12 cm from the sample, resulting in a resolution of 0.04-0.05 degrees per step. The 2-D detector enables measurement of diffracted X-ray intensity as a function of both the Bragg angle (2θ) and along the arc of the Debye rings (denoted χ), as shown in Figure 4-2. This detector distance allowed us to interrogate 41 degrees of 2θ per frame. The scans were acquired using the Bruker Omega scan method, which maintains a constant 2θ by rotating the source (θ_1) and detector (θ_2) around a sample in the same direction (clockwise) through an omega angle (ω). Rotating the detector and source keeping 2θ constant allows the interrogation of a stationary sample by enabling more lattice planes to intersect Ewald's sphere and satisfy Bragg's law. The best parameters for the first frame were: $\theta_1 = 16.0^\circ$, $\theta_2 = 40.0^\circ$ and $\omega = 37.5^\circ$, for the second frame: $\theta_1 = 45.5^\circ$, $\theta_2 = 40.0^\circ$ and $\omega = 7.5^\circ$, where $\theta_1 + \theta_2 = 2\theta$ and each frame was run for 1 hour. The best parameters were determined by empirical trial and error, to maximize the number of lattice plans that satisfied Bragg's law.

A limited number of lattice planes will satisfy Bragg's Law at any point through the scan, which results in a reduced number of lattice planes, as compared to a powder pattern. This limitation combined with the low intensity of peaks, due to poor detection of diffracted rays (because of the relatively low X-ray intensity through the 100 μm pinhole collimator snout), in combination with high X-ray absorption by chromite, required the application of a simple Slice Integration Technique; see Chapter 3 for full process details. The raw 2D GADDS

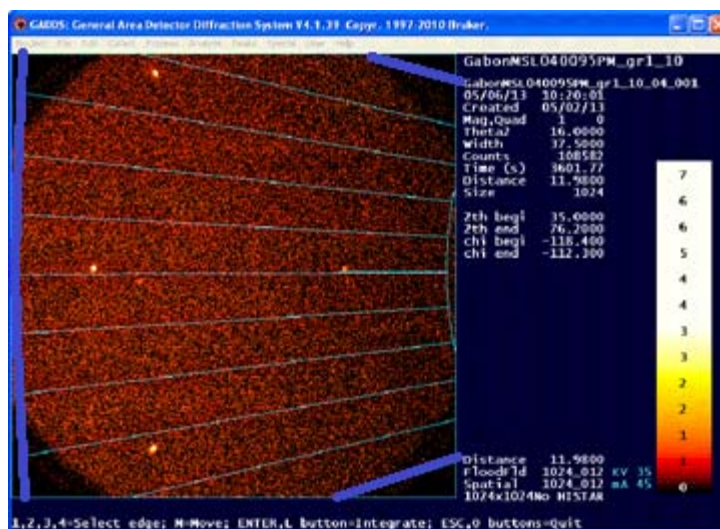


Figure 4-2: Conventional vs Slice Integration. The traditional integration method will integrate the area over the entire frame (thick blue lines) while the slice integration technique subdivides the area of the X-ray detector (seen by the area defined by thin blue lines) to obtain a better signal.

images were integrated along $x^\circ\chi$ slices to produce a series of one-dimensional diffraction patterns of intensity versus 2θ , as can be seen in Figure 4-2. Each slice of the series was searched for peaks and the peaks were used together to define a single *.dif for the conventional 1D-XRD pattern, as can be seen in Figure 4-3. In cases where peaks appeared in multiple frames of the series, the most intense peaks were used for the final pattern. After the process, it was possible to get peaks of sufficient intensity to enable refinement of the unit cell parameters to within acceptable uncertainties ($\sim 0.005 \text{ \AA}$).

The unit cell refinement was completed using the software CELREF employing a non-linear least squares approach (Altermatt and Brown 1987). The program utilizes the user-selected crystal system, space group and starting value for the unit cell parameter a_0 , to calculate all possible diffraction peaks. Then, using the *.dif file created by collection of peaks from the Slice Integration Technique previously described, the observed diffraction peaks can be indexed based on the user-provided information. The unit cell is then

refined, based on least squares refinement of the indexed peaks. All refined unit cells were successfully refined to below acceptable uncertainties (~ 0.005 Å)

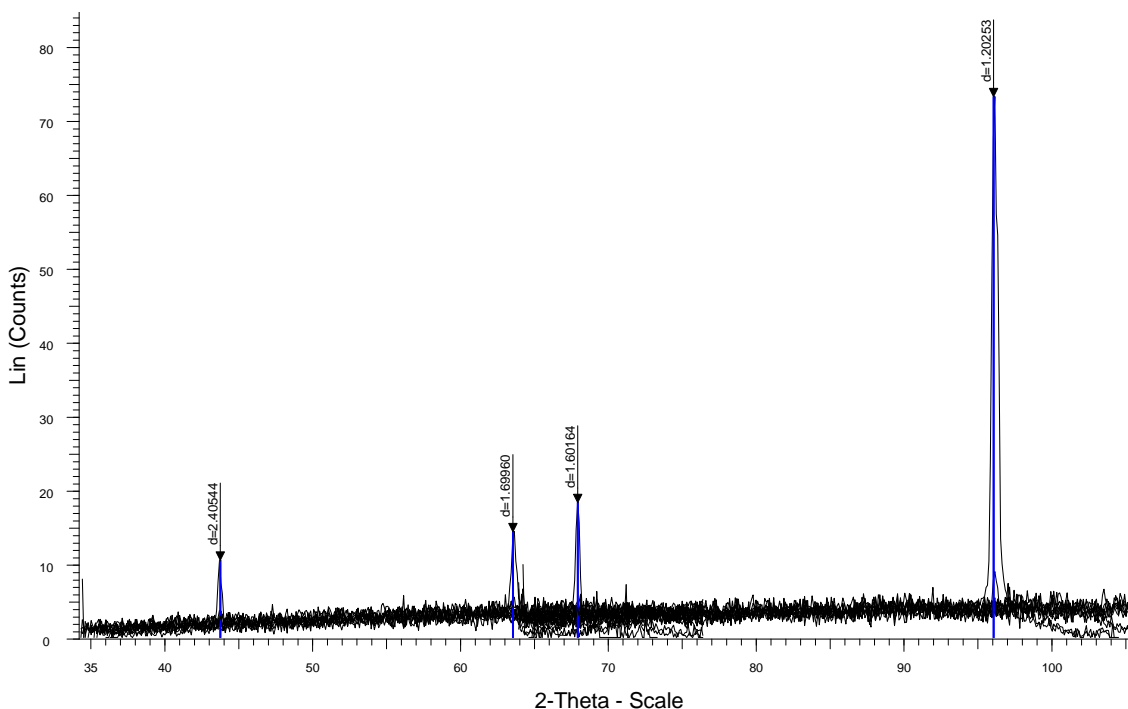


Figure 4-3: 1D *.dif pattern (blue sticks) for use in unit cell refinement after slicing method has been performed. W0062_Disc_3 Slice 1-10 for Frame 1 /2

4.4 Results

4.4.1 Overview

This study focused on the effects of six chemical components, five of which were measured directly: TiO_2 , Al_2O_3 , Cr_2O_3 , FeO , and MgO ; these data have been summarized in Appendix B. The sixth and seventh components, Fe_2O_3 , and FeO were approximated from the Fe (total) content measured along with the major element chemistry by using stoichiometric considerations following the methods described by Droop (1987). The SEM WDS data were supplied as weight percent oxides and subsequently have been converted to atoms per formula unit (apfu). This enabled us to investigate changes in unit cell parameter as a net effect of all substitutions at the various cation sites, and also to relate our results to previous compositional work using conventional exploration plots.

These data demonstrate extensive solid solution in the spread between relevant end-members. In Figure 4-4 a/b, two spinel prisms are displayed where Cr-Al-Fe³⁺ and Cr-Al-Ti are plotted on the ternary ends of the prism and the base and side panels of the spinel prism are plotted as the ratios Fe/(Fe+Mg), Cr/(Cr+Al), and Fe³⁺/(Fe³⁺+Al+Cr) in Figure 4-5a/b and Figure 4-6a/b as seen in Roeder and Schulze (2008) and Barnes and Roeder (2001).

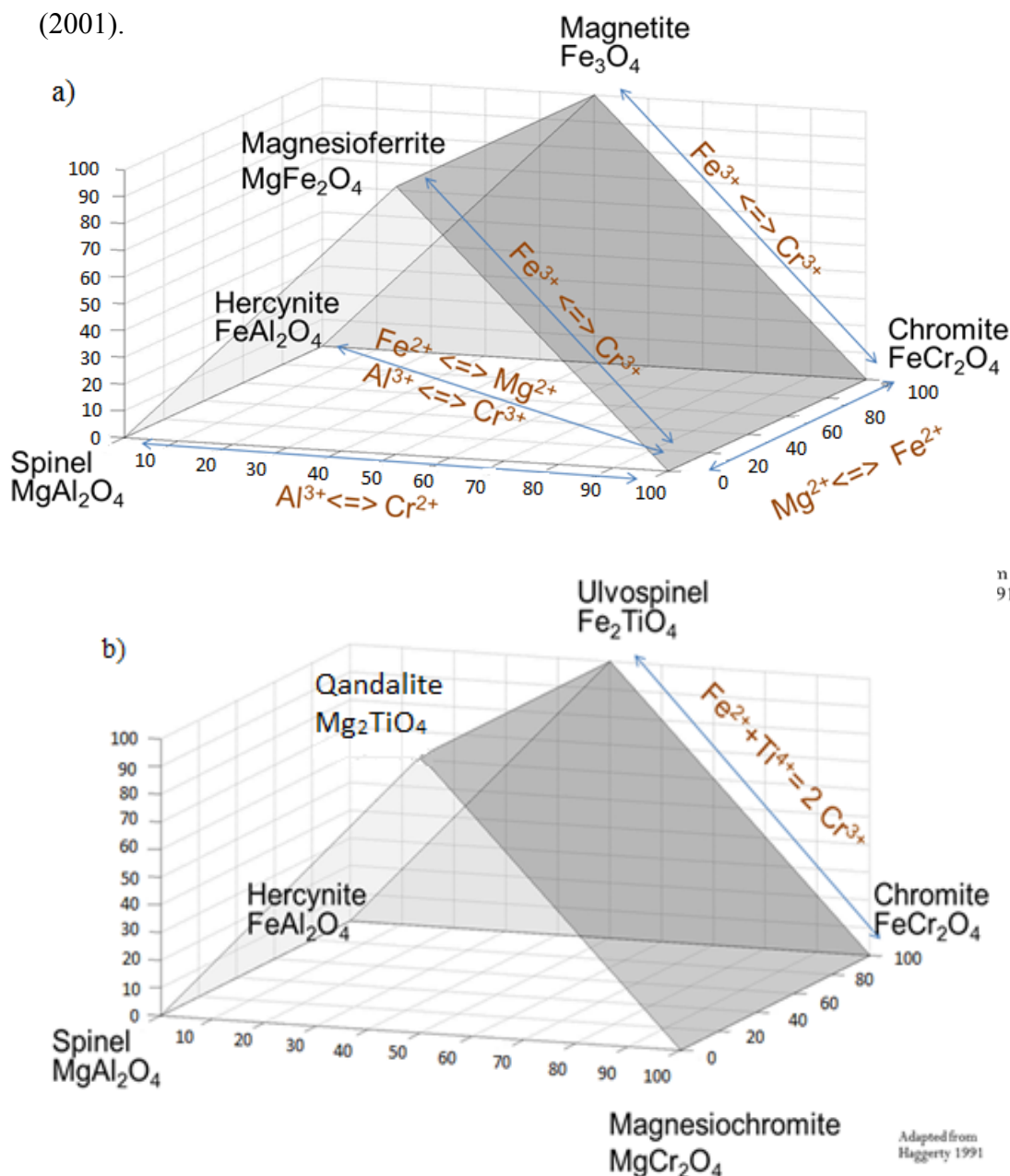


Figure 4-4. The spinel prism. a) Trivalent prism showing the chemical substitution relationships between end members; b) Divalent prism showing the primary relationships seen within our data.

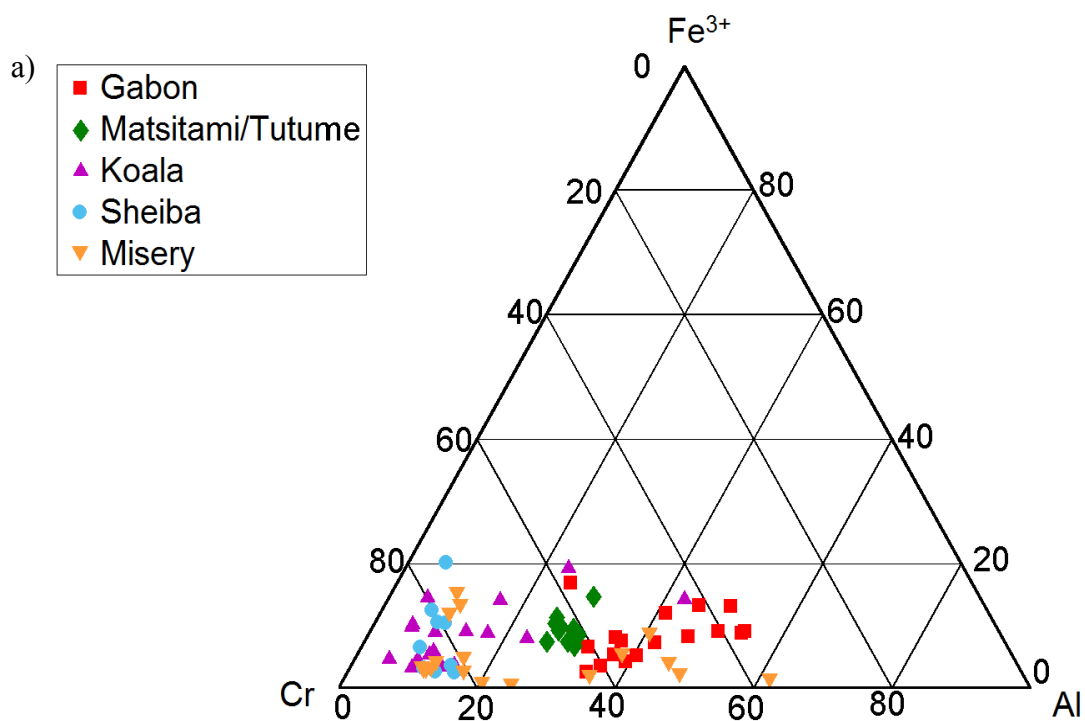
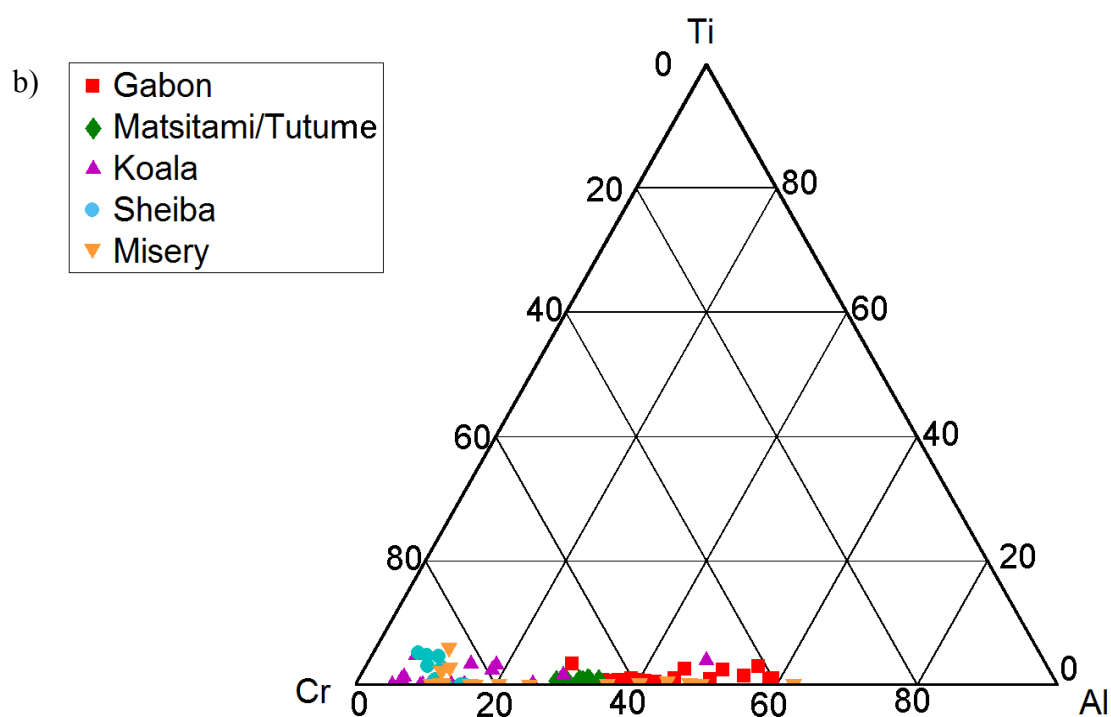


Figure 4-5: Prism Face projections. a) Cr vs Fe^{3+} vs Al plot showing the end projection of the trivalent spinel prism. There is considerable Fe^{3+} in the system, as compared with Ti, as shown in b) the end projection of the divalent prism.



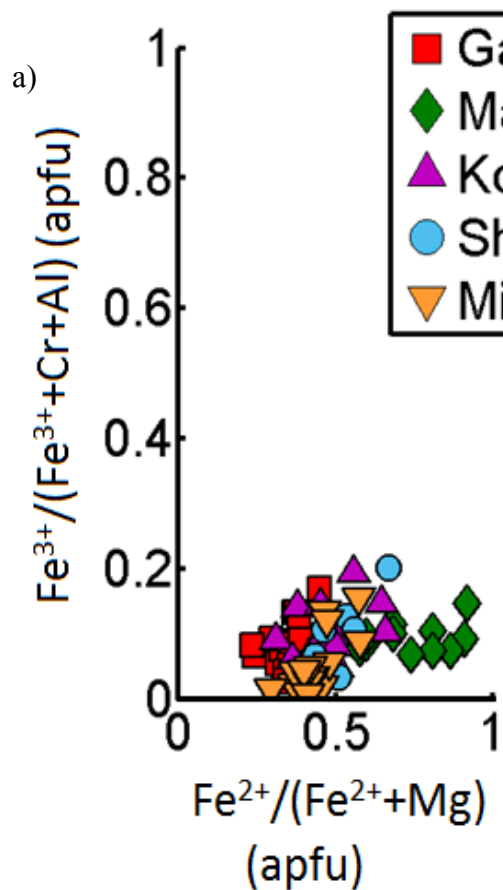
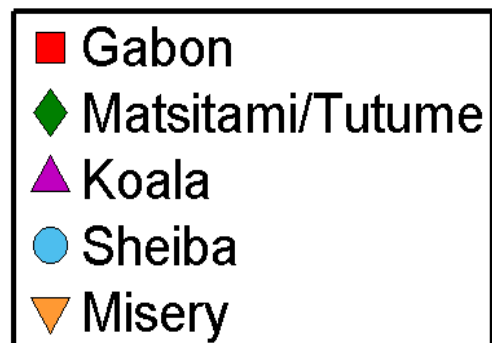
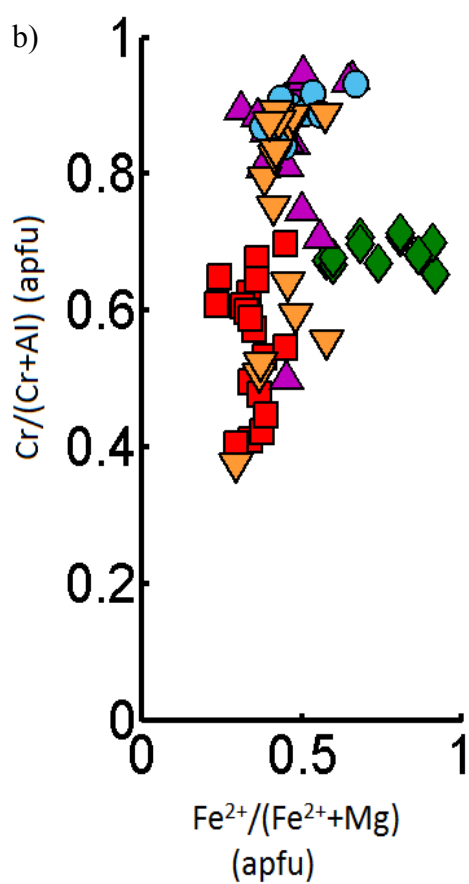


Figure 4-6: The side projection of the prism a) $\text{Fe}/\text{Fe}+\text{Mg}$ versus $\text{Fe}^{3+}/(\text{Fe}^{3+}+\text{Al}+\text{Cr})$ and b) the base of the prism $\text{Fe}^{2+}/(\text{Mg}+\text{Fe}^{2+})$ versus $\text{Cr}/(\text{Cr}+\text{Al})$



The three most common plots employed for discrimination between kimberlite and non-kimberlite minerals in diamond exploration are: Cr_2O_3 vs MgO , TiO_2 vs Cr_2O_3 , and Al_2O_3 vs Cr_2O_3 and Figure 4-7 a/b/c show our data using three common discrimination plots (McClenaghan and Kjarsgaard 2001). Several grains plotted within the diamond inclusion field. On average, non-kimberlitic chromites were 42.3 wt.% Cr_2O_3 compared with 54.6 wt.% Cr_2O_3 for kimberlitic chromites.

4.4.2 Micro X-ray Diffraction as applied to unit cell parameter and textural information

The unit cell parameters were calculated using least-squares refinement and were only deemed acceptable if the error was less than 0.005 Å, as shown in Appendix E: Unit Cells. The error was not reported for the chemical data as supplied by the company. The errors introduced by diffraction data are an order of magnitude less than the errors of the refinement. The errors therefore were based on least-squares refinement and not based on instrument error. Many samples showed an insufficient number of peaks in the XRD diffraction patterns for the unit cell to be refined; approximately 68% of samples were successfully refined. The successfully refined grains showed a cubic symmetry and matched well with various ICDD cards for spinel group minerals. There was no strong evidence for multiple phases in the X-ray diffraction pattern, although previous SEM work from Freckelton and Flemming (2009) showed some zonation. This was not considered to be a problem as non-chromite peaks were not visible. Any additional phases appeared texturally distinct. Some grains did show streaks in the 2D GADDs image along the Debye rings (χ), indicating strain in the chromite grain. It is worth noting that the unit cell parameter is a single value, the size of which is determined by the sum total of all of the chemical elements inside the spinel structure. There are competing effects on the size of the unit cell from different chemical substitutions, which can lead to ambiguity in the interpretation of unit cell size in terms of causal relationships. Correlations between the amount of any chemical element and the unit cell parameter do not necessarily represent causation. However, some generalities should be kept in mind. Volume modeling (Hamecher et al. 2013) has shown the calculated spinel volume to be

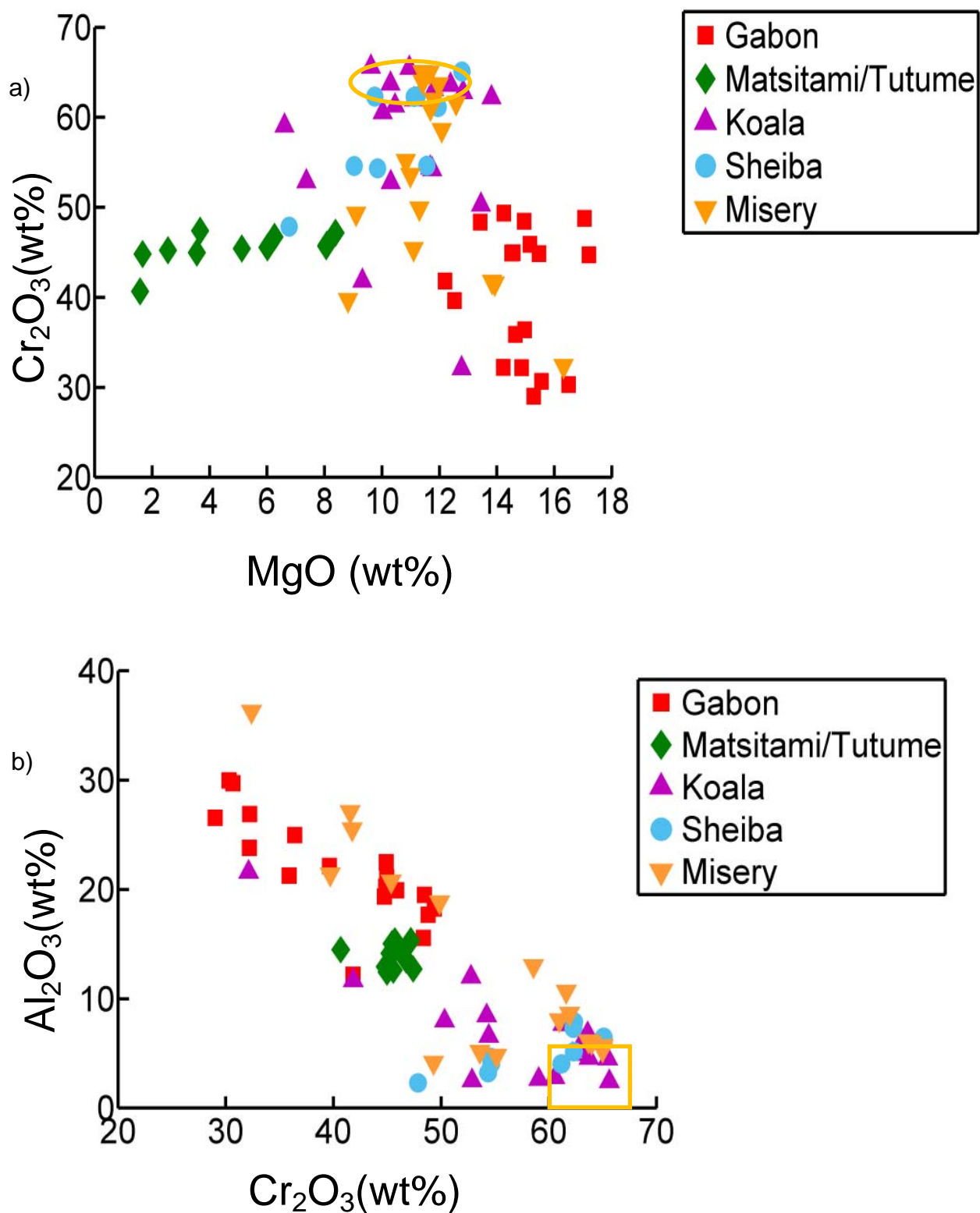


Figure 4-7: Common chromite discrimination diagrams a) MgO vs Cr_2O_3 b) Cr_2O_3 vs Al_2O_3 . See Page 69 for complete caption

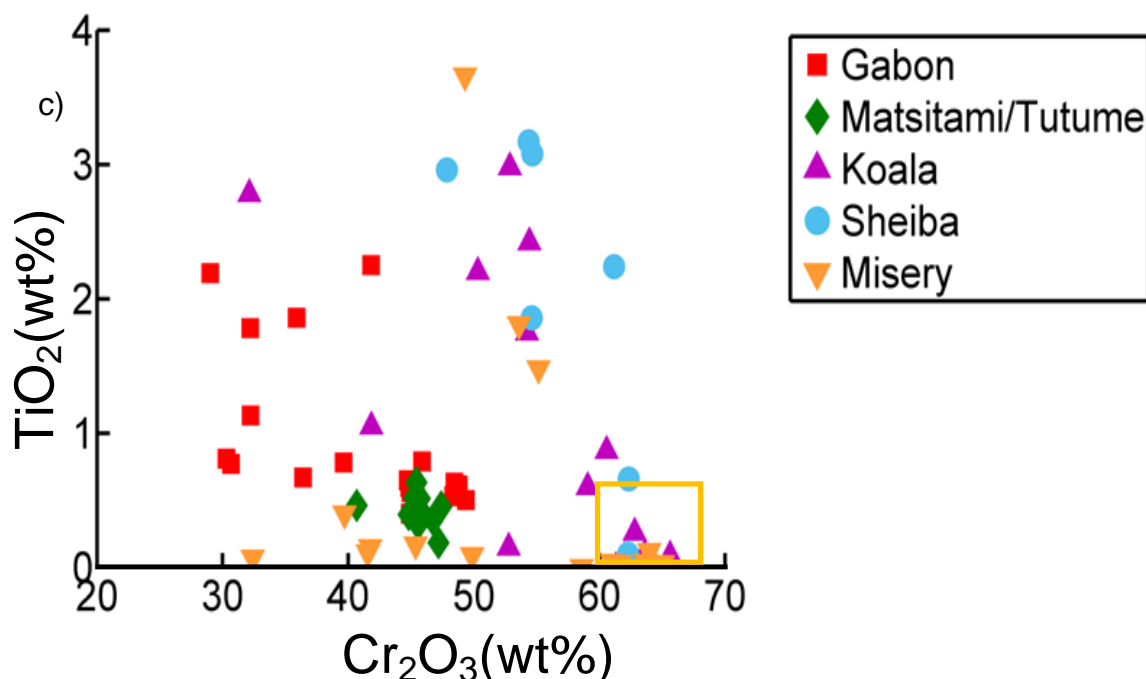


Figure 4-7 : Common discrimination plots used for diamond exploration. a) MgO vs Cr_2O_3 . The constant Cr with varying Mg is a classic example of a non-kimberlite (Nowicki et al. 2004) (e.g. The positive Cr trend with increasing Mg is known as the phenocryst trend (Roeder, 2001), The negative Cr trend with increasing Mg is known as the xenocryst trend. Between 10 and 12% Mg and greater than 61 wt% Cr is known as the diamond inclusion field (~Orange Field). B) TiO_2 vs Cr_2O_3 . The diamond inclusion field can be found in the >61 wt% Cr (McClenaghan 2001) (~Orange Field). C) the diamond inclusion field in the Cr_2O_3 vs Al_2O_3 plots >61 wt% Cr and <8 wt% Al_2O_3 (~Orange Field).

about twice as sensitive to the M–O distance as to the T–O distance. Thus we would expect cation substitution on the octahedral site (M–O) to show a more pronounced effect than cation substitution on the tetrahedral site (T–O). This is consistent with our observations below, where Al–Cr substitution on the octahedral site is correlated with a more pronounced trend in unit cell size, while Fe–Mg substitution on the tetrahedral site has a less pronounced effect on the unit cell parameter.

Furthermore, order-disorder between cations of different ionic size, charge, and coordination environment can have a significant effect on unit cell size (O'Neil and Navrotsky 1983; Hazen and Navrotsky 1996; Hazen and Yang 1999). This will further perturb the observed unit cell. This is likely causing some of the scatter in the data below.

4.4.3 Unit Cell and Composition Correlations

4.4.3.1 Unit Cell vs. Octahedral Site Cations

In our samples, Cr^{3+} and Al^{3+} cations are the predominant substituents in the octahedral sites. In general, an increase in Cr^{3+} (0.615 Å) results in a larger unit cell parameter; in contrast, increasing Al^{3+} (0.53 Å) results in a smaller unit cell parameter (Figure 4-8 a/b) (Radii from (O'Neill and Navrotsky 1983)). It should be noted that for all figures of composition vs the unit cell parameter it is the general trend within all sample location that is more important than what sub-populations are doing. Although Ti^{4+} (0.60 Å) also substitutes into octahedral sites, the Ti concentrations in the chromite samples investigated were insufficient to create significant trends. There is significant scatter of the data from the trendline for Cr, Figure 4-8a. This is due, in part, to other compositional effects of the four major end members: hercynite, spinel, magnesiochromite and chromite, but it is also a product of spreading in the data toward the ulvöspinel, magnesioferrite and magnetite, which have large unit cells, due to the cations having large radii ($\text{Ti} = 0.60$ Å, $\text{Fe}^{3+} = 0.645$ Å, $\text{Fe}^{2+} = 0.74$ Å, $\text{Mn} = 0.80$ Å (galaxite), radii from O'Neill and Navrotsky (1983) and so substitution of these elements clearly will increase the unit cell parameter even when in small quantities. Some scatter may also be caused by order-disorder effects between cations of differing coordination environment (O'Neill and Navrotsky 1983; Hamecher et al. 2013; Hazen and Navrotsky 1996). Figure 4-9 shows the unit cell parameter increasing with increasing Fe^{3+} content but there is significant scatter. This could be due to the minimal Fe^{3+} in the system and the stronger influence of Al-Cr substitution on the unit cell parameter. This is likely not due to Fe^{2+} - Fe^{3+} order-disorder because this has been previously reported that Fe^{3+} does not occupy the tetrahedral site at low concentrations of ferric iron end member (Osborne et al. 1981; Chen et al. 1992; Lenaz and Lughi 2013). However, Fe is reported to be sensitive to next nearest neighbor (NNN) chemical substitution (Chen et al. 1992).

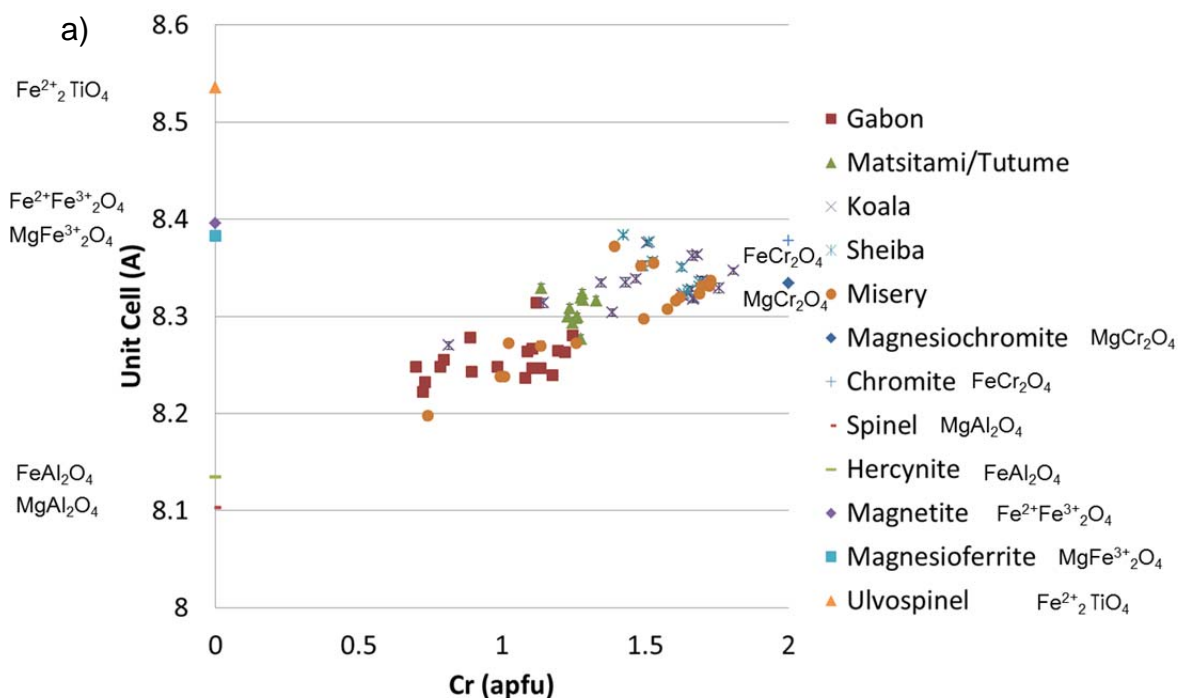
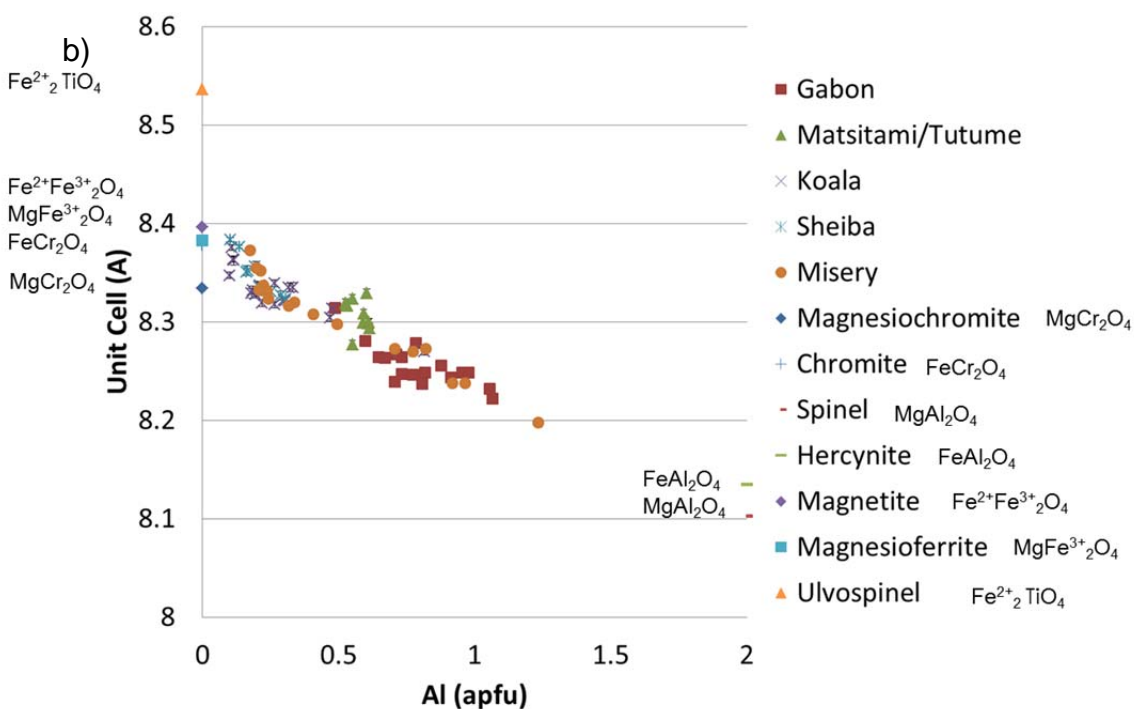


Figure 4-8. Unit cell vs. B cation. a) Unit cell vs Cr plot, showing increasing unit cell with Cr because it is large relative to Al; b) the converse relationship occurs with Al due to its smaller size relative to Cr.



Aluminous end members have unit cells which are closer in size to each other than the equivalent chromian end members; this leads to greatly reduced scatter in the Al plot, which suggests the potential use of unit cell as a proxy for Al content in low-Ti spinels, Figure 4-8 (b).

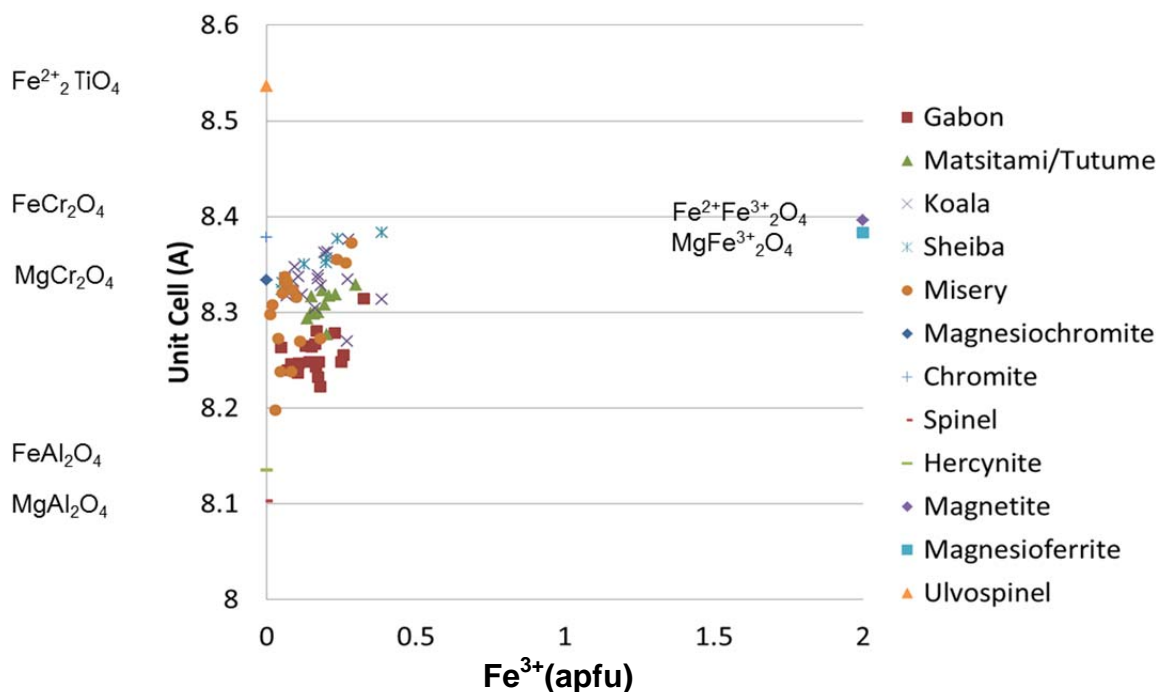


Figure 4-9: Unit cell vs. Fe^{3+} . Fe^{3+} shows a loosely increasing correlation with unit cell size

4.4.3.2 Unit Cell vs. Tetrahedral Site Cations

The tetrahedral site in normal spinel is commonly filled with Mg^{2+} (0.585 Å) and Fe^{2+} (0.615 Å). The $\text{Fe}^{3+}/\text{Fe}^{2+}$ ratio was determined from the chemical analyses (with all Fe reported as wt.% FeO) by using the Droop method (Droop 1987), which assumes full site occupancy and that Fe is the only polyvalent element; these assumptions are reasonable for most situations. Figure 4-10a shows Fe_{tot} compared to the unit cell parameter. As Fe^{2+} is increased, Figure 4-10b, there is an increase in unit cell size. The opposite relationship is seen with Mg^{2+} and the unit cell parameter Figure 4-11 where, as Mg^{2+} increases the unit cell shrinks. This relationship is expected from cation size, as the smaller Mg^{2+}

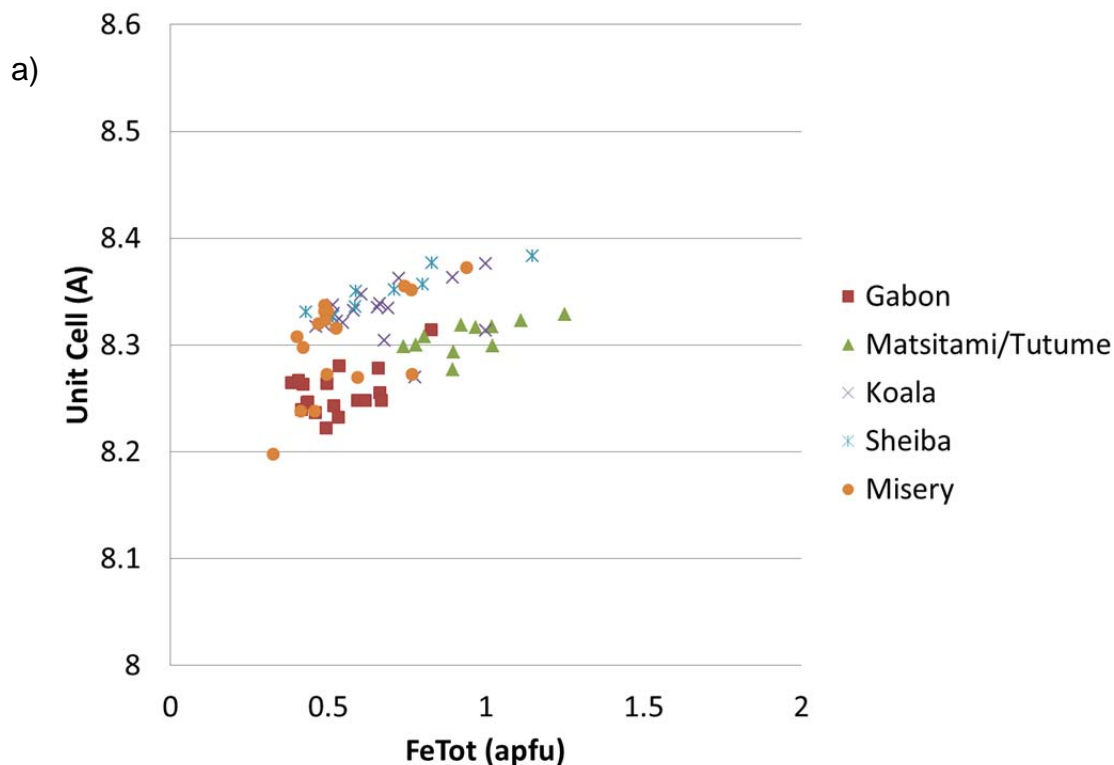
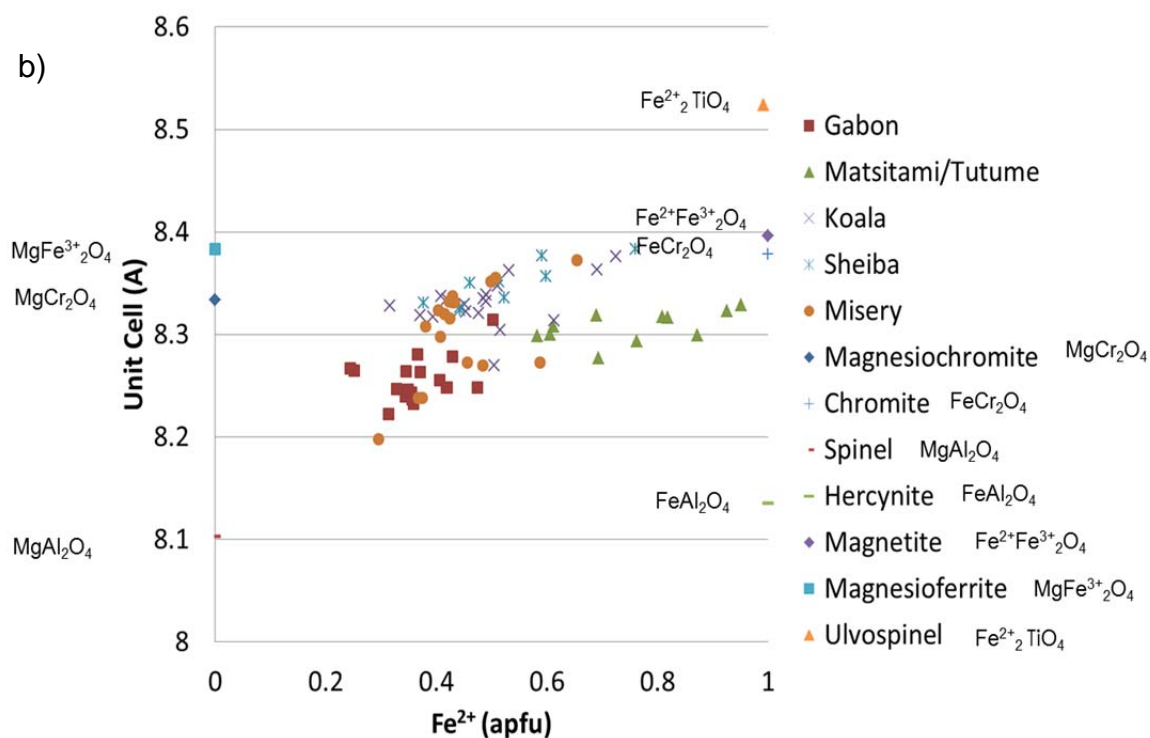


Figure 4-10. Unit cell vs A cation (and Fe total). a) The unit cell vs Fe_{tot} plot shows a clear separation of two populations due to the Cr-Al substitution in addition to the Fe^{3+} in the system. b) Unit cell shows a clear positive trend with Fe^{2+} and is a mirror image of Mg.



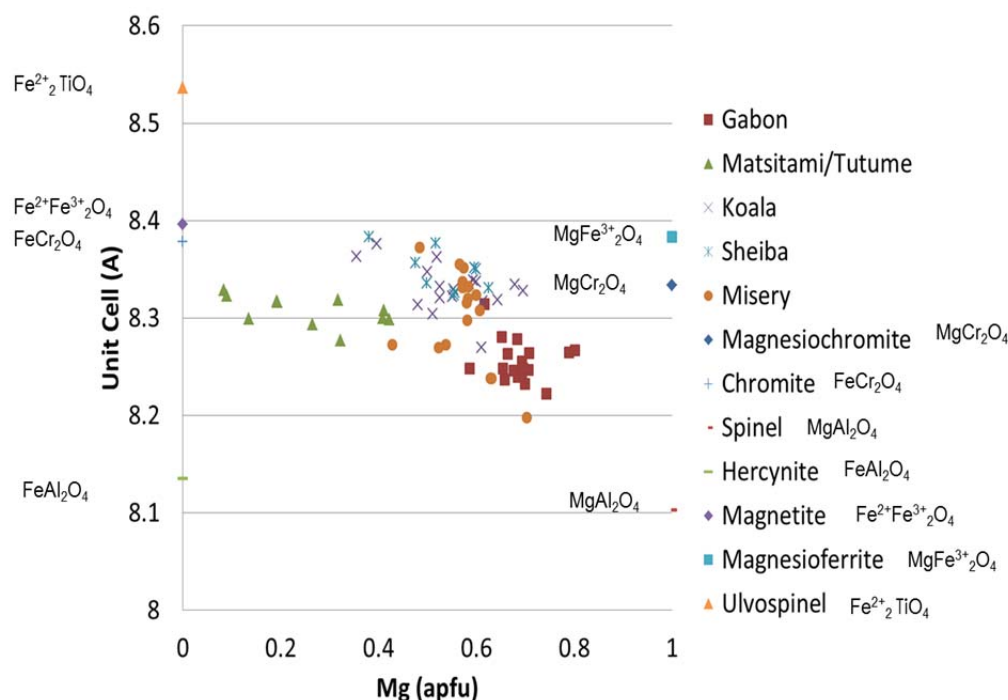


Figure 4-11: Unit cell vs A cation. Unit cell decreases with increased Mg, which substitutes for Fe^{2+} .

cation (0.585 \AA) substitutes for the larger Fe^{2+} cation (0.615 \AA), in the tetrahedral site in normal spinels (Figure 4-11). As with the octahedral site, some of the scatter is due to composition of the relevant end members for the element being analyzed but also due to other cation substitutions. This is most clearly seen in Fe_{tot} , Figure 4-10 (a), where two distinct populations can be seen, primarily separated by the Cr-Al content, with the upper trend being Cr-rich spinels (ie magnesiochromite to chromite) while the lower trend is Al-rich spinels (ie spinel to hercynite).

4.4.4 Unit Cell Parameter in Reference to End-member Spinel

The unit cell parameter data have been superimposed onto compositional data on the faces of the spinel prism, and this shows the change in unit cell as a function of composition between end members. The smallest unit cells are associated with spinel (*sensu stricto*), MgAl_2O_4 , having Mg^{2+} (0.585 Å) and Al^{3+} (0.53 Å). The largest unit cells are associated with magnesiochromite, MgFe_2O_4 ; this is due to Fe^{2+} (0.615 Å) and Cr^{3+} (0.615 Å) being relatively large. The base of the prism is composed of normal spinel-group minerals: hercynite, chromite, magnesiochromite, and spinel. The first three are completely normal but spinel is 7% inverse (Hill and Roeder 1974). The top of the prism is defined by inverse spinel-group minerals, with ulvöspinel being 100% inverse and magnesioferrite being 90% inverse (Haggerty 1986).

4.4.4.1 Ternary Element Plots—Prism Faces

The trivalent prism, as seen in Figure 4-4(a) is defined by the Fe^{3+} on the vertical axis and the divalent prism is defined by the Ti^{4+} , as seen in Figure 4-4(b). Considering the ternary of the spinel prism enables a better understanding of how unit cell becomes affected by multiple substitutions at once. As a general measure of composition it is critical to understand how these relationships work in the natural environment and simultaneous to each other, as only through this understanding can we reduce ambiguity. Figure 4-12a shows the ternary projection of the elements controlling the prism of the oxidized trivalent prism. The most obvious driver of the unit cell parameter in this view is the Cr-Al relationship, but the unit cell parameter does increase slightly with increased Fe^{3+} . Figure 4-12b shows the relationship between Cr-Al-Ti but due to the paucity of Ti in the system it is difficult to discern a trend.

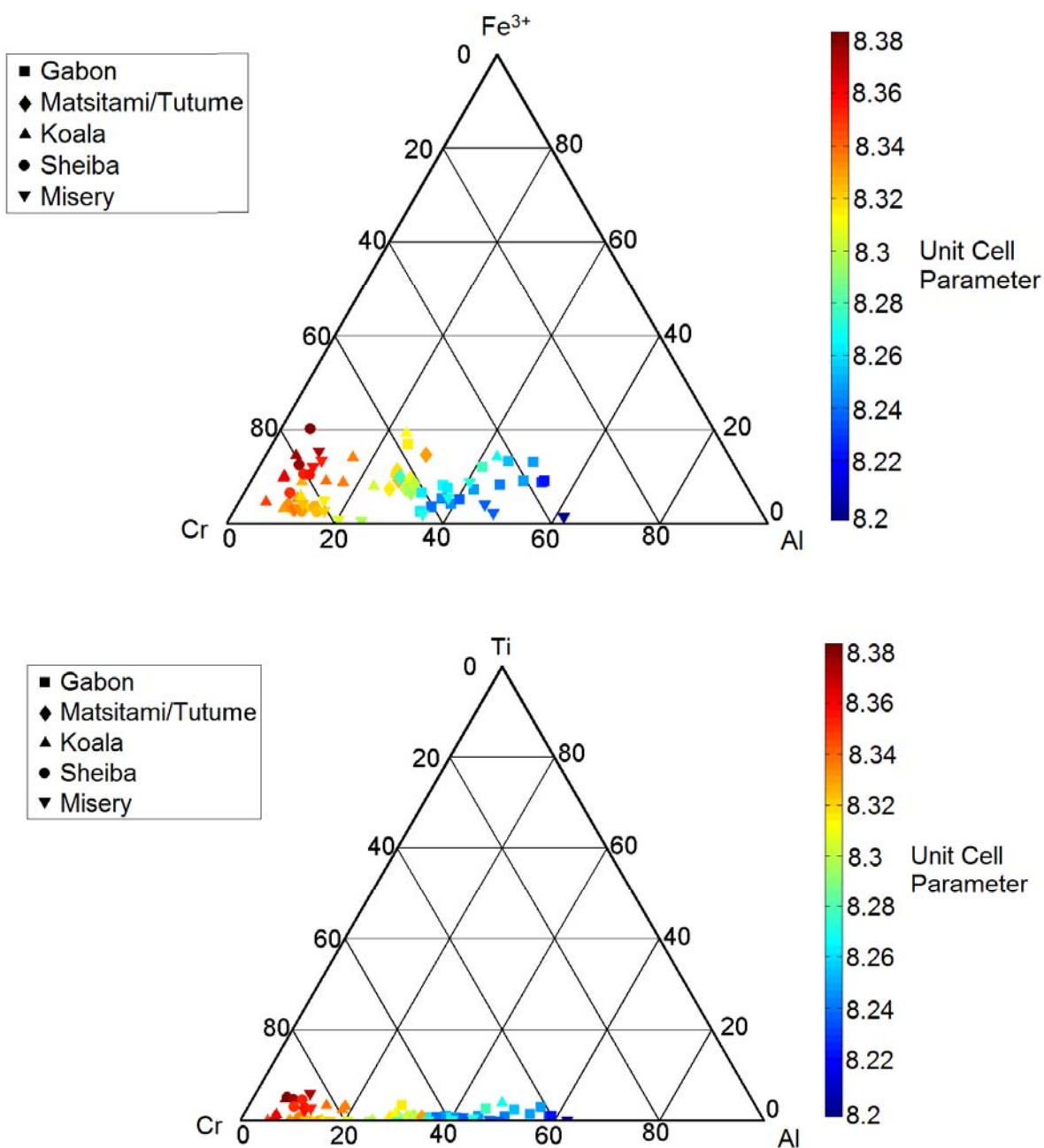


Figure 4-12. Ternary projections. a) This plot shows the relationship between Cr, Al, Fe³⁺ and unit cell. There is a clear increase in unit cell size with increasing Cr (and decreasing Al); a slight increase in unit cell can be observed toward Fe³⁺. **b)** This plot shows the relationship between Cr, Al, Ti and unit cell. There is minimal Ti in our data set. Plotting software adapted from (Sandrock, 2002).

4.4.4.2 Trivalent Plot Sides / Divalent Plot Sides

Some data did spread upwards toward the magnesioferrite and magnetite end members, as can be seen on the side view of the prism in Figure 4-13. A slight spread toward the ulvöspinel (Fe_2TiO_4) may exist, but there was only a small amount of Ti. It is worth noting Fe^{3+} and Ti often are linked since Ti has a greater ability to partition in magnetite (Barnes and Roeder 2001). It is important that there be minimal Fe^{3+} and Ti^{4+} in the samples, when deciding on populations to attempt using the unit cell parameter as a compositional proxy, because order-disorder relationships will lead to scattering. When greater proportions of end-member inverse spinels are included in the system, the data become more scattered. This could be due to cation order-disorder (O'Neill and Navrotsky 1983).

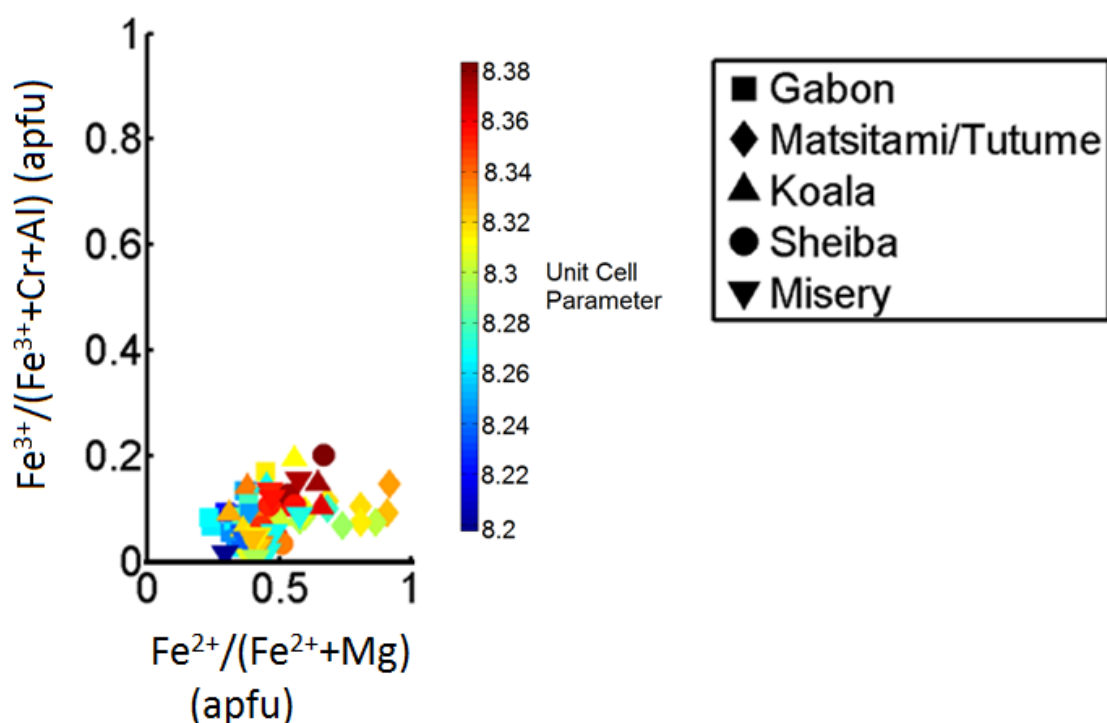


Figure 4-13: Side view of spinel prism that emphasizes the importance of a constrained system when using unit cell as a proxy for composition. (Note: Fe^{2+} and Fe^{3+} are calculated values.)

4.4.4.3 Prism Base

The base of the prism, Figure 4-14, shows the clear spread from spinel through to chromite, with increasing unit cell size toward the chromite. A limitation of unit cell as a chemical proxy in spinel group minerals is illustrated by the Matsitami/Tutume series where the more Fe-rich end members provide similar unit cells to a subset of Cr-rich grains with lower Fe. The spinel gap described by Barnes and Roeder (2001) will limit the number of possible overlaps but will not eliminate the issue entirely. This can be most easily seen in the base of the spinel prism which is common to both the divalent and trivalent prisms as seen below. The utility of using unit cell as a proxy is caused by the substitution of Cr^{3+} (0.615Å) for Al^{3+} (0.53Å) and, as the larger ionic radius atom is

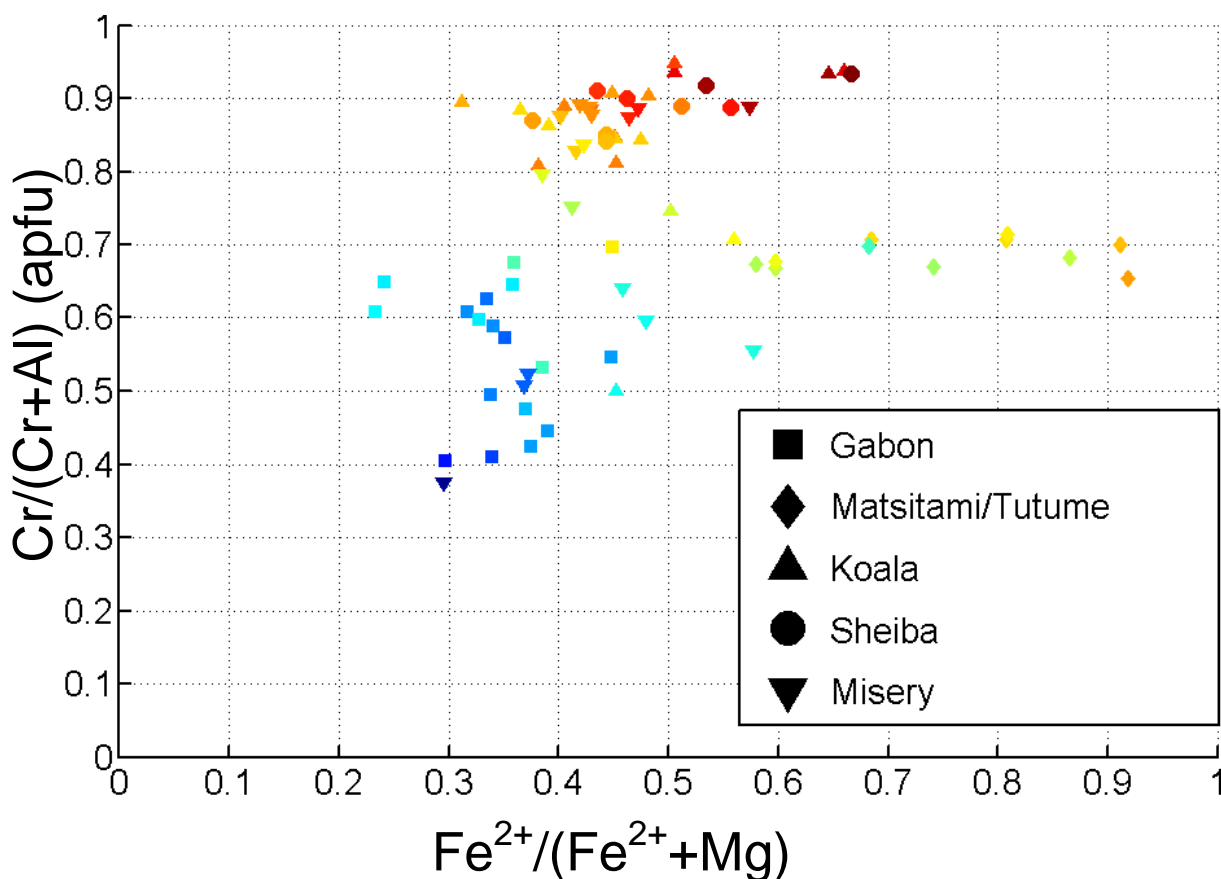


Figure 4-14: Spinel prism base, showing the clear use of unit cell in binary systems. The Cr substitution for Al is clearly demarcated by an increase in unit cell size.

substituted in the unit cell, it swells. We also see a similar increase in unit cell from chromite to magnesiochromite, with the substitution of Fe^{2+} (0.615 Å) for Mg^{2+} (0.585 Å). The multiple substitutions lead to ambiguity, because any of these larger ions can cause a swelling or shrinking of the unit cell parameter. Again, some scatter is also caused by order-disorder relationships, but these effects should be small compared with chemical substitutions, because the crystallization and subsequent annealing histories of most of the studied grains should be reasonably similar. A double substitution reaction occurs between hercynite and chromite, where Cr^{3+} (0.615 Å) substitutes for Al^{3+} (0.53 Å) simultaneous with Mg^{2+} (0.585 Å) substituting for Fe^{2+} (0.615 Å). The Cr^{3+} for Al^{3+} substitution has the greater net effect, because the radii difference is greater and there are twice as many Cr^{3+} substitutions occurring as Fe^{2+} , but as mentioned previously, in the Matsitami/Tutume series there is some ambiguity because the system is not constrained to a binary solid solution. There is some spread in the divalent pyramid due to magnesioferrite and magnetite components, but it is minimal due to the low amount of Fe^{3+} in the system. The spread can be seen in the largest unit cells with a high Cr number (Cr/Cr+Al). The unit cell parameter of the compositions around Cr # 90 increases more rapidly with increasing Fe^{2+} than the unit cells with a Cr number of 70. This is because as the spinel composition evolves toward magnetite or magnesioferrite with greater than ~40 mol% according to Raman observations of Lenz et al. (2013), the Fe^{2+} or Mg^{2+} instead of being in the tetrahedral site is in the octahedral site and has a larger atomic radii (0.74 and 0.71 Å, respectively). The Ti substitution would produce a similar increase in unit cell size but due to the limited extent of Ti substitution and the greater amount of Fe^{3+} , as seen in Figure 12a/b, it is most likely due to the Fe^{3+} .

4.4.5 Unit Cell Applied to KIM vs Non-KIM discrimination

Alone, a unit cell parameter measurement cannot unambiguously discriminate between kimberlitic and non-kimberlitic chromite. The primary reason for this is that multiple chemical compositions, and to a lesser extent ordering states, will result in identical unit cell parameters. If the chemical compositions can be constrained, for example, due to a known kimberlitic origin, unit cell can be used as a first approximation for chemical

composition. The diamond inclusion field in the three bi-variant plots defines the composition range of chromites associated with diamonds. All bivariate discrimination plots can distinguish the diamond inclusion field composition on the basis of unit cell size, with values between 8.31 Å and 8.33 Å, when constrained to lower Fe compositions. These results are consistent with those of Lenaz et al. (2009) on kimberlites from Siberia

4.4.5.1 Bi-variant discrimination plots

Three commonly-used chemical discrimination plots have been overlaid with unit cell data, to demonstrate the applicability of unit cell as a proxy for composition, for discrimination purposes. The areas that are typically associated with the diamond inclusion field are overlaid in the diagrams.

4.4.5.1.1 Cr₂O₃ vs Al₂O₃ Discrimination plot

The Cr₂O₃ vs Al₂O₃ discrimination diagram, Figure 4-15, shows the diamond-associated (or diamond inclusion) field above ~61 wt% Cr₂O₃ and below 8 wt% Al₂O₃.

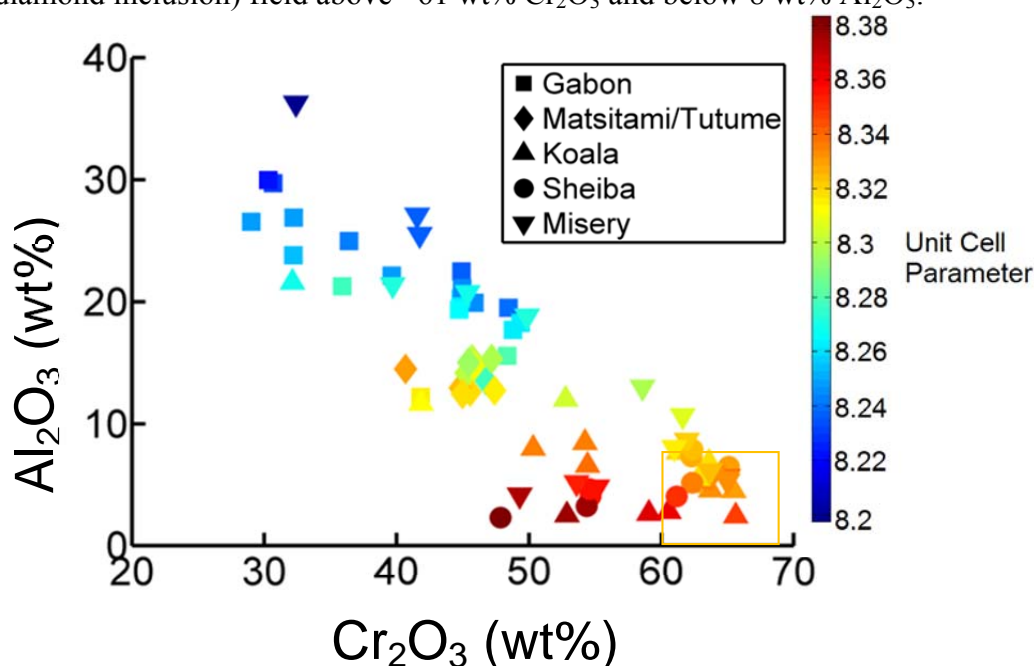


Figure 4-15: Cr₂O₃ vs Al₂O₃ discrimination diagram. This plot shows the diamond inclusion compositional field <8 wt% Al₂O₃ and >61 wt% Cr₂O₃. (see boxed area) (Sobolev, 1977)

There are, however; some kimberlitic samples mixed in this area. The diamond inclusion field samples have unit cells between 8.31 and 8.33 Å. This discrimination plot shows one general trend from high Al_2O_3 to high Cr_2O_3 . This trend is associated with Cr-Al substitution, as there is increasing Cr as described above. At low Al_2O_3 levels, there is an increase in unit cell size as Cr_2O_3 decreases. This is a result of spread between chromite/magnetite and magnesiocromite due to the Fe-Mg substitution leading to the increased unit cell size of the chromite/magnetite end members.

4.4.5.1.2 Cr_2O_3 vs TiO_2 Discrimination Plot

The Cr_2O_3 vs TiO_2 discrimination plot, Figure 4-16, is commonly used to discriminate kimberlites from non-kimberlites by separating the field that is created by the transect from 8-9 wt% TiO_2 to 60 wt% Cr_2O_3 (Nowicki 2014; Grütter and Apter 1998). Currently those grains in the “kimberlite” trend have unit cell parameter dimensions above 8.34 Å (Roeder 2001). This is likely due to the grains also having high Fe^{2+} in conjunction with the high Cr, as seen in Figure 4-15.

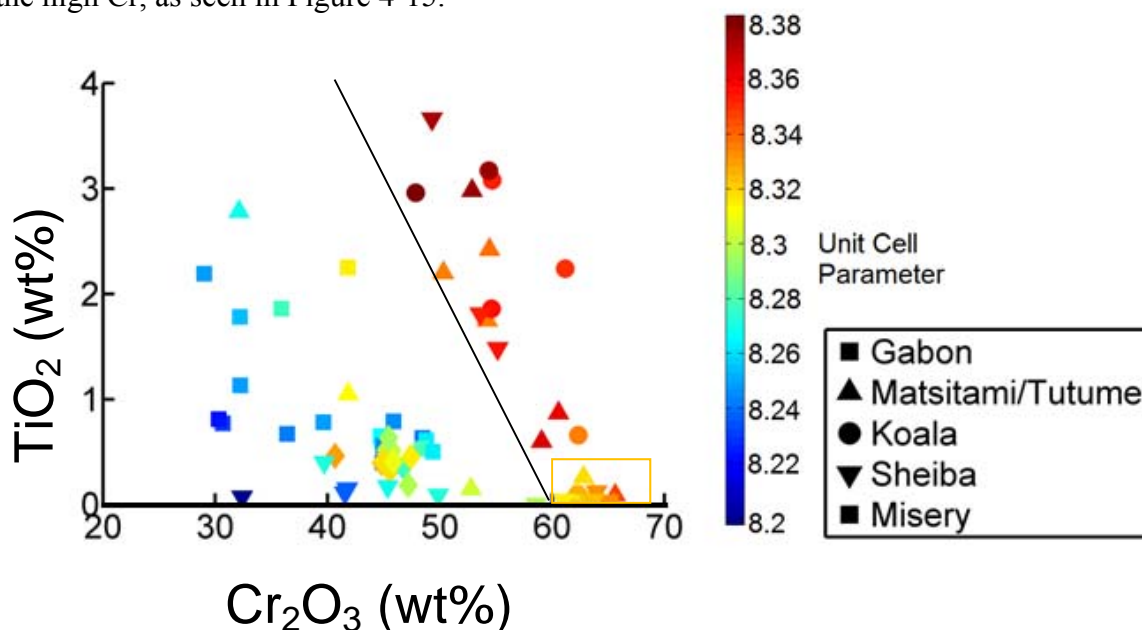


Figure 4-16: Kimberlite discrimination can be done on the basis of those grains that are above the Ti-Cr discrimination field (defined by the black line). This is likely due to Fe^{2+} rather than Ti. Note the diamond inclusion field by a box. (Sobolev, 1977)

It is unlikely that Ti is driving the unit cell size significantly enough to conclude that it will be able to the unit cell parameter will be able to discriminate TiO_2 once more data is added to the plot. Ti does partition into spinels with Fe^{3+} meaning it may trace the Fe^{3+} . This could partially explain the unit cell size discrimination combined with the larger unit cell size of high Ti grain. Figure 14 shows the diamond inclusion field below 0.5 wt% TiO_2 and greater than ~62 wt% Cr_2O_3 . Among the chromite grains below 8.31 Å there is a mix of non-kimberlitic and kimberlitic samples.

4.4.5.1.3 Cr_2O_3 vs MgO Discrimination Plot

The Cr_2O_3 vs MgO diagram, Figure 4-17, demonstrates some of the limitations to the use of unit cell as a compositional proxy. The ‘phenocryst trend’ is found to have increasing unit cell size from 8.33 Å with decreasing MgO content along the positive linear chemical trend. The trend is linked to an increase in unit cell size toward more Fe^{2+} rich spinels, mainly from chromite to magnesiochromite, because of the larger radius for Fe^{2+} than Mg, as discussed previously. The mixed xenocryst and non-kimberlite field represents unit cells of less than 8.31 Å and the negative linear trend toward higher MgO contents, as seen from chromite to spinel in the chemical composition, correlates with the decreasing unit cell. The diamond inclusion field ranges from 8.31 to 8.33 Å and is shown in the region above ~61 wt% Cr_2O_3 and 10-16 wt% MgO (Fipke et al. 1989; Fipke et al. 1995). The technique is, however, unable at this time to discriminate between chemical substitutions driving identical unit cell changes between different populations. This makes it impossible in the general case (i.e., without any chemical constraint or context) to discern kimberlite-specific trends within unit cell data, which is essential for KIM discrimination (Nowicki et al. 2004).

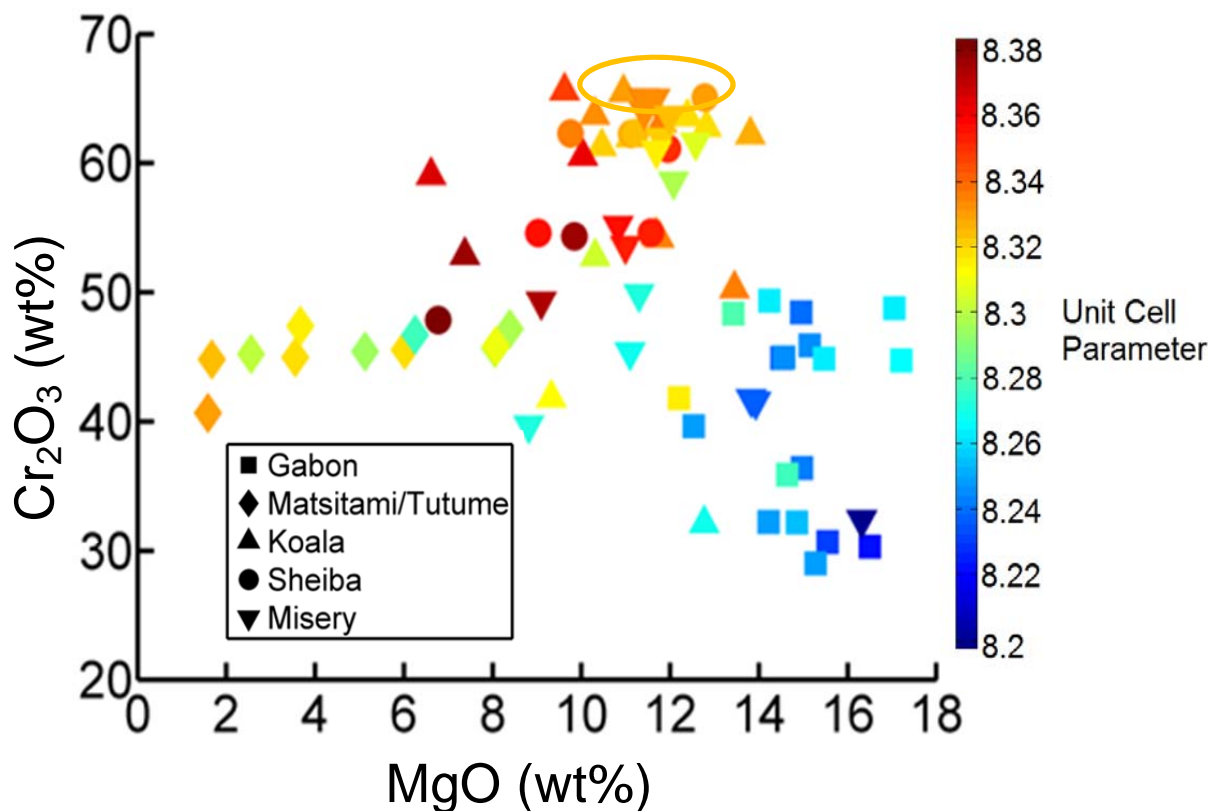


Figure 4-17 : Cr_2O_3 vs MgO discrimination diagram showing the typical kimberlite trends for phenocryst (large unit cells - red) and xenocryst (small unit cells - blue), as exhibited by Koala/Sheiba/Misery, as compared to Matsitami exhibiting the classic flat non-kimberlite trend. Note that the non-kimberlitic Matsitami samples have similar unit cell size to those in the diamond inclusion field (yellow). Diamond inclusion field is indicated by the shaded box. Thus, the use of unit cell for these purposes is limited without context or other constraints.

4.4.5.2 3D-variant discrimination plots

The Cr_2O_3 vs MgO and Cr_2O_3 vs TiO_2 diagrams were combined to see the net effect of these two discrimination plots on unit cell, Figure 4-19. The result was that the diamond inclusion field became highly defined and unit cells of 8.31-8.33 Å described the area. The kimberlitic trend of the Cr_2O_3 vs TiO_2 diagram and the Cr_2O_3 vs MgO are clearly discriminated using the >8.33 Å unit cells. This diagram has the same caveats as all unit cell compositional proxies, but displays data in a clear manner. The xenocryst and non-kimberlite field of the Cr_2O_3 vs MgO diagram is spread upward by the TiO_2 content, as unit cell increases with TiO_2 , although unlikely driven by it except in the Sheiba population.

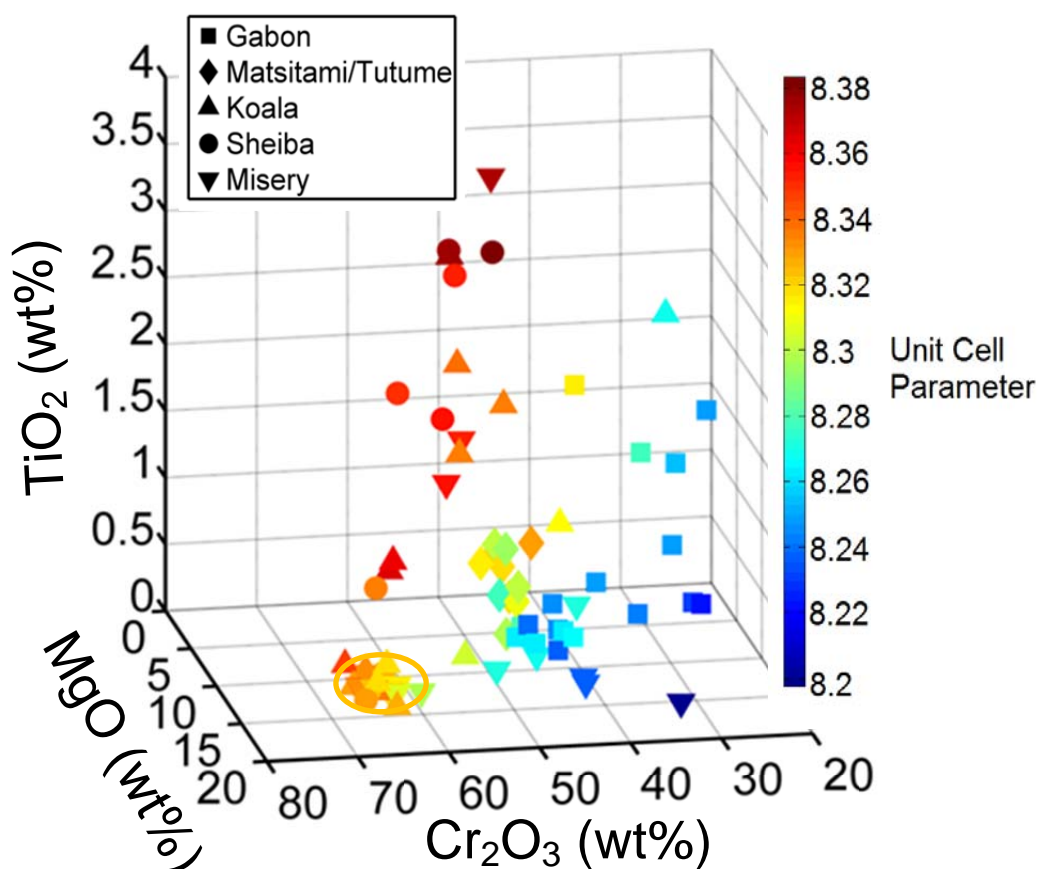


Figure 4-18: Cr_2O_3 vs TiO_2 vs MgO , a 3D diagram that provides a convenient method to display chemical compositions for discrimination purposes. It also demonstrates the utility of unit cell as a discriminator in kimberlitic terrains.

4.5 Conclusions

Unit cell provides a reasonable proxy of composition in spinels in binary systems, as can be clearly seen in the spinel prism plots, with end members plotting in distinctive fields at the base of the prism. It can be used in low Ti, low Mn settings as a rough proxy for Al content due to the tight grouping between end-members. Unit cell alone cannot be used to unambiguously discriminate between kimberlite and non-kimberlitic chromites, but when in a kimberlitic or other well-constrained terrain it could potentially be used as compositional proxy. The constraints would be needed to ensure the system cannot have identical unit cell sizes for different compositions or ordering states. Low levels of Fe^{3+} and/or Ti^{4+} likely to be an important constraint, because the chemical substitutions and order-disorder relations involving those cations will greatly increase unit cell scatter and increase the possibilities of identical cell edges for different compositions. It is also likely that broadly similar crystallization and annealing histories are necessary to reduce scatter due to variable ordering. Unit cell could make a useful vector in the field for diamond exploration, with new field-ready technologies, particularly in combination with other structural discriminators e.g., oxygen-metal distance parameter, or measurements from other field-portable instrumentation such as Raman spectra (Jehlička et al. 2009) and X-ray fluorescence (Glanzman and Closs 2007) to further constrain the structural and chemical properties of chromites.

Acknowledgements: Matt Izawa, Tom Nowicki, Herb Helmstaedt and John Gurney for useful discussions.

4.6 References

- Altermatt, U. and Brown, I. (1987) A real-space computer-based symmetry algebra. *Acta Crystallographica Section A: Foundations of Crystallography*, 1, 125-130
- Barnes, S.J. and Roeder, P.L. (2001) The Range of Spinel Compositions in Terrestrial Mafic and Ultramafic Rocks. *Journal of Petrology*, 12, 2279-2302
- Chen, Y., Xu, B., Chen, J. and Ge, Y. (1992) Fe^{2+} – Fe^{3+} ordered distribution in chromite spinels. *Physics and Chemistry of Minerals*, 4, 255-259

Deer, W.A., Howie, R.A. and Zussman, J. (1992) An introduction to the rock-forming minerals Longman Scientific & Technical, Harlow, Essex, England

Droop, G. (1987) A general equation for estimating Fe³ concentrations in ferromagnesian silicates and oxides from microprobe analyses, using stoichiometric criteria. Mineralogical magazine, 361, 431-435

Fipke, C., Gurney, J. and Moore, R. (1995) Diamond exploration techniques emphasising indicator mineral geochemistry and Canadian examples

Fipke, C., Gurney, J., Moore, R. and Nassichuk, W. (1989) The development of advanced technology to distinguish between diamondiferous and barren diatremes. Geological Survey of Canada, Open File, 559

Freckelton, C.N. and Flemming, R.L. (2009) Crystal-Chemical Correlations in Chromites from Kimberlitic and Non-Kimberlitic Sources. . EOS Trans. AGU, 22, Abstract MA71C-05

Glanzman, R. and Closs, L. (2007) Field portable X-Ray fluorescence geochemical analysis-its contribution to onsite real-time project evaluation. In Proceedings of Exploration, p. 291-301

Grütter, H. and Apter, D. (1998) Kimberlite-and lamproite-borne chromite phenocrysts with “diamond-inclusion”-type chemistries. In Extended abstract 7th International Kimberlite Conference, Cape Town, p. 280-282

Gurney, J.J., Hildebrand, P.R., Carlson, J.A., Fedortchouk, Y. and Dyck, D.R. (2004) The morphological characteristics of diamonds from the Ekati property, Northwest Territories, Canada. Lithos, 1, 21-38

Haggerty, S.E. (1986) Diamond genesis in a multiply-constrained model

Hamecher, E.A., Antoshechkina, P.M., Ghiorso, M.S. and Asimow, P.D. (2013) The molar volume of FeO–MgO–Fe₂O₃–Cr₂O₃–Al₂O₃–TiO₂ spinels. Contributions to Mineralogy and Petrology, 1, 25-43

Hazen, R. and Navrotsky, A. (1996) Effects of pressure on order-disorder reactions. *American Mineralogist*, 1021-1035

Hill, R. and Roeder, P. (1974) The crystallization of spinel from basaltic liquid as a function of oxygen fugacity. *The Journal of geology*, 709-729

Hill, R.J., Craig, J.R. and Gibbs, G.V. (1979) Systematics of the spinel structure type. *Physics and Chemistry of Minerals*, 4, 317-339

Jehlička, J., Vitek, P., Edwards, H., Heagraves, M. and Čapoun, T. (2009) Application of portable Raman instruments for fast and non-destructive detection of minerals on outcrops. *Spectrochimica Acta Part A: Molecular and Biomolecular Spectroscopy*, 3, 410-419

Klein, C. and Dutrow, B. (2008) The 23rd edition of the manual of mineral science:(after James D. Dana) Wiley

Lenaz, D., Logvinova, A.M., Princivalle, F. and Sobolev, N.V. (2009) Structural parameters of chromite included in diamond and kimberlites from Siberia: A new tool for discriminating ultramafic source. *American Mineralogist*, 7, 1067-1070

Lenaz, D., De Min, A., Garuti, G., Zaccarini, F. and Princivalle, F. (2010) Crystal chemistry of Cr-spinels from the lherzolite mantle peridotite of Ronda. *American Mineralogist*, 8-9, 1323-1328

Lenaz, D. and Luggi, V. (2013) Raman study of MgCr_2O_4 – $\text{Fe}_2\text{Cr}_2\text{O}_4$ and MgCr_2O_4 – MgFe_2O_4 synthetic series: the effects of Fe^{2+} and Fe^{3+} on Raman shifts. *Physics and Chemistry of Minerals*, 6, 491-498

Lewis, H.C. (1888) The Matrix of the Diamond . *Geological Magazine, New Series*, 5, 129-131

McClenaghan, M. and Kjarsgaard, B. (2001) Indicator mineral and geochemical methods for diamond exploration in glaciated terrain in Canada. Geological Society, London, Special Publications, 1, 83-123

Nowicki, T. (2014) Chomite and Kimberlite vs Non-Kimberlite Discrimination

Nowicki, T., Crawford, B., Dyck, D., Carlson, J., McElroy, R., Oshust, P. and Helmstaedt, H. (2004) The geology of kimberlite pipes of the Ekati property, Northwest Territories, Canada. *Lithos*, 1–4, 1-27

O'Neill, H.S.C. and Navrotsky, A. (1983) Simple spinels; crystallographic parameters, cation radii, lattice energies, and cation distribution. *American Mineralogist*, 1-2, 181-194

Osborne, M.D., Fleet, M.E. and Bancroft, G.M. (1981) Fe²⁺-Fe³⁺ ordering in chromite and Cr-bearing spinels. *Contributions to Mineralogy and Petrology*, 3, 251-255

Roeder, P.L. and Schulze, D.J. (2008) Crystallization of Groundmass Spinel in Kimberlite. *Journal of Petrology*, 8, 1473-1495

Sandrock, C. (2002) TernPlot. MatLab Central

Co-Authorship Statement

I processed and analyzed the Terra XRD data, provided by Paul Mann, Matt Izawa, Ed Cloutis from University of Wininpeg. Natalie and Jim Renaud of Renaud Geological consulting provided the EPMA data for the portable collected. The calibration data's chemistry was provided by Mineral Services Canada Inc. The μ XRD and refinements were collected by myself at Western University. I also developed the ideas, and wrote the paper. Dr. Flemming provided guidance and instrument training.

Chapter 5

5 Portable Structural Refinement and Compositional proxy using a Terra XRD/XRF

5.1 Abstract

Crystal structure parameters are an important tool for the study of minerals and have been limited, until recently, to a lab based setting. The advent of portable integrated X-ray diffraction and fluorescence (XRD/XRF) technology, adapted from the Mars Science Laboratory Curiosity Rover, has enabled a novel method for acquisition of structural parameters in the field. Exploration for new diamond deposits often relies on indicator minerals to expand the footprint of the target deposit. Indicator minerals can be identified in the field by XRD through the use of a powder matrix. The characterization of these often very small grains in the field would allow for the potential to increase efficiency and pace of exploration projects by reducing time for grain processing through minimization of sample shipping. This study aims to show the potential and limitations of the use of unit cell parameter as a proxy for composition in a field-based exploration context. A proof-of-concept for unit cell parameter as a proxy for aluminum content of natural spinels in the field context has been demonstrated by this study.

5.2 Introduction

Spinel group minerals are important as petrogenetic indicators, as exploration vectors, and as ore minerals. This group of minerals has been extensively studied, but the ability to characterize them in the field has been limited. This has been due to a lack of portable field equipment capable of measuring the relevant chemical and structural properties of grains of the size of most spinels of interest are <425 microns in a diamond exploration context. This study pioneers a method to attain unit cell data from small grains in a field setting, opening the potential for innovation with structural parameters in a field setting.

In the exploration context, the unit cell dimension (a_0) provides a potential asset to the growing trend toward field-portable analytical techniques. The unit cell dimension can be considered as a function of all the chemical substitutions within a structure for the

smallest repeating unit (Deer et al. 1992; Klein and Dutrow 2008). Unit cell dimension has the potential to act as a bulk compositional proxy within binary systems or within well-constrained systems with grains too small to target with current portable XRF or Raman spectrometers.

Chromites are used as indicator minerals because of their resistance to erosion and relative stability, which leads to their wide dispersal from small kimberlite sources and provides a larger footprint for exploration (McClenaghan and Kjarsgaard 2001). This study will build on the work in Chapter 4 for application of unit cell parameter in the field setting.

5.3 Methods

5.3.1 Electron probe microanalysis (EPMA)

Electron microprobe analysis (EPMA) was used as a baseline for the chemical composition calibration of the unit cell proxy because it is a non-destructive technique and can target the small grain size. EPMA uses a high-energy focused beam of electrons to generate characteristic X-rays which diffract through a curved crystal spectrometer and are counted using sealed proportional detectors and gas-flow. The intensity of X-rays produced by the unknown samples were compared to those produced by natural and synthetic standards to allow for quantitative analysis. The calibration standards used were natural minerals from the Smithsonian Institution (Jarosewich 2002). The use of secondary standards was employed to increase analytical accuracy for Ca, Ni and major elements (Jarosewich (2002). Data reduction was performed using the $\Phi(\rho Z)$ oxide correction of Armstrong (1995). The grain mounts were covered with a thin film of carbon using a vacuum carbon evaporator. Analyses were completed at Renaud Geological Consulting on a JEOL JXA-733 electron microprobe equipped with an energy-dispersive spectrometer (EDS) and 5-wavelength-dispersive spectrometers (WDS). The electron microprobe was operated with a beam diameter of 5 microns, with a 15 kV accelerating voltage and a 11 nA probe current. Major elements (Fe, Mg, and Si) were counted for 10 seconds, and minor elements (Ti, Ni, Ca, Mn, Co, and Na) for 50 s. The background was counted for 20 seconds for major elements and 50 seconds for

minor elements. For trace elements, detection limits (DL) were better than 60 ppm and 0.01 wt% of major elements.

5.3.2 Terra XRD/XRF Methods

The kimberlitic indicator spinels used as a vector for exploration are very small ($<425\mu$), making them challenging to get a signal from. A split from a single chromite grain (~ 1 mg) was mixed with halite (NaCl) and ground to $<45\mu\text{m}$ powder with an agate mortar and pestle to allow for the small grain to be successfully analyzed. The use of matrix material was chosen to fill the vibrating sample chamber and allow for laminar flow within the sample holder to increase diffraction opportunities (Sarrazin et al. 2005). Halite has only a few diffraction peaks and because only a few peaks overlap with chromite diffraction peaks, this makes it an ideal matrix. The mixture of halite and chromite was then placed within the Terra's kapton-window cell. Due to halite's high solubility it can easily be flushed out of the sample. Integration times of 8 hours (corresponding to 2400 individual frames) were used to improve the signal-to-noise ratio of the diffraction data.

Both X-ray diffraction patterns and X-ray fluorescence spectra were acquired using an InXitu Terra 299 portable X-ray device, equipped with a 1024×256 pixels – 2-dimensional Peltier-cooled charge-coupled device detector at the University of Winnipeg. The Terra instrument provides XRD data from 5° to $55^\circ 2\theta$ (1.668 \AA to 17.660 \AA d-spacing) with 0.05° angular resolution, and XRF spectra covering 3 to 25 keV. X-rays are produced with a sealed Cu source (Cu $K\alpha$ radiation, $\lambda=1.5418\text{ \AA}$) operating at 30 kV accelerating voltage and 10 W power. A total of 200 exposures were collected and averaged to increase signal-to-noise ratio.

5.3.3 Unit Cell

The Celref software program was used to perform the cell refinements for the chromite sample (Altermatt and Brown 1987). The program uses a non-linear least squares optimization to refine the unit cell dimension based (assuming a known space group) on input starting unit cell values from a Bruker *.dif pattern (peak location file) and outputs

a refined unit cell dimension with a standard deviation. The software also has the ability to visually monitor the refinement of the peaks calculated compared to observed data.

5.4 Results

5.4.1 Power XRD

The majority of expected chromite peaks, and all expected halite peaks, are detectable in the powder pattern of the chromite and halite mixture (Figure 5-1). Due to the small quantity of chromite, it is expected that some weaker peaks might not be detectable above background. Four strong and distinctive chromite peaks were observed ($d_{111}=4.8013 \text{ \AA}$, $d_{220}=2.9452 \text{ \AA}$, $d_{331}=2.5119 \text{ \AA}$, $d_{400}=2.0819 \text{ \AA}$), which is sufficient to refine the unit cell. The unit cell of the chromite sample was determined to be $8.3292 \pm 0.0049 \text{ \AA}$.

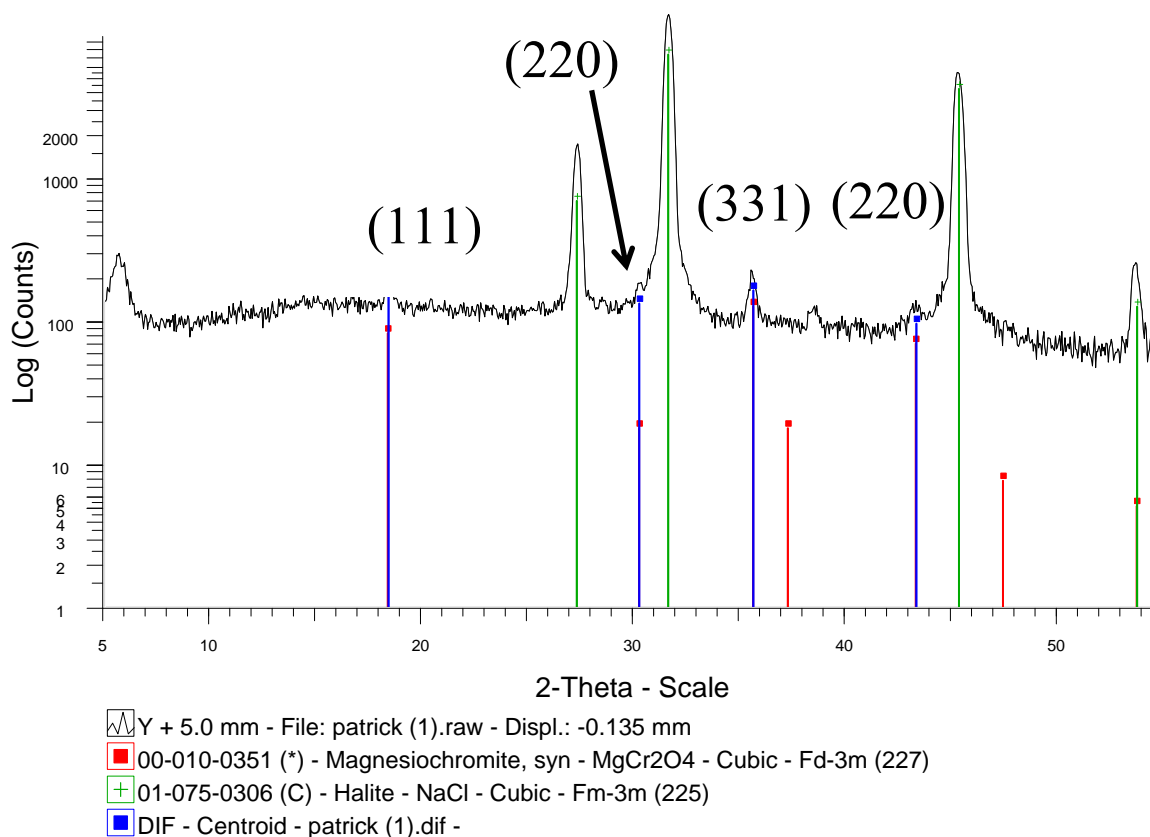


Figure 5-1: Terra powder XRD pattern of halite and chromite mixture clearly showing signal from the spinel for use in structural refinement.

5.4.2 Exposure Times

The Terra instrument was run in 200 exposure sessions of 45 min duration to improve the signal-to-noise ratio, in Figure 5-2. The initial powder pattern only exhibits peaks from the dominant halite phase, once at 600 exposures the first two chromite peaks become visible ($d_{111}=4.8013 \text{ \AA}$, $d_{331}=2.5119 \text{ \AA}$). The third peak, allowing for a potential unit cell, becomes detectable at 1200 exposures ($d_{400}=2.0819 \text{ \AA}$). As a proof of concept, additional exposures were taken until a fourth chromite peak was detectable at 2400 counts and then an additional 400 exposures were performed ($d_{220}=2.9452 \text{ \AA}$).

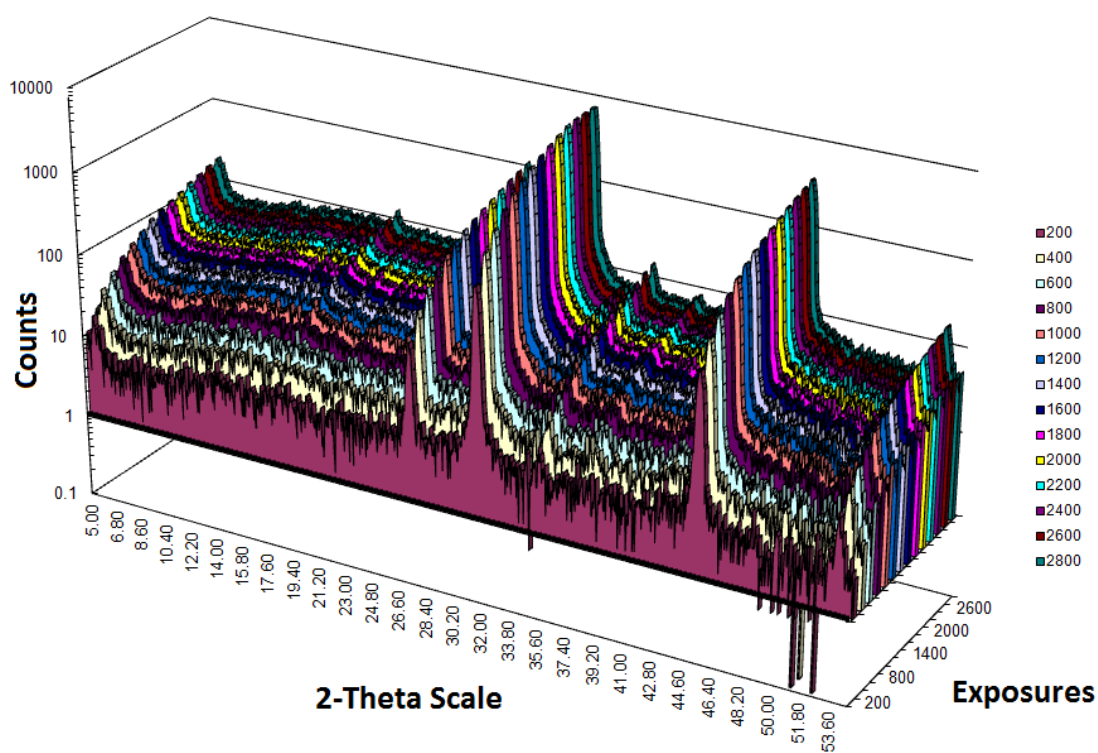


Figure 5-2: Terra XRD plot showing improved signal to noise with greater exposure time. This method leads to the first visible chromite peaks at 600 exposures, a third peak at 1200 exposures and a fourth peak at 2400 exposures. Note that the vertical axis is logarithmic.

5.4.3 Powder XRF

The XRF spectrum of the sample was collected simultaneously with the XRD pattern. It showed the expected Fe and Cr K-alpha peaks corresponding to chromite, but the Mg and Al K-alpha peaks were not detected, see Figure 5-3. The sensitivity of the Terra instrument to light elements is poor due to the low fluorescence yield and strong air attenuation of characteristic X-rays of light elements. The Cl and Br K α peaks are due to halite (Na was not detected for the reasons previously outlined). The strong Cu K α peak is due to detection of scattered primary radiation from the Cu source.

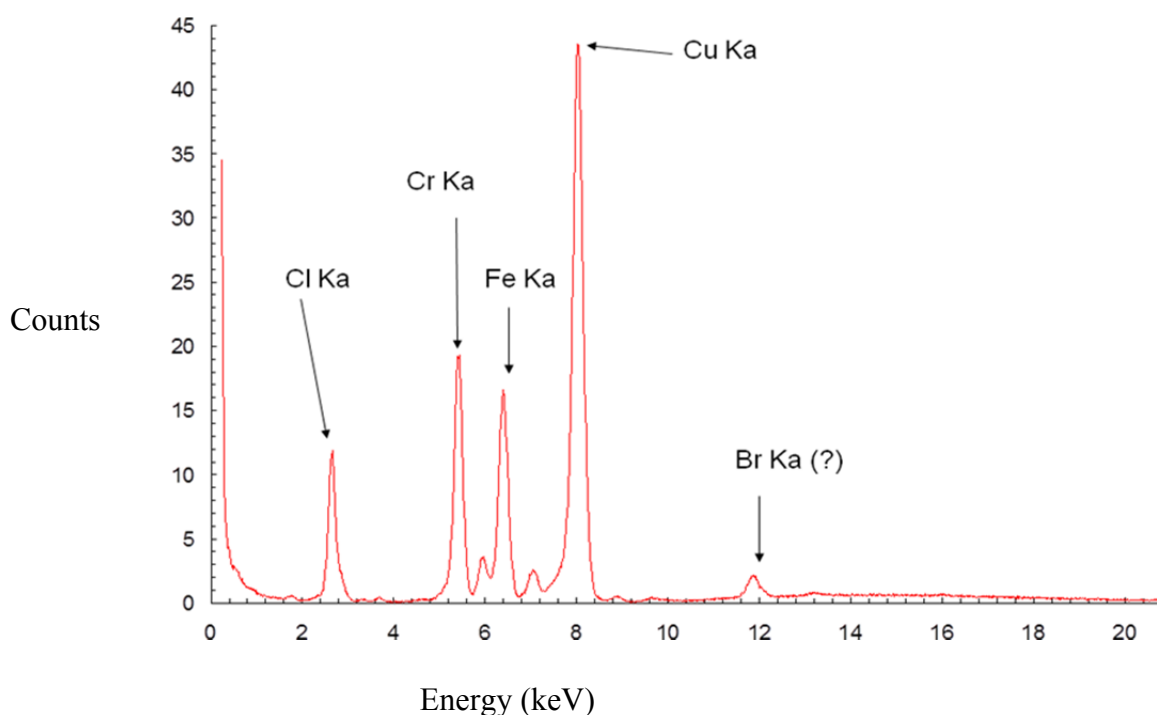


Figure 5-3: XRF pattern shows Fe and Cr detected from chromite but the XRF is unable to detect the light elements Al or Mg.

5.5 Discussion

5.5.1 Estimating Al content from unit cell parameter

As discussed in Chapter 4, unit cell parameter has a narrower spread with respect to Al content than with respect to the other elements due to relevant end member spinels plotting with relatively similar unit cell parameters. Magnesioferrite, magnetite, and chromite all have unit cell parameter of approximately 8.37-8.40 Å (see Table 1.2 in

Chapter 1). They have approximately the same size because the tetrahedral Fe^{2+} found in chromite is larger than the tetrahedral Fe^{3+} found in magnetite and magnesioferrite (because these are inverse spinels). The octahedral sites of magnesioferrite and magnetite contain octahedral Fe^{2+} , Fe^{3+} and Mg, which are all larger, and in some cases, much larger than octahedral Cr (see ionic radii Table 1.1 in Chapter 1). The competing effects of these different substituents averaged over the XRD interaction volume, resulting in an approximately identical unit cell size for high Cr /low Fe grains and high Fe/ low Cr grains. This means that the Al-Cr substitution will have the dominant effect on the unit cell parameter. Using this previously correlated data (Chapter 4, Fig 4-8b) and the known end member unit cell sizes, an approximated unit cell to Al content ‘calibration curve’ was created, Figure 5-4 (central line through data in Figure 5-4 is a guide to the eye only). The upper and lower error of the approximation are defined by the tie lines between the end members spinel-magnesiochromite (lower limit) and the magnetite-hercynite (upper limit). Magnetite was used instead of chromite as the upper limit because it is larger and provides the higher estimate (These tielines assume minimal ulvospinel component). The chromite grain analyzed by the Terra XRD had a unit cell parameter of $8.3292 \pm 0.0049 \text{ \AA}$ and Al content 0.18 apfu (by EPMA). Based on visual interpolation of the ‘best fit’ line through the unit cell data in Figure 5-4, a grain with a unit cell parameter of 8.329 \AA would have an Al content estimated to be 0.29 apfu as compared with the measured value of 0.18 apfu. The observed Al value lies within the extreme limits of the unit cell data, as the upper limit was interpolated to be 0.51 apfu and the lower limit was 0.05 apfu.

An alternative is to fit a mathematical best-fit line through the unit cell vs. Al (apfu) data, as shown in Figure 5-5. The best fit line is no longer parallel to the composition tie lines in this case, likely reflecting the structural influence of other end-member components, particularly magnetite or slight ulvospinel content. The regression line of best fit approximated an Al content of 0.31 apfu based on the portable unit cell measure. This is close to the value of 0.29 approximated from error limits.

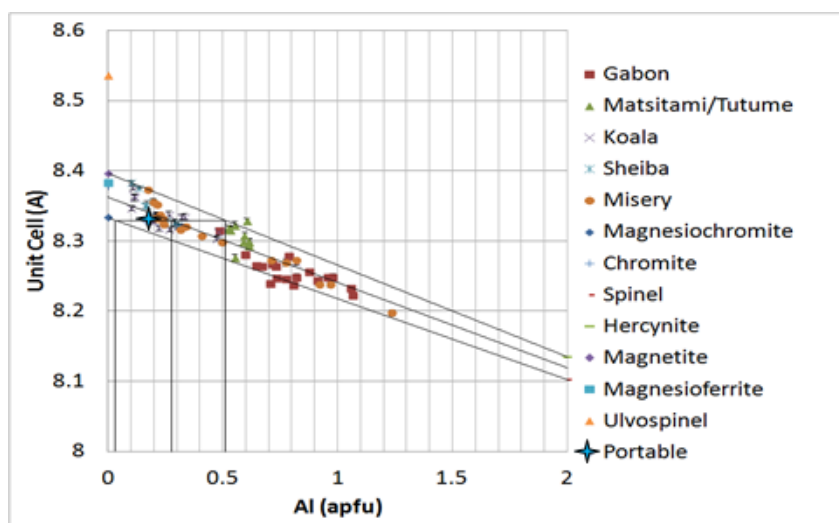


Figure 5-5: The aluminum content approximated through visual interpolation.

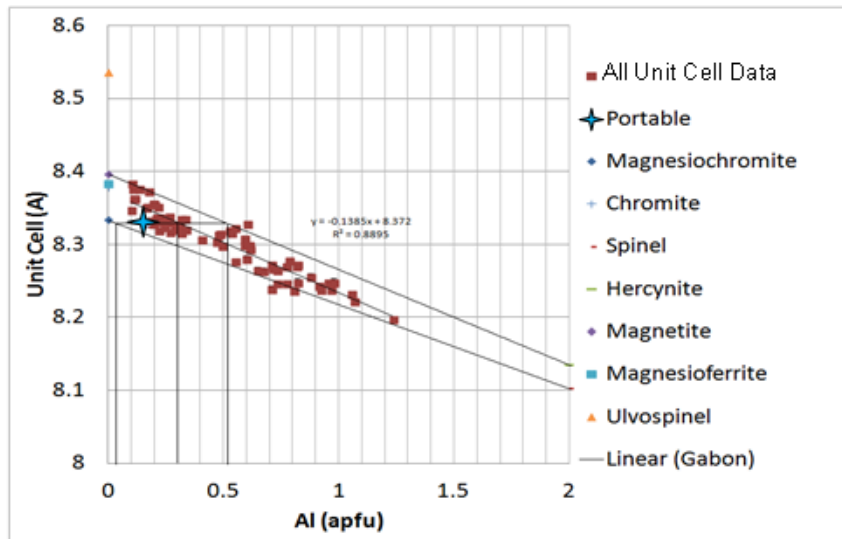


Figure 5-4: The aluminum content approximated through a best fit regression line.

5.5.2 Field Proxy

Field-portable analysis of indicator minerals could reduce shipping expense by doing preliminary processing of the grains in a field setting. This could be done either using indicator minerals in a glacial till, stream sediment, or a soil sample. In order to do work with indicator minerals in a field setting, the indicator minerals must be preconcentrated in the field. The primary methods to preconcentrate indicator minerals in the field are jigging and panning, both of which require significant amounts of water. This means that field based indicator work will be best suited to stream sediment sampling environments. Although we demonstrate the general application of unit cell as a compositional proxy in this study, it could be applied to any deposit with spinel as an indicator mineral such as the Thompson Nickle Belt, Thompson, Manitoba.

The unit cell dimension of the ‘portable’ grain was successfully refined and is plotted on the base of the spinel prism in Figure 5-6. This demonstrates proof-of-concept that unit cell dimensions of small mineral grains of a size equivalent to most indicator mineral samples (e.g. 100-300 μm) can be successfully measured using field-portable diffraction instrumentation. It has been shown elsewhere (Ch. 4) that, under suitable conditions, unit cell parameter can be a useful compositional proxy. The herein-refined chromite grain has a unit cell parameter and composition similar to the previously investigated grains on the unit cell-composition plot (Fig. 5-6) developed from μXRD in Chapter 4. In a field context, with no quantitative chemical data for the grain, some ambiguity would remain due to the similar unit cell sizes for some high Cr# and low Fe# versus low Cr# and high Fe# grains. Future work might include developing a means to quantify the Fe/Cr ratio from the concurrently detected XRF spectra.

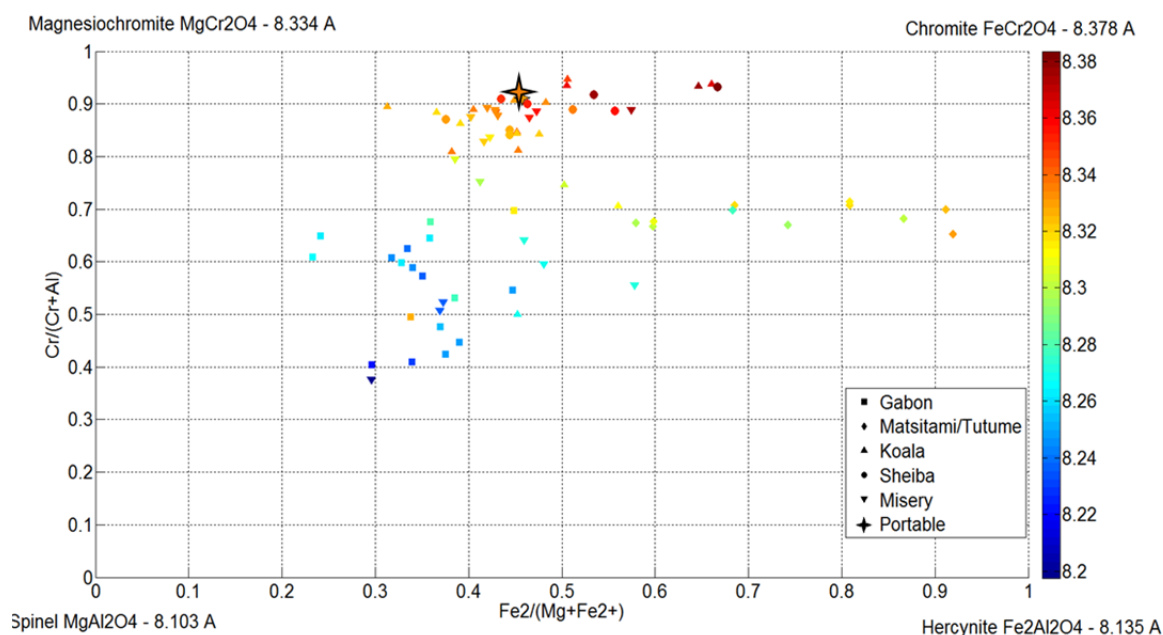


Figure 5-6: Terra XRD can be used as a proxy for spinel composition but this application is limited by the compositional ambiguity between high Cr# and low Fe# and the reverse. The initial potential use of XRD can be seen for binary spinels systems.

5.6 Conclusions and Future work

The use of a halite matrix works as an effective method to collect XRD data for small grains that cannot be collected in the field otherwise. Isochemical (but not necessarily isostructural) grains could potentially be differentiated in the field by this method. XRD-derived structural parameters can be used to estimate aluminium content through the use of the unit cell-composition ‘calibration line’, which has been demonstrated for a chromite grain of composition 0.29 apfu Al (see Figure 5.4 and 5.5).

The application of this technique would be best suited to a stream sediment sampling program, where jigging and panning could be easily applied. If applied, this sort of method could reduce shipping costs of samples and allow potential for greater

understanding in the field of where to continue a search by identifying significant indicator minerals. Presently, the ambiguity in the unit cell parameter between high Cr# and low Fe# (and vice versa) limits the use of the unit cell parameter as a compositional proxy for exploration purposes. The Terra XRD, however, does have a XRF function and through tracking Ti, Cr and Fe (the heavier elements) it should be possible to remove this ambiguity.

Quantification of Terra XRF data is presently an underdeveloped area, and could be pursued in order to produce quantitative inter-element ratios of detectable elements (e.g., Fe, Cr, Ti, Mn) and while representing a considerable undertaking, is potentially of broad interest and applicability. Using currently available X-ray sources, the integration times required to acquire high-quality data are impractically long (many hours to several days). Development of higher flux portable X-ray sources could greatly reduce the time required for XRD data collection in the field. Cu X-ray source induces significant Fe fluorescence in the chromite sample, which necessitates longer exposure times. The use of different X-ray sources (e.g., Mo, Re, or Ag) could both reduce the fluorescence problem and increase the range of observable d-spacings.

Acknowledgments: Natalie Pietrzak-Renaud is thanked for electron probe microanalysis. Paul Mann (U of Winnipeg), Ed Cloutis (U of Winnipeg) and Matt Izawa are thanked for collecting the Terra data. Matt Izawa is thanked for reviewing this chapter and for discussions.

5.7 References

Altermatt, U. and Brown, I. (1987) A real-space computer-based symmetry algebra. *Acta Crystallographica Section A: Foundations of Crystallography*, 1, 125-130

Armstrong, J.T., 1995, CITZAF: a package of correction programs for the quantitative electron microbeam X-ray analysis of thick polished materials, thin films, and particles. *Microbeam Analysis*, 4, 177 - 200.

Deer, W.A., Howie, R.A. and Zussman, J. (1992) *An introduction to the rock-forming minerals* Longman Scientific & Technical, Harlow, Essex, England

Jarosevich, E., 2002, Smithsonian Microbeam Standards, *Journal of Research of the National Institute of Standards and Technology*, 107, 681-685.

Klein, C. and Dutrow, B. (2008) *The 23rd edition of the manual of mineral science:(after James D. Dana)* Wiley

McClenaghan, M. and Kjarsgaard, B. (2001) *Indicator mineral and geochemical methods for diamond exploration in glaciated terrain in Canada*. Geological Society, London, Special Publications, 1, 83-123

Sarrazin, P., Blake, D., Feldman, S., Chipera, S., Vaniman, D. and Bish, D. (2005) Field deployment of a portable X-ray diffraction/X-ray fluorescence instrument on Mars analog terrain. *Powder diffraction*, 02, 128-133

Chapter 6

6 Conclusions and Future Directions

6.1 Slicing

The Slice Integration Technique has improved peak intensity of data retrieved from a GADDS image above background by 6.47% compared to the single slice option for the least improved peak and 189% for the best improved peak, as compared to conventional full frame integration, using the manual addition and merge method. The signal-to-noise ratio improvement using the Max Intensity Plot (MIP) method improved the one-dimensional pattern from one detectable peak with conventional integration to up to seven resolved peaks with the preferred number of slices. The technique is simple and has already been partially automated, but is currently limited to the processing of the data; the selection of the ideal number of slices currently requires user input. Overslicing is an easily identifiable issue where peak distortion occurs with slicing. The identification of overslicing is currently limited to a visual inspection. The Slice Integration Technique will allow the recognition of new data on GADDS images, leading to additional phase-identification. Measurement of structural (i.e. unit cell) information from *in-situ* XRD data for a wide range of target materials is now possible through the use of the Slice Integration Technique.

Future work could involve the complete automation of the slice integration process, which requires the development of an algorithm able to detect overslicing of peaks. This will require the accurate ability to identify signal to noise ratio of the 1D patterns and decide on a cut-off point to guard against passing the over slicing threshold. The development of a standalone program for processing the data would improve the speed of the processing and would decrease user input. The ability to automatically subtract initial background noise from the input slice data would be very advantageous because this process currently relies on macros. The combination of a standalone processing program and inspection element for signal to noise could allow for the application of this technique more broadly to *in-situ* XRD and would not require a skilled operator.

The various slice integration methods developed in this study may have applications to enhancing weak signals in other forms of two-dimensional diffraction data. One potential application is to synchrotron-based micro diffraction or Laue diffraction data. Slice integration methods are not limited to X-ray diffraction and could, for example, be applied to electron diffraction images or powder neutron diffraction patterns.

6.2 Unit Cell Parameters

Compositions of binary spinels can be approximated through the use of a correlation with unit cell parameter as, provided the end member compositions plot in distinctive fields. The unit cell parameter can discriminate spinel composition, with appropriate constraints. An example of a highly-constrained system would be found in late stage exploration; where the differentiation of grade has been established using crystal chemical methods. Future work should aim to investigate other well constrained binary spinel systems for similar compositional proxy applications of the unit cell parameter. This could be completed through samples of known grade and origin that are already discriminated on the basis of composition. The use of spinel unit cell as a proxy for composition may have applications outside of diamond exploration. Possible applications include gemology and curatorial studies, where the nondestructive nature of micro-XRD is highly advantageous. Spinel group minerals including magnetite, maghemite and chromite have been detected in many meteorites from Mars, and the Moon; and non-destructive compositional estimation may be of high value in the study of these rare materials. The Mars Science Laboratory Curiosity rover carries a portable XRD instrument, CheMin, which is similar to the Terra instrument described in Chapter 5 of this work. Spinel compositional estimates could be attempted using CheMin XRD data for suitable materials (e.g., samples rich in (titano)magnetite or chromite).

The power of unit cell measurement to discriminate between kimberlitic and non-kimberlitic chromites is presently hampered by the fact that in many cases, chromite grains with different compositions will have identical unit cell dimensions. If a system

can be well-constrained, in particular to lie within a compositional subdomain that lacks multiple compositions with identical unit cell dimensions, then unit cell dimension can be used as an unambiguous compositional proxy. Such conditions are expected in some kimberlitic systems. The chemical substitutions and order-disorder relations involving even low levels of Fe^{3+} or Ti^{4+} are likely to cause issues. Similar crystallization and annealing histories would be required to reduce the scatter from cation disorder and variable ordering. Further studies could investigate lab synthesized minerals of known compositions and that have known order-disorder relationships and post-crystallization annealing histories. Synthesis studies would allow for a better understanding of potential constraints on the selected terrains, because the effect of chemical substitutions and order-disorder on unit cell dimension could be studied individually.

An important future direction should be the expansion of *in situ* and field based structural characterization methods to include other structural parameters, most notably the oxygen-metal bond lengths (M-O and T-O). The oxygen positional parameter, combined with the unit cell parameter is most likely to have a discrimination potential for diamond exploration and should, therefore, be thoroughly investigated. It is worth noting though that this is not presently possible through *in-situ* XRD and is already being investigated through the single crystal methods (see Chapter 4). A focus of instrument development should be improvements in the quality of data produced (and rate of data collection) for both lab micro-XRD and field-based XRD instrumentation. One potential means towards this end is the development of field-portable micro-XRD instruments.

6.3 Field Proxy

Unit cell could make a useful vector in the field for exploration projects in assistance to other new field-portable technologies, such as Raman spectrometry and portable XRF. A key structural parameter which cannot yet be reliably determined from either lab micro-XRD or field portable instruments is the oxygen positional parameter distance parameter. Single crystal methods have shown that, in combination with unit cell dimension, oxygen

parameter can effectively discriminate among kimberlitic and non-kimberlitic chromian spinels. There is no physical reason that a field portable instrument could not produce data of sufficient quality to refine the oxygen parameter, as has been demonstrated by the successful Rietveld refinement of CheMin XRD data from the MSL Curiosity rover. Current practical limitations include the brightness of field-portable X-ray sources which lead to impractically long integration times. Improvements to X-ray source and detector technology could lead to greatly increased portable XRD source brightness and, therefore, lower the integration times required to obtain crystal structure refinement quality data from field XRD data.

The use of a halite matrix could be used for other grains in an exploration setting either as a method to acquire structural parameter information or phase identification. At the current time, use of unit cell for diamond exploration is limited by the ambiguity (multiple chemistries with identical unit cells) between high Cr# and low Fe# and the vice versa. Unit cell dimension can be used to estimate aluminum concentration in a field setting and has been used to successfully approximate a grain's Al content, see Chapter 5. Future work should look into other potential matrices that could be used to host other grains. Ideal candidates for matrix material must have few diffraction lines, which do not overlap with the target grains' peak positions and preferably be a poor diffractor, or even amorphous.

Another direction for improvement of the field-portable methods developed in this thesis is the quantification of Terra XRF data. Obtaining quantitative chemical data for detectable elements (e.g., Fe, Cr, Ti) would enable the determination of inter-element ratios to better constrain unit cell. It is, however, worth noting that the Terra is limited by the sample chamber being at ambient pressure since it makes lighter elements like Mg very difficult to quantify. The development of a vacuum sealed (or light gas filled) vibration holder could allow for the collection of Mg contents of grains in the field. Composition of other indicator minerals could be potentially constrained also by this quantification of the XRF component of the Terra XRD, including previous work by Harwood et al. (2009). As noted above, collection of data of sufficiently high signal-to-noise ratio with the Terra instrument is, at this time, impractically slow for exploration

application. This is primarily due to the low flux of X-rays emitted by the Terra X-ray source due to constraints of size and power consumption, as discussed above.

Some benefits might also be obtained through changes to the X-ray source material. The shorter-wavelength X-rays produced by Mo, Re or Ag target materials could allow for higher structural resolution. In addition, changing to an X-ray energy other than Cu K-alpha would mitigate the problem of iron fluorescence common in the X-ray analysis of geological materials.

Appendices

Appendix A: Slice Macro

Using the GADDs scripting language the slice technique was partially automated. The main filecalibrate sliver passes the appropriate data like frame size and number of intended slices to IntRP script file. It runs a loop that sets the parameters based on the number of slices and determines the width and frame size. INRP then passes the numbers for the integration to the files that actually perform the integration for each frame IntRP1 and IntRP2.

Appendix B: Max Intensity Plot

This Excel macro is used to create a max intensity plot based on sliced data. The data need to be first processed by merging and background subtracting the XRD files. These data can then be converted into a .plv that can be read by the excel macro. The macro has a gui interface that will accept the required information to process the input data and will output a single max intensity plot in a .dat file. This file then needs to be converted back into a *.raw file for unit cell refinement. See Chapter 3 for a more complete discussion of how the max intensity plot works.

Appendix C: ADK Macros

The two ADK macros are used in conjunction with AutoHotKey, which is a macro that moves the mouse. The first one automates the movement of the mouse for refinement using the software CelRef. This speeds up refinement of spinel-group minerals by reducing the amount of mouse usage. The second macro automates the setup of CelRef for a user opening the software with the appropriate conditions for refining a spinel-group mineral.

Appendix D: XRD Data

The appendix contains all of the unprocessed GADDs images for the project. These files can be used to identify any overlap issues if they had occurred since repletion of peaks would be visible.

Appendix E: Unit Cells

Unit cells were refined using Celref, which generates an output file. The file contains the miller indexes, the d-spacings and the unit cell parameter.

Appendix F: EPMA Data

All of the chemical data presented in this thesis is contained in this appendix. The data is presented in weight percent oxide and atoms per formula unit. The Fe^{3+} and Fe^{2+} values are calculated as has been explained in Chapter 4 using the Droop method (1987).

Appendix G: MatLab Code

The use of MatLab was employed to overlay unit cell information on the typical compositional diagrams to show the relation between the unit cell parameter and composition. The ternary plots require extra code for plotting and were modified from a previous ternary plotting software package to add unit cell as a colour on the plots. The code to create all of the Matlab figures can be found in this appendix.

Appendix A: Slice Macro

Calibrate Sliver Macro

The Calibrate Sliver Macro (CSM) runs a series of submacros that subdivides a single 2D Pattern into chi slices based on desired width

%N is the File Base Name!

%R is the first grain!

%E is the last grain!

InRP pass the appropriate variable into the inner macro IN1RP/Int2RP, this use of two macros allows for the cycling through of different run names and different slices. The Bruker scripting language is unable to contain a loop within a loop

In1RP/Int2RP must have the Frame width and Chi Start values inputted in to them

@C:\Frames\SlivInt\IntRP Int1RP %N %R %E (Frame) (#of Slices)

--Start--

#Let %N ="File Base Name"

#let %R =01

#let %E =01

@C:\Frames\SlivInt\IntRP Int1RP %N %R %E 001 01

@C:\Frames\SlivInt\IntRP Int1RP %N %R %E 001 02

@C:\Frames\SlivInt\IntRP Int1RP %N %R %E 001 05

@C:\Frames\SlivInt\IntRP Int1RP %N %R %E 001 10

@C:\Frames\SlivInt\IntRP Int1RP %N %R %E 001 20

@C:\Frames\SlivInt\IntRP Int1RP %N %R %E 001 30

@C:\Frames\SlivInt\IntRP Int1RP %N %R %E 001 40

@C:\Frames\SlivInt\IntRP Int1RP %N %R %E 001 50

@C:\Frames\SlivInt\IntRP Int1RP %N %R %E 001 60

@C:\Frames\SlivInt\IntRP Int1RP %N %R %E 001 70

@C:\Frames\SlivInt\IntRP Int1RP %N %R %E 001 80

@C:\Frames\SlivInt\IntRP Int1RP %N %R %E 001 90

@C:\Frames\SlivInt\IntRP Int2RP %N %R %E 002 01

@C:\Frames\SlivInt\IntRP Int2RP %N %R %E 002 02

@C:\Frames\SlivInt\IntRP Int2RP %N %R %E 002 05

@C:\Frames\SlivInt\IntRP Int2RP %N %R %E 002 10

@C:\Frames\SlivInt\IntRP Int2RP %N %R %E 002 20

@C:\Frames\SlivInt\IntRP Int2RP %N %R %E 002 30

@C:\Frames\SlivInt\IntRP Int2RP %N %R %E 002 40

@C:\Frames\SlivInt\IntRP Int2RP %N %R %E 002 50

@C:\Frames\SlivInt\IntRP Int2RP %N %R %E 002 60

@C:\Frames\SlivInt\IntRP Int2RP %N %R %E 002 70

@C:\Frames\SlivInt\IntRP Int2RP %N %R %E 002 80

@C:\Frames\SlivInt\IntRP Int2RP %N %R %E 002 90

-End--

The IntRP macro

Passes Variables from the calibrate Sliver to the Int1RP and Int2RP loops

```
--Start--
!Octagon!
MASK /OCTAGON 2. 164. 4. 856. 1018. 1884. 1018. 866.
#let %R=%3
#while ('%R' <= '%4') do

DISPLAY /NEW ""%2'_%R'_%5'.gfrm"
"@C:\Frames\SlivInt\%1"" %2 %6 %5
```

```
#inc %R
#wend
--End--
```

Int1RP/ Int2RP – Same code except one you will input Frame 001 data and the other Frame 002
Integrates designated area of frame and assigns appropriate name

%S = First Slice - Usually stays at 1
 %W = User must input Frame width. This this the divided by the number of slices to determine slice width
 %X = User must input Chi start value. This then has the one slice width removed to prepare for slicing.
 This defines the top of the slice
 %Y = Use must input Chi start value. This will define the bottom of the Frame.

```
--Start--
#let %S = 001
#let %W = Frame width / %2
#let %X = Chi Start Value- %W
#let %Y = Chi Start Value

#while ('%S' <= '%2') do

#let %X = %X + %W
#let %Y = %Y + %W
INTEGRATE /CHI 034.10 076.40 '%X' '%Y' /NORMAL=5 /STEPSIZE=0.1
INTEGRATE /WRITE ""%1'Slit_%2'_%R'_%S'_New_Oct_%3"" &
/FILENAME=%1'-Slit_%2'_%R'_%S'_New_Oct_%3' /FORMAT=DIFFRAC-AT &
/APPEND /SCALE=1.0
#inc %S
#wend

--End--

MJJ
```

Appendix B: Max Intenity Plot Macro

```

Sub ImportSliceDataFrames_Max_Min()

Dim wb As Workbook
Dim saveFileEx As String
Dim WorkRng As Range
On Error Resume Next

Dim LastRow As Long
Dim Cell As String
Dim ThetaStart1, ThetaFinal1, ThetaStart2, ThetaFinal2, StepSize As Double
Dim FolderLocation As String
Dim Filename As String
Dim NumSlices As String
Dim FileNum As String
Dim FileNum As String
Dim FileLocationText As String
Dim DeleteSize, Steps1, Steps2 As Double
Dim Slice As Integer
Dim Calibrate As Integer
Dim FirstDRange, SecondDRange, FirstDeleteRange1, FirstDeleteRange2, SecondDeleteRange1, SecondDeleteRange2 As String
Dim Deletesrows, LastRowDelete2, LastRowDelete1 As Double
Dim SheetLocation1, SheetLocation2, SheetSearch1, SheetSearch2 As String
Dim Lookup As String
Dim Cell11, Cell21, Cell12, Cell22 As String
Dim StartSheet1, SheetSlice1, StartSheet2, SheetSlice2 As Integer
Dim CellLook As String
Dim Ofset, r1, r2, Run, G, i, f As Integer
Dim delete, LastRowDelete As Integer
Dim RangeDelete1, RangeDelete2, RowsL As String
Dim ChiStart1, ChiFinal1, ChiStart2, ChiF2Width, ChiFinal2 As Double
Dim Frame1, Frame2 As Integer

' Application.ScreenUpdating = False
' Run the Input Box.
ThetaStart1 = Application.InputBox("Enter Start of Theta Frame 1 Range.", _
"Number Entry", , 250, 75, "", , 1)

ThetaFinal1 = Application.InputBox("Enter End of Theta Frame 2 Range.", _
"Number Entry", , 250, 75, "", , 1)

ThetaStart2 = Application.InputBox("Enter Start of Theta Frame 1 Range.", _
"Number Entry", , 250, 75, "", , 1)

ThetaFinal2 = Application.InputBox("Enter End of Theta Frame 2 Range.", _
"Number Entry", , 250, 75, "", , 1)

StepSize = Application.InputBox("Step Size.", _
"Number Entry", , 2, 75, "", , 1)

DeleteSize = Application.InputBox("Delete Step.", _
"Number Entry", , 2, 75, "", , 1)

ChiS1Input = Application.InputBox("Enter Start of Chi Frame 1 Range.", _
"Number Entry", , 250, 75, "", , 1)

ChiF1WInput = Application.InputBox("Enter Chi Frame 2 Range.", _
"Number Entry", , 250, 75, "", , 1)

ChiS2Input = Application.InputBox("Enter Start of Chi Frame 1 Range.", _
"Number Entry", , 250, 75, "", , 1)

ChiF2WInput = Application.InputBox("Enter Chi Frame 2 Range.", _
"Number Entry", , 250, 75, "", , 1)

ChiTopR1 = Application.InputBox("Enter Chi Frame 1 Top Delete Restrictions.", _
"Number Entry", , 250, 75, "", , 1)

```

```

Module1 - 2

ChiBotR1 = Application.InputBox("Enter Chi Frame 2 Bottom Delete Restrictions.", _
"Number Entry", , 250, 75, "", , 1)

ChiTopR2 = Application.InputBox("Enter Chi Frame 1 Top Delete Restrictions.", _
"Number Entry", , 250, 75, "", , 1)

ChiBotR2 = Application.InputBox("Enter Chi Frame 2 Bottom Delete Restrictions.", _
"Number Entry", , 250, 75, "", , 1)

FolderLocation = Application.InputBox("Folder Location")
Filename = Application.InputBox("File Name")
Run = Application.InputBox("Run Number")
Grain1 = Application.InputBox("Grain Number 1")
Grain2 = Application.InputBox("Grain Number 1")
Frame1 = Application.InputBox("Frame 1.", _
"Number Entry", , 250, 75, "", , 1)
Frame2 = Application.InputBox("Frame 2.", _
"Number Entry", , 250, 75, "", , 1)
Calibrate = Application.InputBox("Are You Calibrating? Yes=1 No=2")
w = 1

For G = Grain1 To Grain2

Do While (Calibrate = 1) Or (Calibrate = 2)
If Calibrate = 1 Then
'NumSlices inputs the number of slices into the file name
' Only Starts at 20 slices due to erradicate ends of patterns.
If w = 1 Then
NumSlices = 1
Slicecount = 1
ElseIf w = 2 Then
NumSlices = 20
Slicecount = 1
ElseIf w = 3 Then
NumSlices = 30
Slicecount = 1
ElseIf w = 4 Then
NumSlices = 40
Slicecount = 1
ElseIf w = 5 Then
NumSlices = 50
Slicecount = 1
ElseIf w = 6 Then
NumSlices = 60
Slicecount = 1
ElseIf w = 7 Then
NumSlices = 70
Slicecount = 1
ElseIf w = 8 Then
NumSlices = 80
Slicecount = 1
ElseIf w = 9 Then
NumSlices = 90
Slicecount = 1
End If

ElseIf (Calibrate = 2) Then
NumSlices = Application.InputBox("Number of Slices")
End If

'Sets up Width of Slices in Chi
ChiF1Width = ChiF1WInput / NumSlices
ChiF2Width = ChiF2WInput / NumSlices

'Preps Variables for the tracking of chi ie prepares for the loop by taking one chi "step" backwards.
ChiFinal1 = ChiS1Input
ChiStart1 = ChiS1Input - ChiF1Width
ChiFinal2 = ChiS2Input
ChiStart2 = ChiS2Input - ChiF2Width

```

Module1 - 3

```

x = 1
y = 1
Steps1 = Round((((ThetaFinal1 - ThetaStart1) / StepSize) + 1), 1)
Sheets("Sheet1").Select
For x = 1 To Steps1

    Cell = "A" & x
    Range(Cell).Select
    Test = Round((ThetaStart1 + (StepSize * (x - 1))), 1)
    ActiveCell.FormulaR1C1 = Test
    Range(Cell).Select
Next x

x = 1
y = 1
Steps2 = ((ThetaFinal2 - ThetaStart2) / StepSize) + 1
Sheets("Sheet2").Select
For x = 1 To Steps2

    Cell = "A" & x
    Range(Cell).Select
    Test = Round((ThetaStart2 + (StepSize * (x - 1))), 1)
    ActiveCell.FormulaR1C1 = Test
    Range(Cell).Select
Next x

Sheets("Sheet1").Select
LastRow1 = (ActiveSheet.Cells(ActiveSheet.Rows.Count, "A").End(xlUp).Row) + 1

Sheets("Sheet2").Select
LastRow2 = (ActiveSheet.Cells(ActiveSheet.Rows.Count, "A").End(xlUp).Row) + 1

'Schulze_Sept_3 -Slit_02 _01_ 001_New_Oct_001
Sheets("Sheet1").Select

For f = Frame1 To Frame2

'Orginal - before Calibrate Sliver created the files could reach twice number of slices for naming in
second frame
'If f = Frame1 Then
'i = 1
'NumSlices2 = NumSlices

'ElseIf f = Frame2 Then
'i = NumSlices + 1
'NumSlices2 = (NumSlices * 2)
'End If

'For i = i To NumSlices2

'Chi Track'
'If f = Frame1 Then
'ChiFinal1 = ChiFinal1 + ChiF1Width
'ChiStart1 = ChiStart1 + ChiF1Width
'ElseIf f = Frame2 Then
'ChiFinal2 = ChiFinal2 + ChiF2Width
'ChiStart2 = ChiStart2 + ChiF2Width
'End If'

'Current form uses Calibrate Sliver
If f = Frame1 Then
i = 1
NumSlices2 = NumSlices

ElseIf f = Frame2 Then

```

```

Module1 - 4

i = 1
NumSlices2 = NumSlices
End If

For i = i To NumSlices2

'Chi Track'
If f = Frame1 Then
ChiFinal1 = ChiFinal1 + ChiF1Width
ChiStart1 = ChiStart1 + ChiF1Width
ElseIf f = Frame2 Then
ChiFinal2 = ChiFinal2 + ChiF2Width
ChiStart2 = ChiStart2 + ChiF2Width
End If

'Name Create'

If Run = 2 Then

Run2Name Filenum, FileLocationText, Filename, FolderLocation, G, i, f, NumSlices

ElseIf Run = 3 Then

Run3Name Filename, FolderLocation, G, i, f, NumSlices

ElseIf Run = 4 Then

Run4Name Filename, FolderLocation, G, i, f, NumSlices
End If


'export'
ActiveWorkbook.Worksheets.Add
With ActiveSheet.QueryTables.Add(Connection:= _
    FileLocationText, _
    Destination:=Range("$A$2"))
    .Name = Filenum
    .FieldNames = True
    .RowNumbers = False
    .FillAdjacentFormulas = False
    .PreserveFormatting = True
    .RefreshOnFileOpen = False
    .RefreshStyle = xlOverwriteCells
    .SavePassword = False
    .SaveData = True
    .AdjustColumnWidth = True
    .RefreshPeriod = 0
    .TextFilePromptOnRefresh = False
    .TextFilePlatform = 437
    .TextFileStartRow = 50
    .TextFileParseType = xlDelimited
    .TextFileTextQualifier = xlTextQualifierDoubleQuote
    .TextFileConsecutiveDelimiter = True
    .TextFileTabDelimiter = False
    .TextFileSemicolonDelimiter = False
    .TextFileCommaDelimiter = False
    .TextFileSpaceDelimiter = True
    .TextFileColumnDataTypes = Array(1, 1, 1, 1, 1, 1, 1, 1)
    .TextFileTrailingMinusNumbers = True
    .Refresh BackgroundQuery:=False
End With
Cells(1, 1) = Filenum

LastRow = ActiveSheet.Cells(ActiveSheet.Rows.Count, "A").End(xlUp).Row

```

```

Module1 - 5

'Rounding Column'
For r = 1 To LastRow
Cell = "D" & r
Range(Cell).Select
ActiveCell.FormulaR1C1 = "=ROUND(RC[-3],2)"
ActiveCell.Offset(0, 1) = "=RC[-3]"

Next r

'Export PreDelete Frame 1'
LastRowExport = ActiveSheet.Cells(ActiveSheet.Rows.Count, "A").End(xlUp).Row
Range(Cells(2, 4), Cells(LastRowExport, 5)).Select
Set WorkRng = Application.Selection
Set wb = Application.Workbooks.Add
WorkRng.Copy
Selection.PasteSpecial Paste:=xlPasteValues, Operation:=xlNone, SkipBlanks _
:=False, Transpose:=False

If f = Frame1 Then
SavenumEx = Filename & "_" & "0" & NumSlices & "_" & i & "_New_Oct" & "_" & "001"
saveFileEx = FolderLocation & "\" & SavenumEx & ".dat"
ActiveWorkbook.SaveAs Filename:= _
    saveFileEx, FileFormat:=xlTextMSDOS, _
    CreateBackup:=False
Elseif f = Frame2 Then
SavenumEx = Filename & "_" & "0" & NumSlices & "_" & i & "_New_Oct" & "_" & "002"
saveFileEx = FolderLocation & "\" & SavenumEx & ".dat"
ActiveWorkbook.SaveAs Filename:= _
    saveFileEx, FileFormat:=xlTextMSDOS, _
    CreateBackup:=False
End If
wb.Close Saved = True
Application.CutCopyMode = False

'Deletes Frame 1'
'Dim ChiStart1, ChiF1Width, ChiFinal1, ChiStart2, ChiF2Width, ChiFinal2 As Double
If f = Frame1 And ((ChiStart1 <= ChiTopR1) Or (ChiFinal1 >= ChiBotR1)) Then
Deletesrows = Application.Ceiling(((DeleteSize / StepSize) + 2), 1)

FirstDeleteRange1 = "A" & 2
FirstDeleteRange2 = "E" & Deletesrows
FirstDRange = FirstDeleteRange1 & ":" & FirstDeleteRange2

Range(FirstDRange).Select
Selection.delete Shift:=xlUp

LastRowDelete2 = (ActiveSheet.Cells(ActiveSheet.Rows.Count, "A").End(xlUp).Row) + 1
LastRowDelete1 = LastRowDelete2 - Deletesrows
SecondDeleteRange1 = "A" & LastRowDelete1
SecondDeleteRange2 = "E" & LastRowDelete2
SecondDRange = SecondDeleteRange1 & ":" & SecondDeleteRange2

Range(SecondDRange).Select
Selection.delete Shift:=xlUp

Elseif f = Frame2 And ((ChiStart2 <= ChiTopR2) Or (ChiFinal2 >= ChiBotR2)) Then
Deletesrows = Application.Ceiling(((DeleteSize / StepSize) + 2), 1)

FirstDeleteRange1 = "A" & 2
FirstDeleteRange2 = "E" & Deletesrows
FirstDRange = FirstDeleteRange1 & ":" & FirstDeleteRange2

Range(FirstDRange).Select
Selection.delete Shift:=xlUp

LastRowDelete2 = (ActiveSheet.Cells(ActiveSheet.Rows.Count, "A").End(xlUp).Row)
LastRowDelete1 = LastRowDelete2 - Deletesrows + 2

```

```

Module1 - 6

SecondDeleteRange1 = "A" & LastRowDelete1
SecondDeleteRange2 = "E" & LastRowDelete2
SecondDRange = SecondDeleteRange1 & ":" & SecondDeleteRange2

Range(SecondDRange).Select
Selection.delete Shift:=xlUp
End If

'Delete Frame 2'
LastRowExport = ActiveSheet.Cells(ActiveSheet.Rows.Count, "A").End(xlUp).Row
Range(Cells(2, 4), Cells(LastRowExport, 5)).Select
Set WorkRng = Application.Selection
Set wb = Application.Workbooks.Add
WorkRng.Copy
Selection.PasteSpecial Paste:=xlPasteValues, Operation:=xlNone, SkipBlanks _
:=False, Transpose:=False

If f = Frame1 Then
SavenumEx = Filename & "_" & "0" & NumSlices & "_" & i & "_Del" & "_New_Oct" & "_" & "001"
saveFileEx = FolderLocation & "\" & SavenumEx & ".dat"
ActiveWorkbook.SaveAs Filename:= _
    saveFileEx, FileFormat:=xlTextMSDOS, _
    CreateBackup:=False
ElseIf f = Frame2 Then
SavenumEx = Filename & "_" & "0" & NumSlices & "_" & i & "_Del" & "_New_Oct" & "_" & "002"
saveFileEx = FolderLocation & "\" & SavenumEx & ".dat"
ActiveWorkbook.SaveAs Filename:= _
    saveFileEx, FileFormat:=xlTextMSDOS, _
    CreateBackup:=False
End If
wb.Close Saved = True
Application.CutCopyMode = False

Next i
Next f

Sheets("Sheet1").Select

'LastRow = ActiveSheet.Cells(ActiveSheet.Rows.Count, "A").End(xlUp).Row

For s = 1 To (NumSlices)
StartSheet1 = 4
SheetSlic1 = s + StartSheet1 - 1
SheetSearch1 = "Sheet" & SheetSlic1

For r1 = 1 To (LastRow1 - 1)
Cell = "A" & r1
Range(Cell).Select
Cell11 = "R2C4"
Cell21 = "R" & LastRow1 & "C5"
CellLook = "R" & r1 & "C" & 1
SheetLocation = SheetSearch1 & "!" & Cell11 & ":" & Cell21
Lookup = "=IFERROR(VLOOKUP(" & CellLook & "," & SheetLocation & ",2,0)," & Chr(34) & "T" & Chr(34) & "
)"
'Lookup = "=IFERROR(VLOOKUP(" & CellLook & "," & SheetLocation & ",2,0)," & Chr(34) & Chr(34) & ")"
ActiveCell.Offset(0, s) = Lookup

Next r1

Next s

Sheets("Sheet2").Select
s = 1
r2 = 1
For s = 1 To (NumSlices)
StartSheet2 = SheetSlic1

```

Module1 - 7

```

SheetSlice2 = s + StartSheet2
SheetSearch2 = "Sheet" & SheetSlice2

For r2 = 1 To (LastRow2 - 1)
    Cell = "A" & r2
    Range(Cell).Select
    Cell12 = "R2C4"
    Cell22 = "R" & LastRow2 & "C5"
    CellLook = "R" & r2 & "C" & 1
    SheetLocation = SheetSearch2 & "!" & Cell12 & ":" & Cell22
    Lookup = "=IFERROR(VLOOKUP(" & CellLook & "," & SheetLocation & ",2,0)," & Chr(34) & "T" & Chr(34) & "
    )"
    'Lookup = "=IFERROR(VLOOKUP(" & CellLook & "," & SheetLocation & ",2,0)," & Chr(34) & Chr(34) & ")"
    ActiveCell.Offset(0, s) = Lookup

Next r2

Next s

```

```

Sheets("Sheet1").Select
'Second frame max min'
For m = 1 To (LastRow1 - 1)
    Cell = "A" & m
    Range(Cell).Select
    Offset = (NumSlices) + 1
    Offsetmin = (NumSlices) + 2
    RangeLook1 = "R" & m & "C" & 2
    RangeLook2 = "R" & m & "C" & Offset
    ActiveCell.Offset(0, Offset) = "= Max(" & RangeLook1 & ":" & RangeLook2 & ")"
    ActiveCell.Offset(0, Offsetmin) = "= Min(" & RangeLook1 & ":" & RangeLook2 & ")"
Next m

```

'Second Frame Delete

```

LastRowDelete = ActiveSheet.Cells(ActiveSheet.Rows.Count, "A").End(xlUp).Row
For delete = 1 To LastRowDelete
    Range(Cells(delete, 2), Cells(delete, (NumSlices + 1))).Select
    'If WorksheetFunction.CountA(Selection.Rows) = 0 Then
    If WorksheetFunction.CountIf(Selection.Rows, "T") = NumSlices Then
        Selection.Rows.EntireRow.delete
    If delete < LastRowDelete Then
        delete = delete - 1
    LastRowDelete = ActiveSheet.Cells(ActiveSheet.Rows.Count, "A").End(xlUp).Row
    End If
    End If
Next delete

```

```

Sheets("Sheet2").Select

For m = 1 To (LastRow2 - 1)
    Cell = "A" & m
    Range(Cell).Select
    Offset = (NumSlices) + 1
    Offsetmin = (NumSlices) + 2
    RangeLook1 = "R" & m & "C" & 2
    RangeLook2 = "R" & m & "C" & Offset
    ActiveCell.Offset(0, Offset) = "= Max(" & RangeLook1 & ":" & RangeLook2 & ")"
    ActiveCell.Offset(0, Offsetmin) = "= Min(" & RangeLook1 & ":" & RangeLook2 & ")"
Next m

```

```

LastRowDelete = ActiveSheet.Cells(ActiveSheet.Rows.Count, "A").End(xlUp).Row
For delete = 1 To LastRowDelete

```



```

Module1 - 8

Range(Cells(delete, 2), Cells(delete, (NumSlices + 1))).Select
'If WorksheetFunction.CountA(Selection.Rows) = 0 Then
If WorksheetFunction.CountIf(Selection.Rows, "T") = NumSlices Then
Selection.Rows.EntireRow.delete
If delete < LastRowDelete Then
delete = delete - 1
LastRowDelete = ActiveSheet.Cells(ActiveSheet.Rows.Count, "A").End(xlUp).Row
End If
End If
Next delete

'max plot

Sheets.Add After:=Sheets(Sheets.Count)
'LastRow1 could be changed so it it only does the number of cells in each case
x = 0
y = 0

Line = y + 1
Savenum1 = 3 + (NumSlices * 2) + 1
SaveSheet1 = "Sheet" & Savenum1
For x = 0 To (LastRow1 - 1)
Sheets("Sheet1").Select
Range("A1").Select
ActiveCell.Offset(x, y).Range("A1").Select
Selection.Copy
'Stuff to add here for differnt numbers
Sheets(SaveSheet1).Select
Range("A1").Select
ActiveCell.Offset(x, y).Range("A1").Select
Selection.PasteSpecial Paste:=xlPasteValues, Operation:=xlNone, SkipBlanks _
:=False, Transpose:=False

Sheets("Sheet1").Select
Range("A1").Select
ActiveCell.Offset(x, Offset).Range("A1").Select
Selection.Copy
Sheets(SaveSheet1).Select
Range("A1").Select
ActiveCell.Offset(x, Line).Range("A1").Select
Selection.PasteSpecial Paste:=xlPasteValues, Operation:=xlNone, SkipBlanks _
:=False, Transpose:=False
Next x

'min plot

Sheets.Add After:=Sheets(Sheets.Count)
'LastRow1 could be changed so it it only does the number of cells in each case
x = 0
y = 0

Line = y + 1
Savenum1min = 3 + (NumSlices * 2) + 2
SaveSheet1min = "Sheet" & Savenum1min
For x = 0 To (LastRow1 - 1)
Sheets("Sheet1").Select
Range("A1").Select
ActiveCell.Offset(x, y).Range("A1").Select
Selection.Copy
'Stuff to add here for differnt numbers
Sheets(SaveSheet1min).Select
Range("A1").Select
ActiveCell.Offset(x, y).Range("A1").Select
Selection.PasteSpecial Paste:=xlPasteValues, Operation:=xlNone, SkipBlanks _
:=False, Transpose:=False

Sheets("Sheet1").Select
Range("A1").Select

```

Module1 - 9

```

    ActiveCell.Offset(x, Offsetmin).Range("A1").Select
    Selection.Copy
    Sheets(SaveSheet1min).Select
    Range("A1").Select
    ActiveCell.Offset(x, Line).Range("A1").Select
    Selection.PasteSpecial Paste:=xlPasteValues, Operation:=xlNone, SkipBlanks _
        :=False, Transpose:=False
Next x

```

```

Sheets.Add After:=Sheets(Sheets.Count)
Savenum2 = 3 + (NumSlices * 2) + 3
SaveSheet2 = "Sheet" & Savenum2
x = 0
y = 0

Line = y + 1

For x = 0 To (LastRow2 - 1)
    Sheets("Sheet2").Select
    Range("A1").Select
    ActiveCell.Offset(x, y).Range("A1").Select
    Selection.Copy
    'Stuff to add here for differnt numbers
    Sheets(SaveSheet2).Select
    Range("A1").Select
    ActiveCell.Offset(x, y).Range("A1").Select
    Selection.PasteSpecial Paste:=xlPasteValues, Operation:=xlNone, SkipBlanks _
        :=False, Transpose:=False

```

```

Sheets("Sheet2").Select
    Range("A1").Select
    ActiveCell.Offset(x, Offset).Range("A1").Select
    Selection.Copy
    Sheets(SaveSheet2).Select
    Range("A1").Select
    ActiveCell.Offset(x, Line).Range("A1").Select
    Selection.PasteSpecial Paste:=xlPasteValues, Operation:=xlNone, SkipBlanks _
        :=False, Transpose:=False
Next x
"G:\SlicePaper\Schulze\Export Slice 1\Book5.dat"

```

```

Sheets.Add After:=Sheets(Sheets.Count)
Savenum2 = 3 + (NumSlices * 2) + 4
SaveSheet2min = "Sheet" & Savenum2
x = 0
y = 0

Line = y + 1

For x = 0 To (LastRow2 - 1)
    Sheets("Sheet2").Select
    Range("A1").Select
    ActiveCell.Offset(x, y).Range("A1").Select
    Selection.Copy
    'Stuff to add here for differnt numbers
    Sheets(SaveSheet2min).Select
    Range("A1").Select
    ActiveCell.Offset(x, y).Range("A1").Select
    Selection.PasteSpecial Paste:=xlPasteValues, Operation:=xlNone, SkipBlanks _
        :=False, Transpose:=False

```

```

Sheets("Sheet2").Select
    Range("A1").Select
    ActiveCell.Offset(x, Offsetmin).Range("A1").Select
    Selection.Copy

```

Module1 - 10

```

    Sheets(SaveSheet2min).Select
    Range("A1").Select
    ActiveCell.Offset(x, Line).Range("A1").Select
    Selection.PasteSpecial Paste:=xlPasteValues, Operation:=xlNone, SkipBlanks _
        :=False, Transpose:=False
Next x

```

```

Sheets(SaveSheet1).Select
Savenum = Filename & "_" & "0" & NumSlices & "_New_Oct_Max" & "001"
SaveFile1 = FolderLocation & "\" & Savenum & ".dat"
ActiveWorkbook.SaveAs Filename:= _
    SaveFile1, FileFormat:=xlTextMSDOS, _
    CreateBackup:=False

```

```

Sheets(SaveSheet1min).Select
Savenum = Filename & "_" & "0" & NumSlices & "_New_Oct_Min" & "001"
SaveFile1min = FolderLocation & "\" & Savenum & ".dat"
ActiveWorkbook.SaveAs Filename:= _
    SaveFile1min, FileFormat:=xlTextMSDOS, _
    CreateBackup:=False

```

```

Sheets(SaveSheet2).Select
Savenum = Filename & "_" & "0" & NumSlices & "_New_Oct_Max" & "002"
SaveFile2 = FolderLocation & "\" & Savenum & ".dat"
ActiveWorkbook.SaveAs Filename:= _
    SaveFile2, FileFormat:=xlTextMSDOS, _
    CreateBackup:=False

```

```

Sheets(SaveSheet2min).Select
Savenum = Filename & "_" & "0" & NumSlices & "_New_Oct_Min" & "002"
SaveFile2min = FolderLocation & "\" & Savenum & ".dat"
ActiveWorkbook.SaveAs Filename:= _
    SaveFile2min, FileFormat:=xlTextMSDOS, _
    CreateBackup:=False

```

```

Sheets.Add After:=Sheets(Sheets.Count)
Range("A1").Select
ActiveCell.FormulaR1C1 = "ThetaStart1"
Range("A2").Select
ActiveCell.FormulaR1C1 = "ThetaFinal1"
Range("A3").Select
ActiveCell.FormulaR1C1 = "ThetaStart2"
Range("A4").Select
ActiveCell.FormulaR1C1 = "ThetaFinal2"
Range("A5").Select
ActiveCell.FormulaR1C1 = "StepSize"
Range("A6").Select
ActiveCell.FormulaR1C1 = "DeleteSize"
Range("A7").Select

ActiveCell.FormulaR1C1 = "ChiS1Input"
Range("A8").Select
ActiveCell.FormulaR1C1 = "ChiF1Input"
Range("A9").Select
ActiveCell.FormulaR1C1 = "ChiS2Input"
Range("A10").Select
ActiveCell.FormulaR1C1 = "ChiF2Input"
Range("A11").Select

ActiveCell.FormulaR1C1 = "ChiTopR1"

```

Module1 - 11

```

Range("A12").Select
ActiveCell.FormulaR1C1 = "ChiBotR1"
Range("A13").Select
ActiveCell.FormulaR1C1 = "ChiTopR2"
Range("A14").Select
ActiveCell.FormulaR1C1 = "ChiBotR2"
Range("A15").Select

ActiveCell.FormulaR1C1 = "FolderLocation"
Range("A16").Select
ActiveCell.FormulaR1C1 = "FileName"
Range("A17").Select
ActiveCell.FormulaR1C1 = "Run"
Range("A18").Select
ActiveCell.FormulaR1C1 = "G"
Range("A19").Select

ActiveCell.FormulaR1C1 = "Frame1"
Range("A20").Select
ActiveCell.FormulaR1C1 = "Frame2"
Range("A21").Select
ActiveCell.FormulaR1C1 = "Calbrate"
Range("A22").Select

Range("B1").Select
ActiveCell.FormulaR1C1 = ThetaStart1
Range("B2").Select
ActiveCell.FormulaR1C1 = ThetaFinal1
Range("B3").Select
ActiveCell.FormulaR1C1 = ThetaStart2
Range("B4").Select
ActiveCell.FormulaR1C1 = ThetaFinal2
Range("B5").Select
ActiveCell.FormulaR1C1 = StepSize
Range("B6").Select
ActiveCell.FormulaR1C1 = DeleteSize
Range("B7").Select

ActiveCell.FormulaR1C1 = ChiS1Input
Range("B8").Select
ActiveCell.FormulaR1C1 = ChiF1WInput
Range("B9").Select
ActiveCell.FormulaR1C1 = ChiS2Input
Range("B10").Select
ActiveCell.FormulaR1C1 = ChiF2WInput
Range("B11").Select

ActiveCell.FormulaR1C1 = ChiTopR1
Range("B12").Select
ActiveCell.FormulaR1C1 = ChiBotR1
Range("B13").Select
ActiveCell.FormulaR1C1 = ChiTopR2
Range("B14").Select
ActiveCell.FormulaR1C1 = ChiBotR2
Range("B15").Select

ActiveCell.FormulaR1C1 = FolderLocation
Range("B16").Select
ActiveCell.FormulaR1C1 = Filename
Range("B17").Select
ActiveCell.FormulaR1C1 = Run
Range("B18").Select
ActiveCell.FormulaR1C1 = G
Range("B19").Select

ActiveCell.FormulaR1C1 = Frame1
Range("B20").Select
ActiveCell.FormulaR1C1 = Frame2
Range("B21").Select
ActiveCell.FormulaR1C1 = Calbrate
Range("B22").Select

```

Module1 - 12

```
SaveWholeBook = Filename & "_" & "0" & NumSlices
SaveBook = FolderLocation & "\" & SaveWholeBook & ".xlsm"
```

```
ActiveWorkbook.SaveAs Filename:=SaveBook, FileFormat:= _
xlOpenXMLWorkbookMacroEnabled, CreateBackup:=False
```

```
If (Calibrate = 1) Then
```

```
ActiveWindow.Close Saved = True
```

```
Workbooks.Add
w = w + 1
```

```
If w > 9 Then
Calibrate = 3
End If
```

```
Else
```

```
Exit Do
```

```
End If
Loop
Next G
```

```
Application.ScreenUpdating = True
End Sub
```

```
Function Run2Name(Filenum As String, FileLocationText As String, ByVal Filename As String, ByVal FolderLocation As String, ByVal G As Integer, ByVal i As Integer, ByVal f As Integer, ByVal NumSlices As String)
```

```
If (G < 10) Then
```

```
If (NumSlices < 10) Then
If (i < 10) Then
Filenum = Filename & "_" & "0" & NumSlices & "_0" & G & "_" & "00" & i & "_New_Oct" & "_00" & f & "_Subtract"
FileLocationText = "TEXT;" & FolderLocation & "\" & Filenum & ".plv"
ElseIf (i >= 10) And (i < 100) Then
Filenum = Filename & "_" & "0" & NumSlices & "_0" & G & "_" & "0" & i & "_New_Oct" & "_00" & f & "_Subtract"
FileLocationText = "TEXT;" & FolderLocation & "\" & Filenum & ".plv"
ElseIf (i >= 100) Then
Filenum = Filename & "_" & "0" & NumSlices & "_0" & G & "_" & i & "_New_Oct" & "_00" & f & "_Subtract"
FileLocationText = "TEXT;" & FolderLocation & "\" & Filenum & ".plv"
End If
```

```
ElseIf (NumSlices >= 10) Then
If (i < 10) Then
Filenum = Filename & "_" & NumSlices & "_0" & G & "_" & "00" & i & "_New_Oct" & "_00" & f & "_Subtract"
FileLocationText = "TEXT;" & FolderLocation & "\" & Filenum & ".plv"
ElseIf (i >= 10) And (i < 100) Then
Filenum = Filename & "_" & NumSlices & "_0" & G & "_" & "0" & i & "_New_Oct" & "_00" & f & "_Subtract"
FileLocationText = "TEXT;" & FolderLocation & "\" & Filenum & ".plv"
ElseIf (i >= 100) Then
Filenum = Filename & "_" & NumSlices & "_0" & G & "_" & i & "_New_Oct" & "_00" & f & "_Subtract"
FileLocationText = "TEXT;" & FolderLocation & "\" & Filenum & ".plv"
End If
End If
```

```
Else
If (NumSlices < 10) Then
If (i < 10) Then
Filenum = Filename & "_" & "0" & NumSlices & "_" & G & "_" & "00" & i & "_New_Oct" & "_00" & f & "_Subtract"
```

Module1 - 13

```

tract"
FileLocationText = "TEXT;" & FolderLocation & "\" & Filenum & ".plv"
ElseIf (i >= 10) And (i < 100) Then
Filenum = Filename & "_" & "0" & NumSlices & "_" & G & "_" & "0" & i & "_New_Oct" & "_00" & f & "_Subt
ract"
FileLocationText = "TEXT;" & FolderLocation & "\" & Filenum & ".plv"
ElseIf (i >= 100) Then
Filenum = Filename & "_" & "0" & NumSlices & "_" & G & "_" & i & "_New_Oct" & "_00" & f & "_Subtract"
FileLocationText = "TEXT;" & FolderLocation & "\" & Filenum & ".plv"
End If

ElseIf (NumSlices >= 10) Then
If (i < 10) Then
Filenum = Filename & "_" & NumSlices & "_" & G & "_" & "00" & i & "_New_Oct" & "_00" & f & "_Subtract"
FileLocationText = "TEXT;" & FolderLocation & "\" & Filenum & ".plv"
ElseIf (i >= 10) And (i < 100) Then
Filenum = Filename & "_" & NumSlices & "_" & G & "_" & "0" & i & "_New_Oct" & "_00" & f & "_Subtract"
FileLocationText = "TEXT;" & FolderLocation & "\" & Filenum & ".plv"
ElseIf (i >= 100) Then
Filenum = Filename & "_" & NumSlices & "_" & G & "_" & i & "_New_Oct" & "_00" & f & "_Subtract"
FileLocationText = "TEXT;" & FolderLocation & "\" & Filenum & ".plv"
End If

End If

End If

End Function
Private Sub Run3Name(ByVal Filename As String, ByVal FolderLocation As String, ByVal G As Integer, ByV
al i As Integer, ByVal f As Integer, ByVal NumSlices As String)

If (G < 10) Then

If (NumSlices < 10) Then
If (i < 10) Then
Filenum = Filename & "_" & "0" & NumSlices & "_00" & G & "_" & "00" & i & "_New_Oct" & "_00" & f & "_S
ubtract"
FileLocationText = "TEXT;" & FolderLocation & "\" & Filenum & ".plv"
ElseIf (i >= 10) And (i < 100) Then
Filenum = Filename & "_" & "0" & NumSlices & "_00" & G & "_" & "0" & i & "_New_Oct" & "_00" & f & "_Su
btract"
FileLocationText = "TEXT;" & FolderLocation & "\" & Filenum & ".plv"
ElseIf (i >= 100) Then
Filenum = Filename & "_" & "0" & NumSlices & "_00" & G & "_" & i & "_New_Oct" & "_00" & f & "_Subtract
"
FileLocationText = "TEXT;" & FolderLocation & "\" & Filenum & ".plv"
End If

ElseIf (NumSlices >= 10) Then
If (i < 10) Then
Filenum = Filename & "_" & NumSlices & "_00" & G & "_" & "00" & i & "_New_Oct" & "_00" & f & "_Subtrac
t"
FileLocationText = "TEXT;" & FolderLocation & "\" & Filenum & ".plv"
ElseIf (i >= 10) And (i < 100) Then
Filenum = Filename & "_" & NumSlices & "_00" & G & "_" & "0" & i & "_New_Oct" & "_00" & f & "_Subtract
"
FileLocationText = "TEXT;" & FolderLocation & "\" & Filenum & ".plv"
ElseIf (i >= 100) Then
Filenum = Filename & "_" & NumSlices & "_00" & G & "_" & i & "_New_Oct" & "_00" & f & "_Subtract"
FileLocationText = "TEXT;" & FolderLocation & "\" & Filenum & ".plv"
End If
End If

ElseIf (G >= 10) And (G < 100) Then
If (NumSlices < 10) Then
If (i < 10) Then
Filenum = Filename & "_" & "0" & NumSlices & "_0" & G & "_" & "00" & i & "_New_Oct" & "_00" & f & "_Su
btract"
FileLocationText = "TEXT;" & FolderLocation & "\" & Filenum & ".plv"
ElseIf (i >= 10) And (i < 100) Then

```

Module1 - 14

```

Filename = Filename & "_" & "0" & NumSlices & "_0" & G & "_" & "0" & i & "_New_Oct" & "_00" & f & "_Sub
tract"
FileLocationText = "TEXT;" & FolderLocation & "\" & Filename & ".plv"
ElseIf (i >= 100) Then
Filename = Filename & "_" & "0" & NumSlices & "_0" & G & "_" & i & "_New_Oct" & "_00" & f & "_Subtract"
FileLocationText = "TEXT;" & FolderLocation & "\" & Filename & ".plv"
End If

ElseIf (NumSlices >= 10) Then
If (i < 10) Then
Filename = Filename & "_" & NumSlices & "_0" & G & "_" & "00" & i & "_New_Oct" & "_00" & f & "_Subtract
"
FileLocationText = "TEXT;" & FolderLocation & "\" & Filename & ".plv"
ElseIf (i >= 10) And (i < 100) Then
Filename = Filename & "_" & NumSlices & "_0" & G & "_" & "0" & i & "_New_Oct" & "_00" & f & "_Subtract"
FileLocationText = "TEXT;" & FolderLocation & "\" & Filename & ".plv"
ElseIf (i >= 100) Then
Filename = Filename & "_" & NumSlices & "_0" & G & "_" & i & "_New_Oct" & "_00" & f & "_Subtract"
FileLocationText = "TEXT;" & FolderLocation & "\" & Filename & ".plv"
End If
End If

ElseIf (G >= 100) Then
If (NumSlices < 10) Then
If (i < 10) Then
Filename = Filename & "_" & "0" & NumSlices & "_" & G & "_" & "00" & i & "_New_Oct" & "_00" & f & "_Sub
tract"
FileLocationText = "TEXT;" & FolderLocation & "\" & Filename & ".plv"
ElseIf (i >= 10) And (i < 100) Then
Filename = Filename & "_" & "0" & NumSlices & "_" & G & "_" & "0" & i & "_New_Oct" & "_00" & f & "_Subt
ract"
FileLocationText = "TEXT;" & FolderLocation & "\" & Filename & ".plv"
ElseIf (i >= 100) Then
Filename = Filename & "_" & "0" & NumSlices & "_" & G & "_" & i & "_New_Oct" & "_00" & f & "_Subtract"
FileLocationText = "TEXT;" & FolderLocation & "\" & Filename & ".plv"
End If
End If

ElseIf (NumSlices >= 10) Then
If (i < 10) Then
Filename = Filename & "_" & NumSlices & "_" & G & "_" & "00" & i & "_New_Oct" & "_00" & f & "_Subtract"
FileLocationText = "TEXT;" & FolderLocation & "\" & Filename & ".plv"
ElseIf (i >= 10) And (i < 100) Then
Filename = Filename & "_" & NumSlices & "_" & G & "_" & "0" & i & "_New_Oct" & "_00" & f & "_Subtract"
FileLocationText = "TEXT;" & FolderLocation & "\" & Filename & ".plv"
ElseIf (i >= 100) Then
Filename = Filename & "_" & NumSlices & "_" & G & "_" & i & "_New_Oct" & "_00" & f & "_Subtract"
FileLocationText = "TEXT;" & FolderLocation & "\" & Filename & ".plv"
End If
End If

End If
End Sub
Private Sub Run4Name(ByVal Filename As String, ByVal FolderLocation As String, ByVal G As Integer, ByV
al i As Integer, ByVal f As Integer, ByVal NumSlices As String)

If (G < 10) Then

If (NumSlices < 10) Then
If (i < 10) Then
Filename = Filename & "_" & "0" & NumSlices & "_000" & G & "_" & "00" & i & "_New_Oct" & "_00" & f & "_
Subtract"
FileLocationText = "TEXT;" & FolderLocation & "\" & Filename & ".plv"
ElseIf (i >= 10) And (i < 100) Then
Filename = Filename & "_" & "0" & NumSlices & "_000" & G & "_" & "0" & i & "_New_Oct" & "_00" & f & "_S
ubtract"
FileLocationText = "TEXT;" & FolderLocation & "\" & Filename & ".plv"
ElseIf (i >= 100) Then
Filename = Filename & "_" & "0" & NumSlices & "_000" & G & "_" & i & "_New_Oct" & "_00" & f & "_Subtrac
t"
FileLocationText = "TEXT;" & FolderLocation & "\" & Filename & ".plv"
End If

```


Module1 - 16

```

Filename = Filename & "_" & NumSlices & "_0" & G & "_" & i & "_New_Oct" &
"_00" & f & "_Subtract" FileLocationText = "TEXT;" & FolderLocation & "\" &
Filename & ".plv"
End If
End If
ElseIf (G >= 1000) Then
If (NumSlices < 10) Then
If (i < 10) Then
Filename = Filename & "_" & "0" & NumSlices & "_" & G & "_" & "00" & i &
"_New_Oct" & "_00" & f & "_Subtract"
FileLocationText = "TEXT;" & FolderLocation & "\" & Filename & ".plv"
ElseIf (i >= 10) And (i < 100) Then
Filename = Filename & "_" & "0" & NumSlices & "_" & G & "_" & "0" & i &
"_New_Oct" & "_00" & f & "_Subtract"
FileLocationText = "TEXT;" & FolderLocation & "\" & Filename & ".plv"
ElseIf (i >= 100) Then
Filename = Filename & "_" & "0" & NumSlices & "_" & G & "_" & i & "_New_Oct" &
"_00" & f & "_Subtract" FileLocationText = "TEXT;" & FolderLocation & "\" &
Filename & ".plv"
End If
ElseIf (NumSlices >= 10) Then
If (i < 10) Then
Filename = Filename & "_" & NumSlices & "_" & G & "_" & "00" & i & "_New_Oct" &
"_00" & f & "_Subtract" FileLocationText = "TEXT;" & FolderLocation & "\" &
Filename & ".plv"
ElseIf (i >= 10) And (i < 100) Then
Filename = Filename & "_" & NumSlices & "_" & G & "_" & "0" & i & "_New_Oct" &
"_00" & f & "_Subtract" FileLocationText = "TEXT;" & FolderLocation & "\" &
Filename & ".plv"
ElseIf (i >= 100) Then
Filename = Filename & "_" & NumSlices & "_" & G & "_" & i & "_New_Oct" & "_00" &
f & "_Subtract" FileLocationText = "TEXT;" & FolderLocation & "\" & Filename &
".plv"
End If
End If
End If
End Sub

```

Appendix C: AHK Files

Clicks the mouse through the refinement steps saving time

^!r::

WinWait, CELREF V3 (17/10/03),

IfWinNotActive, CELREF V3 (17/10/03), , WinActivate, CELREF V3 (17/10/03),

WinWaitActive, CELREF V3 (17/10/03),

MouseClick, left, 552, 101

Sleep, 100

MouseClick, left, 465, 68

Sleep, 100

MouseClick, left, 209, 100

Sleep, 100

MouseClick, left, 568, 66

Sleep, 100

MouseClick, left, 519, 99

Sleep, 100

return

Setups Celref for Unit Cell Refinement

^!z::

WinWait, Start,

IfWinNotActive, Start, , WinActivate, Start,

WinWaitActive, Start,

MouseClick, left, 12, 25

Sleep, 100

WinWait, Start menu,

IfWinNotActive, Start menu, , WinActivate, Start menu,

WinWaitActive, Start menu,

MouseClick, left, 112, 61

Sleep, 100

WinWait, CELREF V3 (17/10/03),

IfWinNotActive, CELREF V3 (17/10/03), , WinActivate, CELREF V3 (17/10/03),

WinWaitActive, CELREF V3 (17/10/03),

Sleep, 100

MouseClick, left, 341, 63

Sleep, 100

MouseClick, left, 227, 102

Sleep, 100

MouseClick, left, 207, 159

Sleep, 100

MouseClick, left, 246, 297

Sleep, 100

MouseClick, left, 190, 340

Sleep, 100

Click WheelDown

Click WheelDown

Click WheelDown

Click WheelDown

Click WheelDown

Click WheelDown

Click WheelDown

Click WheelDown

Click WheelDown

Click WheelDown

Click WheelDown

Sleep, 500

MouseClick, left, 190, 340

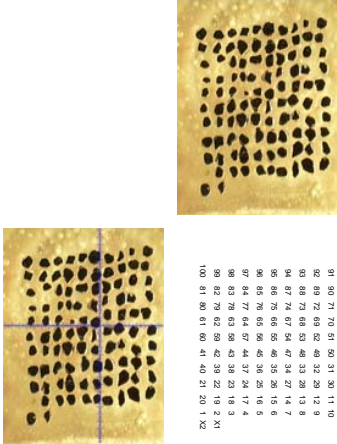
Sleep, 100

Appendix D GADDs Images
Gabbon

Gabon MSL040095 PM
Grains 11-21
May 5th 2013
Patrick Shepherd

Appendix D: GADDs Images

Overview Image



91	92	71	72	51	52	31	32	11	12	
93	94	73	74	53	54	33	34	13	14	
95	96	75	76	55	56	35	36	15	16	
97	98	77	78	57	58	37	38	17	18	
99	100	79	80	59	60	39	40	19	20	
96	86	76	66	46	36	26	16	6		
98	85	78	65	48	38	28	18	5		
97	84	77	64	47	37	27	17	4		
99	83	79	63	49	39	29	19	3		
98	82	78	62	48	38	28	18	2	X1	
100	81	80	71	60	41	40	21	20	1	X2

Gabon Disc 1

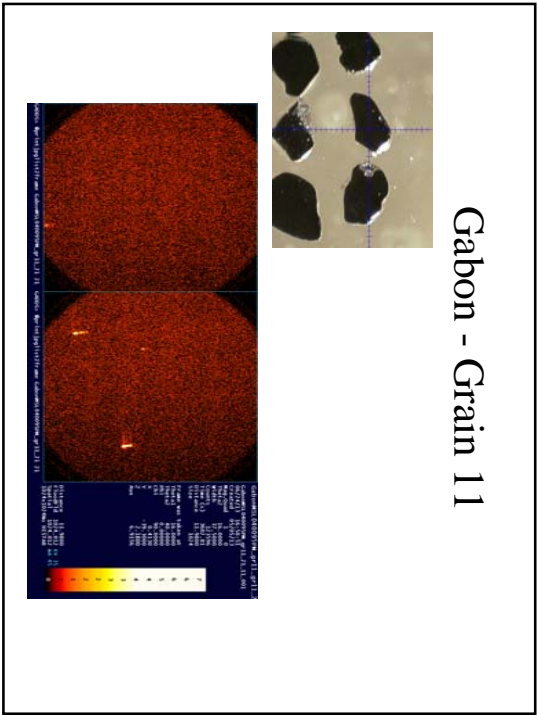
Frame 1

Theta 1 = 16
Theta 2 =40
W = 37.5
T = 60min

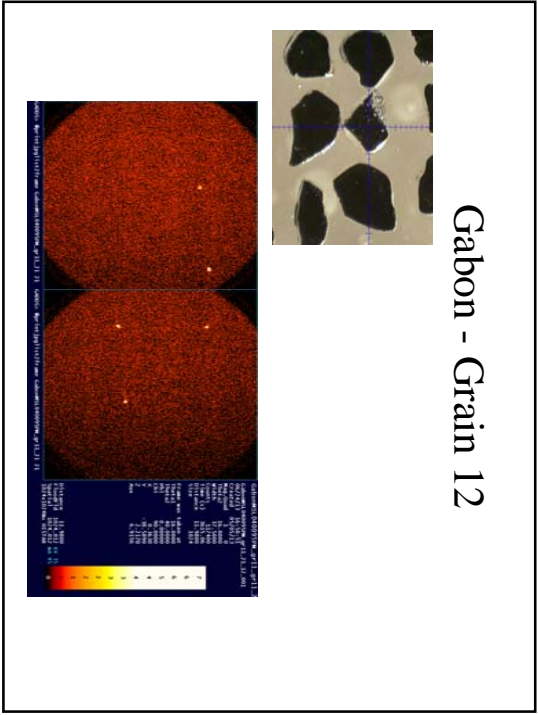
Frame 2

Theta 1 = 45.5
Theta 2 =40
W = 7.5
T = 60min

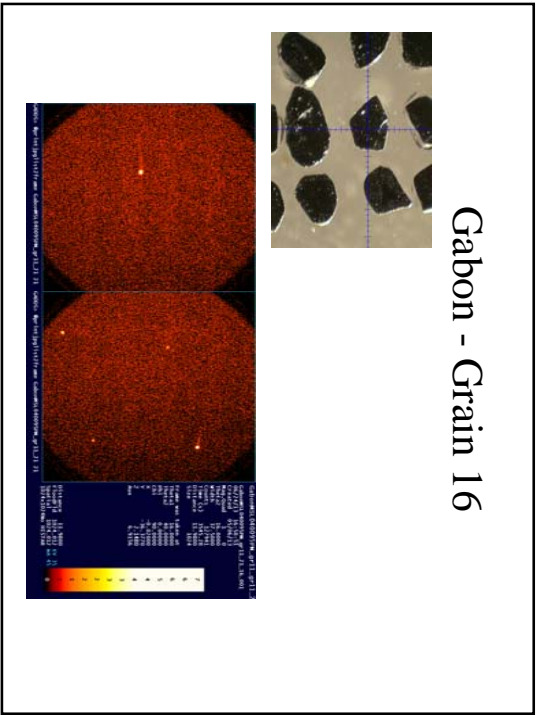
Gabon - Grain 11



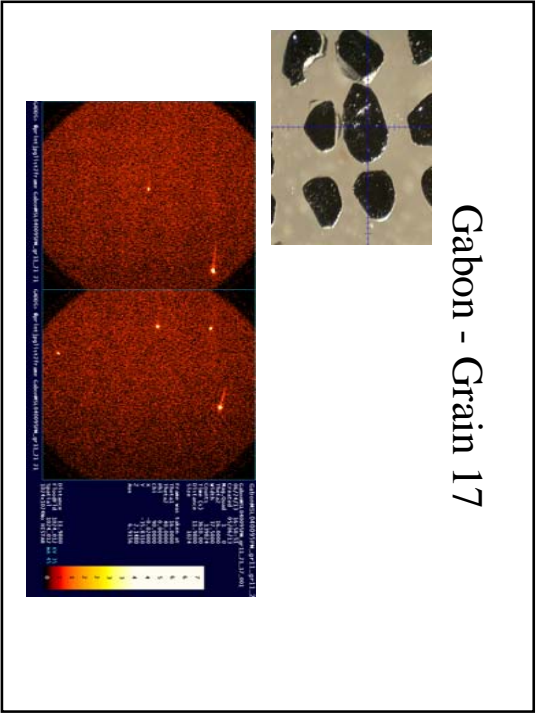
Gabon - Grain 12



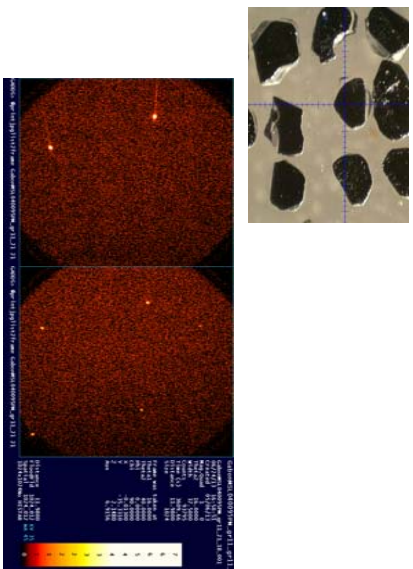
Gabon - Grain 16



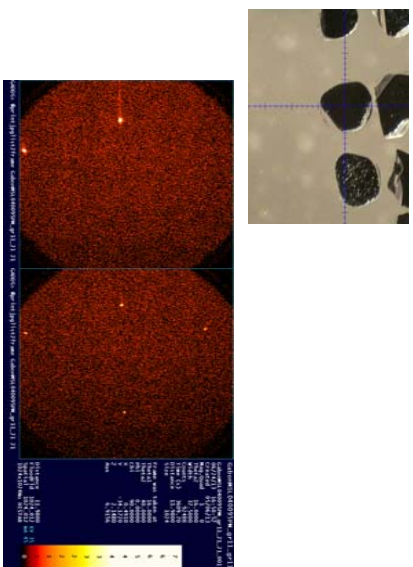
Gabon - Grain 17



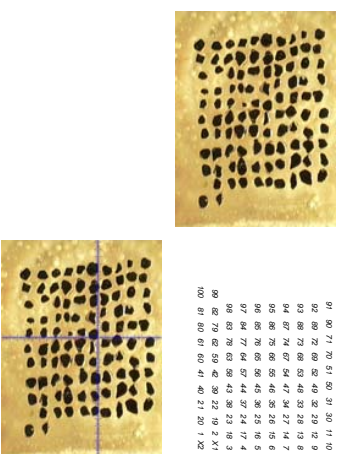
Gabon - Grain 18



Gabon - Grain 21



Overview Image



Run By Slam File : Frame 1 Config

Options for Collect Scan MultiTargets

Frames1

Thick116Thin240Phi0.0Chi 30.000

Scan box # 1-0mmFrame width 17.5Seconds/frame 60.00

Job name GabonMSL040095PM_gr22_100

Title GabonMSL040095PM_gr22_100

Sample name GabonMSL040095PM_gr22_100

Sample number1

Max display counts15Realtime display

Sequence # at starting run22Sequence # at ending run100

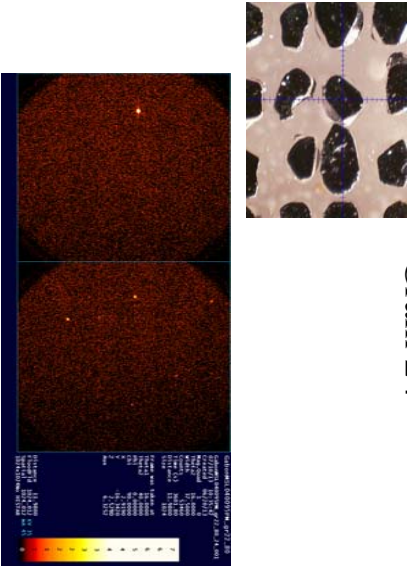
ModeSCANRotate sampleSample Disc NameAmplitude 0mm

Auto Z alignment

OKCancel

Capture Video Image

GabonMSL040095PM Grain 22-80:
Grain 24



Run By Slam File : Frame 2 Config

Options for Collect Scan MultiTargets

Frames1

Thick146.5Thin240Phi0.0Chi 30.000

Scan box # 1-0mmFrame width 17.5Seconds/frame 60.00

Job name GabonMSL040095PM_gr22_100

Title GabonMSL040095PM_gr22_100

Sample name GabonMSL040095PM_gr22_100

Sample number1

Max display counts15Realtime display

Sequence # at starting run22Sequence # at ending run100

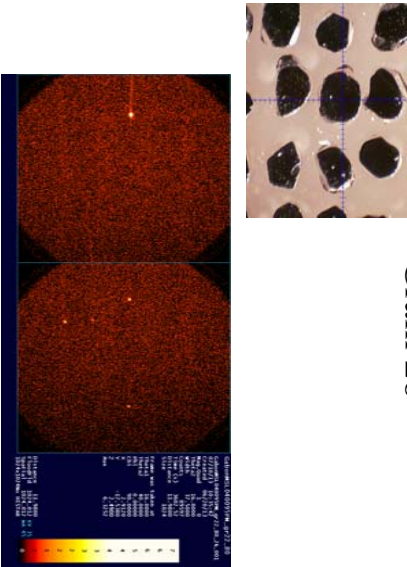
ModeSCANRotate sampleSample Disc NameAmplitude 0mm

Auto Z alignment

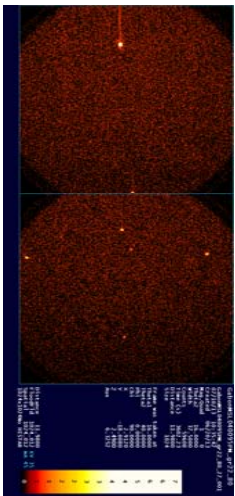
OKCancel

Capture Video Image

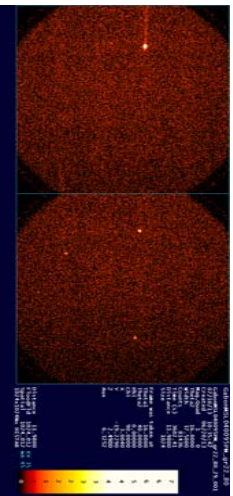
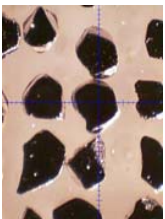
GabonMSL040095PM Grain 22-80:
Grain 26



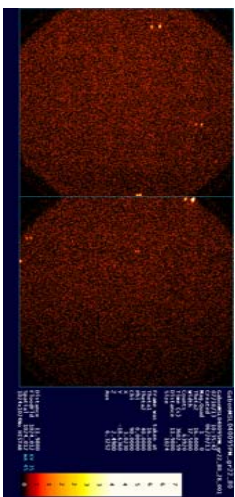
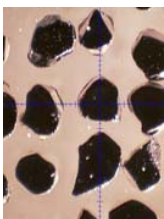
Grain 27



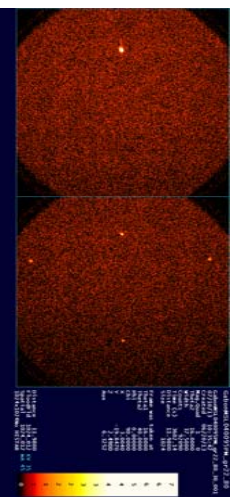
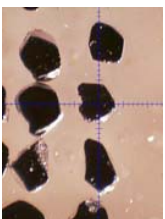
Grain 29



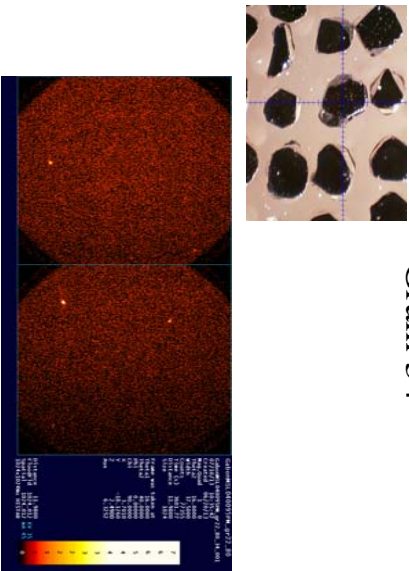
Grain 28



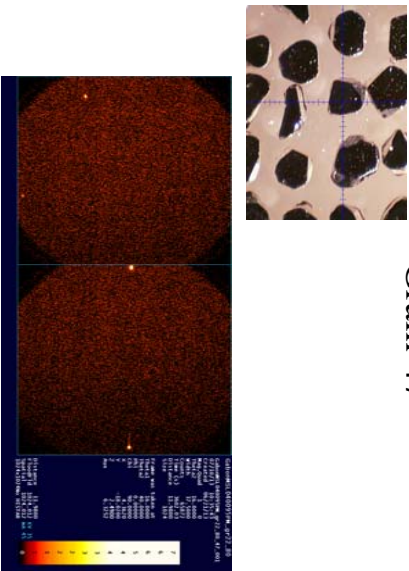
Grain 30



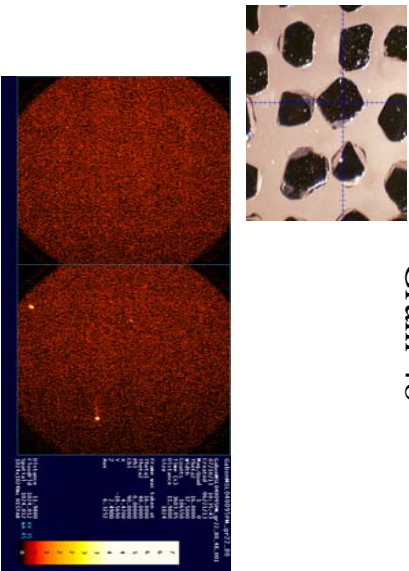
GabonMSL040095PM Grain 22-80:
Grain 34



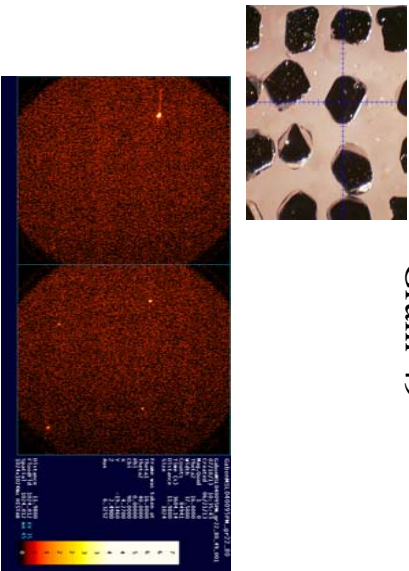
GabonMSL040095PM Grain 22-80:
Grain 47



GabonMSL040095PM Grain 22-80:
Grain 48

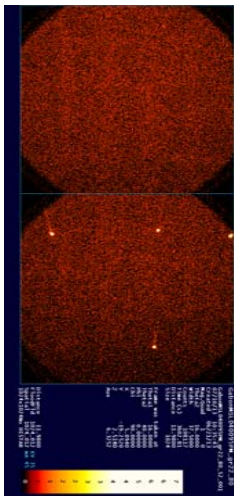
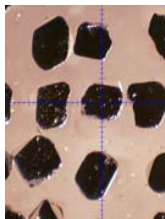


GabonMSL040095PM Grain 22-80:
Grain 49



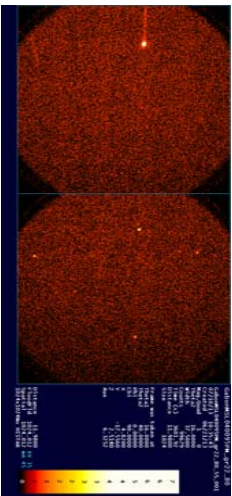
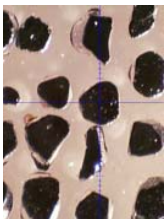
GabonMSL040095PM Grain 22-80:

Grain 52



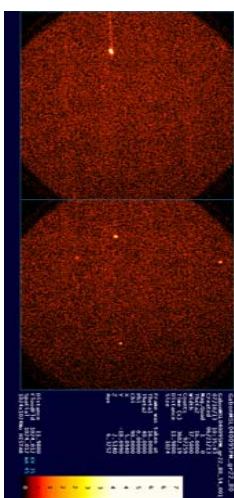
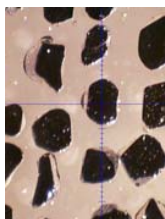
GabonMSL040095PM Grain 22-80:

Grain 55



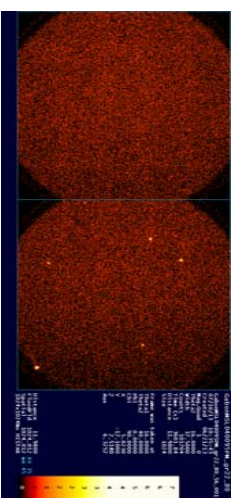
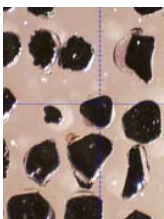
GabonMSL040095PM Grain 22-80:

Grain 54



GabonMSL040095PM Grain 22-80:

Grain 56

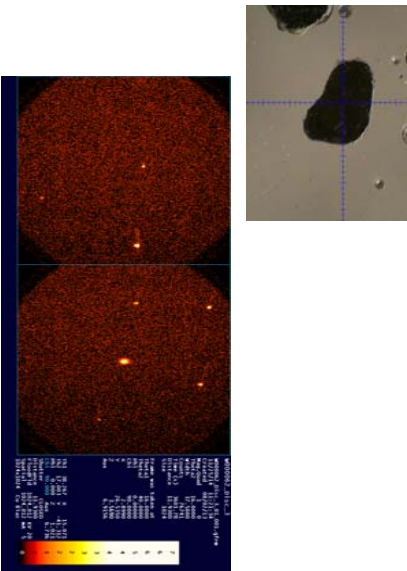


Matistama W000062 PM
Grains 1-30
August 2nd 2013
Patrick Shepherd

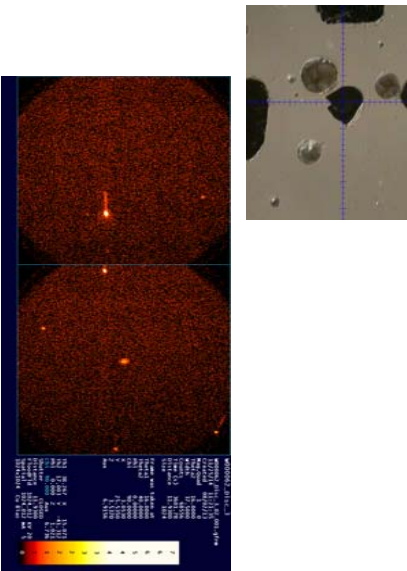
Matistama Disc 3

Frame 1	Frame 2
Theta 1 = 16	Theta 1 = 45.5
Theta 2 = 40	Theta 2 = 40
W = 37.5	W = 7.5
T = 60min	T = 60min

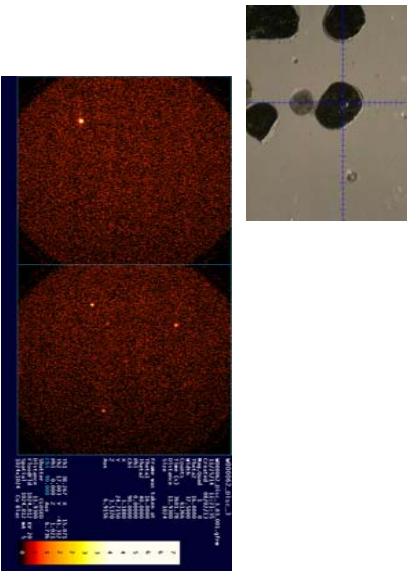
Matsitama Grain 1



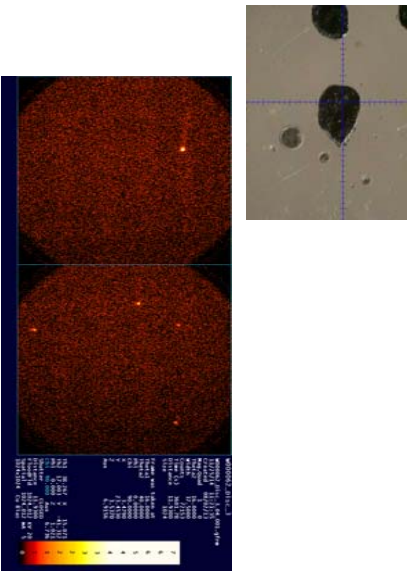
Matsitama Grain 2



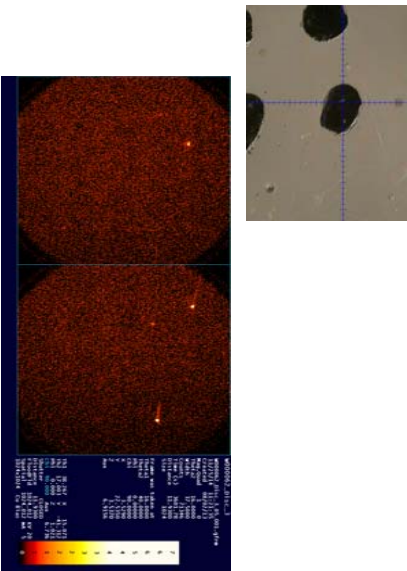
Matsitama Grain 3



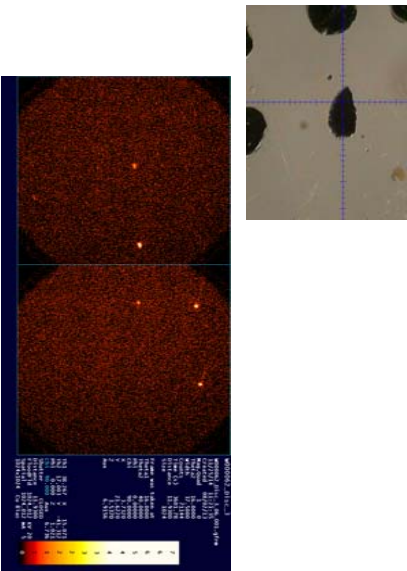
Matsitama Grain 4



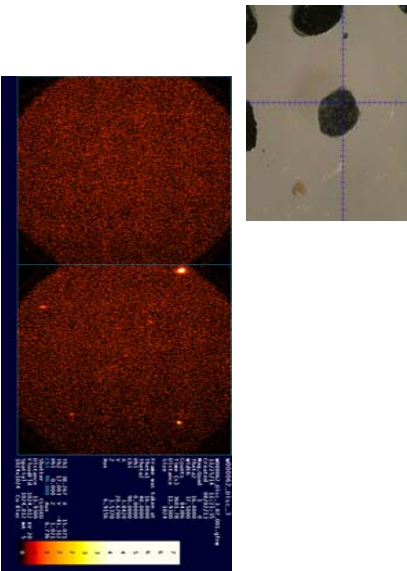
Matsitama Grain 5



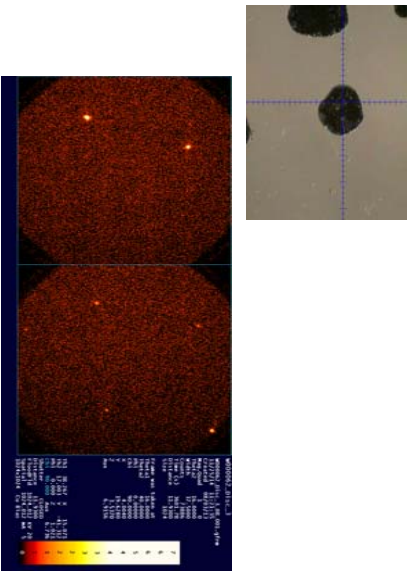
Matsitama Grain 6



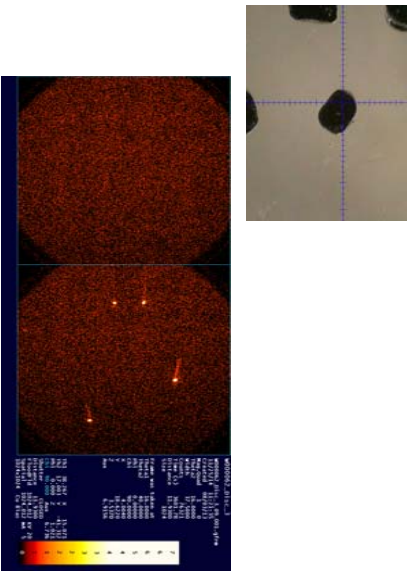
Matsitama Grain 7



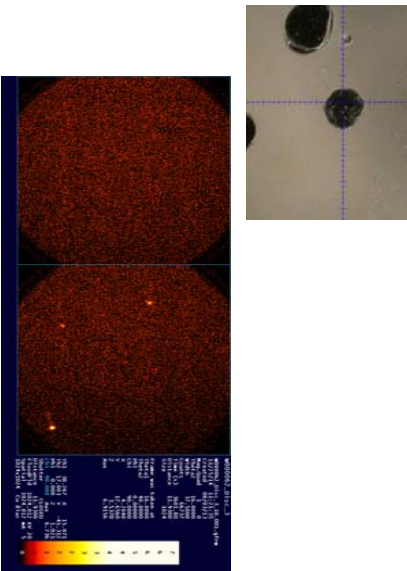
Matsitama Grain 8

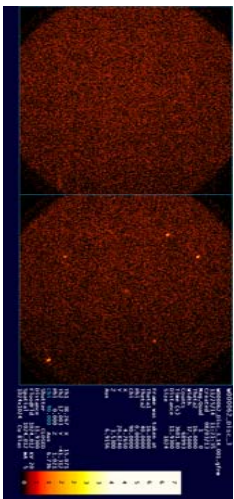

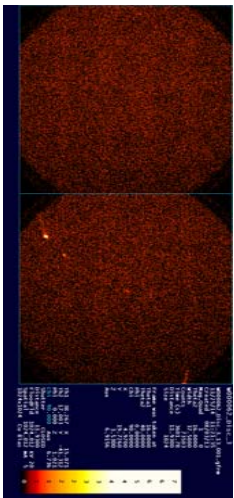

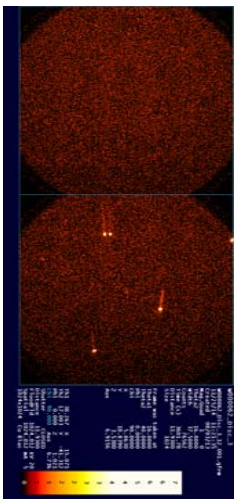
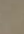
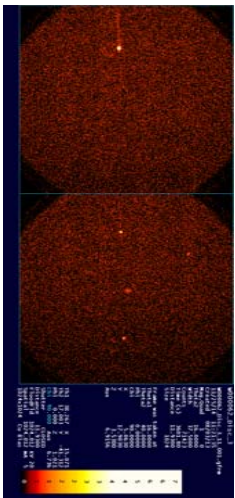
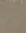


Matsitama Grain 9

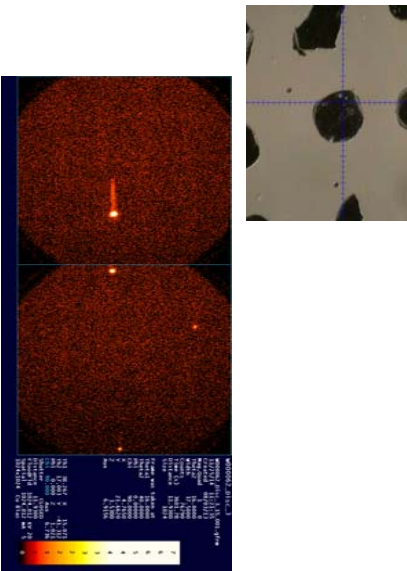


Matsitama Grain 10

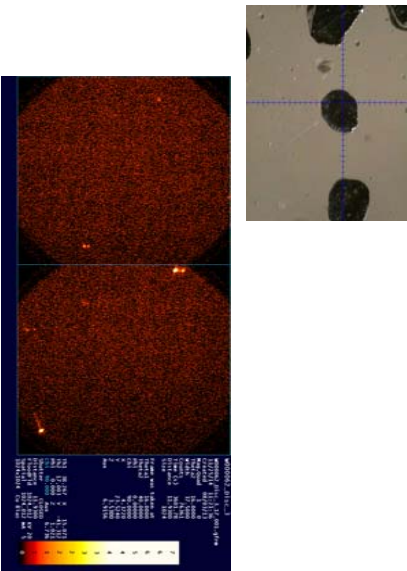




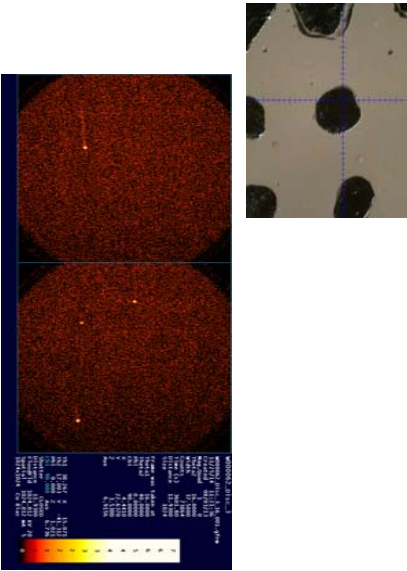
Matsitama Grain 15



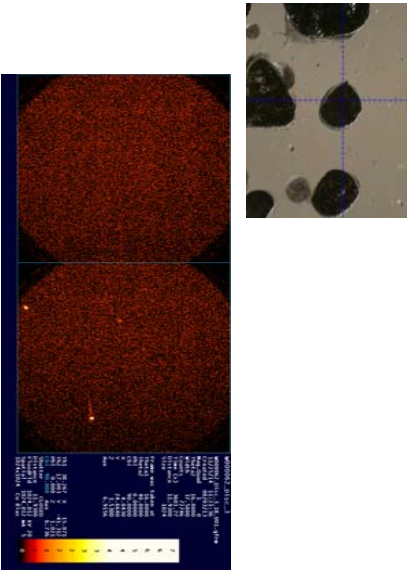
Matsitama Grain 17

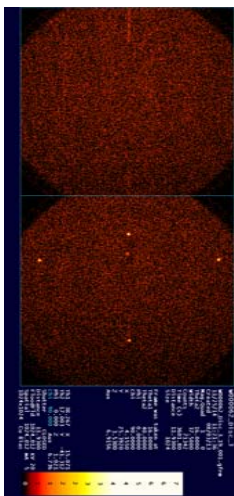
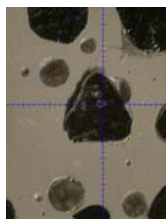


Matsitama Grain 16

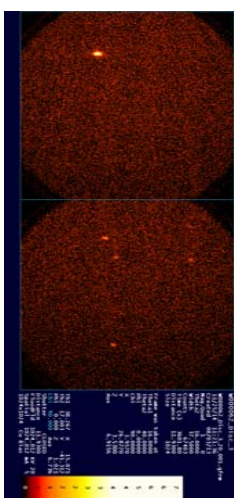
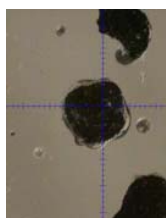


Matsitama Grain 18

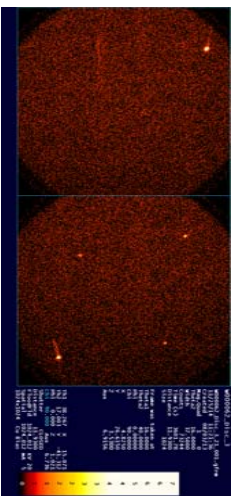
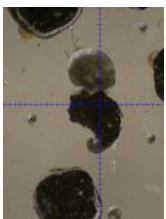




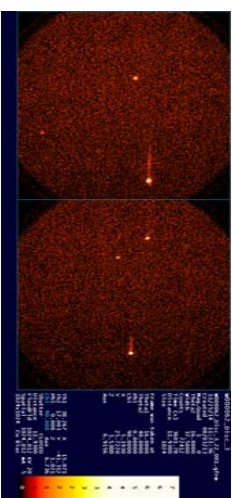
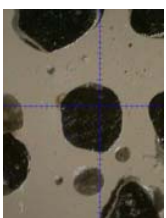
Matsitama Grain 20



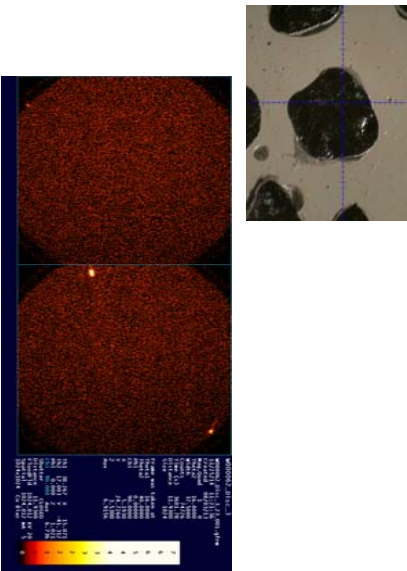
Matsitama Grain 21



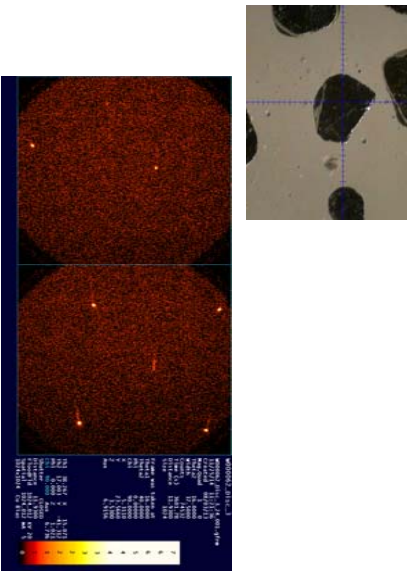
Matsitama Grain 22



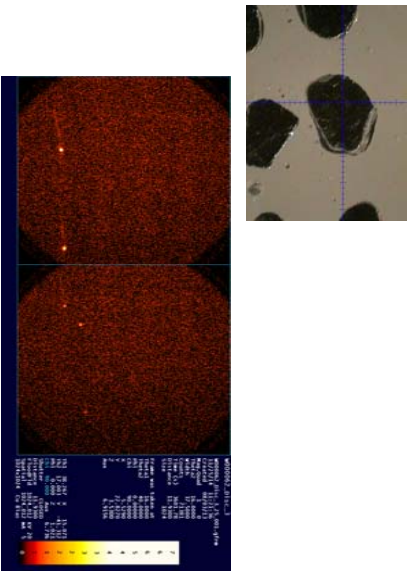
Matsitama Grain 23



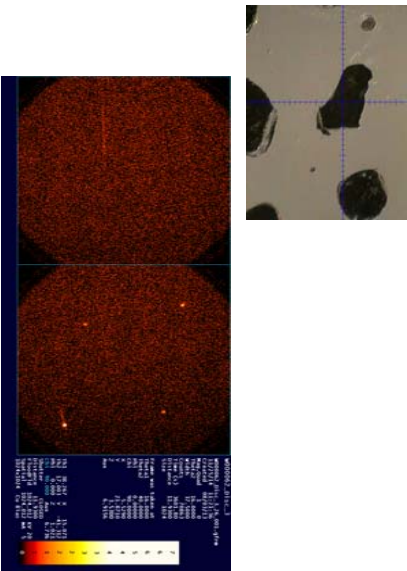
Matsitama Grain 24



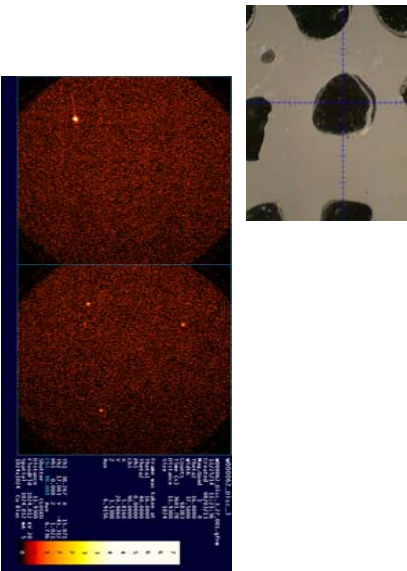
Matsitama Grain 25



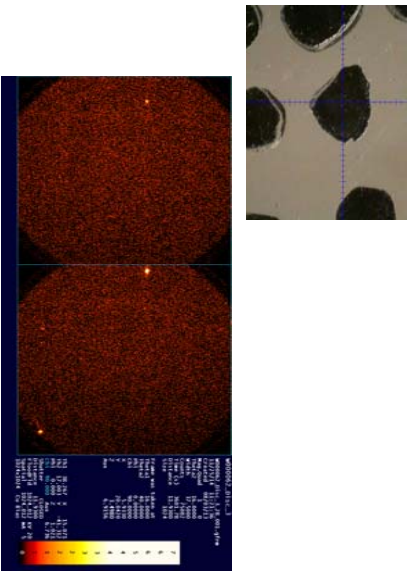
Matsitama Grain 26



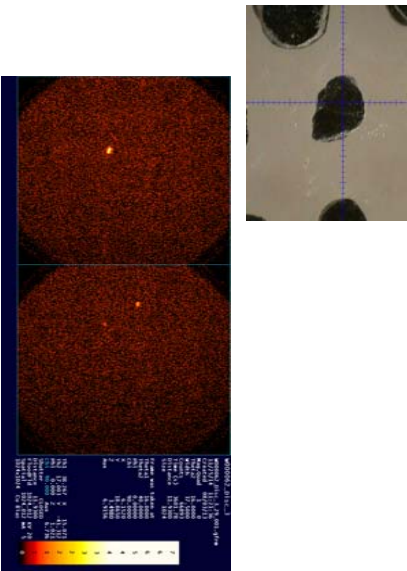
Matsitama Grain 27



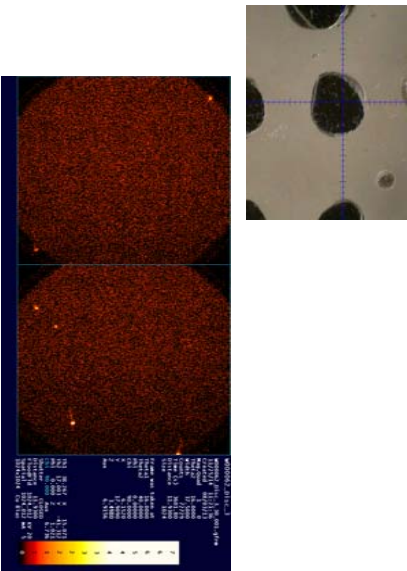
Matsitama Grain 28



Matsitama Grain 29



Matsitama Grain 30

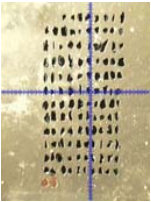


Misery_WO_03_58_PMO

By Patrick Shepherd



111110 01 30 71 70 61 50 31 30 11 10
112109 02 80 72 60 52 49 32 29 12 9
113108 03 88 79 68 53 48 33 28 13 8
114107 04 87 74 67 54 47 34 27 14 7
115106 05 86 73 66 55 46 35 26 15 6
116105 06 85 75 65 56 45 36 25 16 5
117104 07 84 76 64 57 44 37 24 17 4
118103 08 83 78 63 58 43 38 23 18 3
119102 09 82 79 62 59 42 39 22 19 2 31
120100 81 80 81 80 41 40 21 20 1 32



Misery_WO_03_58_PMO

May 18th, 2013
Bruker D8 Discover
100um Gobel Mirror

Options for Collect Scan Multi-Steps

# Frames: 1	Theta: 10	Phi: 0.0	Chi: 90.000
Scan Rate: # 2.0m	Frame width: 37.5	Seconds/frame: 0.000	
Job name: Misery_WO_03_58_PMO			
Title: Misery_WO_03_58_PMO			
Sample name: Misery_WO_03_58_PMO			
Sample number: 1			
Max display count: 15	Realtime display	Pre-clear	
Sequence # of starting run: 001		Sequence # of ending run: 118	
Mode: SCAN	Rotate sample	Sample Size: None	Amplitude: 0 mm
<input checked="" type="checkbox"/> Capture Video Image <input type="checkbox"/> Auto Z alignment			
<input type="button" value="OK"/> <input type="button" value="Cancel"/>			

Options for Collect Scan MultiTargets

Frames1

Thick145.5

Thin210

Pin0.0

Ch390.000

Scan Axis #2.0m

Frame width7.5

Second/frame60.00

Job nameMateriy_WO_03_58_PM0

Title Materiy_WO_03_58_PM

Sample nameMateriy_WO_03_58_PM

Sample number1

Max display counts15

Realtime display

Sequence # of starting run001

Sequence # of ending run118

ModeSCAN

Rotate sample

Sample Disc Name

Amplitude0

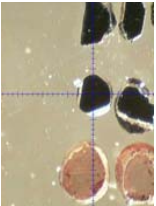
mm

Capture Video Image

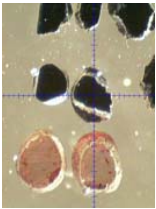
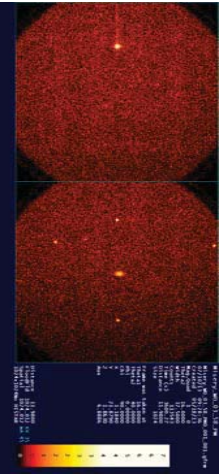
Auto Z alignment

OK

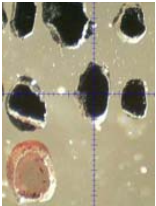
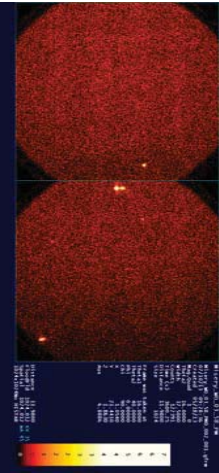
Cancel



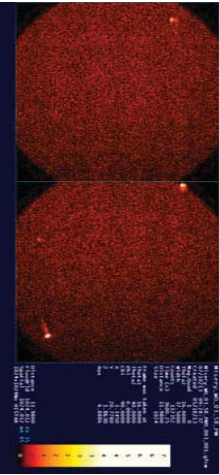
WO_03_58_PM0 Disc 3: Grain 1



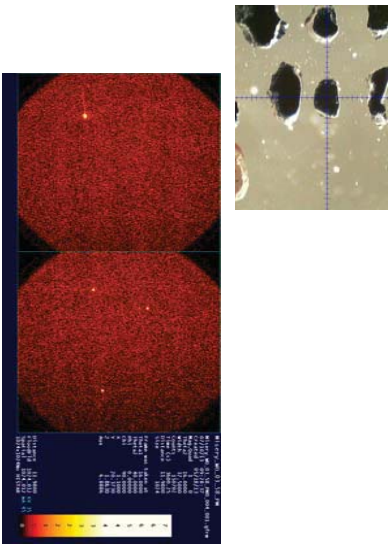
WO_03_58_PM0 Disc 3: Grain 2



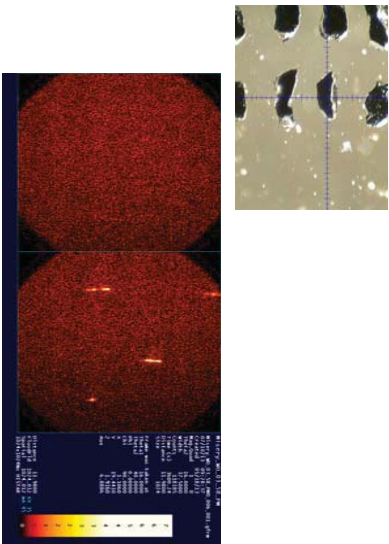
WO_03_58_PM0 Disc 3: Grain 3



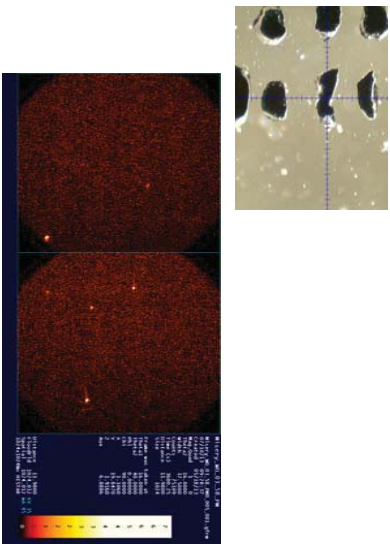
WO_03_58_PM0 Disc 3: Grain 4



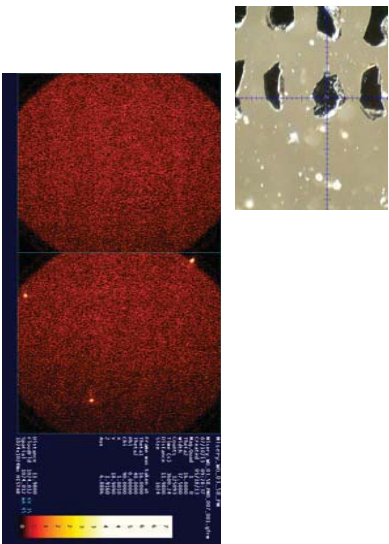
WO_03_58_PM0 Disc 3: Grain 6



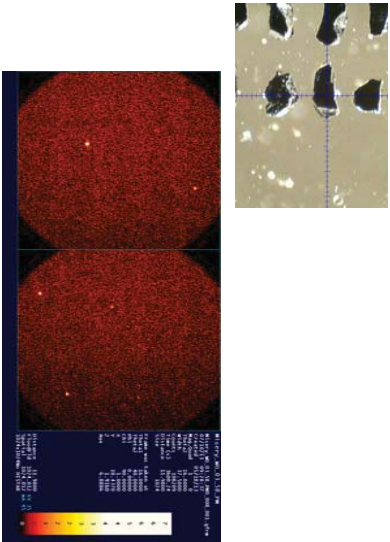
WO_03_58_PM0 Disc 3: Grain 5



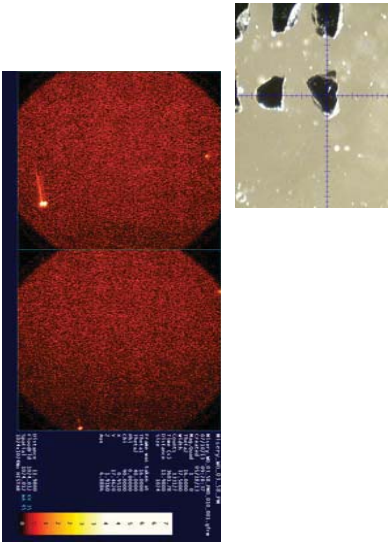
WO_03_58_PM0 Disc 3: Grain 7



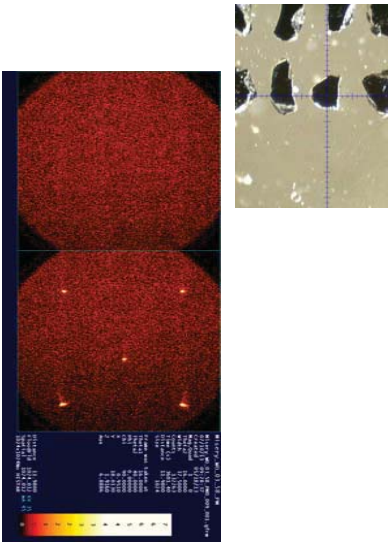
WO_03_58_PM0 Disc 3: Grain 8



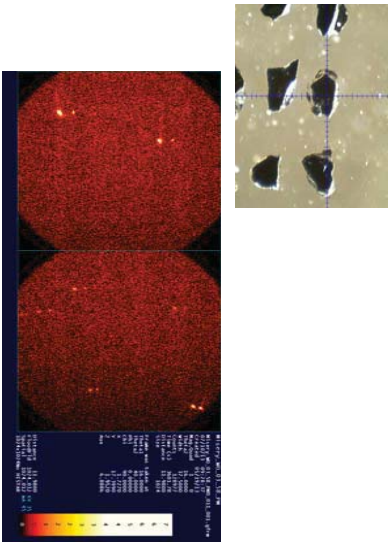
WO_03_58_PM0 Disc 3: Grain 10



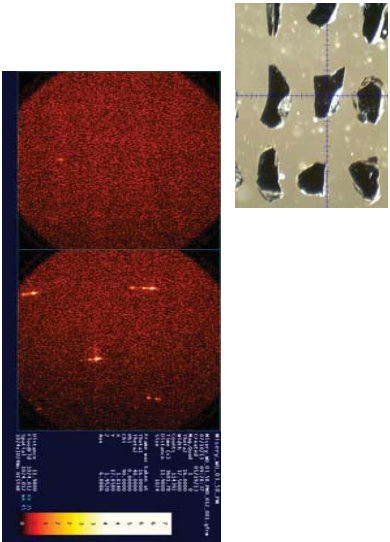
WO_03_58_PM0 Disc 3: Grain 9



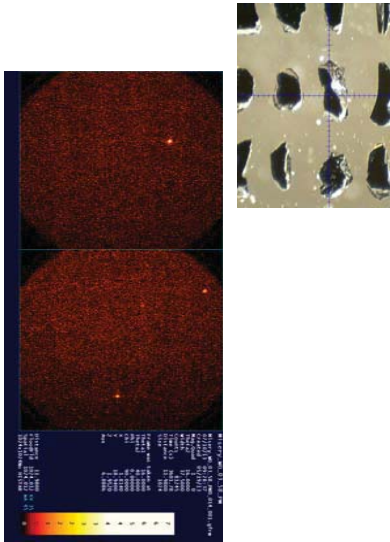
WO_03_58_PM0 Disc 3: Grain 11



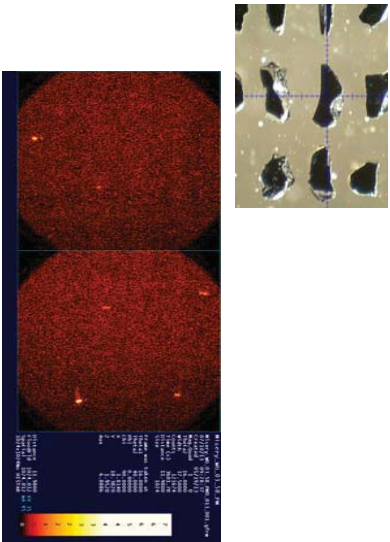
WO_03_58_PM0 Disc 3: Grain 12



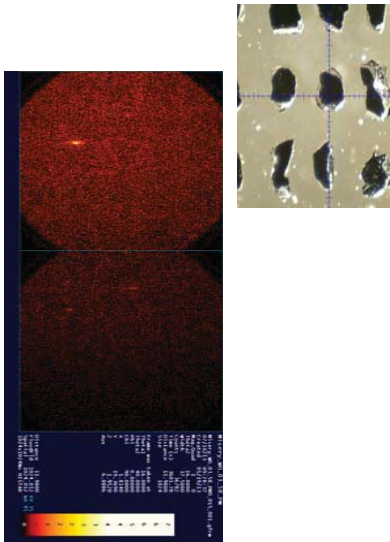
WO_03_58_PM0 Disc 3: Grain 14



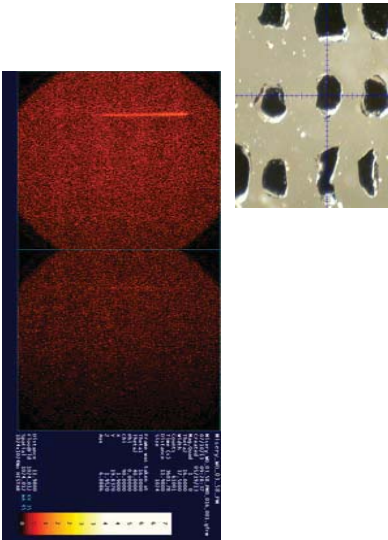
WO_03_58_PM0 Disc 3: Grain 13



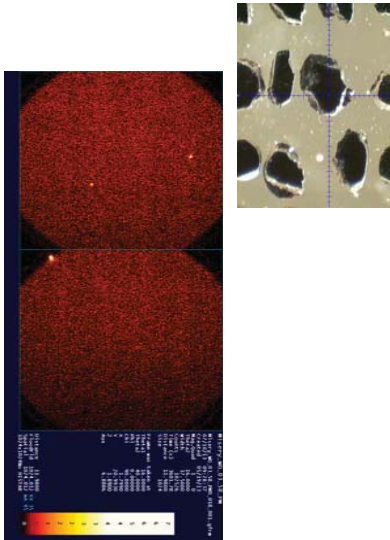
WO_03_58_PM0 Disc 3: Grain 15



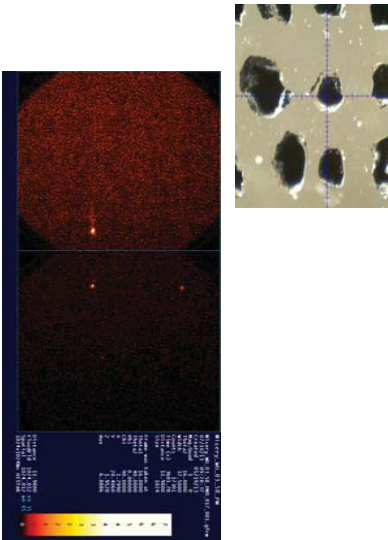
WO_03_58_PM0 Disc 3: Grain 16



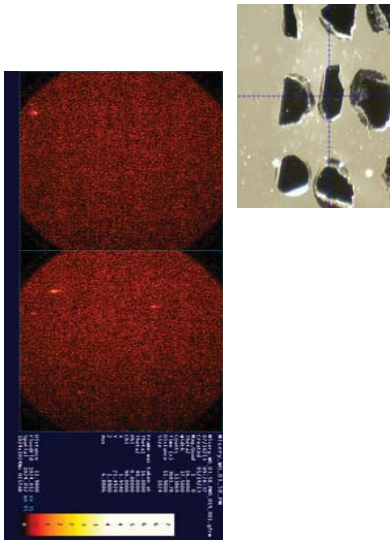
WO_03_58_PM0 Disc 3: Grain 18



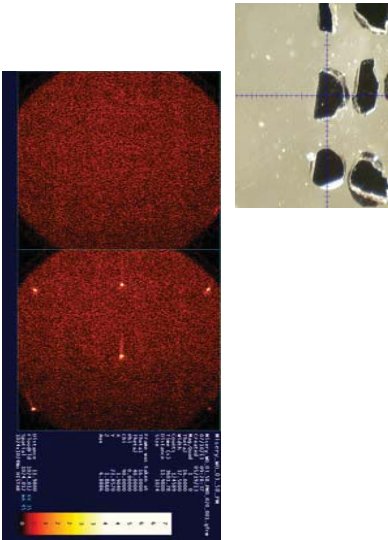
WO_03_58_PM0 Disc 3: Grain 17



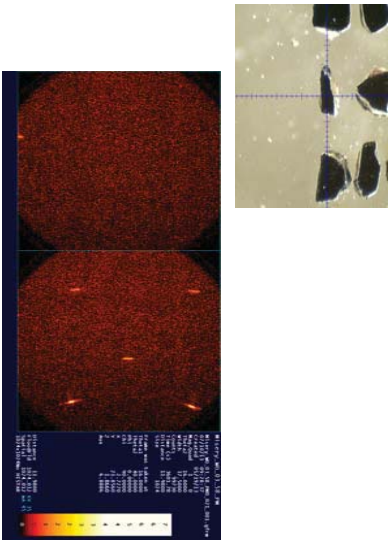
WO_03_58_PM0 Disc 3: Grain 19



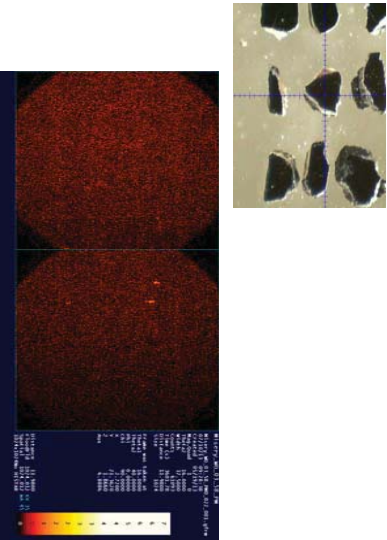
WO_03_58_PM0 Disc 3: Grain 20



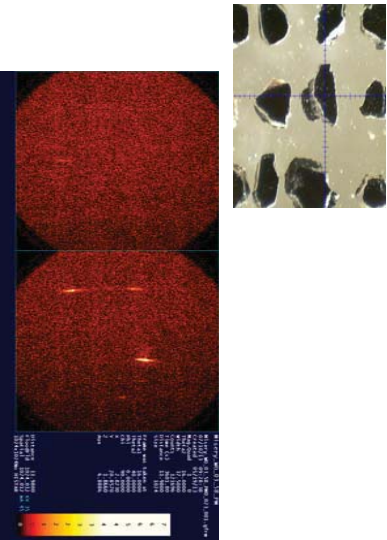
WO_03_58_PM0 Disc 3: Grain 21

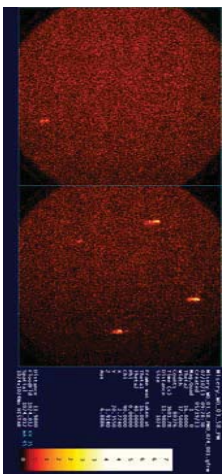
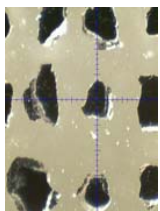


WO_03_58_PM0 Disc 3: Grain 22

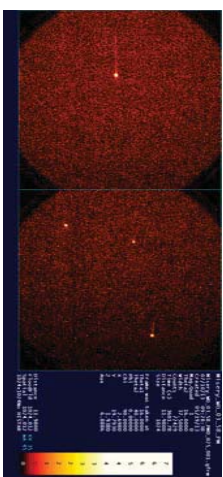
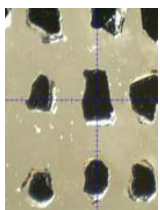


WO_03_58_PM0 Disc 3: Grain 23

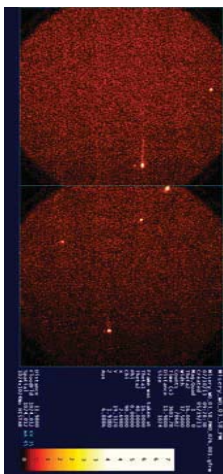
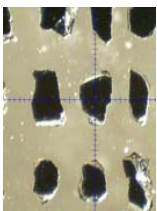




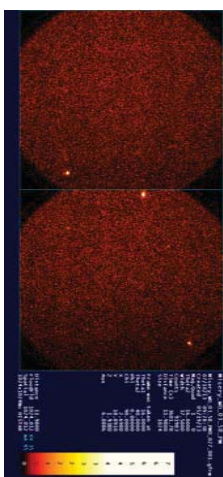
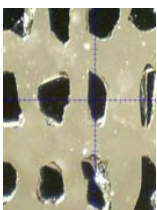
WO_03_58_PM0 Disc 3: Grain 25



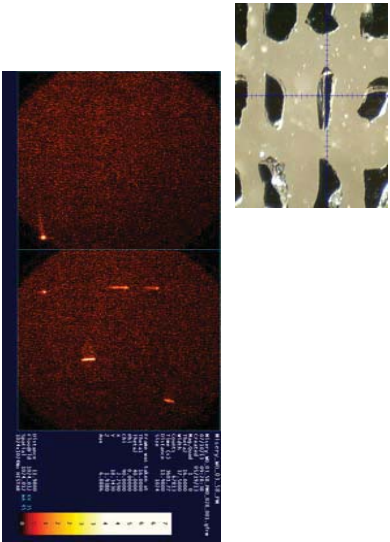
WO_03_58_PM10 Disc 3: Grain 26



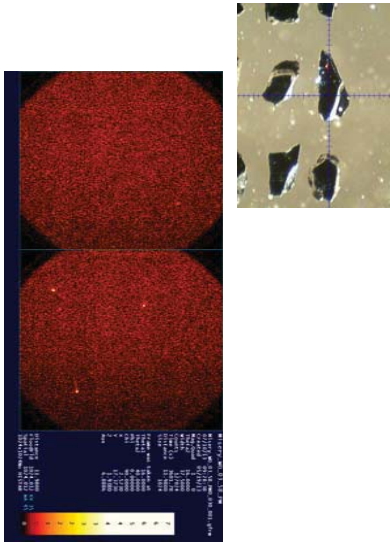
WO_03_58_PM0 Disc 3: Grain 27



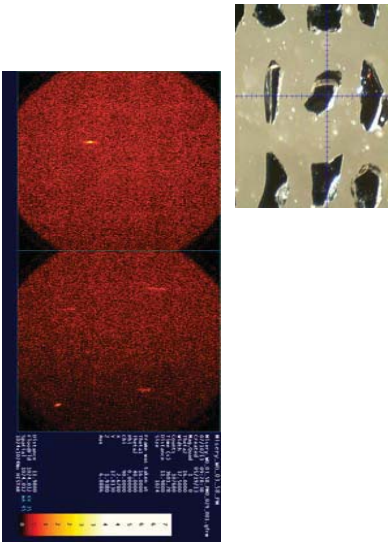
WO_03_58_PM0 Disc 3: Grain 28



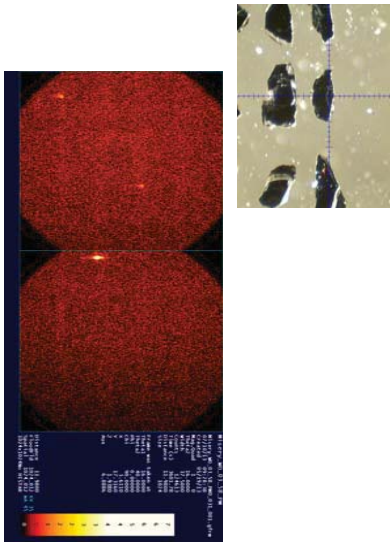
WO_03_58_PM0 Disc 3: Grain 30



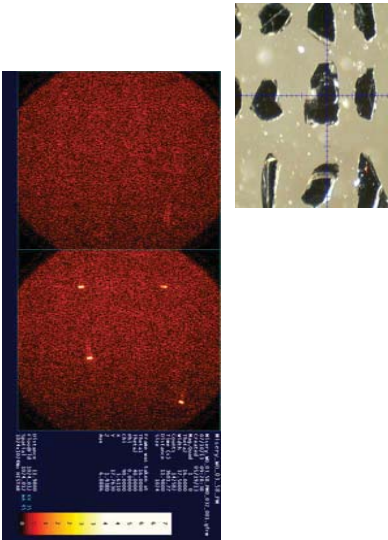
WO_03_58_PM0 Disc 3: Grain 29



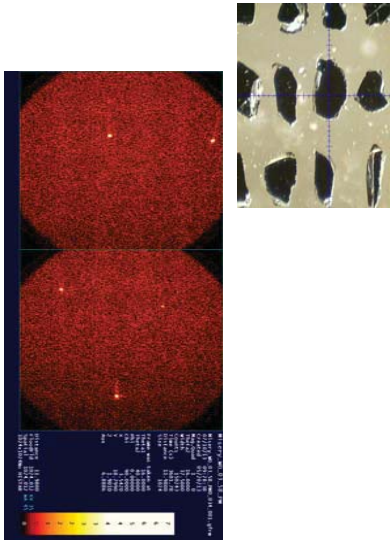
WO_03_58_PM0 Disc 3: Grain 31



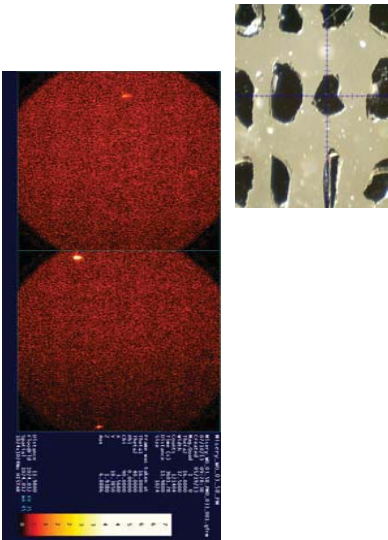
WO_03_58_PM0 Disc 3: Grain 32



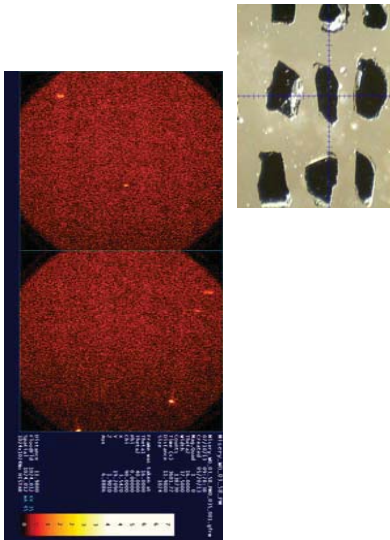
WO_03_58_PM0 Disc 3: Grain 34



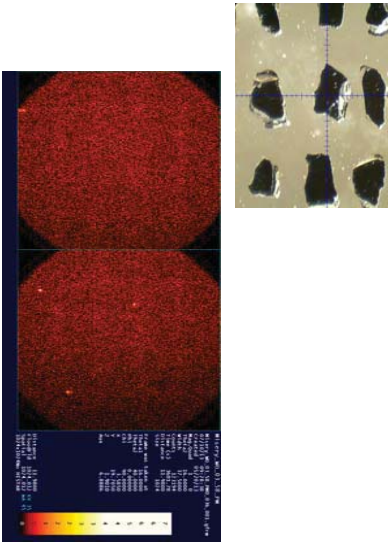
WO_03_58_PM0 Disc 3: Grain 33



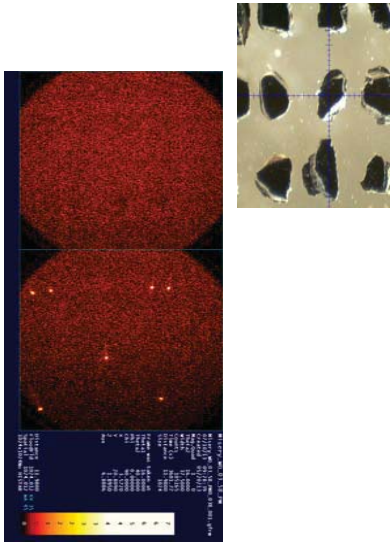
WO_03_58_PM0 Disc 3: Grain 35



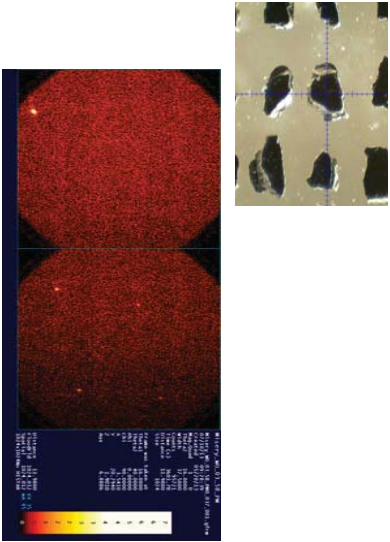
WO_03_58_PM0 Disc 3: Grain 36



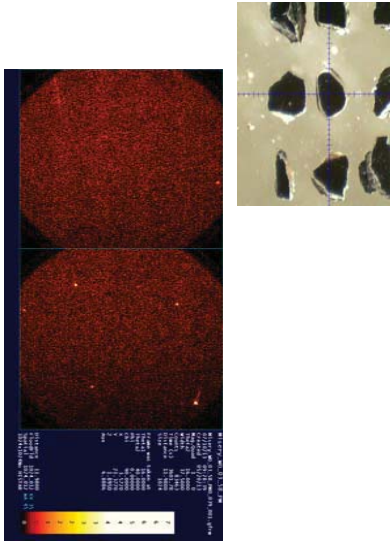
WO_03_58_PM0 Disc 3: Grain 38



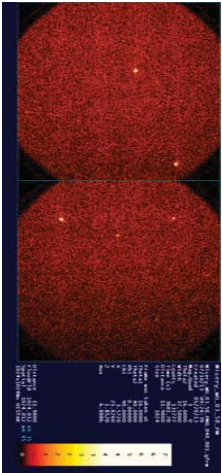
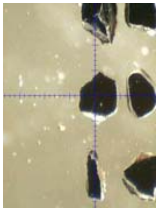
WO_03_58_PM0 Disc 3: Grain 37



WO_03_58_PM0 Disc 3: Grain 39



WO_03_58_PMO Disc 3: Grain 40



Sheiba_W002_084

By Patrick Shepherd

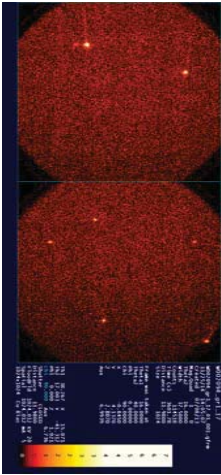
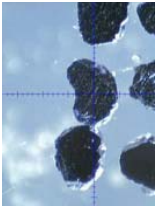
W002094_gr1_17

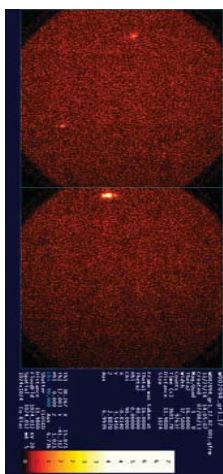
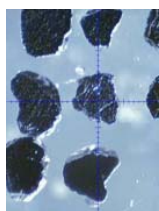
Frame 1	Frame 2
Theta 1 = 16	Theta 1 = 45.5
Theta 2 = 40	Theta 2 = 40
W = 37.5	W = 7.5
T = 60min	T = 60min

Sheiba_W002_084

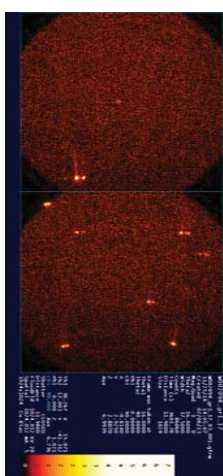
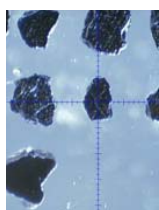
July 3rd 2013
Bruker D8 Discover
100 Micron Mirror

W002084 Grain 1

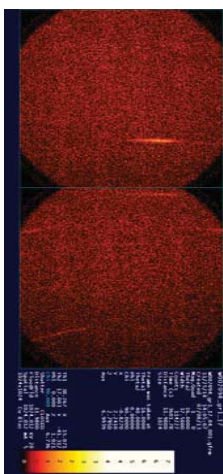
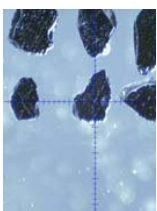




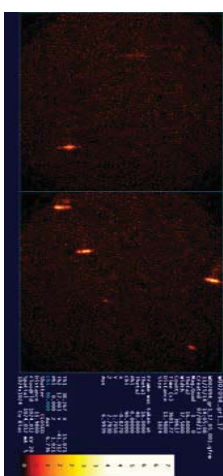
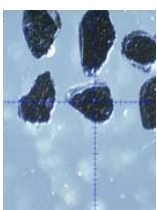
W002084 Grain 3



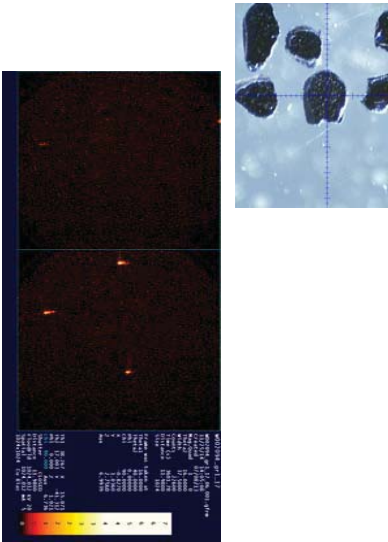
W002084 Grain 4



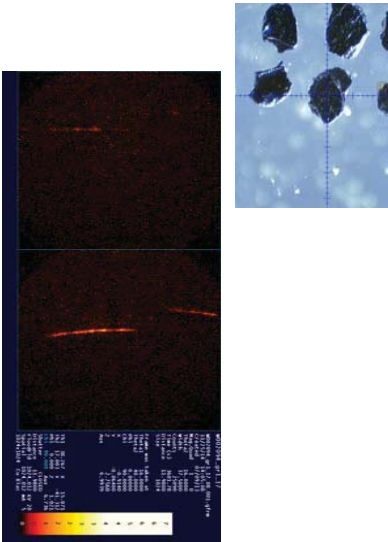
W002084 Grain 5



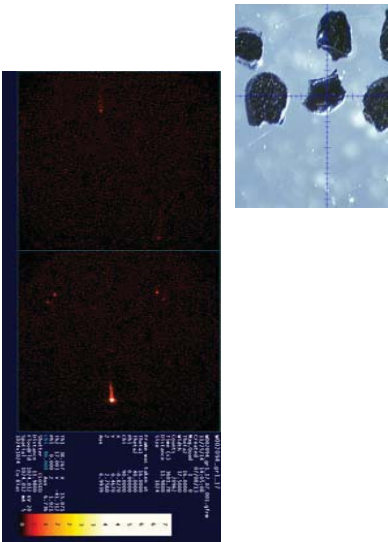
W002084 Grain 6



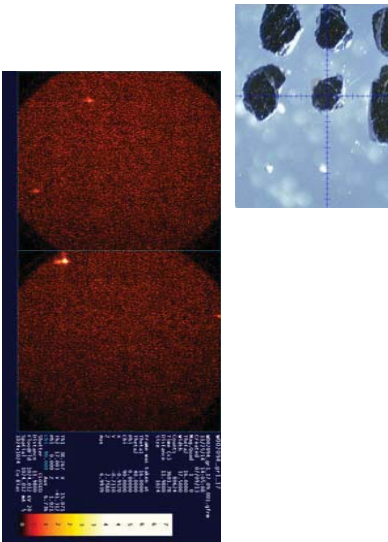
W002084 Grain 8



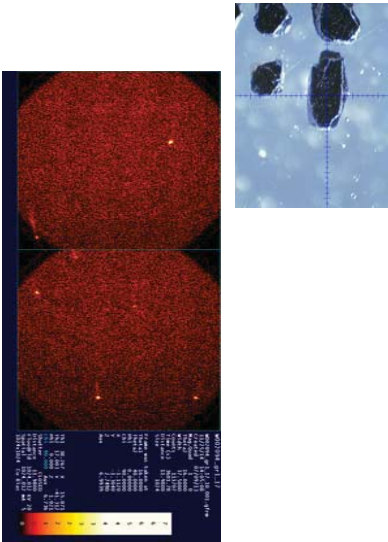
W002084 Grain 7



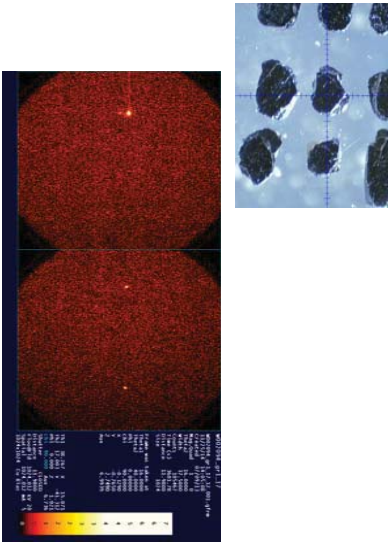
W002084 Grain 9



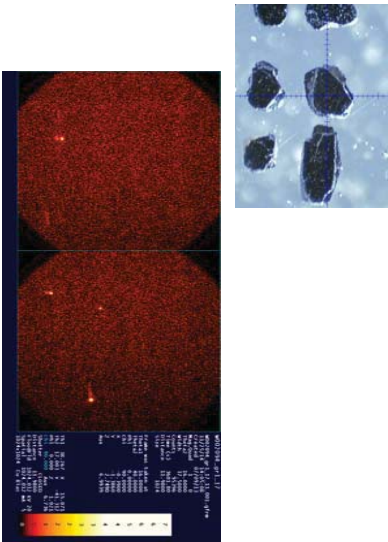
W002084 Grain 10



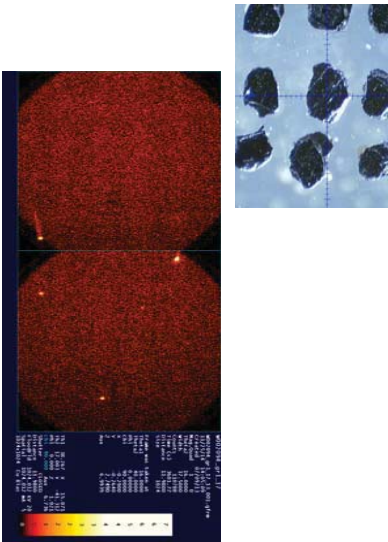
W002084 Grain 12



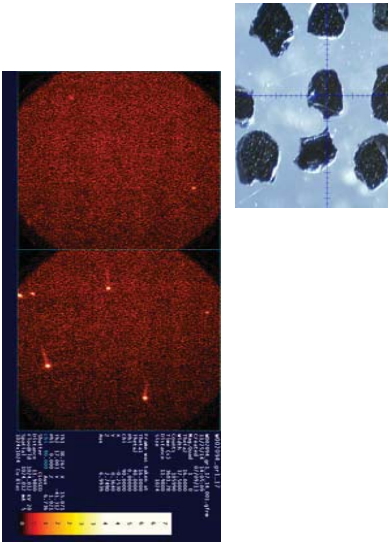
W002084 Grain 11



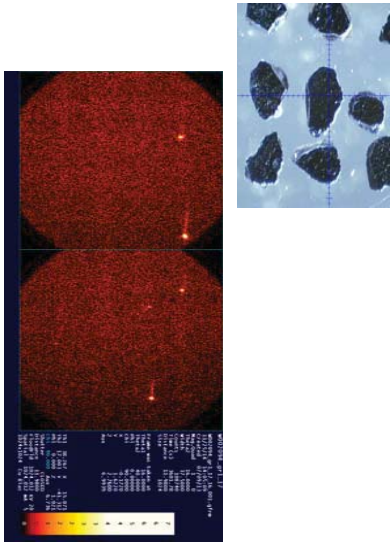
W002084 Grain 13



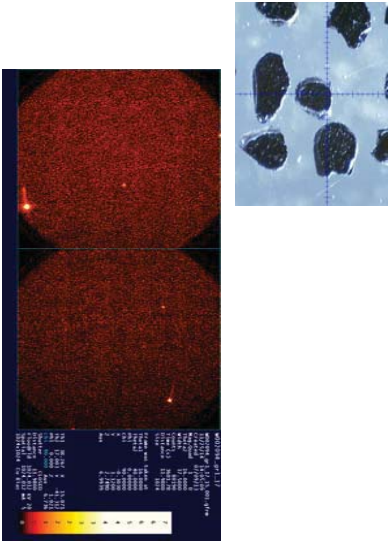
W002084 Grain 14



W002084 Grain 16



W002084 Grain 15



KOALAW002_2048PM

By Patrick Shepherd

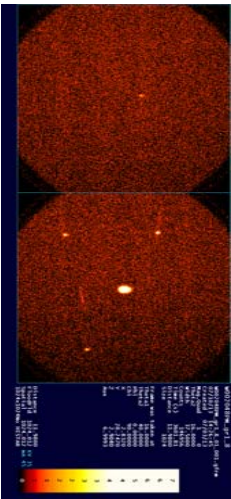
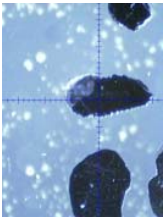
KOALAW002_48gr1_8

July 3rd 2013
Bruker D8 Discover
100 Micron Mirror

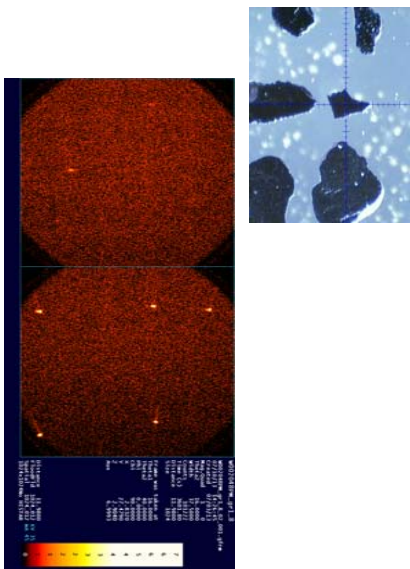
KOALAW002_48gr1_8
Koala Disc 3

Frame 1	Frame 2
Theta 1 = 16	Theta 1 = 45.5
Theta 2 =40	Theta 2 =40
W = 37.5	W = 7.5
T = 60min	T = 60min

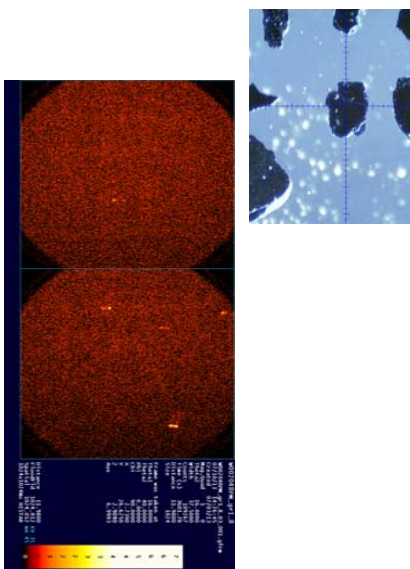
W002048PM_gr1_8 Disc 3 : Grain 1



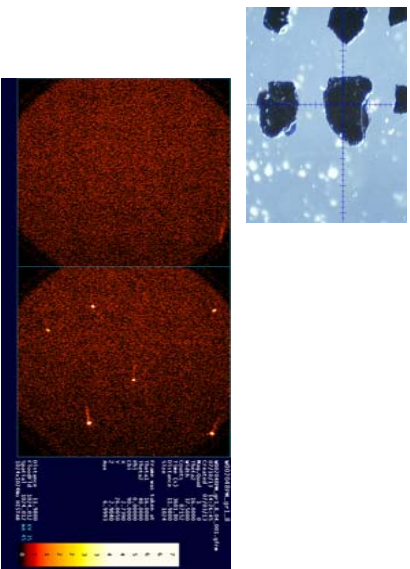
W002048PM_gr1_8 Disc 3 : Grain 2



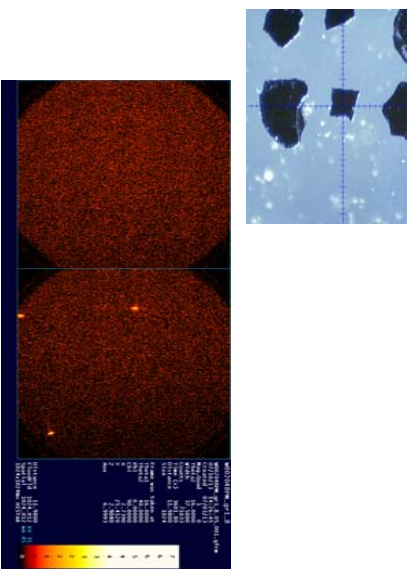
W002048PM_gr1_8 Disc 3 : Grain 3



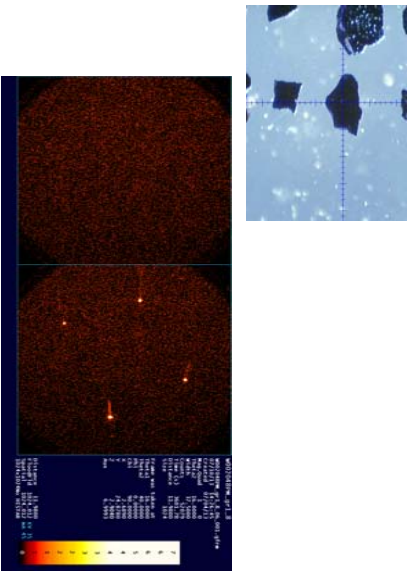
W002048PM_gr1_8 Disc 3 : Grain 4



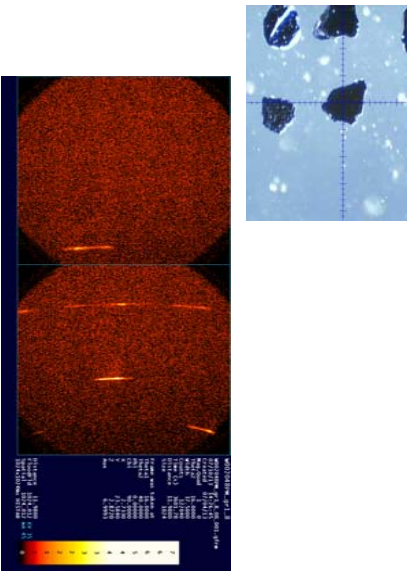
W002048PM_gr1_8 Disc 3 : Grain 5



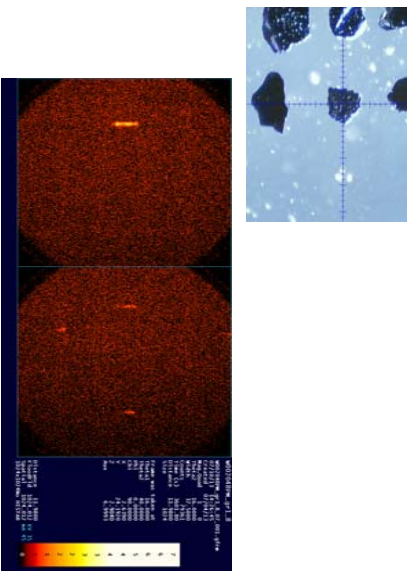
W002048PM_gr1_8 Disc 3 : Grain 6



W002048PM_gr1_8 Disc 3 : Grain 8



W002048PM_gr1_8 Disc 3 : Grain 7



KOALAW002_48gr9_30

July 6th 2013
Bruker D8 Discover
100 Micron Mirror


Frame 2

 $\theta_1 = 45.5^\circ$


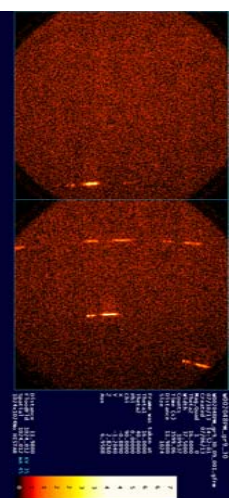

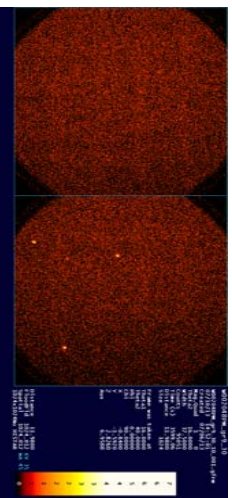
Theta 2 = 40

$$W = 7.5$$

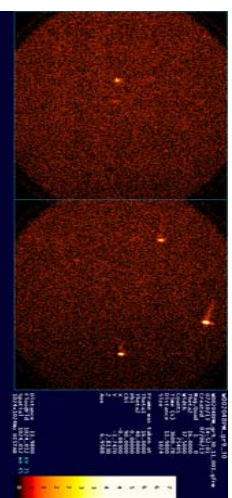
T = 60min



A black and white micrograph showing a cell with a large, dark, irregularly shaped nucleus. A prominent, lighter-colored nucleolus is visible within the nucleus. The surrounding cytoplasm is granular and contains various organelles.



A micrograph showing a single cell with a crosshair overlay, likely used for size measurement or tracking.



Appendix E: Unit Cell Refinements

Non-Kims

Gabon

MSL05/0040 Disc 1

Grain 11								
CELREF Version 3. 6/20/2013 8:03:46 PM								
GabonMSL040095PM_gr11_21-11.dif								
Initial values : (Refinement keys on 2nd line)								
Zero	Lambda	a	b	c	alpha	beta	gamma	Vol.
0	1.789	8.29	8.29	8.29	90	90	90	569.7
0	0	1	0	0	0	0	0	
Final values : (Standard errors on 2nd line)								
Zero	Lambda	a	b	c	alpha	beta	gamma	Vol.
0	1.789	8.2889	8.2889	8.2889	90	90	90	569.5
0	0	0.0264	0	0	0	0	0	
H	K	L	2T(Obs)	2T-Zero	2Th(Cal)	Dif		
1	1	3	41.9926	41.9926	41.9443	0.0483		
2	2	4	63.8054	63.8054	63.8319	-0.0265		
1	1	5	68.2328	68.2328	68.2145	0.0183		

Grain 12								
CELREF Version 3. 7/25/2013 5:42:20 PM								
GabonMSL040095PM_gr11_2110-12.dif								
Initial values : (Refinement keys on 2nd line)								
Zero	Lambda	a	b	c	alpha	beta	gamma	Vol.
0	1.789	8.24	8.24	8.24	90	90	90	559.5
0	0	1	0	0	0	0	0	
Final values : (Standard errors on 2nd line)								
Zero	Lambda	a	b	c	alpha	beta	gamma	Vol.
0	1.789	8.2394	8.2394	8.2394	90	90	90	559.4
0	0	0.0039	0	0	0	0	0	
H	K	L	2T(Obs)	2T-Zero	2Th(Cal)	Dif		
0	0	4	51.4297	51.4297	51.4758	-0.0461		
6	0	2	86.726	86.726	86.7259	0.0001		

Grain 16								
CELREF Version 3. 7/25/2013 6:19:57 PM								
GabonMSL040095PM_gr11_2110-16.dif								
Initial values : (Refinement keys on 2nd line)								
Zero	Lambda	a	b	c	alpha	beta	gamma	Vol.
0	1.789	8.25	8.25	8.25	90	90	90	561.5
0	0	1	0	0	0	0	0	
Final values : (Standard errors on 2nd line)								
Zero	Lambda	a	b	c	alpha	beta	gamma	Vol.
0	1.789	8.2466	8.2466	8.2466	90	90	90	560.8
0	0	0.0035	0	0	0	0	0	
H	K	L	2T(Obs)	2T-Zero	2Th(Cal)	Dif		
1	1	3	42.2193	42.2193	42.17	0.0493		
2	2	2	44.1692	44.1692	44.1412	0.028		
4	2	2	64.1259	64.1259	64.1987	-0.0728		
5	1	1	68.6088	68.6088	68.6135	-0.0047		
5	3	3	90.7012	90.7012	90.6785	0.0227		

Grain 17								
CELREF Version 3. 11/24/2014 10:34:16 AM								
GabonMSL040095PM_gr11_2110-17(mod1).dif								
Initial values : (Refinement keys on 2nd line)								
Zero	Lambda	a	b	c	alpha	beta	gamma	Vol.
0	1.789	8.2675	8.2675	8.2675	90	90	90	565.1
0	0	1	0	0	0	0	0	
Final values : (Standard errors on 2nd line)								
Zero	Lambda	a	b	c	alpha	beta	gamma	Vol.
0	1.789	8.2644	8.2644	8.2644	90	90	90	564.5
0	0	0.0049	0	0	0	0	0	
H	K	L	2T(Obs)	2T-Zero	2Th(Cal)	Dif		
0	0	4	51.325	51.325	51.3085	0.0165		
2	2	4	63.9825	63.9825	64.0434	-0.0609		
5	1	1	68.4673	68.4673	68.4445	0.0228		
2	0	6	86.3626	86.3626	86.3984	-0.0358		
Note: Moved peak 1,2,4 to centre of mass								

Grain 18								
CELREF Version 3. 7/25/2013 6:42:22 PM								
GabonMSL040095PM_gr11_2110-18.dif								
Initial values : (Refinement keys on 2nd line)								
Zero	Lambda	a	b	c	alpha	beta	gamma	Vol.
0	1.789	8.2464	8.2464	8.2464	90	90	90	560.8
0	0	1	0	0	0	0	0	
Final values : (Standard errors on 2nd line)								
Zero	Lambda	a	b	c	alpha	beta	gamma	Vol.
0	1.789	8.2433	8.2433	8.2433	90	90	90	560.1
0	0	0.0031	0	0	0	0	0	
H	K	L	2T(Obs)	2T-Zero	2Th(Cal)	Dif		
2	2	2	44.1376	44.1376	44.1596	-0.022		
2	2	4	64.2096	64.2096	64.2271	-0.0175		
1	1	5	68.6511	68.6511	68.6444	0.0067		
4	4	4	97.5044	97.5044	97.4921	0.0123		

Grain 20								
CELREF Version 3. 7/29/2013 11:14:45 AM								
GabonMSL040095PM_gr11_2110-20.dif								
Initial values : (Refinement keys on 2nd line)								
Zero	Lambda	a	b	c	alpha	beta	gamma	Vol.
0	1.789	8.2413	8.2413	8.2413	90	90	90	559.7
0	0	1	0	0	0	0	0	
Final values : (Standard errors on 2nd line)								
Zero	Lambda	a	b	c	alpha	beta	gamma	Vol.
0	1.789	8.2383	8.2383	8.2383	90	90	90	559.1
0	0	0.0253	0	0	0	0	0	
H	K	L	2T(Obs)	2T-Zero	2Th(Cal)	Dif		
2	2	2	44.1202	44.1202	44.1877	-0.0675		
2	2	4	64.2866	64.2866	64.2706	0.016		
1	1	5	68.7426	68.7426	68.6917	0.0509		

CELREF Version 3. 7/29/2013 11:20:34 AM								
GabonMSL040095PM_gr11_2110-21.dif								
Initial values : (Refinement keys on 2nd line)								
Zero	Lambda	a	b	c	alpha	beta	gamma	Vol.
0	1.789	8.2555	8.2555	8.2555	90	90	90	562.6
0	0	1	0	0	0	0	0	
Final values : (Standard errors on 2nd line)								
Zero	Lambda	a	b	c	alpha	beta	gamma	Vol.
0	1.789	8.2555	8.2555	8.2555	90	90	90	562.6
0	0	0.0043	0	0	0	0	0	
H	K	L	2T(Obs)	2T-Zero	2Th(Cal)	Dif		
2	2	2	44.0997	44.0997	44.0912	0.0085		
2	2	4	64.1358	64.1358	64.1213	0.0145		
1	1	5	68.5649	68.5649	68.5293	0.0356		
4	4	4	97.282	97.282	97.3001	-0.0181		

Grain 23 - Insufficient Peaks

Grain 24								
CELREF Version 3. 7/29/2013 11:31:02 AM								
GabonMSL040095PM_gr22_80-24.dif								
Initial values : (Refinement keys on 2nd line)								
Zero	Lambda	a	b	c	alpha	beta	gamma	Vol.
0	1.789	8.23	8.23	8.23	90	90	90	557.4
0	0	1	0	0	0	0	0	
Final values : (Standard errors on 2nd line)								
Zero	Lambda	a	b	c	alpha	beta	gamma	Vol.
0	1.789	8.2323	8.2323	8.2323	90	90	90	557.9
0	0	0.0009	0	0	0	0	0	
H	K	L	2T(Obs)	2T-Zero	2Th(Cal)	Dif		
2	2	4	64.316	64.316	64.3231	-0.0071		
3	3	3	68.7519	68.7519	68.7488	0.0031		
4	4	4	97.6675	97.6675	97.6666	0.0009		
Note: Peak 1 Manual Selected due to assemetry								

Grain 25								
CELREF Version 3. 7/29/2013 11:35:52 AM								
GabonMSL040095PM_gr22_80-25.dif								
Initial values : (Refinement keys on 2nd line)								
Zero	Lambda	a	b	c	alpha	beta	gamma	Vol.
0	1.789	8.2553	8.2553	8.2553	90	90	90	562.6
0	0	1	0	0	0	0	0	
Final values : (Standard errors on 2nd line)								
Zero	Lambda	a	b	c	alpha	beta	gamma	Vol.
0	1.789	8.2561	8.2561	8.2561	90	90	90	562.8
0	0	0.0122	0	0	0	0	0	
H	K	L	2T(Obs)	2T-Zero	2Th(Cal)	Dif		
1	1	3	42.2163	42.2163	42.1189	0.0974		
5	3	3	90.5239	90.5239	90.5447	-0.0208		
Note: Peak 3 did not fit, but is small and may not be real								

Grain 26								
CELREF Version 3. 7/29/2013 11:52:23 AM								
GabonMSL040095PM_gr22_80-26.dif								
Initial values : (Refinement keys on 2nd line)								
Zero	Lambda	a	b	c	alpha	beta	gamma	Vol.
0	1.789	8.2641	8.2641	8.2641	90	90	90	564.4
0	0	1	0	0	0	0	0	
Final values : (Standard errors on 2nd line)								
Zero	Lambda	a	b	c	alpha	beta	gamma	Vol.
0	1.789	8.2641	8.2641	8.2641	90	90	90	564.4
0	0	0.003	0	0	0	0	0	
H	K	L	2T(Obs)	2T-Zero	2Th(Cal)	Dif		
2	2	2	44.075	44.075	44.0425	0.0325		
2	2	4	64.045	64.045	64.046	-0.001		
3	3	3	68.446	68.446	68.4474	-0.0014		
4	4	4	97.153	97.153	97.1635	-0.0105		

Grain 27								
CELREF Version 3. 7/29/2013 1:31:36 PM								
GabonMSL040095PM_gr22_80-27.dif								
Initial values : (Refinement keys on 2nd line)								
Zero	Lambda	a	b	c	alpha	beta	gamma	Vol.
0	1.789	8.25	8.25	8.25	90	90	90	561.5
0	0	1	0	0	0	0	0	
Final values : (Standard errors on 2nd line)								
Zero	Lambda	a	b	c	alpha	beta	gamma	Vol.
0	1.789	8.2482	8.2482	8.2482	90	90	90	561.1
0	0	0.0027	0	0	0	0	0	
H	K	L	2T(Obs)	2T-Zero	2Th(Cal)	Dif		
2	2	2	44.094	44.094	44.1322	-0.0382		
4	2	2	64.223	64.223	64.1848	0.0382		
5	1	1	68.586	68.586	68.5984	-0.0124		
4	4	4	97.408	97.408	97.4154	-0.0074		

Grain 31								
CELREF Version 3. 7/29/2013 2:18:49 PM								
GabonMSL040095PM_gr22_80-31.dif								
Initial values : (Refinement keys on 2nd line)								
Zero	Lambda	a	b	c	alpha	beta	gamma	Vol.
0	1.789	8.2597	8.2597	8.2597	90	90	90	563.5
0	0	1	0	0	0	0	0	
Final values : (Standard errors on 2nd line)								
Zero	Lambda	a	b	c	alpha	beta	gamma	Vol.
0	1.789	8.2558	8.2558	8.2558	90	90	90	562.7
0	0	0.0298	0	0	0	0	0	
H	K	L	2T(Obs)	2T-Zero	2Th(Cal)	Dif		
2	2	2	44.006	44.006	44.0892	-0.0832		
2	2	4	64.136	64.136	64.1183	0.0177		
1	1	5	68.58	68.58	68.526	0.054		

Grain 32								
CELREF Version 3. 7/29/2013 2:40:00 PM								
GabonMSL040095PM_gr22_80-32.dif								
Initial values : (Refinement keys on 2nd line)								
Zero	Lambda	a	b	c	alpha	beta	gamma	Vol.
0	1.789	8.2429	8.2429	8.2429	90	90	90	560.1
0	0	1	0	0	0	0	0	
Final values : (Standard errors on 2nd line)								
Zero	Lambda	a	b	c	alpha	beta	gamma	Vol.
0	1.789	8.2423	8.2423	8.2423	90	90	90	559.9
0	0	0.0159	0	0	0	0	0	
H	K	L	2T(Obs)	2T-Zero	2Th(Cal)	Dif		
1	1	3	42.2722	42.2722	42.1929	0.0793		
2	2	4	64.2343	64.2343	64.236	-0.0017		
3	3	3	68.5696	68.5696	68.6541	-0.0845		
3	1	5	79.941	79.941	79.8892	0.0518		

Grain 34								
CELREF Version 3. 7/29/2013 2:51:52 PM								
GabonMSL040095PM_gr22_80-34.dif								
Initial values : (Refinement keys on 2nd line)								
Zero	Lambda	a	b	c	alpha	beta	gamma	Vol.
0	1.789	8.24	8.24	8.24	90	90	90	559.5
0	0	1	0	0	0	0	0	
Final values : (Standard errors on 2nd line)								
Zero	Lambda	a	b	c	alpha	beta	gamma	Vol.
0	1.789	8.2367	8.2367	8.2367	90	90	90	558.8
0	0	0.0035	0	0	0	0	0	
H	K	L	2T(Obs)	2T-Zero	2Th(Cal)	Dif		
2	2	4	64.341	64.341	64.2852	0.0558		
1	1	5	68.699	68.699	68.7076	-0.0086		
6	0	2	86.747	86.747	86.7619	-0.0149		

Grain 52								
CELREF Version 3. 7/30/2013 10:45:30 AM								
GabonMSL040095PM_gr22_80-52.dif								
Initial values : (Refinement keys on 2nd line)								
Zero	Lambda	a	b	c	alpha	beta	gamma	Vol.
0	1.789	8.25	8.25	8.25	90	90	90	561.5
0	0	1	0	0	0	0	0	
Final values : (Standard errors on 2nd line)								
Zero	Lambda	a	b	c	alpha	beta	gamma	Vol.
0	1.789	8.2429	8.2429	8.2429	90	90	90	560.1
0	0	0.0006	0	0	0	0	0	
H	K	L	2T(Obs)	2T-Zero	2Th(Cal)	Dif		
1	1	3	42.184	42.184	42.1894	-0.0054		
5	1	1	68.649	68.649	68.6478	0.0012		
Note: 2 peaks								

Grain 53								
No complete peaks								

Grain 54								
CELREF Version 3. 7/30/2013 11:02:39 AM								
GabonMSL040095PM_gr22_80-54(mod).dif								
Initial values : (Refinement keys on 2nd line)								
Zero	Lambda	a	b	c	alpha	beta	gamma	Vol.
0	1.789	8.2682	8.2682	8.2682	90	90	90	565.2
0	0	1	0	0	0	0	0	
Final values : (Standard errors on 2nd line)								
Zero	Lambda	a	b	c	alpha	beta	gamma	Vol.
0	1.789	8.2668	8.2668	8.2668	90	90	90	565
0	0	0.0045	0	0	0	0	0	
H	K	L	2T(Obs)	2T-Zero	2Th(Cal)	Dif		
2	2	2	44.057	44.057	44.0275	0.0295		
5	1	1	68.461	68.461	68.4222	0.0388		
4	4	4	97.078	97.078	97.1216	-0.0436		
Note: Only 3 peaks and fourth peak was recentered due to ka2								

Grain 55								
CELREF Version 3. 7/30/2013 11:18:42 AM								
GabonMSL040095PM_gr22_80-55.dif								
Initial values : (Refinement keys on 2nd line)								
Zero	Lambda	a	b	c	alpha	beta	gamma	Vol.
0	1.789	8.25	8.25	8.25	90	90	90	561.5
0	0	1	0	0	0	0	0	
Final values : (Standard errors on 2nd line)								
Zero	Lambda	a	b	c	alpha	beta	gamma	Vol.
0	1.789	8.2463	8.2463	8.2463	90	90	90	560.8
0	0	0.0008	0	0	0	0	0	
H	K	L	2T(Obs)	2T-Zero	2Th(Cal)	Dif		
2	2	2	44.154	44.154	44.1427	0.0113		
5	1	1	68.615	68.615	68.6159	-0.0009		
4	4	4	97.442	97.442	97.4446	-0.0026		

Grain 4									
CELREF Version 3. 11/7/2014 8:25:55 PM									
W000062_Disc_3-Slit_10_04-mod1.dif									
Initial values : (Refinement keys on 2nd line)									
Zero	Lambda	a	b	c	alpha	beta	gamma	Vol.	
0	1.789	8.3201	8.3201	8.3201	90	90	90	576	
0	0	1	0	0	0	0	0		
Final values : (Standard errors on 2nd line)									
Zero	Lambda	a	b	c	alpha	beta	gamma	Vol.	
0	1.789	8.3189	8.3189	8.3189	90	90	90	575.7	
0	0	0.0043	0	0	0	0	0		
H	K	L	2T(Obs)	2T-Zero	2Th(Cal)	Dif			
1	1	3	41.8226	41.8226	41.7862	0.0364			
4	2	2	63.5455	63.5455	63.575	-0.0295			
5	1	1	68.0048	68.0048	67.9353	0.0695			
5	3	3	89.6266	89.6266	89.6751	-0.0485			
Note: Peak 1 and Peak 3 moved to centre of gravity									

Grain 5								
CELREF Version 3. 11/7/2014 8:29:54 PM								
W000062_Disc_3-Slit_10_05.dif								
Initial values : (Refinement keys on 2nd line)								
Zero	Lambda	a	b	c	alpha	beta	gamma	Vol.
0	1.789	8.3215	8.3215	8.3215	90	90	90	576.2
0	0	1	0	0	0	0	0	
Final values : (Standard errors on 2nd line)								
Zero	Lambda	a	b	c	alpha	beta	gamma	Vol.
0	1.789	8.3231	8.3231	8.3231	90	90	90	576.6
0	0	0.0049	0	0	0	0	0	
H	K	L	2T(Obs)	2T-Zero	2Th(Cal)	Dif		
3	1	1	41.7471	41.7471	41.7642	-0.0171		
2	2	4	63.51	63.51	63.5393	-0.0293		
1	1	5	67.9942	67.9942	67.8964	0.0978		
6	2	2	90.9457	90.9457	90.9414	0.0043		

Grain 6								
CELREF Version 3. 11/7/2014 10:20:59 PM								
W000062_Disc_3-Slit_10_06-mod1.dif								
Initial values : (Refinement keys on 2nd line)								
Zero	Lambda	a	b	c	alpha	beta	gamma	Vol.
0	1.789	8.3	8.3	8.3	90	90	90	571.8
0	0	1	0	0	0	0	0	
Final values : (Standard errors on 2nd line)								
Zero	Lambda	a	b	c	alpha	beta	gamma	Vol.
0	1.789	8.2994	8.2994	8.2994	90	90	90	571.7
0	0	0.0041	0	0	0	0	0	
H	K	L	2T(Obs)	2T-Zero	2Th(Cal)	Dif		
0	0	4	51.0565	51.0565	51.0764	-0.0199		
1	1	5	68.1793	68.1793	68.116	0.0633		
6	0	2	85.9426	85.9426	85.9453	-0.0027		
Note: Peak 1,2 and Peak 3 moved to centre of gravity								

Grain 7
Could Not Refine Within Error

Grain 8								
CELREF Version 3. 11/7/2014 11:03:23 PM								
W000062_Disc_3-Slit_10_08-mod.dif								
Initial values : (Refinement keys on 2nd line)								
Zero	Lambda	a	b	c	alpha	beta	gamma	Vol.
0	1.789	8.277	8.277	8.277	90	90	90	567
0	0	1	0	0	0	0	0	
Final values : (Standard errors on 2nd line)								
Zero	Lambda	a	b	c	alpha	beta	gamma	Vol.
0	1.789	8.2767	8.2767	8.2767	90	90	90	567
0	0	0.0047	0	0	0	0	0	
H	K	L	2T(Obs)	2T-Zero	2Th(Cal)	Dif		
1	1	3	41.9762	41.9762	42.0091	-0.0329		
2	2	4	63.9187	63.9187	63.9372	-0.0185		
3	3	3	68.2618	68.2618	68.329	-0.0672		
5	3	3	90.3131	90.3131	90.257	0.0561		
4	4	4	96.9658	96.9658	96.9664	-0.0006		
Note: Peak 2,5,6 moved to centre of gravity. Peak 2 ignored due to weird shape								

Grain 9								
CELREF Version 3. 11/7/2014 11:13:01 PM								
W000062_Disc_3-Slit_10_09-mod2.dif								
Initial values : (Refinement keys on 2nd line)								
Zero	Lambda	a	b	c	alpha	beta	gamma	Vol.
0	1.789	8.3023	8.3023	8.3023	90	90	90	572.3
0	0	1	0	0	0	0	0	
Final values : (Standard errors on 2nd line)								
Zero	Lambda	a	b	c	alpha	beta	gamma	Vol.
0	1.789	8.2981	8.2981	8.2981	90	90	90	571.4
0	0	0.0049	0	0	0	0	0	
H	K	L	2T(Obs)	2T-Zero	2Th(Cal)	Dif		
3	1	1	41.85	41.85	41.8956	-0.0456		
0	0	4	51.1019	51.1019	51.0852	0.0167		
2	2	4	63.6953	63.6953	63.7527	-0.0574		
5	1	1	68.1635	68.1635	68.1285	0.035		
Note: Peaks 1,2 and 3 moved to the centre of gravity								

Grain 10
Could Not Refine Within Error

Grain 11								
CELREF Version 3. 11/7/2014 11:44:53 PM								
W000062_Disc_3-Slit_10_11-mod.dif								
Initial values : (Refinement keys on 2nd line)								
Zero	Lambda	a	b	c	alpha	beta	gamma	Vol.
0	1.789	8.3	8.3	8.3	90	90	90	571.8
0	0	1	0	0	0	0	0	
Final values : (Standard errors on 2nd line)								
Zero	Lambda	a	b	c	alpha	beta	gamma	Vol.
0	1.789	8.2996	8.2996	8.2996	90	90	90	571.7
0	0	0.004	0	0	0	0	0	
H	K	L	2T(Obs)	2T-Zero	2Th(Cal)	Dif		
2	2	2	43.8704	43.8704	43.8443	0.0261		
1	1	5	68.1258	68.1258	68.1143	0.0115		
4	4	4	96.597	96.597	96.6095	-0.0125		
Note: Peak 2 was determined to be the phantom spot and removed								

Grain 12
Could Not Refine Within Error
Grain 13
Insufficient peaks

Grain 14									
CELREF Version 3. 11/8/2014 12:20:41 AM									
W000062_Disc_3-Slit_10_14-mod.dif									
Initial values : (Refinement keys on 2nd line)									
Zero	Lambda	a	b	c	alpha	beta	gamma	Vol.	
0	1.789	8.3202	8.3202	8.3202	90	90	90	576	
0	0	1	0	0	0	0	0		
Final values : (Standard errors on 2nd line)									
Zero	Lambda	a	b	c	alpha	beta	gamma	Vol.	
0	1.789	8.317	8.317	8.317	90	90	90	575.3	
0	0	0.0049	0	0	0	0	0		
H	K	L	2T(Obs)	2T-Zero	2Th(Cal)	Dif			
1	1	3	41.7355	41.7355	41.7961	-0.0606			
2	2	2	43.6901	43.6901	43.7481	-0.058			
4	2	2	63.6214	63.6214	63.5911	0.0303			
5	1	1	67.9531	67.9531	67.9527	0.0004			
Note:Moved peak 4 to centre of gravity									
Grain 15									
Could Not Refine Within Error									

Grain 16								
CELREF Version 3. 11/8/2014 12:31:30 AM								
W000062_Disc_3-Slit_10_16.dif								
Initial values : (Refinement keys on 2nd line)								
Zero	Lambda	a	b	c	alpha	beta	gamma	Vol.
0	1.789	8.3172	8.3172	8.3172	90	90	90	575.4
0	0	1	0	0	0	0	0	
Final values : (Standard errors on 2nd line)								
Zero	Lambda	a	b	c	alpha	beta	gamma	Vol.
0	1.789	8.3165	8.3165	8.3165	90	90	90	575.2
0	0	0.0039	0	0	0	0	0	
H	K	L	2T(Obs)	2T-Zero	2Th(Cal)	Dif		
1	1	3	41.7264	41.7264	41.7985	-0.0721		
4	2	2	63.5553	63.5553	63.595	-0.0397		
5	1	1	67.9663	67.9663	67.957	0.0093		
5	3	3	89.7339	89.7339	89.7071	0.0268		

Grain 17
Could Not Refine Within Error

Grain 18								
CELREF Version 3. 11/8/2014 12:40:34 AM								
W000062_Disc_3-Slit_10_18-mod1.dif								
Initial values : (Refinement keys on 2nd line)								
Zero	Lambda	a	b	c	alpha	beta	gamma	Vol.
0	1.789	8.3073	8.3073	8.3073	90	90	90	573.3
0	0	1	0	0	0	0	0	
Final values : (Standard errors on 2nd line)								
Zero	Lambda	a	b	c	alpha	beta	gamma	Vol.
0	1.789	8.3081	8.3081	8.3081	90	90	90	573.5
0	0	0.0046	0	0	0	0	0	
H	K	L	2T(Obs)	2T-Zero	2Th(Cal)	Dif		
3	1	1	41.8206	41.8206	41.8431	-0.0225		
2	2	4	63.6852	63.6852	63.6674	0.0178		
1	1	5	68.0433	68.0433	68.0357	0.0076		
Note: Peak 1,2,3 moved to centre of mass								

Grain 19								
Could not refine Robbie								

Grain 20								
CELREF Version 3. 11/8/2014 12:50:59 AM								
W000062_Disc_3-Slit_10_20-mod1.dif								
Initial values : (Refinement keys on 2nd line)								
Zero	Lambda	a	b	c	alpha	beta	gamma	Vol.
0	1.789	8.2939	8.2939	8.2939	90	90	90	570.5
0	0	1	0	0	0	0	0	
Final values : (Standard errors on 2nd line)								
Zero	Lambda	a	b	c	alpha	beta	gamma	Vol.
0	1.789	8.2936	8.2936	8.2936	90	90	90	570.5
0	0	0.0049	0	0	0	0	0	
H	K	L	2T(Obs)	2T-Zero	2Th(Cal)	Dif		
2	2	2	43.8099	43.8099	43.8777	-0.0678		
4	2	2	63.8097	63.8097	63.7912	0.0185		
3	3	3	68.1611	68.1611	68.1704	-0.0093		
4	4	4	96.7167	96.7167	96.7025	0.0142		

Koala

W002048PM Disc 3

Grain 2								
CELREF Version 3. 7/31/2013 11:01:14 AM								
W002048PM_gr1_8-02.dif								
Initial values : (Refinement keys on 2nd line)								
Zero	Lambda	a	b	c	alpha	beta	gamma	Vol.
0	1.789	8.3213	8.3213	8.3213	90	90	90	576.2
0	0	1	0	0	0	0	0	
Final values : (Standard errors on 2nd line)								
Zero	Lambda	a	b	c	alpha	beta	gamma	Vol.
0	1.789	8.3213	8.3213	8.3213	90	90	90	576.2
0	0	0.0076	0	0	0	0	0	
H	K	L	2T(Obs)	2T-Zero	2Th(Cal)	Dif		
1	1	3	41.797	41.797	41.7736	0.0234	113	
3	3	3	67.909	67.909	67.9131	-0.0041	333	

Grain 3								
CELREF Version 3. 7/31/2013 11:06:37 AM								
W002048PM_gr1_8-03(mod).dif								
Initial values : (Refinement keys on 2nd line)								
Zero	Lambda	a	b	c	alpha	beta	gamma	Vol.
0	1.789	8.3197	8.3197	8.3197	90	90	90	575.9
0	0	1	0	0	0	0	0	
Final values : (Standard errors on 2nd line)								
Zero	Lambda	a	b	c	alpha	beta	gamma	Vol.
0	1.789	8.321	8.321	8.321	90	90	90	576.1
0	0	0.0039	0	0	0	0	0	
H	K	L	2T(Obs)	2T-Zero	2Th(Cal)	Dif		
1	1	3	41.814	41.814	41.775	0.039	113	
2	2	4	63.586	63.586	63.5568	0.0292	224	
3	3	3	67.909	67.909	67.9155	-0.0065	333	
5	1	3	78.952	78.952	78.9843	-0.0323	513	

Grain 4								
CELREF Version 3. 7/31/2013 11:11:17 AM								
W002048PM_gr1_8-04.dif								
Initial values : (Refinement keys on 2nd line)								
Zero	Lambda	a	b	c	alpha	beta	gamma	Vol.
0	1.789	8.32	8.32	8.32	90	90	90	575.9
0	0	1	0	0	0	0	0	
Final values : (Standard errors on 2nd line)								
Zero	Lambda	a	b	c	alpha	beta	gamma	Vol.
0	1.789	8.3137	8.3137	8.3137	90	90	90	574.6
0	0	0.005	0	0	0	0	0	
H	K	L	2T(Obs)	2T-Zero	2Th(Cal)	Dif		
1	1	3	41.757	41.757	41.8133	-0.0563	113	
0	0	4	50.958	50.958	50.9825	-0.0245	4	
5	1	1	67.987	67.987	67.9831	0.0039	511	
Note: Scan has 4 peaks only 3 could work								

Grain 5								
CELREF Version 3. 7/31/2013 11:12:59 AM								
W002048PM_gr1_8-05.dif								
Initial values : (Refinement keys on 2nd line)								
Zero	Lambda	a	b	c	alpha	beta	gamma	Vol.
0	1.789	8.333	8.333	8.333	90	90	90	578.6
0	0	1	0	0	0	0	0	
Final values : (Standard errors on 2nd line)								
Zero	Lambda	a	b	c	alpha	beta	gamma	Vol.
0	1.789	8.3323	8.3323	8.3323	90	90	90	578.5
0	0	0.0037	0	0	0	0	0	
H	K	L	2T(Obs)	2T-Zero	2Th(Cal)	Dif		
1	1	3	41.684	41.684	41.7158	-0.0318	113	
5	1	1	67.813	67.813	67.8111	0.0019	511	

Grain 7								
CELREF Version 3. 7/31/2013 11:17:57 AM								
W002048PM_gr1_8-07(mod).dif								
Initial values : (Refinement keys on 2nd line)								
Zero	Lambda	a	b	c	alpha	beta	gamma	Vol.
0	1.789	8.3392	8.3392	8.3392	90	90	90	579.9
0	0	1	0	0	0	0	0	
Final values : (Standard errors on 2nd line)								
Zero	Lambda	a	b	c	alpha	beta	gamma	Vol.
0	1.789	8.3388	8.3388	8.3388	90	90	90	579.9
0	0	0.0036	0	0	0	0	0	
H	K	L	2T(Obs)	2T-Zero	2Th(Cal)	Dif		
2	2	2	43.583	43.583	43.6275	-0.0445	222	
4	2	2	63.404	63.404	63.405	-0.001	422	
3	3	3	67.738	67.738	67.7505	-0.0125	333	
4	4	4	96.031	96.031	96.0063	0.0247	444	
Note: Peak 1 search paramters tweaked to be in centre of mass								

Grain 8									
CELREF Version 3. 7/31/2013 11:34:48 AM									
W002048PM_gr1_8-08(mod).dif									
Initial values : (Refinement keys on 2nd line)									
Zero	Lambda	a	b	c	alpha	beta	gamma	Vol.	
0	1.789	8.3345	8.3345	8.3345	90	90	90	579	
0	0	1	0	0	0	0	0		
Final values : (Standard errors on 2nd line)									
Zero	Lambda	a	b	c	alpha	beta	gamma	Vol.	
0	1.789	8.3346	8.3346	8.3346	90	90	90	579	
0	0	0.0051	0	0	0	0	0		
H	K	L	2T(Obs)	2T-Zero	2Th(Cal)	Dif			
1	1	3	41.725	41.725	41.7035	0.0215		113	
0	0	4	50.841	50.841	50.8455	-0.0045		4	
3	3	3	67.784	67.784	67.7894	-0.0054		333	
Note:Peak 4 centre of gravity adjusted									

Grain 9								
CELREF Version 3. 7/31/2013 11:56:04 AM								
W002048PM_gr9_30-09(mod).dif								
Initial values : (Refinement keys on 2nd line)								
Zero	Lambda	a	b	c	alpha	beta	gamma	Vol.
0	1.789	8.3597	8.3597	8.3597	90	90	90	584.2
0	0	1	0	0	0	0	0	
Final values : (Standard errors on 2nd line)								
Zero	Lambda	a	b	c	alpha	beta	gamma	Vol.
0	1.789	8.3597	8.3597	8.3597	90	90	90	584.2
0	0	0.0087	0	0	0	0	0	
H	K	L	2T(Obs)	2T-Zero	2Th(Cal)	Dif		
1	1	3	41.605	41.605	41.5728	0.0322	113	
0	0	4	50.663	50.663	50.6824	-0.0194	4	
3	3	3	67.554	67.554	67.559	-0.005	333	
Note: Peak 2 tweaked to centre of gravity								

Grain 10								
CELREF Version 3. 7/31/2013 11:48:07 AM								
W002048PM_gr9_30-10(mod).dif								
Initial values : (Refinement keys on 2nd line)								
Zero	Lambda	a	b	c	alpha	beta	gamma	Vol.
0	1.789	8.3691	8.3691	8.3691	90	90	90	586.2
0	0	1	0	0	0	0	0	
Final values : (Standard errors on 2nd line)								
Zero	Lambda	a	b	c	alpha	beta	gamma	Vol.
0	1.789	8.3685	8.3685	8.3685	90	90	90	586
0	0	0.0078	0	0	0	0	0	
H	K	L	2T(Obs)	2T-Zero	2Th(Cal)	Dif		
2	2	2	43.457	43.457	43.4653	-0.0083	222	
2	2	4	63.189	63.189	63.1547	0.0343	224	
3	3	3	67.455	67.455	67.4784	-0.0234	333	

Grain 11								
CELREF Version 3. 8/1/2013 12:33:21 PM								
W002048PM_gr9_30-11.dif								
Initial values : (Refinement keys on 2nd line)								
Zero	Lambda	a	b	c	alpha	beta	gamma	Vol.
0	1.789	8.3349	8.3349	8.3349	90	90	90	579
0	0	1	0	0	0	0	0	
Final values : (Standard errors on 2nd line)								
Zero	Lambda	a	b	c	alpha	beta	gamma	Vol.
0	1.789	8.3346	8.3346	8.3346	90	90	90	579
0	0	0.0042	0	0	0	0	0	
H	K	L	2T(Obs)	2T-Zero	2Th(Cal)	Dif		
1	1	3	41.727	41.727	41.7037	0.0233	113	
0	0	4	50.85	50.85	50.8456	0.0044	4	
4	2	2	63.418	63.418	63.4411	-0.0231	422	
1	1	5	67.823	67.823	67.7897	0.0333	115	
2	2	6	90.767	90.767	90.7802	-0.0132	226	

Grain 12								
CELREF Version 3. 8/1/2013 12:35:16 PM								
W002048PM_gr9_30-12.dif								
Initial values : (Refinement keys on 2nd line)								
Zero	Lambda	a	b	c	alpha	beta	gamma	Vol.
0	1.789	8.3644	8.3644	8.3644	90	90	90	585.2
0	0	1	0	0	0	0	0	
Final values : (Standard errors on 2nd line)								
Zero	Lambda	a	b	c	alpha	beta	gamma	Vol.
0	1.789	8.3634	8.3634	8.3634	90	90	90	585
0	0	0.0028	0	0	0	0	0	
H	K	L	2T(Obs)	2T-Zero	2Th(Cal)	Dif		
2	2	2	43.466	43.466	43.4927	-0.0267	222	
2	2	4	63.175	63.175	63.1969	-0.0219	224	
5	1	1	67.558	67.558	67.5243	0.0337	511	
4	4	4	95.626	95.626	95.6326	-0.0066	444	

Grain 13								
Note: No peaks								

Grain 14								
CELREF Version 3. 8/1/2013 12:44:26 PM								
W002048PM_gr9_30-14.dif								
Initial values : (Refinement keys on 2nd line)								
Zero	Lambda	a	b	c	alpha	beta	gamma	Vol.
0	1.789	8.3666	8.3666	8.3666	90	90	90	585.7
0	0	1	0	0	0	0	0	
Final values : (Standard errors on 2nd line)								
Zero	Lambda	a	b	c	alpha	beta	gamma	Vol.
0	1.789	8.3623	8.3623	8.3623	90	90	90	584.8
0	0	0.0045	0	0	0	0	0	
H	K	L	2T(Obs)	2T-Zero	2Th(Cal)	Dif		
2	2	2	43.448	43.448	43.4989	-0.0509	22	
2	2	4	63.191	63.191	63.2066	-0.0156	224	
5	1	1	67.553	67.553	67.5349	0.0181	511	

Grain 15								
CELREF Version 3. 8/1/2013 12:41:06 PM								
W002048PM_gr9_30-15.dif								
Initial values : (Refinement keys on 2nd line)								
Zero	Lambda	a	b	c	alpha	beta	gamma	Vol.
0	1.789	8.3361	8.3361	8.3361	90	90	90	579.3
0	0	1	0	0	0	0	0	
Final values : (Standard errors on 2nd line)								
Zero	Lambda	a	b	c	alpha	beta	gamma	Vol.
0	1.789	8.3351	8.3351	8.3351	90	90	90	579.1
0	0	0.0048	0	0	0	0	0	
H	K	L	2T(Obs)	2T-Zero	2Th(Cal)	Dif		
2	2	2	43.614	43.614	43.6482	-0.0342	22	
2	2	4	63.509	63.509	63.4369	0.0721	224	
5	1	1	67.792	67.792	67.7852	0.0068	511	
4	4	4	96.034	96.034	96.0637	-0.0297	444	

Grain 16								
CELREF Version 3. 8/1/2013 12:54:16 PM								
W002048PM_gr9_30-16(mod).dif								
Initial values : (Refinement keys on 2nd line)								
Zero	Lambda	a	b	c	alpha	beta	gamma	Vol.
0	1.789	8.3243	8.3243	8.3243	90	90	90	576.8
0	0	1	0	0	0	0	0	
Final values : (Standard errors on 2nd line)								
Zero	Lambda	a	b	c	alpha	beta	gamma	Vol.
0	1.789	8.3219	8.3219	8.3219	90	90	90	576.3
0	0	0.0025	0	0	0	0	0	
H	K	L	2T(Obs)	2T-Zero	2Th(Cal)	Dif		
1	1	3	41.753	41.753	41.7701	-0.0171	113	
3	3	3	67.871	67.871	67.9068	-0.0358	333	
6	0	2	85.67	85.67	85.6571	0.0129	602	
Note: Peak 1 search parameters tweaked								

Grain 17								
CELREF Version 3. 8/1/2013 12:57:24 PM								
W002048PM_gr9_30-17.dif								
Initial values : (Refinement keys on 2nd line)								
Zero	Lambda	a	b	c	alpha	beta	gamma	Vol.
0	1.789	8.3376	8.3376	8.3376	90	90	90	579.6
0	0	1	0	0	0	0	0	
Final values : (Standard errors on 2nd line)								
Zero	Lambda	a	b	c	alpha	beta	gamma	Vol.
0	1.789	8.337	8.337	8.337	90	90	90	579.5
0	0	0.0044	0	0	0	0	0	
H	K	L	2T(Obs)	2T-Zero	2Th(Cal)	Dif		
3	1	1	41.715	41.715	41.6912	0.0238	311	
2	2	4	63.389	63.389	63.4209	-0.0319	224	
3	3	3	67.746	67.746	67.7678	-0.0218	335	
3	1	5	78.817	78.817	78.8036	0.0134	315	

Grain 18								
CELREF Version 3. 8/1/2013 1:06:50 PM								
W002048PM_gr9_30-18.dif								
Initial values : (Refinement keys on 2nd line)								
Zero	Lambda	a	b	c	alpha	beta	gamma	Vol.
0	1.789	8.3478	8.3478	8.3478	90	90	90	581.7
0	0	1	0	0	0	0	0	
Final values : (Standard errors on 2nd line)								
Zero	Lambda	a	b	c	alpha	beta	gamma	Vol.
0	1.789	8.347	8.347	8.347	90	90	90	581.5
0	0	0.0032	0	0	0	0	0	
H	K	L	2T(Obs)	2T-Zero	2Th(Cal)	Dif		
2	2	4	63.378	63.378	63.3362	0.0418	224	
5	1	1	67.689	67.689	67.6757	0.0133	511	
5	3	3	89.264	89.264	89.2923	-0.0283	533	

Grain 19								
CELREF Version 3. 8/1/2013 1:12:21 PM								
W002048PM_gr9_30-19.dif								
Initial values : (Refinement keys on 2nd line)								
Zero	Lambda	a	b	c	alpha	beta	gamma	Vol.
0	1.789	8.27	8.27	8.27	90	90	90	565.6
0	0	1	0	0	0	0	0	
Final values : (Standard errors on 2nd line)								
Zero	Lambda	a	b	c	alpha	beta	gamma	Vol.
0	1.789	8.27	8.27	8.27	90	90	90	565.6
0	0	0.004	0	0	0	0	0	
H	K	L	2T(Obs)	2T-Zero	2Th(Cal)	Dif		
1	1	3	42.059	42.059	42.0447	0.0143	113	
5	3	3	90.335	90.335	90.3502	-0.0152	533	
2	2	6	91.732	91.732	91.6911	0.0409	226	

Grain 20								
CELREF Version 3. 8/1/2013 1:33:05 PM								
W002048PM_gr9_30-20.dif								
Initial values : (Refinement keys on 2nd line)								
Zero	Lambda	a	b	c	alpha	beta	gamma	Vol.
0	1.789	8.3739	8.3739	8.3739	90	90	90	587.2
0	0	1	0	0	0	0	0	
Final values : (Standard errors on 2nd line)								
Zero	Lambda	a	b	c	alpha	beta	gamma	Vol.
0	1.789	8.3767	8.3767	8.3767	90	90	90	587.8
0	0	0.0079	0	0	0	0	0	
H	K	L	2T(Obs)	2T-Zero	2Th(Cal)	Dif		
0	0	4	50.665	50.665	50.5723	0.0927	4	
1	1	5	67.488	67.488	67.4035	0.0845	115	
6	0	2	84.962	84.962	84.9652	-0.0032	602	

Grain 21								
CELREF Version 3. 8/1/2013 1:46:11 PM								
W002048PM_gr9_30-21(mod).dif								
Initial values : (Refinement keys on 2nd line)								
Zero	Lambda	a	b	c	alpha	beta	gamma	Vol.
0	1.789	8.32	8.32	8.32	90	90	90	575.9
0	0	1	0	0	0	0	0	
Final values : (Standard errors on 2nd line)								
Zero	Lambda	a	b	c	alpha	beta	gamma	Vol.
0	1.789	8.328	8.328	8.328	90	90	90	577.6
0	0	0.0024	0	0	0	0	0	
H	K	L	2T(Obs)	2T-Zero	2Th(Cal)	Dif		
1	1	3	41.687	41.687	41.738	-0.051	113	
0	0	4	50.88	50.88	50.8885	-0.0085	4	
2	2	4	63.483	63.483	63.4969	-0.0139	224	
3	3	3	67.833	67.833	67.8503	-0.0173	333	
6	0	2	85.591	85.591	85.5794	0.0116	602	
Note: Peak 1 and 4 tweaked to centre of mass								

Grain 22								
CELREF Version 3. 8/1/2013 1:58:10 PM								
W002048PM_gr9_30-22(mod).dif								
Initial values : (Refinement keys on 2nd line)								
Zero	Lambda	a	b	c	alpha	beta	gamma	Vol.
0	1.789	8.3048	8.3048	8.3048	90	90	90	572.8
0	0	1	0	0	0	0	0	
Final values : (Standard errors on 2nd line)								
Zero	Lambda	a	b	c	alpha	beta	gamma	Vol.
0	1.789	8.304	8.304	8.304	90	90	90	572.6
0	0	0.0033	0	0	0	0	0	
H	K	L	2T(Obs)	2T-Zero	2Th(Cal)	Dif		
2	2	2	43.795	43.795	43.8198	-0.0248	222	
2	2	4	63.658	63.658	63.7019	-0.0439	224	
5	1	1	68.105	68.105	68.0732	0.0318	511	
4	4	4	96.537	96.537	96.5411	-0.0041	444	

Grain 23								
CELREF Version 3. 8/1/2013 2:00:00 PM								
W002048PM_gr9_30-23.dif								
Initial values : (Refinement keys on 2nd line)								
Zero	Lambda	a	b	c	alpha	beta	gamma	Vol.
0	1.789	8.3296	8.3296	8.3296	90	90	90	577.9
0	0	1	0	0	0	0	0	
Final values : (Standard errors on 2nd line)								
Zero	Lambda	a	b	c	alpha	beta	gamma	Vol.
0	1.789	8.3294	8.3294	8.3294	90	90	90	577.9
0	0	0.005	0	0	0	0	0	
H	K	L	2T(Obs)	2T-Zero	2Th(Cal)	Dif		
3	1	1	41.716	41.716	41.7309	-0.0149	311	
3	3	3	67.8	67.8	67.8378	-0.0378	333	
0	4	4	74.828	74.828	74.817	0.011	44	
3	1	5	78.921	78.921	78.8893	0.0317	315	

Grain 24								
CELREF Version 3. 8/1/2013 2:01:47 PM								
W002048PM_gr9_30-24.dif								
Initial values : (Refinement keys on 2nd line)								
Zero	Lambda	a	b	c	alpha	beta	gamma	Vol.
0	1.789	8.32	8.32	8.32	90	90	90	575.9
0	0	1	0	0	0	0	0	
Final values : (Standard errors on 2nd line)								
Zero	Lambda	a	b	c	alpha	beta	gamma	Vol.
0	1.789	8.3174	8.3174	8.3174	90	90	90	575.4
0	0	0.0034	0	0	0	0	0	
H	K	L	2T(Obs)	2T-Zero	2Th(Cal)	Dif		
1	1	3	41.8226	41.8226	41.7942	0.0284	113	
2	2	4	63.6	63.6	63.588	0.012	224	
5	1	1	67.9476	67.9476	67.9494	-0.0018	511	
0	4	4	74.9035	74.9035	74.944	-0.0405	44	

Note: Peak 1, and 4 , moved to centre of mass

Note: Peak 3

Grain 27								
CELREF Version 3. 8/1/2013 2:46:48 PM								
W002048PM_gr9_30-27(mod).dif								
Initial values : (Refinement keys on 2nd line)								
Zero	Lambda	a	b	c	alpha	beta	gamma	Vol.
0	1.789	8.3793	8.3793	8.3793	90	90	90	588.3
0	0	1	0	0	0	0	0	
Final values : (Standard errors on 2nd line)								
Zero	Lambda	a	b	c	alpha	beta	gamma	Vol.
0	1.789	8.3758	8.3758	8.3758	90	90	90	587.6
0	0	0.0028	0	0	0	0	0	
H	K	L	2T(Obs)	2T-Zero	2Th(Cal)	Dif		
2	2	2	43.398	43.398	43.4252	-0.0272	222	
2	2	4	63.122	63.122	63.0929	0.0291	224	
5	1	1	67.427	67.427	67.4113	0.0157	511	
4	4	4	95.424	95.424	95.4462	-0.0222	444	
Note: Peak 1 and 4 tweaked to centre of mass								

Grain 28								
CELREF Version 3. 8/1/2013 3:00:14 PM								
W002048PM_gr9_30-28.dif								
Initial values : (Refinement keys on 2nd line)								
Zero	Lambda	a	b	c	alpha	beta	gamma	Vol.
0	1.789	8.3358	8.3358	8.3358	90	90	90	579.2
0	0	1	0	0	0	0	0	
Final values : (Standard errors on 2nd line)								
Zero	Lambda	a	b	c	alpha	beta	gamma	Vol.
0	1.789	8.3359	8.3359	8.3359	90	90	90	579.2
0	0	0.0209	0	0	0	0	0	
H	K	L	2T(Obs)	2T-Zero	2Th(Cal)	Dif		
1	1	3	41.725	41.725	41.6967	0.0283	113	
2	2	4	63.409	63.409	63.4298	-0.0208	224	
1	1	5	67.806	67.806	67.7774	0.0286	115	
Note: Background does not work								

Grain 29									
CELREF Version 3. 8/1/2013 3:07:22 PM									
W002048PM_gr9_30-29.dif									
Initial values : (Refinement keys on 2nd line)									
Zero	Lambda	a	b	c	alpha	beta	gamma	Vol.	
0	1.789	8.3183	8.3183	8.3183	90	90	90	575.6	
0	0	1	0	0	0	0	0	0	
Final values : (Standard errors on 2nd line)									
Zero	Lambda	a	b	c	alpha	beta	gamma	Vol.	
0	1.789	8.3192	8.3192	8.3192	90	90	90	575.8	
0	0	0.0976	0	0	0	0	0	0	
H	K	L	2T(Obs)	2T-Zero	2Th(Cal)	Dif			
0	0	4	50.914	50.914	50.9463	-0.0323	4		
1	1	5	67.941	67.941	67.9321	0.0089	115		
Note: Insufficient peaks									

Grain 4								
CELREF Version 3. 8/1/2013 4:22:54 PM								
W002094_gr1_17-04(mod).dif								
Initial values : (Refinement keys on 2nd line)								
Zero	Lambda	a	b	c	alpha	beta	gamma	Vol.
0	1.789	8.3321	8.3321	8.3321	90	90	90	578.5
0	0	1	0	0	0	0	0	
Final values : (Standard errors on 2nd line)								
Zero	Lambda	a	b	c	alpha	beta	gamma	Vol.
0	1.789	8.3305	8.3305	8.3305	90	90	90	578.1
0	0	0.0047	0	0	0	0	0	
H	K	L	2T(Obs)	2T-Zero	2Th(Cal)	Dif		
2	2	2	43.624	43.624	43.6733	-0.0493		
5	1	1	67.826	67.826	67.8272	-0.0012	222	
0	4	4	74.887	74.887	74.805	0.082	511	
5	3	3	89.517	89.517	89.5157	0.0013	533	

Grain 9								
CELREF Version 3. 8/1/2013 4:44:28 PM								
W002094_gr1_17-09(mod).dif								
Initial values : (Refinement keys on 2nd line)								
Zero	Lambda	a	b	c	alpha	beta	gamma	Vol.
0	1.789	8.38	8.38	8.38	90	90	90	588.5
0	0	1	0	0	0	0	0	
Final values : (Standard errors on 2nd line)								
Zero	Lambda	a	b	c	alpha	beta	gamma	Vol.
0	1.789	8.3835	8.3835	8.3835	90	90	90	589.2
0	0	0.0023	0	0	0	0	0	
H	K	L	2T(Obs)	2T-Zero	2Th(Cal)	Dif		
4	2	2	63.057	63.057	63.0284	0.0286	422	
0	4	4	74.249	74.249	74.2525	-0.0035	44	
1	3	5	78.297	78.297	78.2822	0.0148	135	
5	1	5	99.256	99.256	99.2771	-0.0211	515	
Note: Peak 4 tweaked to centre of mass								

Grade 10								
CELREF Version 3. 8/7/2013 5:39:57 PM								
W002094_gr1_17-10(mod2).dif								
Initial values : (Refinement keys on 2nd line)								
Zero	Lambda	a	b	c	alpha	beta	gamma	Vol.
0	1.789	8.3359	8.3359	8.3359	90	90	90	579.2
0	0	1	0	0	0	0	0	
Final values : (Standard errors on 2nd line)								
Zero	Lambda	a	b	c	alpha	beta	gamma	Vol.
0	1.789	8.3358	8.3358	8.3358	90	90	90	579.2
0	0	0.0048	0	0	0	0	0	
H	K	L	2T(Obs)	2T-Zero	2Th(Cal)	Dif		
1	1	3	41.676	41.676	41.6972	-0.0212	113	
2	2	2	43.707	43.707	43.6441	0.0629	222	
2	2	4	63.44	63.44	63.4306	0.0094	224	
5	3	3	89.428	89.428	89.4436	-0.0156	533	
Note: 511 reflection off to left								

Grain 11								
CELREF Version 3. 8/1/2013 5:20:02 PM								
W002094_gr1_17-11.dif								
Initial values : (Refinement keys on 2nd line)								
Zero	Lambda	a	b	c	alpha	beta	gamma	Vol.
0	1.789	8.379	8.379	8.379	90	90	90	588.3
0	0	1	0	0	0	0	0	
Final values : (Standard errors on 2nd line)								
Zero	Lambda	a	b	c	alpha	beta	gamma	Vol.
0	1.789	8.3765	8.3765	8.3765	90	90	90	587.8
0	0	0.0014	0	0	0	0	0	
H	K	L	2T(Obs)	2T-Zero	2Th(Cal)	Dif		
3	1	1	41.515	41.515	41.4853	0.0297	311	
2	2	4	63.097	63.097	63.087	0.01	224	
5	1	1	67.408	67.408	67.4049	0.0031	511	
6	2	2	90.185	90.185	90.2004	-0.0154	622	

Grade 12								
CELREF Version 3. 8/1/2013 5:33:40 PM								
W002094_gr1_17-12.dif								
Initial values : (Refinement keys on 2nd line)								
Zero	Lambda	a	b	c	alpha	beta	gamma	Vol.
0	1.789	8.326	8.326	8.326	90	90	90	577.2
0	0	1	0	0	0	0	0	
Final values : (Standard errors on 2nd line)								
Zero	Lambda	a	b	c	alpha	beta	gamma	Vol.
0	1.789	8.3233	8.3233	8.3233	90	90	90	576.6
0	0	0.0018	0	0	0	0	0	
H	K	L	2T(Obs)	2T-Zero	2Th(Cal)	Dif		
2	2	2	43.698	43.698	43.7131	-0.0151	222	
2	2	4	63.564	63.564	63.537	0.027	224	
5	1	1	67.887	67.887	67.894	-0.007	511	
4	4	4	96.251	96.251	96.244	0.007	444	

Grain 13
The three peaks could not be fit to spinel structure within errors

Grain 14
The three peaks could not be fit to spinel structure within errors

Grain 15								
CELREF Version 3. 8/1/2013 5:55:17 PM								
W002094_gr1_17-15(mod).dif								
Initial values : (Refinement keys on 2nd line)								
Zero	Lambda	a	b	c	alpha	beta	gamma	Vol.
0	1.789	8.3542	8.3542	8.3542	90	90	90	583.1
0	0	1	0	0	0	0	0	
Final values : (Standard errors on 2nd line)								
Zero	Lambda	a	b	c	alpha	beta	gamma	Vol.
0	1.789	8.3565	8.3565	8.3565	90	90	90	583.5
0	0	0.0045	0	0	0	0	0	
H	K	L	2T(Obs)	2T-Zero	2Th(Cal)	Dif		
1	1	3	41.617	41.617	41.5893	0.0277	113	
2	2	4	63.244	63.244	63.2555	-0.0115	224	
0	4	4	74.478	74.478	74.533	-0.055	44	
5	1	3	78.595	78.595	78.5837	0.0113	513	
Note: Tweaked Peake 1,2 and 4 to centre of mass								

Grain 16								
CELREF Version 3. 8/1/2013 5:56:28 PM								
W002094_gr1_17-16.dif								
Initial values : (Refinement keys on 2nd line)								
Zero	Lambda	a	b	c	alpha	beta	gamma	Vol.
0	1.789	8.3542	8.3542	8.3542	90	90	90	583.1
0	0	1	0	0	0	0	0	
Final values : (Standard errors on 2nd line)								
Zero	Lambda	a	b	c	alpha	beta	gamma	Vol.
0	1.789	8.3505	8.3505	8.3505	90	90	90	582.3
0	0	0.0034	0	0	0	0	0	
H	K	L	2T(Obs)	2T-Zero	2Th(Cal)	Dif		
1	1	3	41.647	41.647	41.6208	0.0262	113	
2	2	4	63.285	63.285	63.3066	-0.0216	224	
1	1	5	67.678	67.678	67.6436	0.0344	115	
5	1	3	78.652	78.652	78.6517	0.0003	513	

Misery

WO 03 58 PM0 Disc 8

Grain1
Note: Could not refine to structure

Grain 2								
CELREF Version 3. 8/9/2013 11:57:30 AM								
Misery_WO_03_58_PM0-002(mod).dif								
Initial values : (Refinement keys on 2nd line)								
Zero	Lambda	a	b	c	alpha	beta	gamma	Vol.
0	1.789	8.35	8.35	8.35	90	90	90	582.2
0	0	1	0	0	0	0	0	
Final values : (Standard errors on 2nd line)								
Zero	Lambda	a	b	c	alpha	beta	gamma	Vol.
0	1.789	8.3519	8.3519	8.3519	90	90	90	582.6
0	0	0.0028	0	0	0	0	0	
H	K	L	2T(Obs)	2T-Zero	2Th(Cal)	Dif		
2	2	4	63.303	63.303	63.2946	0.0084		
3	3	3	67.628	67.628	67.6305	-0.0025		
0	4	4	74.571	74.571	74.5813	-0.0103		
Note: Peak 1 tweaked doublet to centre of mass								

Grain 3								
CELREF Version 3. 8/9/2013 12:01:38 PM								
Misery_WO_03_58_PM0-003.dif								
Initial values : (Refinement keys on 2nd line)								
Zero	Lambda	a	b	c	alpha	beta	gamma	Vol.
0	1.789	8.2384	8.2384	8.2384	90	90	90	559.1
0	0	1	0	0	0	0	0	
Final values : (Standard errors on 2nd line)								
Zero	Lambda	a	b	c	alpha	beta	gamma	Vol.
0	1.789	8.2379	8.2379	8.2379	90	90	90	559.1
0	0	0.0037	0	0	0	0	0	
H	K	L	2T(Obs)	2T-Zero	2Th(Cal)	Dif		
1	1	3	42.139	42.139	42.2162	-0.0772		
2	2	4	64.204	64.204	64.274	-0.07		
0	4	4	75.804	75.804	75.7931	0.0109		
7	1	1	101.698	101.698	101.6894	0.0086		

Grain 4								
CELREF Version 3. 8/9/2013 12:09:55 PM								
Misery_WO_03_58_PM0-004.dif								
Initial values : (Refinement keys on 2nd line)								
Zero	Lambda	a	b	c	alpha	beta	gamma	Vol.
0	1.789	8.3352	8.3352	8.3352	90	90	90	579.1
0	0	1	0	0	0	0	0	
Final values : (Standard errors on 2nd line)								
Zero	Lambda	a	b	c	alpha	beta	gamma	Vol.
0	1.789	8.3373	8.3373	8.3373	90	90	90	579.5
0	0	0.0035	0	0	0	0	0	
H	K	L	2T(Obs)	2T-Zero	2Th(Cal)	Dif		
2	2	2	43.646	43.646	43.636	0.01		
2	2	4	63.415	63.415	63.4181	-0.0031		
1	1	5	67.796	67.796	67.7647	0.0313		
4	4	4	96.024	96.024	96.0298	-0.0058		

Grain 5								
CELREF Version 3. 8/9/2013 12:24:59 PM								
Misery_WO_03_58_PM0-005.dif								
Initial values : (Refinement keys on 2nd line)								
Zero	Lambda	a	b	c	alpha	beta	gamma	Vol.
0	1.789	8.2739	8.2739	8.2739	90	90	90	566.4
0	0	1	0	0	0	0	0	
Final values : (Standard errors on 2nd line)								
Zero	Lambda	a	b	c	alpha	beta	gamma	Vol.
0	1.789	8.2726	8.2726	8.2726	90	90	90	566.1
0	0	0.0031	0	0	0	0	0	
H	K	L	2T(Obs)	2T-Zero	2Th(Cal)	Dif		
3	1	1	42.077	42.077	42.0311	0.0459		
2	2	4	63.968	63.968	63.9728	-0.0048		
5	1	1	68.361	68.361	68.3678	-0.0068		
3	1	5	79.509	79.509	79.5382	-0.0292		

Grain 6								
CELREF Version 3. 8/9/2013 12:27:10 PM								
Misery_WO_03_58_PM0-006.dif								
Initial values : (Refinement keys on 2nd line)								
Zero	Lambda	a	b	c	alpha	beta	gamma	Vol.
0	1.789	8.3298	8.3298	8.3298	90	90	90	578
0	0	1	0	0	0	0	0	
Final values : (Standard errors on 2nd line)								
Zero	Lambda	a	b	c	alpha	beta	gamma	Vol.
0	1.789	8.331	8.331	8.331	90	90	90	578.2
0	0	0.0166	0	0	0	0	0	
H	K	L	2T(Obs)	2T-Zero	2Th(Cal)	Dif		
1	1	3	41.704	41.704	41.7224	-0.0184		
0	0	4	50.94	50.94	50.869	0.071		
3	3	3	67.825	67.825	67.8227	0.0023		
Note: Unusual peak shape								

Grain 7								
CELREF Version 3. 8/9/2013 1:03:54 PM								
Misery_WO_03_58_PM0-007.dif								
Initial values : (Refinement keys on 2nd line)								
Zero	Lambda	a	b	c	alpha	beta	gamma	Vol.
0	1.789	8.3133	8.3133	8.3133	90	90	90	574.5
0	0	1	0	0	0	0	0	
Final values : (Standard errors on 2nd line)								
Zero	Lambda	a	b	c	alpha	beta	gamma	Vol.
0	1.789	8.3123	8.3123	8.3123	90	90	90	574.3
0	0	0.0078	0	0	0	0	0	
H	K	L	2T(Obs)	2T-Zero	2Th(Cal)	Dif		
1	1	3	41.838	41.838	41.8205	0.0175		
3	3	3	67.981	67.981	67.9959	-0.0149		
0	4	4	75.023	75.023	74.9969	0.0261		

Grain 8								
CELREF Version 3. 8/13/2013 1:15:47 PM								
Misery_WO_03_58_PM0-008(mod).dif								
Initial values : (Refinement keys on 2nd line)								
Zero	Lambda	a	b	c	alpha	beta	gamma	Vol.
0	1.789	8.375	8.375	8.375	90	90	90	587.4
0	0	1	0	0	0	0	0	
Final values : (Standard errors on 2nd line)								
Zero	Lambda	a	b	c	alpha	beta	gamma	Vol.
0	1.789	8.3724	8.3724	8.3724	90	90	90	586.9
0	0	0.0022	0	0	0	0	0	
H	K	L	2T(Obs)	2T-Zero	2Th(Cal)	Dif		
2	2	2	43.438	43.438	43.4438	-0.0058		
4	2	2	63.132	63.132	63.1216	0.0104		
3	3	3	67.406	67.406	67.4424	-0.0364		
5	3	3	88.96	88.96	88.9489	0.0111		
Note: Peak 4 issues discussed with Dr.Flemming again reflection [531]								

Grain 9								
CELREF Version 3. 8/13/2013 5:02:22 PM								
Misery_WO_03_58_PM0_009_sum.dif								
Initial values : (Refinement keys on 2nd line)								
Zero	Lambda	a	b	c	alpha	beta	gamma	Vol.
0	1.789	8.3551	8.3551	8.3551	90	90	90	583.3
0	0	1	0	0	0	0	0	
Final values : (Standard errors on 2nd line)								
Zero	Lambda	a	b	c	alpha	beta	gamma	Vol.
0	1.789	8.3549	8.3549	8.3549	90	90	90	583.2
0	0	0.0009	0	0	0	0	0	
H	K	L	2T(Obs)	2T-Zero	2Th(Cal)	Dif		
1	1	3	41.587	41.587	41.5974	-0.0104		
0	0	4	50.717	50.717	50.7131	0.0039		
5	1	1	67.603	67.603	67.6024	0.0006		
Note: First attempt tried to select peak, which was seperated, due to possible Y-shift. This does not work, as discovered with Dr.Flemming, instead a sum frame (overall).								

CELREF Version 3. 8/9/2013 1:35:29 PM								
Misery_WO_03_58_PM0-009(mod).dif								
Initial values : (Refinement keys on 2nd line)								
Zero	Lambda	a	b	c	alpha	beta	gamma	Vol.
0	1.789	8.3426	8.3426	8.3426	90	90	90	580.6
0	0	1	0	0	0	0	0	
Final values : (Standard errors on 2nd line)								
Zero	Lambda	a	b	c	alpha	beta	gamma	Vol.
0	1.789	8.3417	8.3417	8.3417	90	90	90	580.5
0	0	0.0032	0	0	0	0	0	
H	K	L	2T(Obs)	2T-Zero	2Th(Cal)	Dif		
3	1	1	41.661	41.661	41.6665	-0.0055		
0	0	4	50.757	50.757	50.7992	-0.0422		
5	1	1	67.727	67.727	67.7241	0.0029		

Grain 10								
CELREF Version 3. 8/13/2013 5:20:15 PM								
Misery_WO_03_58_PM0-010(mod).dif								
Initial values : (Refinement keys on 2nd line)								
Zero	Lambda	a	b	c	alpha	beta	gamma	Vol.
0	1.789	8.2819	8.2819	8.2819	90	90	90	568
0	0	1	0	0	0	0	0	
Final values : (Standard errors on 2nd line)								
Zero	Lambda	a	b	c	alpha	beta	gamma	Vol.
0	1.789	8.2813	8.2813	8.2813	90	90	90	567.9
0	0	0.0032	0	0	0	0	0	
H	K	L	2T(Obs)	2T-Zero	2Th(Cal)	Dif		
0	2	2	35.5237	35.5237	35.578	-0.0543		
3	3	3	68.2763	68.2763	68.2863	-0.01		
6	0	2	86.1834	86.1834	86.1801	0.0033		
Note: 333 is exchangeable with 115, as demonstrated through unit cell under both conditions								

Grain 10 b								
CELREF Version 3. 8/13/2013 5:36:05 PM								
Misery_WO_03_58_PM0-010(mod).dif								
Initial values : (Refinement keys on 2nd line)								
Zero	Lambda	a	b	c	alpha	beta	gamma	Vol.
0	1.789	8.2885	8.2885	8.2885	90	90	90	569.4
0	0	1	0	0	0	0	0	
Final values : (Standard errors on 2nd line)								
Zero	Lambda	a	b	c	alpha	beta	gamma	Vol.
0	1.789	8.2861	8.2861	8.2861	90	90	90	568.9
0	0	0.0631	0	0	0	0	0	
H	K	L	2T(Obs)	2T-Zero	2Th(Cal)	Dif		
0	2	2	35.5237	35.5237	35.5566	-0.0329		
1	1	5	68.2763	68.2763	68.2411	0.0352		
0	4	4	75.1545	75.1545	75.2759	-0.1214		
2	0	6	86.1834	86.1834	86.1178	0.0656		

Grain 10 C								
CELREF Version 3. 8/14/2013 12:18:31 PM								
Grain 10								
test.lst								
Initial values : (Refinement keys on 2nd line)								
Zero	Lambda	a	b	c	alpha	beta	gamma	Vol.
0	1.789	8.2866	8.2866	8.2866	90	90	90	569
0	0	1	0	0	0	0	0	
Final values : (Standard errors on 2nd line)								
Zero	Lambda	a	b	c	alpha	beta	gamma	Vol.
0	1.789	8.2823	8.2823	8.2823	90	90	90	568.1
0	0	0.0288	0	0	0	0	0	
H	K	L	2T(Obs)	2T-Zero	2Th(Cal)	Dif		
0	2	2	35.524	35.524	35.5732	-0.0492		
3	3	3	68.276	68.276	68.2761	-0.0001		
0	4	4	75.155	75.155	75.3157	-0.1607		
2	0	6	86.183	86.183	86.166	0.017		

Grain 11								
CELREF Version 3. 8/9/2013 1:58:38 PM								
Misery_WO_03_58_PM0-011.dif								
Initial values : (Refinement keys on 2nd line)								
Zero	Lambda	a	b	c	alpha	beta	gamma	Vol.
0	1.789	8.3	8.3	8.3	90	90	90	571.8
0	0	1	0	0	0	0	0	
Final values : (Standard errors on 2nd line)								
Zero	Lambda	a	b	c	alpha	beta	gamma	Vol.
0	1.789	8.3075	8.3075	8.3075	90	90	90	573.3
0	0	0.0023	0	0	0	0	0	
H	K	L	2T(Obs)	2T-Zero	2Th(Cal)	Dif		
1	1	3	41.861	41.861	41.8462	0.0148		
2	2	2	43.795	43.795	43.8007	-0.0057		
3	3	3	68.014	68.014	68.0411	-0.0271		
5	3	3	89.845	89.845	89.8314	0.0136		

Output from program UnitCell - method of TJB Holland & SAT Redfern 1995

sample title: Synthetic Misery 10

refined in cubic system, using wavelength 1.78897 Å

minimising the sum of squares of residuals in 2 theta

refined ZeroShift 2 theta : 0.0708 ±0.0002

parameter value sigma 95% conf

a 8.2866 0.0043 0.0134

cell vol 569.0220 0.8757 2.7697

residuals: standard, average, and maximum deviations:-

sd (2T) = 0.0726 aad (2T) = 0.0649 maxdev (2T) = 0.1138

sigmafit = 0.083819

students t = 3.16

Reciprocal cell parameters:

a*

params 0.1206768

sigma 0.0000620

Observed and fitted results: {dependent-variable residuals >2sd are bulleted}

(2-Theta observations corrected by ZeroShift of 0.0708)

no	h	k	l	d(obs)	d(calc)	res(d)	2T.obs	2T.calc	res(2T)
1	0	2	2	2.93215	2.92976	0.00239	35.524	35.554	-0.030
2	3	3	3	1.59391	1.59476	-0.00085	68.276	68.235	0.041
3	4	4	0	1.46677	1.46488	0.00189	75.155	75.269	-0.114
4	6	0	2	1.30932	1.31023	-0.00091	86.183	86.109	0.074

Regression diagnostics (for deletion of each observation i):

(a) potentially deleterious or influential observations affecting the fit:

no	h	k	l	hat	dfFits	Rstudt	sigma[i]	d(sig)%
3	4	4	0	0.293	-2.350	-3.650	0.0371	-55.8
4	6	0	2	0.430	1.131	1.301	0.0755	-9.9

limit : 0.500 1.000 2.000

(b) observations most strongly affecting the parameter values

DfBetas: cell parameter changes (as % of their standard deviations):

no	h	k	l	da	dV
3	4	4	0	-104	-104

Output from program UnitCell - method of TJB Holland & SAT Redfern 1995

sample title: Synthetic Misery 10

refined in cubic system, using wavelength 1.78897 Å

minimising the sum of squares of residuals in 2 theta

parameter value sigma 95% conf

a 8.2866 0.0043 0.0134

cell vol 569.0220 0.8757 2.7697

residuals: standard, average, and maximum deviations:-

sd (2T) = 0.0726 aad (2T) = 0.0649 maxdev (2T) = 0.1138

sigmafit = 0.083819

students t = 3.16

Reciprocal cell parameters:

a*

params 0.1206768

sigma 0.0000620

Observed and fitted results: {dependent-variable residuals >2sd are bulleted}

no	h	k	l	d(obs)	d(calc)	res(d)	2T.obs	2T.calc	res(2T)
1	0	2	2	2.93215	2.92976	0.00239	35.524	35.554	-0.030
2	3	3	3	1.59391	1.59476	-0.00085	68.276	68.235	0.041
3	4	4	0	1.46677	1.46488	0.00189	75.155	75.269	-0.114
4	6	0	2	1.30932	1.31023	-0.00091	86.183	86.109	0.074

Regression diagnostics (for deletion of each observation i):

(a) potentially deleterious or influential observations affecting the fit:

no	h	k	l	hat	dfFits	Rstudt	sigma[i]	d(sig)%
3	4	4	0	0.293	-2.350	-3.650	0.0371	-55.8
4	6	0	2	0.430	1.131	1.301	0.0755	-9.9

limit : 0.500 1.000 2.000

(b) observations most strongly affecting the parameter values

DfBetas: cell parameter changes (as % of their standard deviations):

no	h	k	l	da	dV
3	4	4	0	-104	-104
4	6	0	2	102	102

Output from program UnitCell - method of TJB Holland & SAT Redfern 1995

sample title: Synthetic Misery 10

refined in cubic system, using wavelength 1.78897 Å

minimising the sum of squares of residuals in 2 theta

parameter value sigma 95% conf

a 8.2866 0.0043 0.0134

cell vol 569.0220 0.8757 2.7697

residuals: standard, average, and maximum deviations:-

sd (2T) = 0.0726 aad (2T) = 0.0649 maxdev (2T) = 0.1138

sigmafit = 0.083819

students t = 3.16

Reciprocal cell parameters:

a*

params 0.1206768

sigma 0.0000620

Observed and fitted results: {dependent-variable residuals >2sd are bulleted}

no	h	k	l	d(obs)	d(calc)	res(d)	2T.obs	2T.calc	res(2T)
1	0	2	2	2.93215	2.92976	0.00239	35.524	35.554	-0.030
2	1	1	5	1.59391	1.59476	-0.00085	68.276	68.235	0.041
3	0	4	4	1.46677	1.46488	0.00189	75.155	75.269	-0.114
4	2	0	6	1.30932	1.31023	-0.00091	86.183	86.109	0.074

Regression diagnostics (for deletion of each observation i):

(a) potentially deleterious or influential observations affecting the fit:

no	h	k	l	hat	dfFits	Rstudt	sigma[i]	d(sig)%
3	0	4	4	0.293	-2.350	-3.650	0.0371	-55.8
4	2	0	6	0.430	1.131	1.301	0.0755	-9.9

limit : 0.500 1.000 2.000

(b) observations most strongly affecting the parameter values

DfBetas: cell parameter changes (as % of their standard deviations):

no	h	k	l	da	dV
3	0	4	4	-104	-104
4	2	0	6	102	102

Grain 12

CELREF Version 3. 8/14/2013 12:57:19 PM								
Misery_WO_03_58_PM0-012(sum).dif								
Initial values : (Refinement keys on 2nd line)								
Zero	Lambda	a	b	c	alpha	beta	gamma	Vol.
0	1.789	8.3482	8.3482	8.3482	90	90	90	581.8
0	0	1	0	0	0	0	0	
Final values : (Standard errors on 2nd line)								
Zero	Lambda	a	b	c	alpha	beta	gamma	Vol.
0	1.789	8.3473	8.3473	8.3473	90	90	90	581.6
0	0	0.0091	0	0	0	0	0	
H	K	L	2T(Obs)	2T-Zero	2Th(Cal)	Dif		
3	1	1	41.691	41.691	41.6374	0.0536		
0	0	4	50.762	50.762	50.7629	-0.0009		
3	3	3	67.631	67.631	67.6728	-0.0418		

CELREF Version 3. 8/14/2013 3:04:55 PM								
Misery_WO_03_58_PM0-012.dif								
Initial values : (Refinement keys on 2nd line)								
Zero	Lambda	a	b	c	alpha	beta	gamma	Vol.
0	1.789	8.363	8.363	8.363	90	90	90	584.9
0	0	1	0	0	0	0	0	
Final values : (Standard errors on 2nd line)								
Zero	Lambda	a	b	c	alpha	beta	gamma	Vol.
0	1.789	8.3421	8.3421	8.3421	90	90	90	580.5
0	0	0.0764	0	0	0	0	0	
H	K	L	2T(Obs)	2T-Zero	2Th(Cal)	Dif		
1	1	3	41.754	41.754	41.6643	0.0897		
0	0	4	50.709	50.709	50.7965	-0.0875		
1	1	5	67.737	67.737	67.7203	0.0167		
2	0	6	85.266	85.266	85.4005	-0.1345		

Note: First tried using splice technique but peaks 1,3 and 2,4 grouped together.

There does not appear to be a Y problem, but even so an attempt to try a sum frame was attempted

This yielded only 3 peaks and a high sigma value. Then by forcing selections of peaks using celref indexes

in unit cell, only possible with four peaks. This value passed, but when done with same values in celref it failed.

CELREF Version 3. 8/14/2013 1:07:10 PM								
Misery_WO_03_58_PM0-012.dif								
Initial values : (Refinement keys on 2nd line)								
Zero	Lambda	a	b	c	alpha	beta	gamma	Vol.
0	1.789	8.3482	8.3482	8.3482	90	90	90	581.8
0	0	1	0	0	0	0	0	
Final values : (Standard errors on 2nd line)								
Zero	Lambda	a	b	c	alpha	beta	gamma	Vol.
0	1.789	8.3397	8.3397	8.3397	90	90	90	580
0	0	0.0125	0	0	0	0	0	
H	K	L	2T(Obs)	2T-Zero	2Th(Cal)	Dif		
3	1	1	41.754	41.754	41.6769	0.0771		
0	0	4	50.709	50.709	50.8122	-0.1032		
5	1	1	67.737	67.737	67.7425	-0.0055		
2	0	6	85.266	85.266	85.431	-0.165		

Grain 13

CELREF Version 3. 8/21/2013 4:23:25 PM								
Misery_WO_03_58_PM0-073.dif								
Initial values : (Refinement keys on 2nd line)								
Zero	Lambda	a	b	c	alpha	beta	gamma	Vol.
0	1.789	8.277	8.277	8.277	90	90	90	567
0	0	1	0	0	0	0	0	
Final values : (Standard errors on 2nd line)								
Zero	Lambda	a	b	c	alpha	beta	gamma	Vol.
0	1.789	8.276	8.276	8.276	90	90	90	566.8
0	0	0.023	0	0	0	0	0	
H	K	L	2T(Obs)	2T-Zero	2Th(Cal)	Dif		
1	1	3	41.999	41.999	42.0128	-0.0138		
2	2	4	63.938	63.938	63.9432	-0.0052		
1	1	5	68.406	68.406	68.3356	0.0704		
2	2	6	91.569	91.569	91.6057	-0.0367		

Note: All peaks could not be selected at once

Grain 14

CELREF Version 3. 8/21/2013 4:51:59 PM								
Misery_WO_03_58_PM0-014(mod).dif								
Initial values : (Refinement keys on 2nd line)								
Zero	Lambda	a	b	c	alpha	beta	gamma	Vol.
0	1.789	8.3213	8.3213	8.3213	90	90	90	576.2
0	0	1	0	0	0	0	0	
Final values : (Standard errors on 2nd line)								
Zero	Lambda	a	b	c	alpha	beta	gamma	Vol.
0	1.789	8.3196	8.3196	8.3196	90	90	90	575.8
0	0	0.0057	0	0	0	0	0	
H	K	L	2T(Obs)	2T-Zero	2Th(Cal)	Dif		
1	1	3	41.794	41.794	41.7825	0.0115		
5	1	1	67.996	67.996	67.9288	0.0672		
5	3	3	89.6	89.6	89.6656	-0.0656		

CELREF Version 3. 8/21/2013 4:55:14 PM								
Misery_WO_03_58_PM0-014(mod).dif								
Initial values : (Refinement keys on 2nd line)								
Zero	Lambda	a	b	c	alpha	beta	gamma	Vol.
0	1.789	8.326	8.326	8.326	90	90	90	577.2
0	0	1	0	0	0	0	0	
Final values : (Standard errors on 2nd line)								
Zero	Lambda	a	b	c	alpha	beta	gamma	Vol.
0	1.789	8.3232	8.3232	8.3232	90	90	90	576.6
0	0	0.0038	0	0	0	0	0	
H	K	L	2T(Obs)	2T-Zero	2Th(Cal)	Dif		
3	1	1	41.7942	41.7942	41.7635	0.0307		
5	3	3	89.5997	89.5997	89.616	-0.0163		

Note: Forced middle peak to all peaks to be selected,
Peak 3 moved to centre of mass, Two peak shows within error of three peak selection

Grain 15

Note: Insufficient peaks

Grain 16
Note: Insufficient peaks

Grain 17
Note: Insufficient peaks

Grain 18								
CELREF Version 3. 8/21/2013 5:22:57 PM								
Misery_WO_03_58_PM0-018.dif								
Initial values : (Refinement keys on 2nd line)								
Zero	Lambda	a	b	c	alpha	beta	gamma	Vol.
0	1.789	8.2985	8.2985	8.2985	90	90	90	571.5
0	0	1	0	0	0	0	0	
Final values : (Standard errors on 2nd line)								
Zero	Lambda	a	b	c	alpha	beta	gamma	Vol.
0	1.789	8.3018	8.3018	8.3018	90	90	90	572.2
0	0	0.0403	0	0	0	0	0	
H	K	L	2T(Obs)	2T-Zero	2Th(Cal)	Dif		
0	4	4	74.996	74.996	75.1081	-0.1121		
3	1	5	79.145	79.145	79.2024	-0.0574		
2	0	6	86.047	86.047	85.9145	0.1325		
Note: Peaks would never align discussed with Dr.Flemming								

Grain 19								
CELREF Version 3. 8/21/2013 5:27:55 PM								
Misery_WO_03_58_PM0-019(mod).dif								
Initial values : (Refinement keys on 2nd line)								
Zero	Lambda	a	b	c	alpha	beta	gamma	Vol.
0	1.789	8.329	8.329	8.329	90	90	90	577.8
0	0	1	0	0	0	0	0	
Final values : (Standard errors on 2nd line)								
Zero	Lambda	a	b	c	alpha	beta	gamma	Vol.
0	1.789	8.3281	8.3281	8.3281	90	90	90	577.6
0	0	0.0159	0	0	0	0	0	
H	K	L	2T(Obs)	2T-Zero	2Th(Cal)	Dif		
2	2	4	63.603	63.603	63.4963	0.1067		
1	1	5	67.855	67.855	67.8497	0.0053		
4	4	4	96.117	96.117	96.1706	-0.0536		
Note: Examples of Ilmenite and chromite having same peaks,when tuned								

Grain 20								
CELREF Version 3. 8/9/2013 4:21:28 PM								
Misery_WO_03_58_PM0-020.dif								
Initial values : (Refinement keys on 2nd line)								
Zero	Lambda	a	b	c	alpha	beta		
0	1.789	8.2731	8.2731	8.2731	90	90		
0	0	1	0	0	0	0		
Final values : (Standard errors on 2nd line)								
Zero	Lambda	a	b	c	alpha	beta		
0	1.789	8.2728	8.2728	8.2728	90	90		
0	0	0.0018	0	0	0	0		
H	K	L	2T(Obs)	2T-Zero	2Th(Cal)	Dif		
0	0	4	51.237	51.237	51.253	-0.016		
5	1	1	68.366	68.366	68.366	0		

Grain 25
Note: Could not refine to structure

Grain 26								
CELREF Version 3. 8/10/2013 3:28:53 PM								
Misery_WO_03_58_PM0-026(mod).dif								
Initial values : (Refinement keys on 2nd line)								
Zero	Lambda	a	b	c	alpha	beta	gamma	Vol.
0	1.789	8.2393	8.2393	8.2393	90	90	90	559.3
0	0	1	0	0	0	0	0	
Final values : (Standard errors on 2nd line)								
Zero	Lambda	a	b	c	alpha	beta	gamma	Vol.
0	1.789	8.238	8.238	8.238	90	90	90	559.1
0	0	0.0039	0	0	0	0	0	
H	K	L	2T(Obs)	2T-Zero	2Th(Cal)	Dif		
2	2	4	64.176	64.176	64.2739	-0.0979		
5	1	1	68.688	68.688	68.6953	-0.0073		
0	4	4	75.805	75.805	75.793	0.012		
6	0	2	86.763	86.763	86.7449	0.0181		
Note: All peaks tweaked to centre								

Grain 27
Note: Could not refine to structure

Grain 28
Note: Could not refine to structure

Grain 29								
CELREF Version 3. 8/10/2013 4:16:20 PM								
Misery_WO_03_58_PM0-029(mod).dif								
Initial values : (Refinement keys on 2nd line)								
Zero	Lambda	a	b	c	alpha	beta	gamma	Vol.
0	1.789	8.3332	8.3332	8.3332	90	90	90	578.7
0	0	1	0	0	0	0	0	
Final values : (Standard errors on 2nd line)								
Zero	Lambda	a	b	c	alpha	beta	gamma	Vol.
0	1.789	8.3314	8.3314	8.3314	90	90	90	578.3
0	0	0.0044	0	0	0	0	0	
H	K	L	2T(Obs)	2T-Zero	2Th(Cal)	Dif		
1	1	3	41.701	41.701	41.7206	-0.0196		
2	2	2	43.699	43.699	43.6687	0.0303		
5	1	1	67.878	67.878	67.8196	0.0584		
5	3	3	89.446	89.446	89.5044	-0.0584		
Note: Peak 2 tweaked to centre of mass								

Grain 40

CELREF Version 3. 8/12/2013 1:19:20 PM								
Misery_WO_03_58_PM0-040.dif								
Initial values : (Refinement keys on 2nd line)								
Zero	Lambda	a	b	c	alpha	beta	gamma	Vol.
0	1.789	8.2984	8.2984	8.2984	90	90	90	571.5
0	0	1	0	0	0	0	0	
Final values : (Standard errors on 2nd line)								
Zero	Lambda	a	b	c	alpha	beta	gamma	Vol.
0	1.789	8.2978	8.2978	8.2978	90	90	90	571.3
0	0	0.0032	0	0	0	0	0	
H	K	L	2T(Obs)	2T-Zero	2Th(Cal)	Dif		
4	2	2	63.765	63.765	63.7557	0.0093		
3	3	3	68.091	68.091	68.1317	-0.0407		
5	3	3	89.985	89.985	89.9653	0.0197		

Grain 41

Note: Could not refine to structure

Appendix F: Chemistry Plot

[illegible]

Weight Percent - Fe ₂ and Fe ₃ - Lique Droplet Calc. (Mafic) (mol. convex hatched)																			
Location	Minid	Paragenesis	WO number	Probe Disk	Grain Number	Grained	Total	SiO ₂	TiO ₂	Al ₂ O ₃	Cr ₂ O ₃	FeO	Fe ₂ O ₃	MnO	NiO	ZnO	V	Unit Cell (a)	
Gabon	CHR	NK	W03.04.005PM-1		12	55605	100.7983	100.34	0.21	0.63	18.49	46.46	13.4957	2.591048	0.99	14.95	0.26	0	8.2594
Gabon	CHR	NK	W03.04.005PM-1		12	55605	100.7983	100.34	0.21	0.63	18.49	46.46	13.4957	2.591048	0.99	14.95	0.26	0	8.2594
Gabon	CHR	NK	W03.04.005PM-1		17	55611	99.56847	99.76	0.21	0.67	17.98	46.78	9.68946	4.89624	0.46	17.15	0	0	8.2544
Gabon	CHR	NK	W03.04.005PM-1		18	55611	97.98677	99.19	0.19	0.67	24.97	36.41	13.6453	6.122443	0.53	14.97	0.23	0	8.2433
Gabon	CHR	NK	W03.04.005PM-1		21	55614	99.04507	99.22	0.24	1.78	23.79	32.2	15.54125	9.663817	0.47	14.56	0.27	0	8.2527
Gabon	CHR	NK	W03.04.005PM-1		24	55617	98.53343	99.12	0.31	0.77	29.69	30.67	14.2063	6.292795	0.47	15.55	0.27	0	8.2533
Gabon	CHR	NK	W03.04.005PM-1		26	55618	101.0385	101.36	0.31	0.6	20.24	44.86	13.67624	5.970762	0.38	15.47	0	0	8.2641
Gabon	CHR	NK	W03.04.005PM-1		28	55621	100.9378	100.93	0.26	0.6	19.35	44.86	13.67624	5.970762	0.38	15.47	0	0	8.2641
Gabon	CHR	NK	W03.04.005PM-1		29	55622	97.542719	98.15	0.26	0.67	29.96	30.12	12.2052	6.59562	0.33	16.5	0.23	0	8.2722
Gabon	CHR	NK	W03.04.005PM-1		29	55622	97.542719	98.15	0.26	0.67	29.96	30.12	12.2052	6.59562	0.33	16.5	0.23	0	8.2722
Gabon	CHR	NK	W03.04.005PM-1		30	55623	100.6265	100.18	0.21	1.86	21.36	35.9	16.5663	6.59672	0.53	14.64	0.19	0	8.2637
Gabon	CHR	NK	W03.04.005PM-1		30	55623	98.58409	98.19	0	0.53	15.56	48.35	13.42766	6.59672	0.53	13.42	0.21	0	8.2637
Gabon	CHR	NK	W03.04.005PM-1		34	55627	100.9822	101.77	0.24	0.24	22.48	47.31	13.99971	3.812248	0.45	14.51	0.18	0	8.2597
Gabon	CHR	NK	W03.04.005PM-1		47	55628	98.51559	98.8	0.33	1.13	26.87	32.22	16.5714	6.48945	0.45	14.22	0.28	0	8.2455
Gabon	CHR	NK	W03.04.005PM-1		47	55628	98.51559	98.8	0.33	1.13	26.87	32.22	16.5714	6.48945	0.45	14.22	0.28	0	8.2455
Gabon	CHR	NK	W03.04.005PM-1		48	55633	99.30148	99.36	0.38	0.78	22.15	30.62	18.0702	5.554504	0.47	12.53	0.21	0	8.2311
Gabon	CHR	NK	W03.04.005PM-1		54	55633	98.34838	99.48	0	0.65	19.35	44.74	9.32971	6.072466	0.53	17.21	0.19	0	8.2658
Gabon	CHR	NK	W03.04.005PM-1		55	55633	98.87352	98.99	0.23	0.26	21.09	44.95	13.38687	3.116657	0.53	14.57	0.29	0	8.2463
Gabon	CHR	NK	W03.04.005PM-1		55	55633	98.87352	98.99	0.23	0.26	21.09	44.95	13.38687	3.116657	0.53	14.57	0.29	0	8.2463
Gabon	CHR	NK	W03.04.005PM-1		56	55633	100.2586	98.51	0	2.25	12.18	41.81	17.74068	13.24457	0.47	12.2	0.17	0	8.3144
Gabon	CHR	NK	W03.04.005PM-1		56	55633	100.2586	98.51	0	2.25	12.18	41.81	17.74068	13.24457	0.47	12.2	0.17	0	8.3144
Gabon	CHR	NK	W03.04.005PM-1		57	55637	103.0286	100.85	0.024	0	0.46204	40.6718	32.5195	12.74071	0.34001	1.9853	0	0	8.3268
Gabon	CHR	NK	W03.04.005PM-1		57	55637	103.0286	100.85	0.024	0	0.46204	40.6718	32.5195	12.74071	0.34001	1.9853	0	0	8.3268
Gabon	CHR	NK	W03.04.005PM-1		58	55637	98.38441	98.12294	0.0482	0.3832	12.83312	44.80351	30.53807	8.032306	0.80701	1.66887	0	0	8.3231
Gabon	CHR	NK	W03.04.005PM-1		58	55637	98.38441	98.12294	0.0482	0.3832	12.83312	44.80351	30.53807	8.032306	0.80701	1.66887	0	0	8.3231
Gabon	CHR	NK	W03.04.005PM-1		6	28458	99.42738	98.76357	0.8929	0.5004	14.16692	45.23928	29.52486	6.586509	1.05622	2.55538	0	0	8.2767
Gabon	CHR	NK	W03.04.005PM-1		6	28458	99.42738	98.76357	0.8929	0.5004	14.16692	45.23928	29.52486	6.586509	1.05622	2.55538	0	0	8.2767
Gabon	CHR	NK	W03.04.005PM-1		8	28459	100.156	99.11077	0	0.3552	13.55652	46.74608	21.04681	5.657776	0.84862	6.25456	0	0	8.2931
Gabon	CHR	NK	W03.04.005PM-1		8	28459	100.156	99.11077	0	0.3552	13.55652	46.74608	21.04681	5.657776	0.84862	6.25456	0	0	8.2931
Gabon	CHR	NK	W03.04.005PM-1		9	28459	98.5999	98.23111	0	0.15542	15.51947	47.18599	20.61542	6.599425	0.81863	8.58592	0	0	8.2931
Gabon	CHR	NK	W03.04.005PM-1		9	28459	98.5999	98.23111	0	0.15542	15.51947	47.18599	20.61542	6.599425	0.81863	8.58592	0	0	8.2931
Gabon	CHR	NK	W03.04.005PM-1		11	28462	98.7387	98.08311	0.017	0	0.15542	45.7019	21.3336	7.02228	1.0383	8.58592	0	0	8.2931
Gabon	CHR	NK	W03.04.005PM-1		11	28462	98.7387	98.08311	0.017	0	0.15542	45.7019	21.3336	7.02228	1.0383	8.58592	0	0	8.2931
Gabon	CHR	NK	W03.04.005PM-1		16	28458	98.5454	97.28927	0	0.45203	12.44229	47.40033	27.81811	6.586509	0.70113	8.58592	0	0	8.3165
Gabon	CHR	NK	W03.04.005PM-1		16	28458	98.5454	97.28927	0	0.45203	12.44229	47.40033	27.81811	6.586509	0.70113	8.58592	0	0	8.3165
Gabon	CHR	NK	W03.04.005PM-1		18	28458	99.07551	98.17014	0	0.407	14.3732	45.86938	21.43745	7.84745	0.60816	8.07738	0	0	8.3051
Gabon	CHR	NK	W03.04.005PM-1		20	28458	98.56219	97.71894	0.03423	0	0.63385	15.03744	45.44874	5.657776	0.36121	5.12236	0	0	8.2936
Gabon	CHR	NK	W03.04.005PM-1		3	39345	99.8777	99.77	0.12	0	7.67	61.3	16.8953	2.822466	0.27	10.46	0	0	8.321
Gabon	CHR	NK	W03.04.005PM-1		3	39345	99.8777	99.77	0.12	0	7.67	61.3	16.8953	2.822466	0.27	10.46	0	0	8.321
Gabon	CHR	NK	W03.04.005PM-1		4	39345	101.867	99.69	0.27	1.05	11.69	41.85	21.1991	16.0048	0.33	9.32	0	0	8.3137
Gabon	CHR	NK	W03.04.005PM-1		4	39345	101.867	99.69	0.27	1.05	11.69	41.85	21.1991	16.0048	0.33	9.32	0	0	8.3137
Gabon	CHR	NK	W03.04.005PM-1		7	39345	99.88319	99.53	0.15	2.42	6.6	54.42	17.1666	7.10322	0.34	11.48	0	0	8.3398
Gabon	CHR	NK	W03.04.005PM-1		7	39345	99.88319	99.53	0.15	2.42	6.6	54.42	17.1666	7.10322	0.34	11.48	0	0	8.3398
Gabon	CHR	NK	W03.04.005PM-1		11	39346	100.3199	99.79	0.18	2.2	7.99	50.31	14.80817	11.05169	0.35	13.45	0	0	8.3346
Gabon	CHR	NK	W03.04.005PM-1		11	39346	100.3199	99.79	0.18	2.2	7.99	50.31	14.80817	11.05169	0.35	13.45	0	0	8.3346
Gabon	CHR	NK	W03.04.005PM-1		12	39346	101.215	99.89	0.23	0.6	2.65	59.06	22.92124	8.79247	0.35	6.81	0	0	8.3634
Gabon	CHR	NK	W03.04.005PM-1		14	39345	101.5003	100.81	0.28	0.87	2.48	60.57	18.6667	8.06389	0.36	10.03	0	0	8.3633
Gabon	CHR	NK	W03.04.005PM-1		14	39345	101.5003	100.81	0.28	0.87	2.48	60.57	18.6667	8.06389	0.36	10.03	0	0	8.3633
Gabon	CHR	NK	W03.04.005PM-1		16	39345	100.3934	100.8	0.19	0.75	5.48	54.22	17.9501	6.87478	0.29	11.75	0	0	8.3351
Gabon	CHR	NK	W03.04.005PM-1		16	39345	100.3934	100.8	0.19	0.75	5.48	54.22	17.9501	6.87478	0.29	11.75	0	0	8.3351
Gabon	CHR	NK	W03.04.005PM-1		17	39345	99.45589	99.45	0.11	5.27	63.12	14.5252	4.40336	0.227	11.51	0	0	8.337	
Gabon	CHR	NK	W03.04.005PM-1		17	39345	99.45589	99.45	0.11	5.27	63.12	14.5252	4.40336	0.227	11.51	0	0	8.337	
Gabon	CHR	NK	W03.04.005PM-1		18	39346	99.91079	99.87	0.23	0.89	2.45	65.62	17.4575	3.87045	0.43	9.62	0	0	8.347
Gabon	CHR	NK	W03.04.005PM-1		18	39346	99.91079	99.87	0.23	0.89	2.45	65.62	17.4575	3.87045	0.43	9.62	0	0	8.347
Gabon	CHR	NK	W03.04.005PM-1		19	39346	99.21431	99.88	0.38	2.78	21.59	32.13	18.8068	10.42542	0.23	12.77	0	0	8.27
Gabon	CHR	NK	W03.04.005PM-1		19	39346	99.21431	99.88	0.38	2.78	21.59	32.13	18.8068	10.42542	0.23	12.77	0	0	8.27
Gabon	CHR	NK	W03.04.005PM-1		21	39347	100.0718	99.43	0	0	4.53	62.2	11.15072	7.41111	0.43	13.81	0	0	8.328
Gabon	CHR	NK	W03.04.005PM-1		21	39347	100.0718	99.43	0	0	4.53	62.2	11.15072	7.41111	0.43	13.81	0	0	8.328
Gabon	CHR	NK	W03.04.005PM-1		22	39347	100.0718	100.59	0.17	0.15	4.12	62.78	18.57152	6.48918	0.24	10.51	0	0	8.324
Gabon	CHR	NK	W03.04.005PM-1		22	39347	100.0718	100.59	0.17	0.15	4.12	62.78	18.57152	6.48918	0.24	10.51	0	0	8.324
Gabon	CHR	NK	W03.04.005PM-1		22	39347	100.302	100.32	0.14	0.1	6.32	63.81	14.1995	2.822466	0.35	12.38	0	0	8.3174
Gabon	CHR	NK	W03.04.005PM-1		22	39347	100.302	100.32	0.14	0.1	6.32	63.81	14.199						

Appendix G: MatLab Code

Weight Percent Plots

Input Code

```
data = xlsread('Weight Percent.xlsx')
```

```
Tigabon=data(1:18,2)
```

```
Timats=data(19:29,2)
```

```
Tikoala=data(30:47,2)
```

```
Tisheiba=data(48:56,2)
```

```
Timisery=data(57:74,2)
```

```
Algabon=data(1:18,3)
```

```
Almats=data(19:29,3)
```

```
Alkoala=data(30:47,3)
```

```
Alsheiba=data(48:56,3)
```

```
Almisery=data(57:74,3)
```

```
Crgabon=data(1:18,4)
```

```
Crmats=data(19:29,4)
```

```
Crkoala=data(30:47,4)
```

```
Crsheiba=data(48:56,4)
```

```
Crmisery=data(57:74,4)
```

```
Mggabon=data(1:18,8)
```

```
Mgmats=data(19:29,8)
```

```
Mgkoala=data(30:47,8)
```

```
Mgsheiba=data(48:56,8)
```

```
Mgmisery=data(57:74,8)
```

```
Fe2gabon=data(1:18,5)
```

```
Fe2mats=data(19:29,5)
```

```
Fe2koala=data(30:47,5)
```

```
Fe2sheiba=data(48:56,5)
```

```
Fe2misery=data(57:74,5)
```

```
Fe3gabon=data(1:18,6)
```

```
Fe3mats=data(19:29,6)
```

```
Fe3koala=data(30:47,6)
```

```
Fe3sheiba=data(48:56,6)
```

```
Fe3misery=data(57:74,6)
```

```
Unitgabon=data(1:18,12)
```

```
Unitmats=data(19:29,12)
```

```
Unitkoala=data(30:47,12)
```

```
Unisheiba=data(48:56,12)
```

```
Unitmisery=data(57:74,12)
```

Plots with Terra Data require the following lines for input

```
Tiportable=data(75:75,2)
Alportable=data(75:75,3)
Crportable=data(75:75,4)
Mgportable=data(75:75,8)
Fe2portable=data(75:75,5)
Fe3portable=data(75:75,6)
Unitportable=data(75:75,12)
```

Plots without Unit Cell

```
scatter(Mggabon,Crgabon,50,'s','fill');
scatter(Mgmats,Crmats,50,'d','fill');
scatter(Mgkoala,Crkoala,50,'^','fill')
scatter(Mgsheiba,Crsheiba,50,'o','fill');
scatter(Mgmisery,Crmisery,50,'v','fill');
```

```
scatter(Crgabon,Algabon,50,'s','fill');
scatter(Crmats,Almats,50,'d','fill');
scatter(Crkoala,Alkoala,50,'^','fill')
scatter(Crsheiba,Alsheiba,50,'o','fill');
scatter(Crmisery,Almisery,50,'v','fill');
```

```
scatter(Crgabon,Tigabon,50,'s','fill');
scatter(Crmats,Timats,50,'d','fill');
scatter(Crkoala,Tikoala,50,'^','fill')
scatter(Crsheiba,Tisheiba,50,'o','fill');
scatter(Crmisery,Timisery,50,'v','fill');
```

Plots with Unit Cell

Cr₂O₃ vs MgO

```
scatter(Mggabon,Crgabon,50,Unitgabon,'s','fill');
scatter(Mgmats,Crmats,50,Unitmait,'d','fill');
scatter(Mgkoala,Crkoala,50,Unitkoala,'^','fill')
scatter(Mgsheiba,Crsheiba,50,Unitsheiba,'o','fill');
scatter(Mgmisery,Crmisery,50,Unitmisery,'v','fill');
```

Al₂O₃ vs Cr₂O₃

```
scatter(Crgabon,Algabon,50,Unitgabon,'s','fill');
scatter(Crmats,Almats,50,Unitmats,'d','fill');
scatter(Crkoala,Alkoala,50,Unitkoala,'^','fill')
scatter(Crsheiba,Alsheiba,50,Unitsheiba,'o','fill');
scatter(Crmisery,Almisery,50,Unitmisery,'v','fill');
```

Plots with Unit Cell – Cont'dTiO₂ vs Cr₂O₃

```
scatter(Crgabon,Tigabon,50,Unitgabon,'s','fill');
scatter(Crmats,Timats,50,Unitmats,'d','fill');
scatter(Crkoala,Tikoala,50,Unitkoala,'^','fill')
scatter(Crsheiba,Tisheiba,50,Unitsheiba,'o','fill');
scatter(Crmisery,Timisery,50,Unitmisery,'v','fill');
```

Plots with Terra Data require the following lines for output

```
scatter(Mgportable,Crportable,50,Unitportable,*);
scatter(Crportable,Alportable,100,Unitportable,*);
scatter(Crportable,Tiportable,100,Unitportable,*);
scatter3(Crportable,Mgportable,Tiportable,50,Unitportable,*);
```

Extra DiagramsAl₂O₃ vs MgO

```
scatter(Mggabon,Algabon,50,Unitgabon,'s');
scatter(Mgkoala,Alkoala,50,Unitkoala,'^')
scatter(Mgsheiba,Alsheiba,50,Unitsheiba,'o');
scatter(Mgmisery,Almisery,50,Unitmisery,'v');
scatter(Mgmats,Almats,50,Unitmats,'*');
scatter(Mgportable,Alportable,100,Unitportable,'*');
```

Matlab Entry Code for Ratio PlotsInput

```
data = xlsread('Ratios.xlsx')
```

Cr/Cr+Al

```
xcrgabon=data(1:18,1)
xcrmat=data(19:29,1)
xcrkoala=data(30:47,1)
xcrsheiba=data(48:56,1)
xcrmisery=data(57:74,1)
```

Fe²⁺/Mg+Fe²⁺

```
ymggabon=data(1:18,2)
ymgmait=data(19:29,2)
ymgkoala=data(30:47,2)
ymgsheiba=data(48:56,2)
ymgmisery=data(57:74,2)
```

Input – cont'd $Fe^{3+}/Cr+Al+Fe^{3+}$

```

zfegabon=data(1:18,3)
zfemait=data(19:29,3)
zfekoala=data(30:47,3)
zfesheiba=data(48:56,3)
zfemisery=data(57:74,3)

```

Unit cell

```

unitgabon=data(1:18,4)
unitmait=data(19:29,4)
unitkoala=data(30:47,4)
unitsheiba=data(48:56,4)
unitmisery=data(57:74,4)

```

Plots with Terra Data require the following lines for input

```

xcrportable=data(75:75,1)
ymgportable=data(75:75,2)
zfeportable=data(75:75,3)
unitportable=data(75:75,4)

```

hold on

Plots without Unit Cell $Fe^{3+}/Cr+Al+Fe^{3+}$ vs $Fe^{2+}/Mg+Fe^{2+}$

```

scatter(ymggabon,zfegabon,100,'s','fill');
scatter(ymgmats,zfemats,100,'d','fill');
scatter(ymgkoala,zfekoala,100,'^','fill');
scatter(ymgsheiba,zfesheiba,100,'o','fill');
scatter(ymgmisery,zfemisery,100,'v','fill');

```

 $Cr/Cr+Al$ vs $Fe^{2+}/Mg+Fe^{2+}$

```

scatter(ymggabon,xcrgabon,100,'s','fill');
scatter(ymgmats,xcrmats,100,'d','fill');
scatter(ymgkoala,xcrkoala,100,'^','fill');
scatter(ymgsheiba,xcrsheiba,100,'o','fill');
scatter(ymgmisery,xcrmisery,100,'v','fill');

```


Plots with Unit Cell $Fe^{3+}/Cr+Al+Fe^{3+}$ vs $Fe^{2+}/Mg+Fe^{2+}$

```
scatter(ymggabon,zfegabon,100,unitgabon,'s','fill');
scatter(ymgmatt,zfemats,100,unitmats,'d','fill');
scatter(ymgkoala,zfekoala,100,unitkoala,'^','fill');
scatter(ymgsheiba,zfesheiba, 100,unitsheiba,'o','fill');
scatter(ymgmisery,zfemisery,100,unitmisery,'v','fill');
```

 $Cr/Cr+Al$ vs $Fe^{2+}/Mg+Fe^{2+}$

```
scatter(ymggabon,xcrgabon,100,unitgabon,'s','fill');
scatter(ymgmats,xcrmats,100,unitmats,'d','fill');
scatter(ymgkoala,xcrkoala,100,unitkoala,'^','fill');
scatter(ymgsheiba,xcrsheiba, 100,unitsheiba,'o','fill');
scatter(ymgmisery,xcrmisery,100,unitmisery,'v','fill');
```

Plots with Terra Data require the following lines for output

```
scatter(ymgportable,xcrportable,100,unitportable,'*');
```

Matlab Entry Code for Ternary PlotsInput

```
data = xlsread('Tern_Plots.xlsx')
```

```
Tigabon=data(1:18,2)
Timats=data(19:29,2)
Tikoala=data(30:47,2)
Tisheiba=data(48:56,2)
Timisery=data(57:74,2)
```

```
Algabon=data(1:18,3)
Almats=data(19:28,3)
Alkoala=data(30:47,3)
Alsheiba=data(48:56,3)
Almisery=data(57:74,3)
```

```
Crgabon=data(1:18,4)
Crmats=data(19:29,4)
Crkoala=data(30:47,4)
Crsheiba=data(48:56,4)
Crmisery=data(57:74,4)
```

```
Mggabon=data(1:18,8)
Mgmats=data(19:29,8)
```

```
Mgkoala=data(30:47,8)
Mgsheiba=data(48:56,8)
Mgmisery=data(57:74,8)
```

```
Fe2gabon=data(1:18,6)
Fe2mats=data(19:29,6)
Fe2koala=data(30:47,6)
Fe2sheiba=data(48:56,6)
Fe2misery=data(57:74,6)
```

```
Fe3gabon=data(1:18,7)
Fe3mats=data(19:29,7)
Fe3koala=data(30:47,7)
Fe3sheiba=data(48:56,7)
Fe3misery=data(57:74,7)
```

```
Unitgabon=data(1:18,13)
Unitmats=data(19:29,13)
Unitkoala=data(30:47,13)
Unisheiba=data(48:56,13)
Unitmisery=data(57:74,13)
```

Fe3 Ternary

```
ternplot(Algabon,Fe3gabon,Crgabon,Unitgabon,'s')
hold on
ternplot(Almait,Fe3mait,Crmait,Unitmait,'d')
ternplot(Alkoala,Fe3koala,Crkoala,Unitkoala,'^')
ternplot(Alsheiba,Fe3sheiba,Crsheiba,Unitsheiba,'o')
ternplot(Almisery,Fe3misery,Crmisery,Unitmisery,'v')
```

Ti Ternary

```
ternplot(Algabon,Tigabon,Crgabon,Unitgabon,'s')
hold on
ternplot(Almait,Timait,Crmait,Unitmait,'d')
ternplot(Alkoala,Tikoala,Crkoala,Unitkoala,'^')
ternplot(Alsheiba,Tisheiba,Crsheiba,Unitsheiba,'o')
ternplot(Almisery,Timisery,Crmisery,Unitmisery,'v')
```

Make Legend Markers Black

```
hMarkers = findobj(legend,'type','patch');
set(hMarkers, 'MarkerEdgeColor','k', 'MarkerFaceColor','k');
```

Ternary Plots

The Ternary plots from Carl Sandrock was adapted for use with a colour as an additional dimension.

% TERNPLOT plot ternary phase diagram

```
% TERNPLOT(A, B) plots ternary phase diagram for three components. C
is calculated
%      as 1 - A - B.
%
% TERNPLOT(A, B, C) plots ternary phase data for three components A B
and C. If the values
%      are not fractions, the values are normalised by dividing by the
total.
%
% TERNPLOT(A, B, C, LINETYPE) the same as the above, but with a user
specified LINETYPE (see PLOT
%      for valid linetypes).
%
% NOTES
% - An attempt is made to keep the plot close to the default plot
type. The code has been based largely on the
%      code for POLAR.
% - The regular TITLE and LEGEND commands work with the plot from
this function, as well as incremental plotting
%      using HOLD. Labels can be placed on the axes using TERNLABEL
%
% See also TERNLABEL PLOT POLAR

%
%      b
%     /\
%    /\
%   /\
%  c --- a

% Author: Carl Sandrock 20020827

% To do

% Modifications

% Modifiers
% CS Carl Sandrock

function handles = ternplot(A, B, C, D,E, varargin)

majors = 5;

if nargin < 3
    C = 1 - (A+B);
end;

[fA, fB, fC] = fractions(A, B, C);
[x, y] = terncoords(fA, fB, fC);
fD=D;
```

Ternary Plots- Cont'd

```
% Sort data points in x order
[x, i] = sort(x);
y = y(i);
fD = fD(i);

% Make ternary axes
[hold_state, cax, next] = ternaxes(majors);

% plot data
q = scatter(x, y, 50, fD, E, 'fill');

if nargout > 0
    hpol = q;
end
if ~hold_state
    set(gca, 'dataaspectratio', [1 1 1]), axis off;
    set(cax, 'NextPlot', next);
end
```

% TERNAXES create ternary axis

```
% HOLD_STATE = TERNAXES(MAJORS) creates a ternary axis system using
the system
% defaults and with MAJORS major tickmarks.
```

```
% Author: Carl Sandrock 20050211
```

```
% To Do
```

```
% Modifications
```

```
% Modifiers
% (CS) Carl Sandrock
```

```
function [hold_state, cax, next] = ternaxes(majors)
```

```
%TODO: Get a better way of offsetting the labels
xoffset = 0.04;
yoffset = 0.02;
```

```
% get hold state
cax = newplot;
next = lower(get(cax, 'NextPlot'));
hold_state = ishold;
```

```
% get x-axis text color so grid is in same color
tc = get(cax, 'xcolor');
ls = get(cax, 'gridlinestyle');
```

```
% Hold on to current Text defaults, reset them to the
% Axes' font attributes so tick marks use them.
```

```

fAngle = get(cax, 'DefaultTextFontAngle');
fName  = get(cax, 'DefaultTextFontName');
fSize  = get(cax, 'DefaultTextFontSize');
fWeight = get(cax, 'DefaultTextFontWeight');
fUnits  = get(cax, 'DefaultTextUnits');

set(cax, 'DefaultTextFontAngle', get(cax, 'FontAngle'), ...
    'DefaultTextFontName', get(cax, 'FontName'), ...
    'DefaultTextFontSize', get(cax, 'FontSize'), ...
    'DefaultTextFontWeight', get(cax, 'FontWeight'), ...
    'DefaultTextUnits', 'data')

% only do grids if hold is off
if ~hold_state
    %plot axis lines
    hold on;
    plot ([0 1 0.5 0],[0 0 sin(1/3*pi) 0], 'color', tc,
        'linewidth',1,...
            'handlevisibility','off');
    set(gca, 'visible', 'off');

    % plot background if necessary
    if ~isstr(get(cax,'color')),
        patch('xdata', [0 1 0.5 0], 'ydata', [0 0 sin(1/3*pi) 0], ...
            'edgecolor',tc,'facecolor',get(gca,'color'),...
            'handlevisibility','off');
    end

    % Generate labels
    majorticks = linspace(0, 1, majors + 1);
    majorticks = majorticks(1:end-1);
    labels = num2str(majorticks'*100);

    zerocomp = zeros(size(majorticks)); % represents zero composition

    % Plot right labels (no c - only b a)
    [lxc, lyc] = terncoords(1-majorticks, majorticks, zerocomp);
    text(lxc, lyc, [repmat(' ', length(labels), 1) labels]);

    % Plot bottom labels (no b - only a c)
    [lxb, lyb] = terncoords(majorticks, zerocomp, 1-majorticks); % fB =
1-fA
    text(lxb, lyb, labels, 'VerticalAlignment', 'Top');

    % Plot left labels (no a, only c b)
    [lxa, lya] = terncoords(zerocomp, 1-majorticks, majorticks);
    text(lxa-xoffset, lya, labels);

    nlabels = length(labels)-1;
    for i = 1:nlabels
        plot([lxa(i+1) lxb(nlabels - i + 2)], [lya(i+1) lyb(nlabels - i
+ 2)], ls, 'color', tc, 'linewidth',1,...
            'handlevisibility','off');
        plot([lxb(i+1) lxc(nlabels - i + 2)], [lyb(i+1) lyc(nlabels - i
+ 2)], ls, 'color', tc, 'linewidth',1,...

```

```

        'handlevisibility','off');
    plot([lxc(i+1) lxa(nlabels - i + 2)], [lyc(i+1) lya(nlabels - i
+ 2)], ls, 'color', tc, 'linewidth',1,...
        'handlevisibility','off');
    end;
end;

% Reset defaults
set(cax, 'DefaultTextFontAngle', fAngle , ...
    'DefaultTextFontName',    fName , ...
    'DefaultTextFontSize',    fSize, ...
    'DefaultTextFontWeight',  fWeight, ...
    'DefaultTextUnits', fUnits );

```

Patrick Shepherd

EDUCATION

Masters of Geological Sciences, Western University, London, ON 2015 (Expected)

- Chromite Crystal Structure and Chemistry Applied as an Exploration Tool
- Courses/Short Courses Include: Exploration Geochemistry, Kimberlite Petrography in the context of Modern Volcanic Rocks Short Course, Best Practices in Drilling Short Course, Cumulative Average 89%
- Western Graduate Research Scholarship (2012-2014)

Bachelor of Science, Queen's University, Kingston, ON 2011

- Dean's Honour List (2009-2010)
- Courses/ Short Courses Include: Ore Petrology, Advanced Topics in Mineralogy, Diamond Short Course

WORK EXPERIENCE

Western University, London, ON 2012-Present

Graduate Teaching Assistantship – Upper Year Mineralogy and Optics

- Taught course material to upper year students requiring the students to look at mineral hand samples and use optical microscopy in a lab setting to prepare them for future fieldwork.
- Assisted students with labs that required uses of analytical techniques, overseeing their use of a powder X-ray Diffraction (XRD) and their processing of Electron Microprobe (EPMA) data, leading to an understanding of common techniques used by the industry.

Queen's University, Kingston, ON 2009-2011

Teaching Assistant – First Year Engineering and First Year Science Geology classes

- Taught students identification of rock and mineral hand samples, use of stereoscopes, and basic geology concepts in a classroom setting to engineering students to provide them with technical skills for future engineering work.
- Guided fieldwork to ensure students gained experience in the practical application of geological techniques in the engineering sector.

Home Hardware, Almonte, ON 2008-2011

Lumberyard Assistant/Inventory Assistant

- Heavy labour in an outdoor environment leading to the completion of tasks within time-sensitive deadlines.
- Reorganized warehouse leading to increased efficiency, and more accurate inventories.

PUBLICATIONS

- Shepherd, P. & Flemming, R.L. (2014) Unit Cell Parameter as a Proxy for Composition of Kimberlitic and Non-Kimberlitic Chromite (Goldschmidt, 2275).
- Schulze, D.J., Flemming, R.L., Shepherd, P., Helmstaedt, H. (2014) Mantle-derived guyanaite in a Cr-omphacitite xenolith from Moses Rock diatreme, Utah. *American Mineralogist*.

ACTIVITIES

London Gem and Mineral Society, Guest Lecturer 2013

Structure and Chemistry of Minerals and Materials class, Western University, Guest Lecturer 2012

Western Newman Club, Men's Outreach Coordinator 2012-Present

- Increased coordination with off-campus groups, leading to 3x attendance of male participants and leaders.
- Provided mentorship and peer support to younger students, both individually and in small groups, to aid in the shift from high school to university and to develop future leaders in the group

INTERESTS & CERTIFICATIONS

Taekwondo, Black Belt

Amateur Radio License

Basic ioGas, Leapfrog and geosoft operation

Basic C++ and VBA programming skills – Developed in-house software for lab operations, which has been implemented throughout the group.

ArcGIS, Air photo interpretation

P.A.L. Restricted-Canadian Firearms Safety License 2011

APGO Geoscientist-in-Training (GIT) 2012